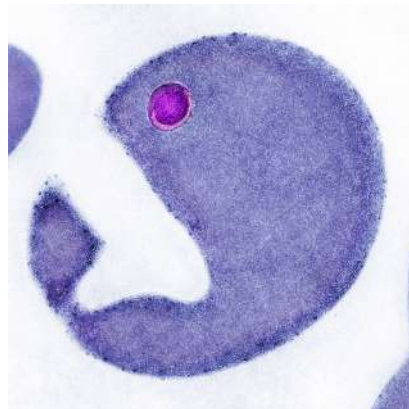


The effects on the malaria parasite
Plasmodium falciparum (WELCH, 1897)
in response to an interaction of
parasitized erythrocytes with
various human endothelial receptors



DISSERTATION

to obtain the degree of
Doctor of Natural Science

Dr. rer. nat.

submitted to the
University of Hamburg
Faculty of Mathematics, Informatics and Natural Sciences
at the Department of Biology

by
Lisa Katharina Roth
from Bad Bergzabern

Hamburg 2019

This work was performed at the Bernhard Nocht Institute for Tropical Medicine in Hamburg in the department of Protozoology under the supervision of Prof. Dr. rer. nat. Iris Bruchhaus

This work is supported by the Joachim Herz Stiftung
& the PIER Helmholtz Graduate School

Date of the disputation

16th of May 2019

Evaluation

Prof. Dr. rer. nat. **Iris Bruchhaus**
Bernhard Nocht Institute for Tropical Medicine (BNITM)
Department of Protozoology
Hamburg

Prof. Dr. rer. nat. **Tim-Wolf Gilberger**
Bernhard Nocht Institute for Tropical Medicine (BNITM)
Department of Cellular Parasitology
Hamburg

SUMMARY

Malaria is still one of the main infectious diseases worldwide, while *Plasmodium falciparum* induces the most severe form, with a high potential of developing devastating clinical symptoms such as hemolytic anemia, obstruction of blood flow, critical and insufficient supply of organs as well as cerebral impairment and death.

Variable surface proteins, such as '*Plasmodium falciparum* erythrocyte membrane protein 1' (PfEMP1) and other multicopy gene families, are involved in the interaction between the malaria pathogen and its human host. PfEMP1 appears in electron dense structures, termed knobs, on the membrane of infected erythrocytes (IE). In particular, the parasitic mechanisms of sequestration and antigenic variation are crucial for immune evasion and parasite survival. They are mainly mediated by PfEMP1 and other surface proteins, thus, the proteins being the major factors for the high pathogenicity of *P. falciparum*. By now, various human receptors are known to bind IE but only for a few of them, PfEMP1 is identified as the parasite ligand.

The overall objective of this work was to characterize the gene expression of *P. falciparum* populations, specifically enriched for binding to different human endothelial receptors.

By conducting static binding assays with various *P. falciparum* culture and field isolates, the initial binding capability of the isolates was evaluated. This revealed a noteworthy binding profile towards 6 promising, so far, only barely if yet described candidates, namely MDR1, TNFR1, TNFR2, CD37, CD55 and CD81.

Consequently, the *P. falciparum* IT4 isolate was utilized for specific sequestration studies, followed by a respective gene expression analysis via next generation RNA sequencing. For each individual and receptor specifically enriched IT4 population, the *var* multigene family as well as other multicopy surface protein clusters were evaluated, while a comprehensive analysis of the whole transcriptomes was performed in the same course.

The obtained results evidenced a differentially upregulation in almost all receptor enriched IT4 populations. The expression of particular *var* genes was observed in IT4-MDR1 for C_var05; in IT4-TNFR1 for A_var03; in IT4-CD55 for B_var11 and in IT4-CD81 for A_var09, B_var11 and B_var12. Furthermore, diverse gene clusters, associated with knob formation on the surface of IE were cumulatively detected in IT4-MDR1, IT4-TNFR2, IT4-CD37 and IT4-CD81. The gene, coding for the major knob associated histidine rich protein (KAHRP), was found to be extensively upregulated in the IT4-CD37 population, while also being present at considerable levels in IT4-MDR1, IT4-CD55 and IT4-CD81.

The quantitative and comparative transmission electron microscopy (TEM) analysis provides an overall view of the morphology, appearance and versatility of distinct *P. falciparum* populations. While exhibiting a definite binding profile towards the particular human receptors as well as cultivated under various febrile conditions, the appearance and distribution of knob formations were focused on. Moreover, a comparison of various *P. falciparum* field isolates was performed.

The TEM analysis revealed a knob positive phenotype apparent within the IT4-CD37 and, in smaller proportions, in the IT4-CD81 population. Additionally, the sequestration towards human endothelial brain cells at febrile temperature manifested knob positive IE. Surprisingly, this phenotype was also achieved within small IT4 populations, specifically sequestered to mock-transfected CHO-GFP as well as to CHO cells expressing human receptor protein CD55, in combination with short periods of febrile temperatures.

Summarizing, the as yet described set of human receptors, interacting with *P. falciparum* infected erythrocytes can be extended, while also a hint towards the interacting PfEMP1 proteins has been revealed. Eventually, the influence of febrile temperatures coupled with sequestration, must be noted. The obtained findings open up new possibilities for further investigations regarding major factors of the high pathogenicity of *P. falciparum*, to get a step closer to fight malaria.

ZUSAMMENFASSUNG

Malaria ist nach wie vor eine der Hauptinfektionskrankheiten weltweit, wobei *Plasmodium falciparum* die schwerste Form auslöst. Diese ist durch die Ausprägung verheerender klinischer Symptome charakterisiert, wie beispielsweise hämolytische Anämie, Blockierung des Blutflusses, kritische und unzureichende Versorgung von Organen, sowie massive Hirnschädigungen und Tod.

Variable Oberflächenproteine, wie 'Plasmodium falciparum erythrocyte membrane protein 1' (PfEMP1) und andere Multigenfamilien sind an der Interaktion zwischen dem Malariaerreger und seinem menschlichen Wirt beteiligt. Die PfEMP1 Proteine sind in hoher Dichte in und um knopfförmige Ausstülpungen, den sogenannten *knobs*, auf der Membranoberfläche von infizierten Erythrozyten (IE) zu finden. Insbesondere die beiden parasitären Mechanismen der Sequestrierung und die antigene Variation sind für die Immunabwehr und das Überleben des Parasiten im Wirt wichtig. Diese werden vor allem durch PfEMP1 und weitere Oberflächenproteine vermittelt und stellen somit die Hauptfaktoren für die hohe Pathogenität von *P. falciparum* dar. Inzwischen wurden einige menschliche Rezeptoren identifiziert, die an der Sequestrierung der IE beteiligt sind. Allerdings konnten bisher nur für einige von ihnen PfEMP1 als Parasitenligand identifiziert werden.

Das Ziel dieser Arbeit ist es, die Genexpression verschiedener *P. falciparum* Populationen zu analysieren, die spezifisch auf die Bindung an verschiedene humane Endothelrezeptoren angereichert wurden.

Mit Hilfe von statischen Bindungsexperimenten diverser *P. falciparum* Kultur- und Feldisolate wurde die anfängliche Bindungsfähigkeit der Isolate bewertet. Diese zeigten bemerkenswerte Bindungsprofile hinsichtlich sechs, bislang nicht, oder nur kaum beschriebener, vielversprechender Rezeptoren, nämlich MDR1, TNFR1, TNFR2, CD37, CD55 und CD81.

Darauf aufbauend wurde das *P. falciparum* IT4 Isolat mittels spezifischer Bindungsstudien auf die entsprechenden Rezeptoren angereichert und durch eine nachfolgende Genexpressionsanalyse via *next generation* RNA-Sequenzierung analysiert. Für jede einzelne der IT4 Population wurden die *var* Multigenfamilie sowie andere Gruppen von Oberflächenproteinen untersucht und eine umfassende Auswertung der gesamten Transkriptome durchgeführt.

Die vorliegenden Ergebnisse zeigen eine erhöhte Expression in fast allen rezeptorspezifisch angereicherten IT4 Populationen. Eine differenzielle Expression der *var* Gene konnte in IT4-MDR1 für C_var05; in IT4-TNFR1 für A_var03; in IT4-CD55 für B_var11 und in IT4-CD81 für A_var09, B_var11 und B_var12 beobachtet werden. Darüber hinaus wurden hauptsächlich in den IT4-MDR1, IT4-TNFR2, IT4-CD37 und IT4-CD81 Populationen erhöhte Genexpressionen detektiert, deren Proteine mit der Ausbildung von *knobs* auf der Oberfläche von IE in Verbindung gebracht werden.

Die quantitative und vergleichende Transmissionselektronenmikroskopie (TEM) lieferte einen Überblick über die Morphologie der untersuchten IT4 Populationen. Diese wurden entweder durch spezifische, rezeptorvermittelte Sequestrierung oder durch Kultivierung in Gegenwart von Hitzestress generiert. Hierbei wurde insbesondere das Vorhandensein von *knobs* innerhalb der verschiedenen Populationen analysiert. Zusätzlich wurde ein Vergleich mit unterschiedlichen *P. falciparum* Feldisolaten angestellt.

Die TEM-Analyse zeigte einen *knob* positiven Phänotyp innerhalb der IT4-CD37 und einer kleineren IT4-CD81 Populationen. Zudem bewirkte die Sequestrierung an humane Gehirndothelzellen bei fieberartigen Temperaturen ebenfalls eine *knob* Ausprägung auf den IE. Überraschenderweise prägte sich dieser Phänotyp auch in geringem Maße in bestimmten IT4-Populationen aus, welche spezifisch an Mock-transfizierte CHO-GFP sowie an CHO-CD55 Zellen sequestrierten, die das menschliche CD55 Protein auf der Oberfläche exprimieren. Dies konnte jedoch nur in Kombination mit kurzen, fieberartigen Temperaturphasen erzielt werden.

Zusammenfassend lässt sich sagen, dass die Gruppe an *P. falciparum* IE interagierenden Rezeptoren erweitert und gleichzeitig Hinweise auf das Zusammenspiel mit bestimmten PfEMP1 Proteinen gefunden wurden.

Außerdem ist der Einfluss von Fieber, im Zusammenspiel mit Sequestrierung besonders zu beachten. Die gewonnenen Erkenntnisse eröffnen neue Möglichkeiten für weitere Untersuchungen hinsichtlich der wesentlichen Pathogenitätsfaktoren von *P. falciparum*, um so neue Strategien zur Bekämpfung der Malaria zu entwickeln.

| | |
|--|-----------|
| SUMMARY | 3 |
| ZUSAMMENFASSUNG | 5 |
| TABLE OF CONTENTS | 7 |
| LIST OF FIGURES | 11 |
| LIST OF TABLES | 13 |
| 1 INTRODUCTION | 14 |
| 1.1 KEY FACTS & DISTRIBUTION OF <i>PLASMODIUM FALCIPARUM</i> | 14 |
| 1.2 TRANSMISSION & SPECIES OF THE GENUS <i>PLASMODIUM</i> | 15 |
| 1.3 PATHOGENESIS & SYMPTOMS | 16 |
| 1.4 DIAGNOSTICS, THERAPY, PREVENTION & PROPHYLAXIS | 16 |
| 1.5 VACCINE APPROACH | 17 |
| 1.6 <i>PLASMODIUM FALCIPARUM</i> LIFE CYCLE | 18 |
| 1.6.1 PRE-ERYTHROCYTIC STAGES | 19 |
| 1.6.2 MEROZOITE INVASION | 20 |
| 1.6.3 RING STAGE | 21 |
| 1.6.4 TROPHOZOITE STAGE | 21 |
| 1.6.5 SCHIZONT STAGE | 22 |
| 1.6.6 GAMETOCYTE STAGE | 23 |
| 1.6.7 MOSQUITO PHASE | 23 |
| 1.7 SEMI-IMMUNITY, IMMUNE EVASION, ANTIGENIC VARIATION AND CYTOADHESION | 24 |
| 1.8 SEQUESTRATION | 25 |
| 1.9 SECRETORY PATHWAYS & PROTEIN TRANSPORT | 26 |
| 1.10 SELECTED MULTIGENE FAMILIES | 28 |
| 1.10.1 THE VAR MULTIGENE FAMILY | 28 |
| 1.10.2 OTHER MULTIGENE FAMILIES: <i>RIF</i> , <i>STEVOR</i> , <i>PFMC-2TM</i> , <i>SURF</i> , <i>PHIST</i> | 29 |
| 1.11 GENOMIC ORGANIZATION, MUTUAL EXCLUSIVITY & VAR GENE SWITCHING | 30 |
| 1.12 KNOB STRUCTURE | 32 |
| 1.13 HUMAN RECEPTORS, INVOLVED IN <i>P. FALCIPARUM</i> MALARIA | 33 |
| 1.13.1 CD36 | 34 |
| 1.13.2 CHONDROITIN SULFATE A (CSA) | 34 |
| 1.13.3 CELLULAR ADHESION MOLECULES | 34 |
| 1.13.4 SELECTINS | 35 |
| 1.13.5 TETRASPANINS | 36 |
| 1.13.6 HRH1 – HISTAMINE RECEPTOR 1 | 36 |
| 1.13.7 CD55 | 37 |
| 1.13.8 MDR1 / CD243 – MULTIDRUG RESISTANCE PROTEIN 1 | 37 |
| 1.13.9 TNFR1 AND TNFR2 – TUMOR NECROSIS FACTORS | 37 |

| | | |
|----------|---|-----------|
| 2 | AIM OF THE THESIS | 39 |
| 3 | MATERIALS | 40 |
| 3.1 | STOCKS & SOLUTIONS | 40 |
| 3.2 | CHEMICALS | 44 |
| 3.3 | ENZYMES | 45 |
| 3.4 | KITS | 45 |
| 3.5 | DEVICES | 45 |
| 3.6 | SOFTWARE | 46 |
| 3.7 | VECTORS & GENES | 46 |
| 3.8 | ANTIBODIES | 47 |
| 4 | METHODS | 48 |
| 4.1 | CELL LINES | 48 |
| 4.1.1 | <i>E. COLI</i> ONE SHOT TOP10 (ATCC PTA-10989) | 48 |
| 4.1.2 | CHINESE HAMSTER OVARY (CHO) CELL LINE (ATCC CRL-2242) | 48 |
| 4.1.3 | HUMAN BRAIN ENDOTHELIAL CELLS (HBEC)-5I CELL LINE | 49 |
| 4.1.4 | <i>P. FALCIPARUM</i> CLINICAL ISOLATES | 49 |
| 4.1.5 | <i>P. FALCIPARUM</i> FIELD ISOLATE NF54 AND 3D7 | 50 |
| 4.1.6 | <i>P. FALCIPARUM</i> FIELD ISOLATE DD2 | 50 |
| 4.1.7 | <i>P. FALCIPARUM</i> FIELD ISOLATE MM | 50 |
| 4.1.8 | <i>P. FALCIPARUM</i> FIELD ISOLATE FCR3/IT4 | 50 |
| 4.2 | MOLECULAR BIOLOGY | 51 |
| 4.2.1 | <i>P. FALCIPARUM</i> CULTURING | 51 |
| 4.2.2 | <i>P. FALCIPARUM</i> THAWING OF CRYOGENIC CONSERVED STOCKS | 51 |
| 4.2.3 | <i>P. FALCIPARUM</i> FREEZING OF CRYOGENIC CONSERVED STOCKS | 52 |
| 4.2.4 | <i>P. FALCIPARUM</i> CULTURING | 52 |
| 4.2.5 | <i>P. FALCIPARUM</i> GIEMSA STAINING | 52 |
| 4.2.6 | <i>P. FALCIPARUM</i> SPLITTING | 52 |
| 4.2.7 | <i>P. FALCIPARUM</i> SYNCHRONIZATION VIA D-SORBITOL | 53 |
| 4.2.8 | CHO AND HBEC-5I CULTURING | 53 |
| 4.2.9 | CHO THAWING OF CRYOGENIC CONSERVED STOCKS | 53 |
| 4.2.10 | CHO FREEZING OF CRYOGENIC CONSERVED STOCKS | 54 |
| 4.2.11 | CHO CULTURING | 54 |
| 4.2.12 | CHO SPLITTING | 54 |
| 4.2.13 | <i>P. FALCIPARUM</i> ISOLATION OF GENOMIC DNA (GDNA) | 55 |
| 4.2.14 | SYNTHESIS OF COMPLEMENTARY DNA | 55 |
| 4.2.15 | POLYMERASE CHAIN REACTION | 55 |
| 4.2.16 | THERMOCYCLER PROGRAMS | 55 |
| 4.2.17 | ENZYMATIC RESTRICTION DIGEST | 57 |
| 4.2.18 | ISOLATION OF DNA – PCR CLEAN UP AND GEL EXTRACTION | 57 |
| 4.2.19 | CHEMICALLY COMPETENT <i>ESCHERICHIA COLI</i> (<i>E. COLI</i>) CELLS | 57 |
| 4.2.20 | TOPOISOMERASE (TOPO) CLONING | 57 |
| 4.2.21 | PLASMID PREPARATION | 57 |
| 4.2.22 | TRANSFECTION OF CHO CELLS | 57 |
| 4.2.23 | <i>P. FALCIPARUM</i> DNA SEQUENCING | 58 |
| 4.2.24 | <i>P. FALCIPARUM</i> TOTAL RNA ISOLATION WITH TRIZOL REAGENT | 58 |
| 4.2.25 | <i>P. FALCIPARUM</i> RNA QUALITY AND QUANTITY CONTROL | 58 |
| 4.2.26 | NEXT GENERATION SEQUENCING (NGS) | 59 |

| | | |
|----------|---|------------|
| 4.2.27 | BIOINFORMATIC ANALYSIS OF <i>P. FALCIPARUM</i> TRANSCRIPTOMES | 59 |
| 4.2.28 | SEEDING OF CHO AND HBEC-5I CELLS | 59 |
| 4.2.29 | <i>P. FALCIPARUM</i> STATIC BINDING ASSAY | 60 |
| 4.2.30 | CYTOADHESION INHIBITION ASSAY WITH SPECIFIC ANTIBODIES | 61 |
| 4.2.31 | CYTOADHESION INHIBITION ASSAY WITH SOLUBLE CSA (sCSA) | 61 |
| 4.2.32 | ENRICHED <i>P. FALCIPARUM</i> POPULATIONS VIA PANNING ASSAYS | 61 |
| 4.2.33 | IE HARVEST FOR USING BIOCOLL SEPARATING SOLUTION | 62 |
| 4.2.34 | <i>P. FALCIPARUM</i> HARVEST FOR RNA ISOLATION USING TRIZOL | 63 |
| 4.2.35 | IFA – IMMUNOFLUORESCENCE ASSAY | 63 |
| 4.3 | BIOTECHNICAL METHODS | 64 |
| 4.3.1 | FACS ANALYSIS FOR FURTHER CULTIVATION | 64 |
| 4.3.2 | FACS STAINING PROCEDURE | 65 |
| 4.3.3 | FACS SORTING PROCEDURE | 66 |
| 4.3.4 | FACS GATING STRATEGY | 66 |
| 4.3.5 | <i>P. FALCIPARUM</i> SEPARATION USING PERCOLL GRADIENT SOLUTION | 68 |
| 4.3.6 | TRANSMISSION ELECTRON MICROSCOPY (TEM) | 69 |
| 5 | RESULTS | 71 |
| 5.1 | PHYSIOLOGICAL RELEVANCE OF A CHOSEN HUMAN RECEPTOR SET | 71 |
| 5.2 | CHO REPERTOIRE, FACS DATA & FLUORESCENCE MICROSCOPY | 73 |
| 5.3 | SPECIFIC CYTOADHESION OF IE TO TRANSGENIC CHO CELLS | 77 |
| 5.4 | STATIC BINDING ASSAYS | 78 |
| 5.5 | INHIBITION ASSAY TO UNKNOWN SURFACE STRUCTURES | 82 |
| 5.6 | CYTOADHESION INHIBITION ASSAY WITH sCSA | 84 |
| 5.7 | ENRICHMENT VIA MULTIPLE ROUNDS OF PANNING ASSAYS | 87 |
| 5.8 | NGS ANALYSIS: COMPARISON OF GENE EXPRESSION LEVELS | 89 |
| 5.8.1 | COMPARISON OF VAR GENE EXPRESSION LEVELS | 89 |
| 5.8.2 | COMPARISON OF OVERALL GENE EXPRESSION LEVELS | 95 |
| 5.8.2.1 | Knob related genes | 96 |
| 5.8.2.2 | Trafficking, membrane & cytoskeleton related genes | 97 |
| 5.8.2.3 | VSA genes | 97 |
| 5.8.2.4 | Merozoites & invasion related genes and others | 98 |
| 5.8.2.5 | Conserved genes with unknown function | 98 |
| 5.9 | KNOB PRESENCE MEDIATED BY A COMBINATION OF HEAT AND SEQUESTRATION | 99 |
| 5.10 | TRANSMISSION ELECTRON MICROSCOPY ANALYSIS | 101 |
| 5.11 | MORPHOLOGICAL ANALYSIS OF KNOB APPEARANCE | 105 |
| 6 | DISCUSSION | 107 |
| 6.1 | PHYSIOLOGICAL RELEVANCE OF A CHOSEN HUMAN RECEPTOR SET | 107 |
| 6.2 | CHO REPERTOIRE, FACS DATA & FLUORESCENCE MICROSCOPY | 108 |
| 6.3 | SPECIFIC CYTOADHESION OF IE TO TRANSGENIC CHO CELLS | 110 |
| 6.4 | STATIC BINDING ASSAYS | 112 |
| 6.5 | CYTOADHESION INHIBITION ASSAY TO UNKNOWN SURFACE STRUCTURES | 114 |
| 6.6 | CYTOADHESION INHIBITION ASSAY WITH sCSA | 115 |
| 6.7 | ENRICHMENT VIA MULTIPLE ROUNDS OF PANNING ASSAYS | 116 |
| 6.8 | NGS ANALYSIS – COMPARISON OF GENE EXPRESSION LEVELS | 117 |
| 6.9 | ANALYZING THE VAR TRANSCRIPTOME | 117 |
| 6.10 | ANALYZING THE WHOLE TRANSCRIPTOME | 118 |
| 6.10.1 | IT4-GFP | 119 |
| 6.10.2 | IT4-MDR1 | 119 |

| | | |
|-----------------------------|--|------------|
| 6.10.3 | IT4-TNFR1 | 120 |
| 6.10.4 | IT4-TNFR2 | 121 |
| 6.10.5 | IT4-CD37 | 122 |
| 6.10.6 | IT4-CD55 | 122 |
| 6.10.7 | IT4-CD81 | 123 |
| 6.11 | OPERATIONAL MATTERS | 125 |
| 6.12 | TEM ANALYSIS OF KNOB APPEARANCE OF THE <i>P. FALCIPARUM</i> IE | 126 |
| 6.12.1.1 | Field isolates | 126 |
| 6.12.1.2 | Culture isolate IT4 | 126 |
| CONCLUSION | | 129 |
| FINAL SUMMARY | | 131 |
| LITERATURE | | 132 |
| ABBREVIATIONS | | 144 |
| APPENDIX | | 147 |
| ANNEX I | | 147 |
| ANNEX II | | 153 |
| LANGUAGE CERTIFICATE | | 154 |
| ACKNOWLEDGEMENTS | | 155 |
| DECLARATION | | 156 |

LIST OF FIGURES

- Figure 1.** Global transmission and distribution of *Plasmodium spp.*
- Figure 2.** The lifecycle of *Plasmodium falciparum*.
- Figure 3.** *P. falciparum* entering the liver phase by invasion of hepatocytes.
- Figure 4.** *P. falciparum* merozoite organization and invasion into host erythrocyte.
- Figure 5.** Transmission electron microscopy of *P. falciparum* intraerythrocytic blood stages.
- Figure 6.** Forms of cytoadhesion of *P. falciparum* IE
- Figure 7.** Schematic overview of the protein export in *P. falciparum*.
- Figure 8.** Predicted gene organization and assumed topology of VSA members.
- Figure 9.** Schema of the mutual exclusivity transcription system of *var* genes.
- Figure 10.** Knob structure of *P. falciparum* IE and involved proteins
- Figure 11.** General gating strategy to sort double positive CHO cell populations using the FACSAriaIII device.
- Figure 12.** FACS analysis and transcriptome analysis* of HBEC-5i cells, incubated at either 37°C, 40°C or stimulated with TNF α
- Figure 13.1.** Fluorescence analysis and FACS analysis of transgenic CHO cells, expressing human endothelial receptors.
- Figure 13.2.** Fluorescence analysis and FACS analysis of transgenic CHO cells, expressing human endothelial receptors.
- Figure 14.** Specific cytoadhesion of *P. falciparum* IT4 parasitized IE towards transgenic CHO-CD81 and CHO-CD55 cells during a static binding assay.
- Figure 15.1** Static binding assays of various isolates over the complete human endothelial receptor set.
- Figure 15.2.** Static binding assays of various isolates over the complete human endothelial receptor set.
- Figure 16.** Cytoadhesion inhibition assay with specific antibodies.
- Figure 17.** Cytoadhesion inhibition assay of specific IE binding towards HBEC-5i with sCSA.
- Figure 18.** Enrichment via multiple rounds of panning assays to generate a homogenous population of *P. falciparum* IE specifically interact to a human endothelial receptor.
- Figure 19.** Comparison of *var* gene expression levels of IT4-ST and IT4-GFP population.

- Figure 20.1.** Comparison of *var* gene expression levels of IT4-MDR1, IT4-TNFR1 and IT4-TNFR2.
- Figure 20.2.** Comparison of *var* gene expression levels of IT4-CD37, IT4-CD55 and IT4-CD81.
- Figure 21.** Immunofluorescence analysis: knob induction of the knobless IT4 isolate via cytoadhesion at febrile temperatures.
- Figure 22.** Transmission electron microscopy: analysis of knob appearance of *P. falciparum* field isolates.
- Figure 23.1.** Transmission electron microscopy: analysis of knob appearance of the *P. falciparum* IE, enriched over human endothelial receptors.
- Figure 23.2.** Transmission electron microscopy: analysis of knob appearance of the *P. falciparum* IE, treated with TNF α , as well as enriched and/or cultivated over HBEC-5i at febrile temperatures
- Figure 24.** TEM analysis of knob structure focusing on the morphological appearance.
- Figure 25.** Overview of the experimental setup and obtained results.

LIST OF TABLES

- Table 1.** Overview of human pathogenic *Plasmodium spp.* with classification and unique characteristics.
- Table 2.** Overview of generated transgenic CHO cell lines.
- Table 3.** Overview of NGS data for control and enriched IT4 population with mean values and respective p- and padj-values focusing on *var* genes.
- Table 4.1.** Overview of NGS data for control and enriched IT4 population with mean values and respective p- and padj-values.
- Table 4.2.** Overview of NGS data for control and enriched IT4 population with mean values and respective p- and padj-values.

1 INTRODUCTION

1.1 Key facts & distribution of *Plasmodium falciparum*

Malaria is a devastating disease and beside HIV and tuberculosis, still the most infectious disease worldwide. Despite over 100 years of scientific investigation, malaria remains the leading cause of death among children living in Sub-Saharan Africa and India.

Currently, malaria occurred in 90 countries with an estimation of concerning 219 million new cases annually and about 435.000 deaths in 2017. Over 90% of all cases occurred in Africa, 5% in South East Asia and 2% in Mediterranean Regions, as shown in **Figure 1**. Sub-Saharan countries and India were hit hardest. So far, compared to the last 2 years, no significant progress in reducing global malaria cases was accomplished, thus the results achieved are profoundly dissatisfying.

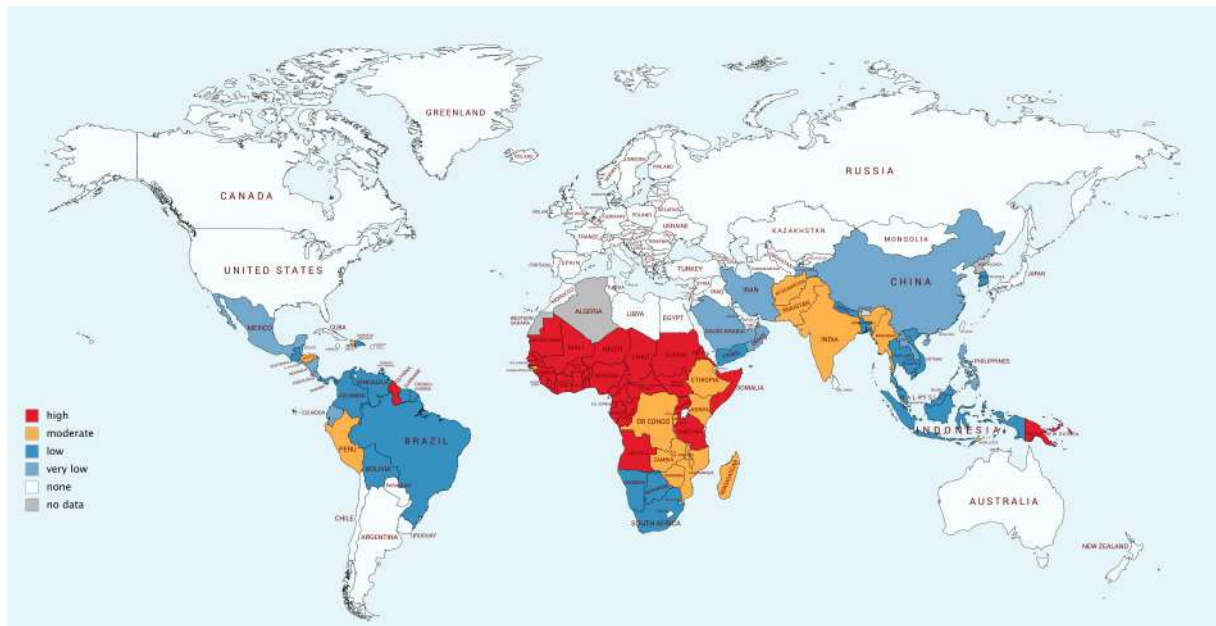


Figure 1. Global transmission and distribution of *Plasmodium spp.* Currently, 90 countries are assigned to boast malaria endemic areas. The estimated risk of being infected is color coded for all countries, ranging from high (red) to moderate (orange), low (dark blue) and very low (light blue). White areas are assigned to be malaria free, while for grey colored countries, no data exist. The global incidence rate comprises about 60 infected persons per 1000 persons at risk, stagnating over the last 3 years. While countries can apply for the 'Malaria-Free' status after 3 consecutive years of zero indigenous cases at the WHO, half of the world population is still in risk of being infected with the devastating disease. The data sourced from the CDC in July 2018.¹

1.2 Transmission & species of the genus *Plasmodium*

Table 1. Overview of human pathogenic *Plasmodium* spp. with classification and unique characteristics.

| phylum | Protozoa / Apicomplexa / Plasmodiidae | | | | |
|----------------------|---|---|---|--|---|
| genus | <i>Plasmodium falciparum</i> | <i>Plasmodium vivax</i> | <i>Plasmodium ovale</i> > <i>P. crustisi</i> & > <i>P. wallikeri</i> | <i>Plasmodium malariae</i> | <i>Plasmodium knowlesi</i> |
| discovery | 1897 Welch | 1890 Grassi & Feletti | 1922 – Stephens > 2010 – Sutherland | 1889 Feletti & Grassi, | 1933 Sinton & Mulligan |
| distribution | most in Africa, also global | most in SEA, also America Africa | most in Sub-Sahara, also SEA India | global | most in SEA |
| vector | mostly <i>A. gambiae</i> also <i>A. walkeri</i> <i>A. stephensi</i> <i>A. culicifacies</i> <i>A. dirus</i> <i>A. subpictus</i> | mostly <i>A. albimanus</i> also <i>A. walkeri</i> <i>A. culicifacies</i> <i>A. punctipennis</i> <i>A. sinensis</i> (Korea) <i>A. subpictus</i> | mostly <i>A. gambiae</i> also <i>A. funestus</i> <i>A. dirus</i> <i>A. albimanus</i> <i>A. freeborni</i> <i>A. subpictus</i> | mostly <i>A. messeae</i> also <i>A. atroparvus</i> | mostly <i>A. latens</i> also <i>A. hackeri</i> <i>A. dirus</i> <i>A. subpictus</i> |
| uniqueness | sequestration via PfEMP1 | hypnozoites – ability to relapse after years via dormant parasitic liver stage possible sequestration Schüffner's dots – hematological feature, associated with lipid rafts of plasma membrane (caveolae) | hypnozoites – ability to relapse after years likely via dormant parasitic liver stage 20 % of parasitized IE are spherical shaped Schüffner's dots / James dots – hematological feature, associated with bigger lipid rafts of plasma membrane (caveolae) two indistinguishable morphological species | NO hypnozoites – but possible relapse after up to 50 years via low blood parasitemia (< 2 parasites / ml) band or basket formed trophozoites | initial simian parasite, but also infecting humans artificially and naturally |
| stage in blood | ring | all | all | all | all |
| host cell | erythrocytes | reticulocytes | erythrocytes | older erythrocytes | erythrocytes |
| febrile phase | falciparum malaria malaria tropica irregular fever every 43 – 48 h | tertian malaria reoccurring fever every 48 h | tertian malaria reoccurring fever every 48h | quartan malaria > most seldom reoccurring fever every 72h | quotidian malaria reoccurring fever every 24h |
| pre- erythrocytic | 5 – 7 days | 6 – 8 days | 9 days | 14 – 16 days | 8 – 12 days |

Malaria is transmitted via a female mosquito of about 100 of 450 different *Anopheles* species² during her blood meal. Within a life cycle of 4 to 30 days, preferentially, the adult insect lays its eggs in stagnant water and the clutch of eggs develop until the larvae hatch and mature to leaves the water as adult mosquitos, feeding on humans to nourish the eggs of the next generation. Thus, new-, multiple-, super- or reoccurring infection happen every couple of seconds.

Malaria parasites of the genus *Plasmodium* spp. are protozoans of the taxon Alveolata,

and the class of Apicomplexa, graded due to their apomorphy of an apicoplast as well as an apical complex including rhoptries and micronemes. Within the genus of *Plasmodium*, there are more than 200 species infecting various host species, such as birds, reptiles and mammals, while only 5 species are known to naturally infect humans, recapped in **Table 1**. *Falciparum* malaria is considered as the strongest effector of disease burden, as 99.7% of all infections in Africa are accounted to *P. falciparum*, while the predominant global distribution in South East Asia is ascribed to 62,8%, in East Mediterranean to 69% and in West Pacific up to 71.9%. *P. vivax* is predominant in the Americas region with 74.1%.¹

1.3 Pathogenesis & symptoms

Falciparum malaria is an acute febrile illness, where the first symptoms appear during 7 to 15 days post infection. Initial complaints can be fever, headache, chills and general malaise. Due to this inconclusive clinical picture, the differential diagnosis compared to e.g. Zika, Dengue, Chikungunya, Yellow fever, bacteremia, influenzas and other illnesses can be challenging. If *falciparum* malaria is not treated within the first 24 hours (h) after onset of symptoms, the course of disease can become very serious. First symptoms may already appear at a parasitemia of 0.01%, *P. falciparum* can reach extremely high parasitemia levels up to 25% within a short period of time. The general definition of the different phases of disease are 'asymptomatic malaria' (AM) with circulating asexual parasite stages within the patient's blood but no expression of symptoms; 'uncomplicated malaria' (UM) with circulating asexual parasites and unspecific symptoms with no clinical or laboratory evidenced (organ) dysfunctions; 'severe malaria' (SM) with circulating asexual blood staged parasites and, with no alternative cause, one of the symptoms of respiratory distress, anemia, low blood pressure, hypoglycemia, metabolic acidosis, splenomegaly, sepsis, multi-organ failure, Glasgow coma score < 11, shock or coma. In case of 'cerebral malaria' (CM) cerebral manifestations like ischemia, aphasia, paralyzes and disturbed consciousness are typical clinical pictures. 'Pregnancy associated malaria' (PAM) is defined by mild to severe symptoms, with a typical lack of a characteristic fever, constituting into a particular hazard regarding early detection of the disease.

1.4 Diagnostics, therapy, prevention & prophylaxis

The current gold standard in diagnosing malaria is still the manual microscopy of Giemsa-stained thin and thick blood film of potent patients. The trained human eye can detect *Plasmodium* infections with a sensitivity of 10 to 100 parasites per microliter, while also the species as well as the parasite quantification can be identified in the same step. Laboratory diagnostics are more sensitive, but also more cost, time and labor-intense, not to mention that proper and maintained laboratory equipment is not available everywhere. Rapid diagnostic tests utilize the lateral flow antigen detection method while being the main tool to diagnose malaria, used in an estimated 75% of

cases.^{3,4} Although no vaccine exists to prevent *Plasmodium* infections and manifestations of the disease, antimalarial therapy is very effective and comparatively well tolerated. A rising parasitemia beyond 36 to 48 h after treatment, indicates therapeutic failure, usually due to high-level drug resistance reinforcing the need for further and variant drug development. So far, the most prevalent schizonticide drug was a combination of quinine and chloroquine. A mostly optimal antimalarial drug was artemisinin, as it fights parasitic sexual and asexual blood stages. Some groups of the population are at higher risk of being infected, such as infants, children under the age of 5, people older than 65, pregnant women, immunocompromised or -deficient, non-immune migrants, refugees, medical staff, mobile populations, travelers, and others. Avoiding mosquitos by persistent repellents, long clothing, not going outside during times of dusk and dawn, sleeping under insecticide treated nets, indoor residual spraying of insecticides and getting rid of stagnant waters, are only some preventive measures to impede malaria disease. In turn, chemoprophylaxis is recommended for pregnant woman and infants in moderate and high endemic areas, as well as in areas of high risk during the whole rainy season. The common advice for travelers is to carry a chemoprophylactic drug as an emergency treatment until the next hospital is reached. In case of an infection, the drug suppresses the parasitic blood and liver stages, avoiding severe symptoms, as *P. falciparum* infection can become very serious within 24 h.^{5,6}

1.5 Vaccine approach

As people can acquire partial or semi-immunity with repeated periods of infection, there is strong evidence that a comprehensive vaccination can be achieved.⁷ Vaccination approaches includes the artificial introduction of the symbiotic-parasitic gram-negative bacteria *Wolbachia spp.* or the generation of genetically altered mosquitos, where sterile insect techniques or heterogenous expression can be utilized to block the parasitic maturation or the egress within the insect's midgut.⁸⁻¹¹

The use of x-ray irradiated, and therefore attenuated sporozoites, induce sterile protection within the host.¹²⁻¹⁵ The circumsporozoite protein of sporozoites is highly conserved across many *Plasmodium* strains and utilized in the leading vaccine candidate RTS,S/AS01, or 'Mosquirux'.^{16,17} Also, intraerythrocytic parasites can be affected by either targeting the unique Maurer's cleft network or inhibiting the hemoglobin digestion. Merozoites and sporozoites are the only extracellular stages without host cell membrane surrounding, and thus defenselessly exposed to the immune system. Those strategies, in principle, could be extended towards whole attenuated *Plasmodium* organisms or exhibited antigens and parasitic proteins on every parasitic stage.¹⁸⁻²⁰

1.6 Plasmodium falciparum life cycle

The *P. falciparum* malaria life cycle obligates a change of the host from the *Anopheles* vector to a human intermediate host, schematically shown in **Figure 2**. The enclosed life cycle can be divided into 3 major phases: The asymptomatic pre-erythrocytic phase contains the infection of the human host, the migration of the transmitted parasites to the liver and the liver stage itself. The clinical symptomatic erythrocytic phase contains the transition of the parasites from the liver to the blood system, as well as the maturation of merozoites via trophozoites into schizonts and gametocytes within infected erythrocytes (IE), as well as the subsequent uptake of infectious sexual staged parasites by the mosquito. The vector phase includes the further development of gametes into oocysts, the production and distribution of sporozoites well as the new infection via the next blood meal.

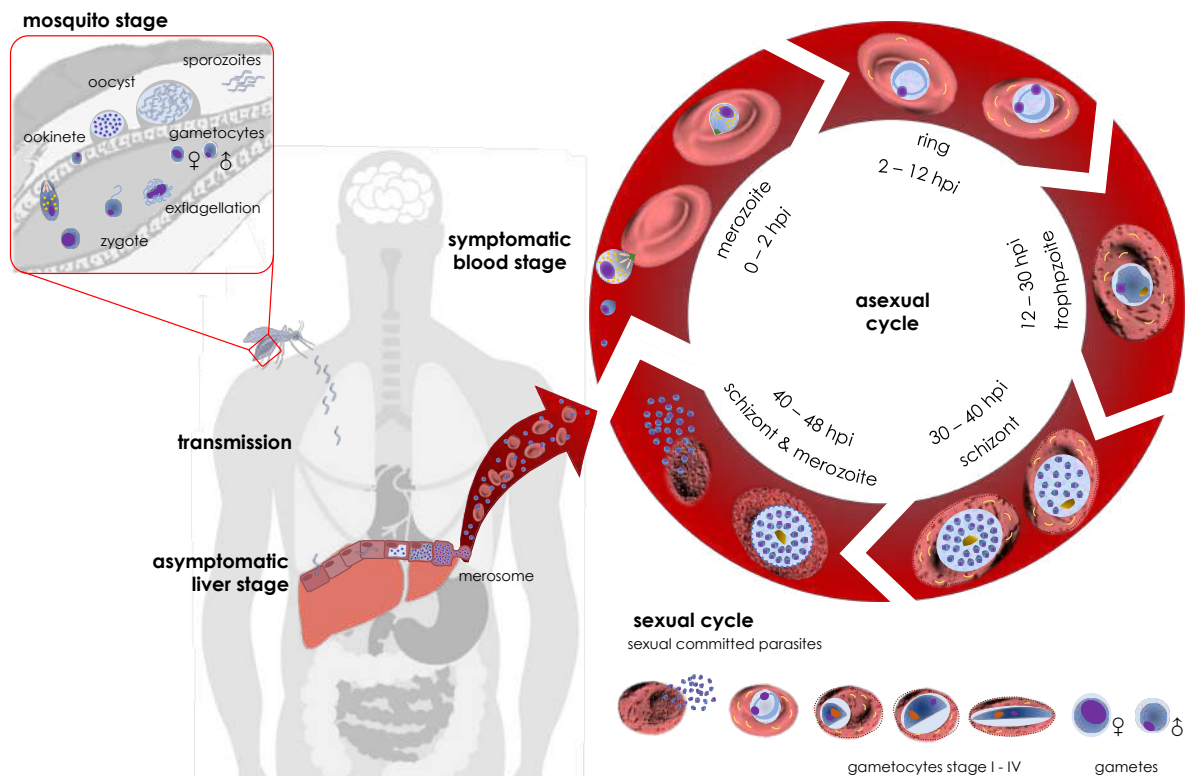


Figure 2. The lifecycle of *Plasmodium falciparum*. A female *Anopheles* mosquito transmits infectious sporozoites during a blood meal into the human host. Parasites transmigrate through the skin to a blood vessel. After reaching the liver, parasites undergo asexual mass reproduction, also called liver-schizogony. Merosomes are formed and pinched off into the blood stream, releasing 10,000 to 30,000 of infectious merozoites. During the symptomatic asexual blood stage, parasites mature from the initial merozoite form, via the ring and trophozoite stage into schizonts, containing 10 to 36 newly formed merozoites. After rupture of the infected erythrocyte, a new cycle of asexual replication takes place, about every 48 h. Some parasites develop into sexual gametocytes, ranging from stage I to V, while only the last stage can be taken up again by a mosquito. Within the insect's gut, male microgamete undergoes an exflagellation and fertilizes a female macrogamete. The zygote develops into an ookinete, transmigrates the midgut wall and matures into an oocyst, containing thousands of infectious sporozoites. After the oocyst rupture, the motile cells migrate through the whole body and can be transmitted into a human host during a blood meal via the injected salivary.

1.6.1 Pre-erythrocytic stages

During a blood meal, a female *Anopheles* mosquito transmits about 50 to 100 infectious sporozoites within her saliva intradermally into the human host, where they stay for about ten minutes. After entering a blood vessel, sporozoites circulate for a few minutes until they reach the liver.

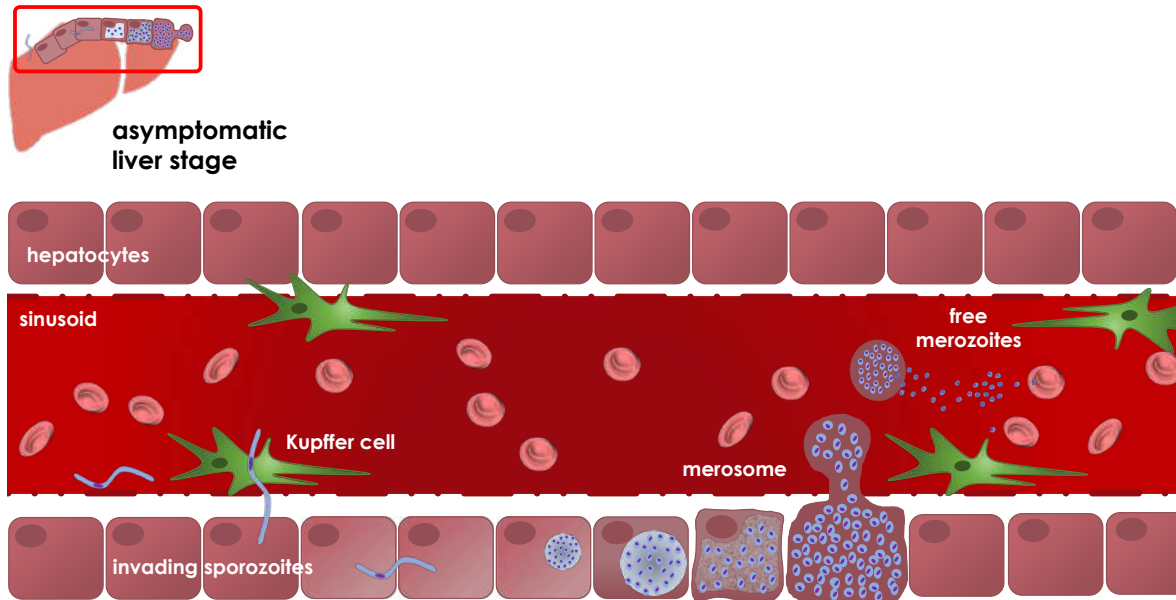


Figure 3. *P. falciparum* entering the liver phase by invasion of hepatocytes. The *P. falciparum* sporozoites migrate from the blood stream to the liver parenchyma via the sinusoidal layer of Kupffer cells. After docking to a hepatocyte, the parasites invade and traverse several liver cells in an unspecific manner. Within the liver schizont, the parasitophorous vacuole membrane degrades after asexual schizogony towards up to 30.000 infectious merozoites. The hepatocyte bulges through the endothelial layer, pumping merozoites via the connecting tube into the sinusoid, where the merozoites are pinched off. After merozoon rupture, the merozoites are free to invade erythrocytes, starting the symptomatic, asexual intraerythrocytic cycle.

Incidentally, *P. vivax* and *P. ovale* can form dormant hypnozoite stages within the liver tissue, undetectably outlasting several months to even years, while still being infectious for human and insect hosts. *P. falciparum* sporozoites migrate from the blood stream to the liver parenchyma via the sinusoidal layer of Kupffer-Cells, usually functional for filtering and degrading exogenous pollution, pathogens, injured erythrocytes and metabolites from the blood. The sporozoites docks onto a hepatocyte, infringe and traverse several liver cells in an unspecific and questionable manner.²¹⁻²⁶ During these 5 to 7 days of asymptomatic and pathogenically 'silent' extra-erythrocytic stage, the parasite undergoes asexual schizogony with in a liver schizont, producing about 10.000 to 30.000 infectious merozoites. The parasitophorous vacuole membrane (PVM) degrade and the hepatocyte pushes through the endothelial lining, pumping merozoites via a connecting tube into small vesicles, called 'merosome', subsequently pinched off by the sinusoidal blood stream. The merosome rupture and the egress of merozoites spreading the infection towards the clinical symptomatic erythrocytic phase, schematically shown in **Figure 3**.²⁷

1.6.2 Merozoite invasion

The process of merozoite invasion into erythrocytes is conserved across *Plasmodium* species, while *P. falciparum* invade erythrocytes of all ages, with a slight favor to younger cells, *P. vivax* evolved an exclusive preference in selecting reticulocytes. The characterization as Apicomplexa is due to the apical complex, present within this stage, including micronemes, rhoptries and dense granules as secretory organelles.^{28,29} The invasion process takes about 30 seconds (sec) and can be separated into 3 phases: attachment, invasion and completion, schematically shown in **Figure 4**.

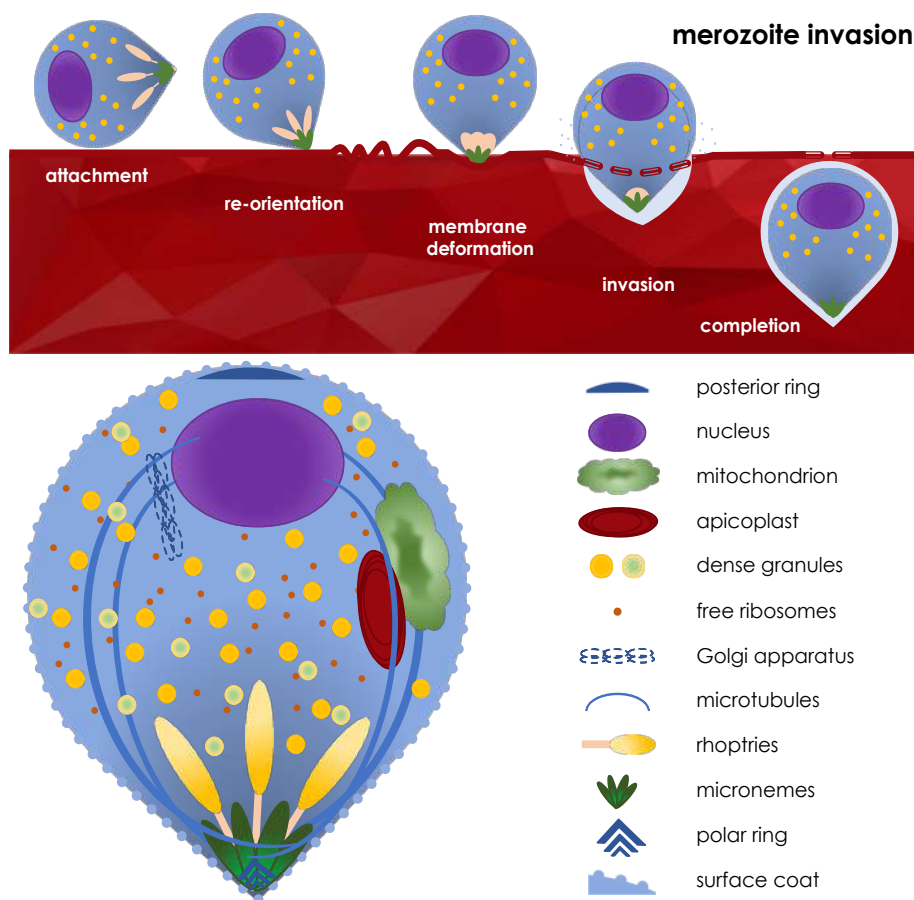


Figure 4. *P. falciparum* merozoite organization and invasion into host erythrocyte. The merozoite invades the host erythrocyte stepwise. After the attachment, the merozoite re-orientates its apical pole vertical to the host cell membrane. Via various protein interactions, released from the secretory organelles, a tight- and then moving junction is induced. Due to gliding motility, the merozoite actively invades the erythrocyte, forming the parasitophorous vacuole, while the surface coat is shed. The junction is pinches off, resealing the PV as well as the erythrocyte membrane and thus completes the invasion.

During attachment, the polar merozoite interacts reversibly at any point of the surface and re-orientates the apical end vertically towards the host erythrocyte surface. Due to tight ligand binding of merozoite surface molecules, the close contact as well as the wrapping of the erythrocytic membrane around the merozoite, the active invasion is triggered. During invasion, the content of parasite's specialized secretory organelles, called rhoptries, micronemes and dense granules are released, promoting the

formation of a ring shaped tight-junction between parasitic surface proteins and junctional host cell protein complexes, previously injected into erythrocyte membrane. The parasite actively enters the host cell, while the tight- or then moving-junction engulf the merozoite from the apical to posterior pole. Thus, the parasite's gliding motility as well as the excretion of the secretory organelles lead to the formation of the parasitophorous vacuole (PV).³⁰ During the completion step, the merozoite surface coat is shed at the moving junction by a protease or 'shedase'. The final cell entry leads to pinching off the junction, resealing and recovery of the erythrocyte and seals the membrane of the PV.

1.6.3 Ring stage

Once inside the erythrocyte, the parasite morphologically matures into the ring and early trophozoite stage; lasting for about 24 h or around half of the parasite's life cycle, shown in **Figure 5 A+B**. The parasite grows and starts to remodel the metabolic inactive host cell within its PV while the organelles are arranged on the outer edges of the spherical shaped parasite, rising the name 'ring stage'. Ring-infected erythrocyte surface proteins (RESA), released from dense granules into the PV are thought to interact with the host cell spectrin, changing the formability and stiffness as well as the probability of further infections.³⁰⁻³² The transportation of essential nutrients and waste products from the extra- or intercellular matrix is accomplished via the establishment of New Permeation Pathways (NPP) within the erythrocyte membrane and the tubulovesicular networks (TVN), reaching from the parasitophorous vacuole membrane (PVM) towards the host cell cytoplasm. Moreover, an additional highly motile membrane system called Maurer's clefts (MC) is established, which transfers cytoadhesion relevant proteins to the host cell surface and is held in place near the PVM by numerous thin holding structures, called 'tethers', presumably including membrane associated histidine rich protein 1 (MAHRP1) and skeleton binding protein 1 (SBP1). Those pathways increase the permeability of the membrane to essential molecules like sugars, amino acids, vitamins, nutrients and other low molecular weight solutes, when endogenous transport systems are not available in the host cell or fail to ensure an adequate supply.³³⁻³⁷ During the ring stage, the metabolic activity is comparatively low, while a high expression level of genes, coding for proteins, exported towards the erythrocyte membrane is detected. Therefore, the long-lasting ring stage is thought to constitute as a lag phase with growth delay, initiating host cell modifications, crucial for antigen variation, immune evasion and hence life and survival of the *Plasmodium*.³⁸⁻⁴⁰

1.6.4 Trophozoite stage

The trophozoite stage is characterized by an enormous enlargement of the parasite up to two thirds of the host cell and a peak in protein synthesis, shown in **Figure 5 C+D**. Those alterations are accompanied by a high metabolic activity due to increased processing and digestion of host cell hemoglobin for further replication via asexual schizogony. The parasite performs the essential catabolic detoxification of α -hematin, the free and toxic byproduct of the digestion, into non-toxic hemozoin (β -hematin)

crystals, within the acidic food vacuole. The final crystals are trapped by polymerization, exhibit paramagnetic properties and are visible by light microscopy as dense yellow-brownish accumulations, also called 'malaria pigment'.^{41–43} Another morphological decisive characteristic of the early and mature trophozoite stage is the abundance of numerous electron-dense knobby protrusions on the host cell membrane, called 'knobs'.⁴⁴ The onset of knob formation correlates with the emergence of PfEMP1 and other variant surface antigens (VSA) proteins at the IE surface and the induction of sequestration to endothelial cells. This important incidence enables the contact and cytoadhesion of the IE with receptors or interaction partners of other cells, antigenic variation, immune evasion and thereby safe replication possibilities and survival of the parasite.^{45–50}

1.6.5 Schizont stage

About 30 hours post infection (hpi), the parasite matures into the schizont stage, producing 8 to 32 daughter merozoites due to asexual schizogony. During multiple rounds of asynchronous and closed mitosis, the nucleus is pinched off while the nucleus membrane stays intact. The dark, hemozoin filled food vacuole is located in the middle while the newly formed merozoites are arranged circular around the malaria pigment over time, shown in **Figure 5 E+F**. The PMV is dissolved and merozoites are free within the intact erythrocyte. They activate their motility system, further deforming and swelling of the erythrocyte takes place, followed by the disruption of the host cell cytoskeleton and the plasma membrane, ensued by merozoite's active exit of the host cell. The clinical symptoms are mainly caused by the abrupt lysis and explosive rupture of the schizont, erythrocytic destruction and the subsequent egress of invasive merozoites as well as the accumulated waste products and the cellular remains.^{51,52} Released merozoites float within the blood stream for approximately 60 seconds prior to invading new erythrocytes.^{53,54}

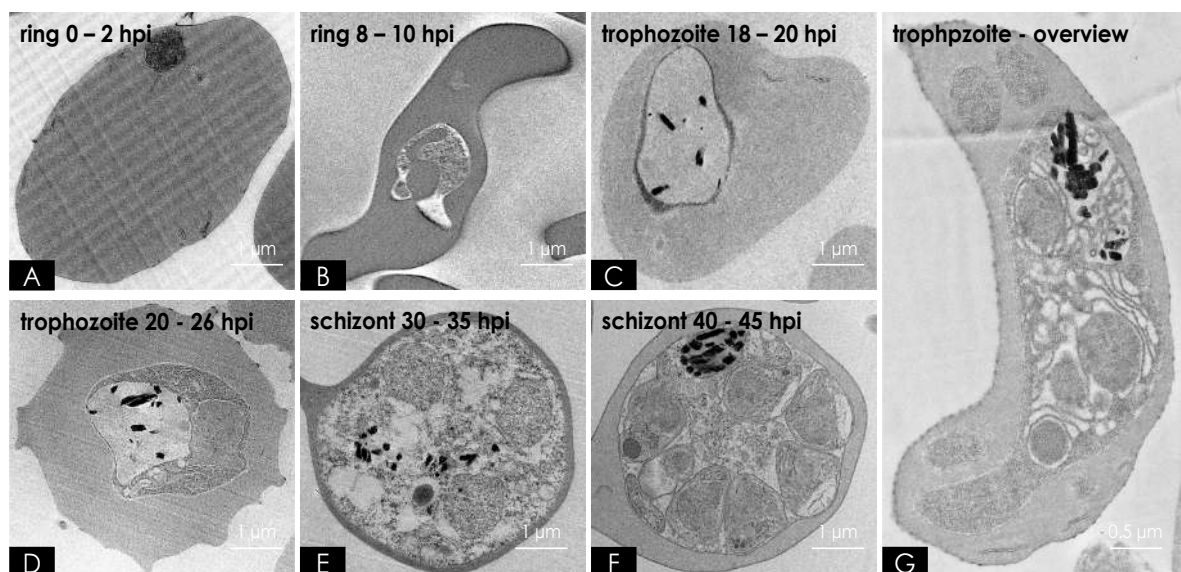


Figure 5. Transmission electron microscopy of *P. falciparum* intraerythrocytic blood stages. The different *P. falciparum* intraerythrocytic blood stages are shown as TEM pictures. **A** shows an early parasite, shortly after invading an erythrocyte, about 0 to 2 hpi. The MC network is visible near the parasite itself and near the cell membrane. **B** shows a young ring staged parasite,

about 8 to 10 hpi, just about to ingest hemozoin via engulfment. Two nuclei are visible at the very left edge, while all other organelles are organized in a ring-shaped manner around the just being formed food vacuole. **C** shows a young trophozoite staged parasite, about 18 to 20 hpi, with an enlarged food vacuole, containing some hemozoin crystals. The MC network is visible in the erythrocytic cytosol. **D** shows a mature trophozoite staged parasite, about 20 to 26 hpi, while the organelles and the multilayer membrane system is visible around the food vacuole. Also knob structures are detected on the surface as electron dense protrusions, visible as black spots. **E** shows a mature schizont staged parasite, about 30 to 35 hpi, while the whole erythrocyte is filled with the parasite. The structures of the newly formed merozoites are already apparent. **F** shows mature merozoites within an intact schizont, about 40 to 45 hpi. The merozoites arrange in a circular manner and the multilayers of each new parasite are visible, while the hemozoin crystals are condensed at the edge. **G** shows an overview of the organelles and membrane system within a trophozoite staged parasite. The knob structure, completely covering the whole erythrocytic membrane, the meshwork of membranes, various Maurer's clefts as well as the vacuoles and organelles are clearly detectable. All pictures were individually taken with FEI Tecnai Spirit TEM at a 14000x magnification. The scale bar for A to F is 1 μm ; for G is 0.5 μm .

1.6.6 Gametocyte stage

During the blood stage, some intraerythrocytic parasites develop into gendered gamete precursors, the so-called gametocytes, able to start the sexual phase of the life cycle after the very first round of asexual replication.⁵⁵ The gametocyte development can be divided into the 5 distinct stages I to V, morphological distinguishable within Giemsa-stained thin blood smears, while the chromatin appears in a single mass within macrogametes (♀), it is spread in a diffuse manner within microgametes (♂), shown in **Figure 2**.^{56,57} Moreover, stage I to IV gametocytes can sequester apart from the peripheral circulation, likewise mature asexual staged parasites. Albeit the particular mechanisms to trigger gametogenesis are yet unknown, some circumstances are known. Thus, the commitment towards sexual differentiation is already set within the asexual stage of the previous generation, while the triggers include ongoing changes in hematocrit levels, temperature and pH values, high asexual parasitemia and antimalarial drug uptake, artificial interferences, such as addition of erythrocytic lysates, mammalian hormones as well as a high number of reticulocytes. As the specific genes for gametogenesis are spread over all chromosomes, all genetic information of gamete development is available within one haploid genome.^{58,59}

1.6.7 Mosquito phase

The female and male gametocytes are ingested by a female *Anopheles* mosquito during the blood meal and develop into gametes. Within only 1 h, the male haploid gamete undergoes exflagellation, then being able to fertilize haploid macrogametes. The further developed diploid and mobile zygote and then ookinete traverses the mosquito's midgut wall to form an oocyst, producing thousands of active, haploid sporozoites. The diploid stages ensure frequently genetic exchange and generation of new genetic combinations. After 10 to 14 days, sporozoites are released into the cavity of the mosquito, migrate through the whole body and are able to be transmitted to a

human host during a blood meal via infectious saliva, causing *Plasmodium* infection.^{51,60,61}

1.7 Semi-immunity, immune evasion, antigenic variation and cytoadhesion

Within holoendemic areas, severe clinical manifestations of *falciparum* malaria mainly occur in children under the age of 5 or in people with little or no immunity and pregnant women in all groups of age. However, older children and adults in malaria endemic areas can archive a clinical semi-immunity due to numerous repeated infections with *P. falciparum*, while a sufficient acquisition takes about 4 years. This semi-immunity can reduce the risk of developing severe clinical symptoms and a serious course of the disease, while still allowing asymptomatic infections not affecting the endemic burden in general.⁶² The reason for the just slowly developing immunity are different immune evasion strategies and the 'antigenic variation' of the malaria pathogen.

Among others, the particular set of surfaces expressed, parasitic PfEMP1 proteins, mostly organized and clustered on knob structures, are described to mediate adhesion to various endothelial receptors within the lining of the microvasculature of the human host. Due to this cytoadhesion, also called 'sequestration', the parasite is able to escape the passage and clearance through the spleen and the local pitting of IE, as well as the detection and elimination of old, deformed or stiff erythrocytes. Only non-sequestering infected erythrocytes with young ring staged or stage V gametocytes are detectable in the peripheral blood.⁶³⁻⁷¹ Other forms of cytoadherence include the formation of rosettes with uninfected erythrocytes, also called 'rosetting', the spontaneous binding of IE to non-IE, providing a parasitic growth advantage or establishing a favorable environment for newly released and invading merozoites or immune evasion.^{72,73} Also, IE can bind to other infected erythrocytes with the help of platelets, termed as 'platelet mediated clumping' or 'autoagglutination' or the interaction with immune cells, schematically shown in **Figure 6**.^{18,74,75} Furthermore, adhesion to dendritic cells inhibits the maturation of these antigen-presenting cells and thus modulates the immune response of the host.⁷⁶⁻⁷⁸ The process of 'antigenic variation' allows the parasite to successively present alternative forms of an antigen to the surface of its host cells, enabling the constant change of the parasitic phenotype and therefore masking from the recognition by host immune cells. Those variant surface antigens (VSA) are proteins, coded by individualized multigene families within each parasitic genome, putatively exhibiting adhesive properties, crucial for immune evasion and sequestration.⁷⁹⁻⁸¹



Figure 6. Forms of cytoadhesion of *P. falciparum* IE. Mainly, 3 different forms of cytoadhesion occur in the human vasculature, mediated by *P. falciparum* IE. Rosetting: IE can bind non-IE, forming clots at the endothelial lining or free within the blood flow of the capillaries. Sequestration: IE bind to the endothelial cells, mediated by an interaction with host receptors or surface structures anywhere in the vasculature. Platelet mediated clumping: IE are accumulated, while the clumping is mediated by human platelets. Cytoadhesion can lead to mechanical obstructions of the blood flow, activation of the vascular endothelium, release of cytokines and inflammation, potentially resulting in endothelial activation and dysfunction, cell death, derangements, mitochondrial and organ dysfunctions.

1.8 Sequestration

Sequestration is a particular form of cytoadhesion and unique in *P. falciparum*, while the existence in *P. vivax* infected hosts is probable, but still discussed. Furthermore, some non-human primate infecting parasites, namely *P. berghei* and *P. chabaudi*, do sequester even without having knobs of PfEMP1-type proteins. While the just infected erythrocytes, early, mid-ring, and most of mature ring staged IE still circulating within the human blood system, trophozoites and schizonts can sequester to endothelial cell receptors or structures within the vascular linings of capillary vessels. Sequestration is thought to be resembling the leucocyte recruiting process, divided in 3 major steps of tethering, rolling and firm adhesion. The IE circulating in human vasculature, driven by the physiological flow conditions and thereby passing matching receptors on endothelial cells. Weak binding interactions slow down the IE within the blood stream indicating the initial tethering, followed by rolling and flipping of mature staged IE above the endothelial cell layer.⁸²⁻⁸⁴ Either weak and firm binding induce signal cascades within the host endothelial cells, resulting in a transformation and remodeling of the cytoskeleton and the surface composition, including the rise of adhesins and other cytoadhesion related proteins.⁸⁵ On the protein level, PfEMP1 are thought to act as the major key player within the sequestration process. Due to an increased research interest in the different forms of cytoadhesion, also other multigene families become increasingly important.

1.9 Secretory pathways & protein transport

Since *P. falciparum* cannot rely on a host cell transport system, the parasite needs to establish its own protein transport network. The *P. falciparum* 'exportome' comprise about 400 proteins, that is 5 to 10 times larger than described in other *Plasmodium* species. About 8% of all genes are defined by the presence of a short amino acid sequence, localized about 20 amino acids downstream of the signal peptide, called *Plasmodium* export element (PEXEL) or vacuolar transport signal (VTS). Exported proteins pass through various membranous structures including the parasite endoplasmic reticulum (ER), parasite plasma membrane (PPM), PVM, MC and finally the IE plasma membrane. The transport of soluble or membrane proteins is thought to start co-translational with the insertion into the lumen or the membrane of the ER, respectively. Here, the PEXEL signal is recognized and proteolytically cleaved by the ER residing Plasmepsin V protease N-acetylated subsequently. However, a smaller number of proteins, including e.g. SBP1 and MHARP1, is also transported via the same routes, despite lacking an identifiable motif and therefore termed PNEP (PEXEL negative exported proteins). The predicted secretory pathway of *Plasmodium* proteins is schematically shown in **Figure 7**. Subsequently, the processed proteins are probably transported by vesicles into the PPM. Here, soluble proteins fuse to the membrane and are released immediately into the PV, while transmembrane proteins are integrated into the PVM and need to be extracted again, prior to further transport. The trafficking via the PVM into the erythrocytic cytosol could take place via the translocon PTEX proteins, whereby chaperones unfold the proteins. The unfolded proteins could form a protein transport aggregate (PTA), together with parasitic HSP40 (heat shock protein) and erythrocytic HSP70 chaperones, perhaps in association with J- or K-dots, heading to further host cell structures. Finally, the MC as well as the continuous membrane transport network, seem to play a decisive role in sorting and exporting the proteins to their final destination. While soluble proteins are eventually trafficked via diffusion and interaction, the export of transmembrane proteins from MC towards the IE surface seem to be achieved due to electron dense vesicles via thin tethers or actin stands forming the bracket between MC and erythrocyte membrane.⁸⁶⁻⁹³

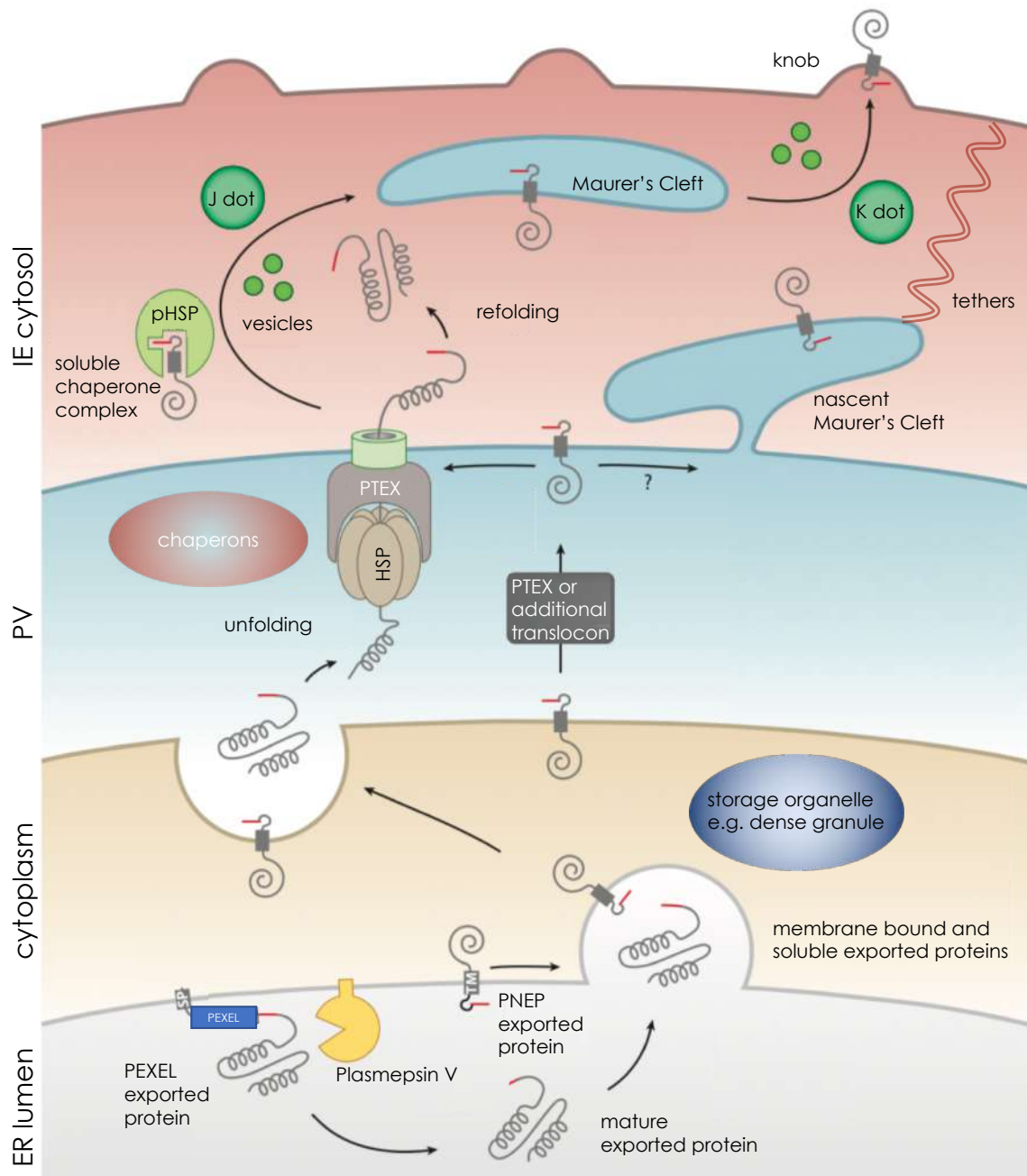


Figure 7. Schematic overview of the protein export in *P. falciparum*. Within the parasite, PEXEL positive proteins are cleaved by the Plasmepsin V kinase, residing in the ER lumen. Mature PEXEL and PNEP proteins are transported via the ER membrane, while for TM containing proteins need to be extracted. Within the parasitic cytoplasm, proteins can be stored or further transported directly, e.g. via PTEX or other translocons. Chaperons, HSP and folding-associated proteins assist the further processing via the PV into the IE cytosol. The parasitic proteins can be transported towards the IE membrane and into knob structures within soluble chaperone complexes, vesicles, J- or K-dots, freely, via diffusion or distributed by Maurer's Clefts and tether structures. Based on Spillmann, 2015.⁹⁴

> Taken together, 3 defined signals are necessary for the transport, including a N-terminal signal sequence for entry into the secretory pathway, a PEXEL(-like) signal for transport across the PVM and, where required, a TM domain for insertion into membrane structures. Eventually, the transport of parasitic proteins is an encompassing and complex process, even studied in detail, many distinct subjects still remain elusive.

1.10 Selected multigene families

For *P. falciparum*, some multigene families have been described so far on gene and protein level: *var*/PfEMP1 (gene: variant gene family/protein: PfEMP1), *rif*/RIFIN (gene: repetitive interspersed family/protein: RIFIN), *stevor* (gene: subtelomeric variable open reading frame/protein: STEVOR), *pfmc-2tm* (gene: *Plasmodium falciparum* maurer's cleft – two transmembrane domains/protein: PfMC-2TM), *surf* (gene: surface-associated interspersed genes/protein: SURFIN).^{29,92,95–101} Those surface proteins are encoded by multigene families that are groups of homologous genes, though to perform similar functions. The genes cluster together in the subtelomeric or central regions of all 14 parasitic chromosomes, as they are spread in the whole genome, it is believed that the proteins play an important role in the survival of the parasite within the human host and therefore in its pathogenicity.¹⁰² While the interaction assigned to the binding process of IE to endothelial cells is considered to be proven for PfEMP1 proteins, this is so far not excluded for the proteins of the other multigene families. **Figure 8** shows the predicted gene organization (A) as well as the assumed topology (B) of the proteins. Similar trafficking routes and localization in different stages of the parasitic asexual blood stages, as well as two time-shifted expression peaks indicate distinct biological functions for members of the same multigene family.^{87,92,97,100,103–105}

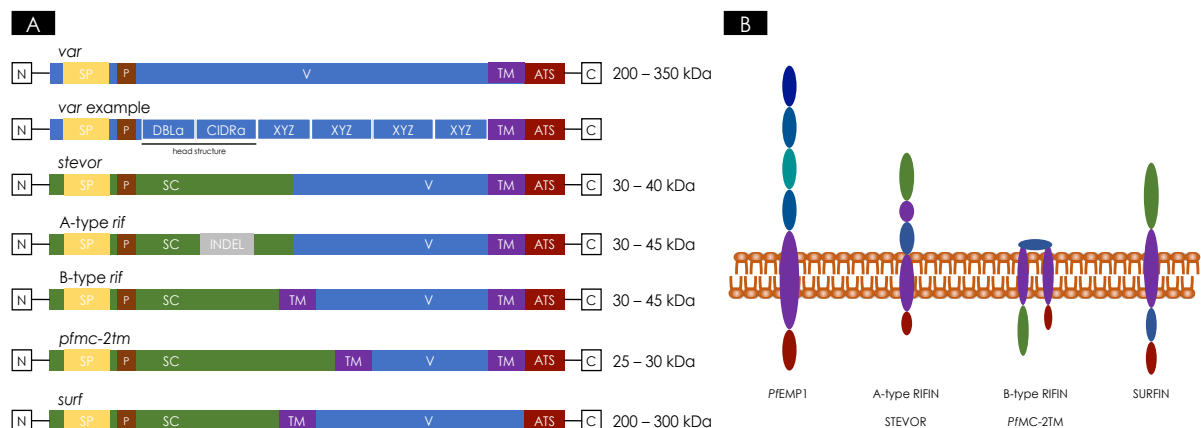


Figure 8. Predicted gene organization and assumed topology of VSA members. In section **A** the predicted gene architecture for *var*, *stevor*, *rifin* (a- and B-type), *pfmc-2tm* and *surf* genes are shown schematically. SP: signal peptide; P: PEXEL: protein export element; SC: semi-conserved region; V: variable region; XYZ: various DBL and CIDR domains or combinations; TM: transmembrane domain; ATS: acidic terminal segment; C: C-terminal segment. Section **B** shows the assumed topology of the corresponding proteins.

1.10.1 The *var* multigene family

The well characterized *P. falciparum var* (variant surface antigen) multigene family consists of about 60 genes per haploid parasite genome, while each of the 200 to 350 kDa gene is constructed by two exons, separated by one intron.^{102,106–110} The first exon encodes a PEXEL marking the protein for intracellular and transmembrane transports towards the host cell surface; the variable extracellular region (V),

containing a various number of Duffy binding like (DBL) and cysteine rich interdomain region (CIDR) domains, including a short N-terminal segment (NTS) and a transmembrane domain (TM), anchoring the proteins on lipid rafts within the host cell membrane. The intron separates the two exons and contains a promotor sequence that, in combination with the 5' upstream promotor sequence (ups), is thought to be necessary for *var* gene silencing within mutually exclusive gene expression. The second exon contains the conserved cytoplasmic domain, including the acidic terminal segment (ATS). This *var* gene organization is conserved across isolates.^{111,112} Although the *var* gene repertoire is highly divergent, most *PfEMP1* proteins can be divided by similarities within their 5' upstream promotor sequence localization and transcriptional direction within the chromosome, resulting in a classification of 4 distinct groups: upsA, upsB, upsC and upsE.^{112–115} Each *PfEMP1* consist of a N-terminal, semi-conserved head structure of two definite protein domains (DBLa and CIDRa) but can also imply up to 9 DBL and CIDR domains, arranged in a particular manner. The so-called 'domain cassettes' (DC) are thought to be decisive for the actual and individual binding phenotype. Group A and B/A *PfEMP1* restrictively include DC8 and DC13 that are thought to be the predominant cause of clinical symptoms. Both, DC8, DC13, as well as a subset of other group A *PfEMP1* proteins are strongly selected on human brain vascularity and highly expressed in children with SM or CM.⁶

1.10.2 Other multigene families: *rif*, *stevor*, *pfmc-2tm*, *surf*, *phist*

The largest multigene family of *P. falciparum* is the *rif* (repetitive interspersed family) family, while the 30 to 45 kDa proteins mostly appearing about 16 to 20 hpi, coherently with *PfEMP1*. Due to the presence or absence of a 25 amino acid peptide in the coding sequence of the second exon, most of the RIFIN proteins are divided into subgroups A- and B-type.⁸⁷ While A-type RIFIN are localized within the MC of the IE as well as in the erythrocytic membrane, B-type RIFIN are predominantly detected in the cytosol of the host cell. The *stevor* (subtelomeric variant open reading frame) multigene family transcription peaks in mid trophozoite stage, and within the merozoite stage, while STEVOR are colocalized on the surface with MSP1 (merozoite surface protein 1) throughout the invasion process.¹⁰⁰ The overall structural organization of the highly conserved gene family is very similar to that of A-type RIFIN proteins. The members of the *rif* and *stevor* gene family could be detected in both sexual and asexual stages as well as in extracellular stages such as merozoites and sporozoites, whereby the *rif* gene expression emerging a little earlier in the parasitic maturation process.^{105,116–118} As the function of *rif* and *stevor* family members are not clearly identified, the binding abilities towards erythrocytic glycophorin (GYP) A and C, their higher detection frequency on ex vivo IE, compared to long term cultivated *Plasmodium* isolates as well as a recent study of a splenectomized patient, indicate a strong dependency between the A-type RIFIN and STEVOR proteins with sequestration, antigenic variation, erythrocytic deformability and invasion, rosetting and immune evasion.^{87,100,104,105,118–120}

The *pfmc-2tm* (*Plasmodium falciparum* Maurer's cleft – two transmembrane domains) multigene family produced small proteins of about 25 kDa with a similar topology as B-type RIFIN.¹⁰² Additionally, the localization was mostly termed to the MC transport

system, to the erythrocytic membrane of the host cell as well as to the apical tip of newly formed merozoites within schizont staged IE and just uncertainly to the knob structures.^{87,101,105,121} However, it has been shown that members of this family also undergo switching and the highly polymorphic stretch between the two TM domains is thought to generate antigenic variation, though not necessarily in relation with immune evasion and sequestration. Furthermore, sequence similarities and comparable annotation raise suspicions of related characteristics with *P. falciparum* gametocyte-exported proteins.^{87,105,122,123}

The *surf* (surface-associated interspersed proteins) multigene family is localized in the subtelomeric regions of only 5 chromosomes. The gene structure consists of 3 exons, while the first is thought to carry a PNEP (PEXEL negative exported protein) or modified PEXEL motif, marking the proteins to be transported through the ER of the host cell.^{89,124} They are described to be conserved across and outside of human pathogen malaria parasites and not mutually exclusively transcribed. Within hierarchical clustering, they troop together with *var*, some DBL containing and MSP3 genes, while sharing structural and sequence similarities with the firsts. Even this gene family is not extensively investigated, at least, 2 members were focused on: SURFIN4.1 (PFIT_0400900), present in mid-trophozoite, early schizont and merozoite staged parasites, while yet being detected on IE surface. SURFIN4.2 (PFIT_0422600) is expressed within the merozoite apical tip, co-localized with STEVOR proteins, as well as co-transported with PfEMP1 and RIFIN towards the surface of IE.^{72,124-128}

The *phist* (*Plasmodium* helical interspersed subtelomeric) multigene family is defined by the presence of a conserved 150 amino acid domain, containing 4 consecutive alpha helices, unique in sequence and predicted structure, producing exported PHIST proteins of unclear function. The genes can be further sub grouped into *phist-a*, *phist-b* and *phist-c* and are described to be conserved across human, rodent and avian affecting *Plasmodium* species. So far, some PHIST, or PHIST domain containing proteins, are described to play a role in knob formation, alteration of IE membrane integrity and sequestration by interaction with PfEMP1, MC residing SBP1 or protein4.1.

> Taken together, the members of the multigene families are localized in chromosomal areas characterized by a high rate of recombination events, exhibit a large number of over 200 genes and contain variable regions, likely to be involved in antigenic variation and immune evasion processes. The 2 peaks of expression during different stages of development for most of the members, strongly indicate distinct, or at least dual, biological functions for the proteins during the course of malaria infection, mainly including the merozoite invasion process and cytoadhesion. Nonetheless, the identification of the exact biological role remains elusive.

1.11 Genomic organization, mutual exclusivity & var gene switching

Each chromosome contains 1 to 3 of the totals of about 60 *var* genes, clustered together with groups of *rif*, *stevor*, *pfmc-2tm*, *surfin* and other gene families, such as *etramp* (early transcribed membrane protein), *phist* (*Plasmodium* helical interspersed

subtelomeric protein), *clag* (cytoadherence-linked asexual protein) and *fikk* (serine-threonine kinase), arranged in the core, near the periphery. The *var* gene expression takes place at 3 to 18 hpi, while the *PfEMP1* proteins are detectable on the IE surface at 16 hpi. The transcription mechanism, when only one single *PfEMP1* type is expressed on the surface of the host cell at a time, and the remaining *var* genes appear in a silent state, is called 'mutual exclusivity', schematically shown in **Figure 9**. This is evident in the case for *PfEMP1*, while for RIFIN and STEVOR proteins, it is clear that several gene variants can be expressed at the same time within the same cell, and therefore do not fulfill the conditions for a mutually exclusive expression pattern.^{72,129}

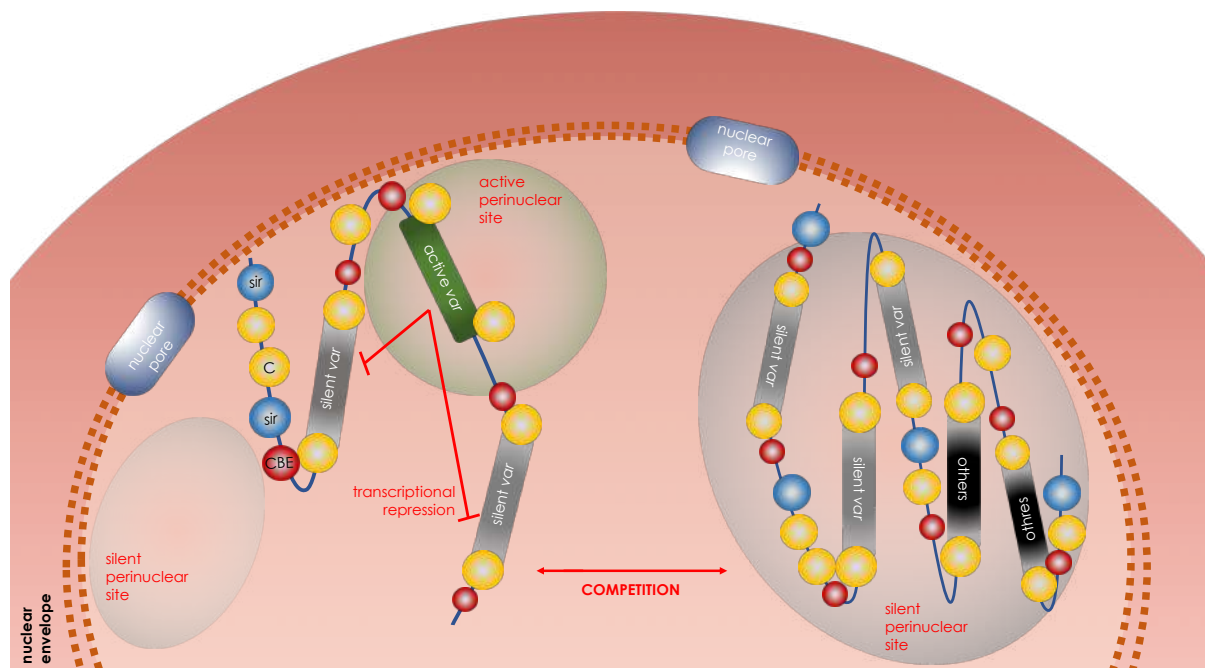


Figure 9. Schema of the mutual exclusivity transcription system of *var* genes. The model for the mutually exclusive transcription of *var* genes comprises silent and active perinuclear sites, within the parasite's nucleus. An active *var* gene resides within an active cluster, while the activation can be either induced by activation due to molecular factors, maybe in correlation with a positional movement, or by moving away from silencing effects of the nuclear periphery, or by dissociation from other, interfering *var* clusters. The activation suggests an involvement of chromatin structures (C) and sirtuin proteins (sir) or a looping out of the respective gene. An activated *var* gene, located in the active site inhibit the expression of other *var* genes, as they remain in a silent state, while a competition of the perinuclear sites is likely. This model does not explain how adjacent *var* genes on the same chromosome are differentially activated, but an attractive possibility is that chromatin barrier elements (CBE) interact with nuclear pores to maintain distinct chromatin states for neighboring genes.

The actual phenotype determines the antigenic variation as well as the virulence of the parasitized IE and is stably inherited through successive cell cycles, avoiding premature expenditure of the whole *var* gene repertoire. Due to histone methylation and deacetylation, another, different *var* gene can be expressed by a mechanism, called 'switching' during the course of infection, ensuring the antigenic variation, immune evasion and thus the parasite survival over an ongoing course of (chronic) malaria infection.^{130,131} For example, it has recently been shown that each successive

parasite generation is able to express another *var* gene, making it almost impossible for the immune system to recognize and combat infected cells.¹¹⁸ Furthermore, gene recombination between *var* genes and paralogs support the extreme diversity in the variant antigen repertoire. The underlying procedures of both mechanisms, mutual exclusively transcription and switching of *var* genes, could be controlled epigenetically but until now, they are not yet fully understood.^{49,113,132–136}

1.12 Knob structure

Knobs are cup shaped protrusions, appearing about 16 hpi on the IE surface with a diameter of about 50 to 150 nm and a height of about 50 nm, schematically shown in **Figure 10A**. Erythrocytic proteins include the main players of the cytoskeleton construction such as spectrin, actin and ankyrin, forming a two-dimensional meshwork of hexagonal structures below the cell membrane. GYPC, in association with protein4.1 as well as protein Band3 in combination with protein4.2 and Rhesus-associated glycoproteins, maintain the erythrocytic shape, preserve the cellular flexibility and vertically connect the membrane skeleton with the overlaying plasma membrane. Many parasitic proteins are evidenced to affect knob formation, erythrocytic rigidity and the capability of cytoadhesion, while only a few are studied in detail. The main actor of knob formation is the essential and self-assembling protein KHARP, directly interacting with actin and spectrin. It can bind N- and C-terminally to the cytoplasmic ATS region *PfEMP1*. Furthermore, *PfEMP3* also binds spectrin and is involved in *PfEMP1* trafficking and increasing the cell rigidity, thus altering the membrane deformability within mature staged IE. *MESA/PfEMP2* interacts with protein4.1, complexing with GYPC. *RESA* is described to contain a DnaJ domain binding spectrin to stabilize the host cell membrane, prevent subsequent invasions of already hosted IE and avoid thermal damages due to elevated body temperatures during the course of infection. The cluster of DnaJ proteins translocate via J-dots, which are implicated in the regulation of HSP, general protein folding, assembly and disassembly of higher order protein structures as well as thought to play a key role in knob formation. Moreover, phosphorylation status and thus general or parasite-favoring functions are maintained and controlled by the serine/threonine protein kinases FIKK, exported via K-dots towards the membrane-associated host cell region.^{40,47,137} Furthermore, the *CLAG* (cytoadherence linked asexual gene) family is released by rhoptries during invasion but is also located within the IE membrane, within or close to the knob structure and is, at least partly, responsible for *PfEMP1* trafficking and cytoadhesion.^{94,126,138–140} The tracing of the knob structures in 3D, schematically shown in **Figure 10 B+C**, revealed a conical spiral filament underlying each knob protrusion, turning counterclockwise when viewed from the intracellular matrix and could imply parasitic vacuolar sorting proteins.

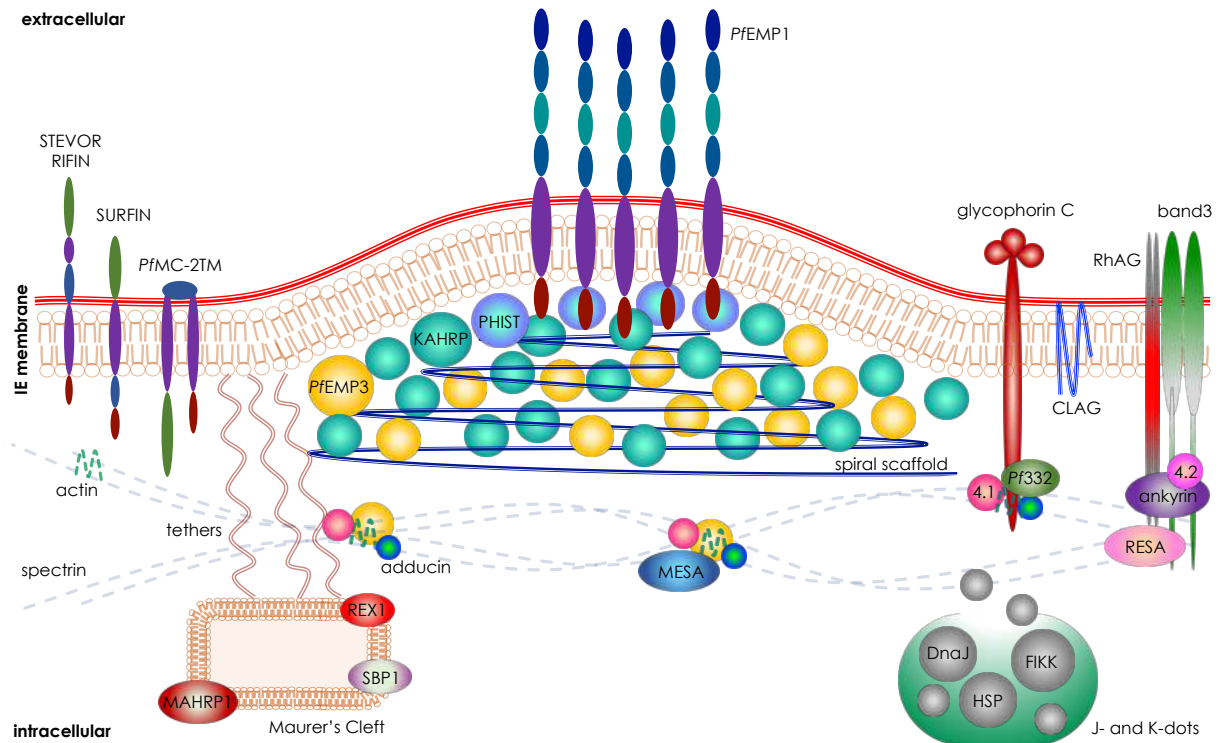


Figure 10. Knob structure of *P. falciparum* infected erythrocyte and involved proteins. Knobs are cone like structures appearing about 16 hpi on the surface of IE. Erythrocytic proteins include mainly spectrin, actin and ankyrin as cytoskeleton-builder, as well as band3, protein4.1 and 4.2, GYPC, RhAG, and others. Main player on the parasitic side are KAHRP, PfEMP3, PHISTs, PfEMP2/MESA and the spiral scaffold, influencing the shape and rigidity. PfEMP1 proteins are cluster wise arranged either on the tip of a knob or as patches spread across the IE membrane. While STEVOR, RIFIN, PfMC-2TM, CLAG and other proteins are located at the IE membrane, MAHRP1, SBP1 or REX1 are MC residing at the MC, while MC are held in place by tether structures. DnaJ, FIKK, HSP and other transported proteins are shifted via J- or K-dots or in a vesicle(-like) manner.

However, not every IE display knob structure on its surface, as knobless *Plasmodium* isolates can occur either due to KAHRP or PfEMP3-deletions, during artificial long-term cultivation or via so far unknown reasons; albeit, a knobby phenotype can be restored. Even though the amount of PfEMP1 on knobless IE is reduced by about 50%, the overall distribution of adhesins appears unaltered. Nevertheless, knobless IE are also able to cytoadhere, albeit in a considerable attenuated manner, under both, static and flow conditions.^{57,141,142} It is conceivable that the presentation and organization of specific PfEMP1 variants on host cell surface depends on distinct *var* and knob-related gene expression profiles and thereby ensuring optimal host receptor affinity.^{139,143,144}

1.13 Human receptors, involved in *P. falciparum* malaria

So far, various human endothelial receptors or cell surface structures and molecules are known to interact with *P. falciparum* IE, albeit for only a few, PfEMP1 is described as the interacting partner on the parasitic side.

1.13.1 CD36

CD36 is a glycosylated integrated membrane protein of about 50 to 90 kDa, also called platelet glycoprotein IV. CD36 is present on numerous vertebrate's tissues like liver, muscles, small blood vessels, while only barely detectable within the brain. Ligands are various and include thrombospondin, fibronectin, collagen as well as (bacterial) lipoproteins. The interaction induced formation of CD36 clusters, internalization of receptor-ligand-complexes and therefore initiating intracellular signaling. The promotion of proinflammatory host immune response is induced by CD36 function as co-receptor for TLR4:TLR6 heterodimer and therefore leading to NFκB dependent production of cytokines. CD36 plays a major role in malaria infection, as within nearly all field isolates and most of culture isolates, 80% of known *PfEMP1* proteins carry a CD36-binding domain. Albeit, CD36 is clearly involved in firm cytoadhesion, sequestration, and rosetting and thus trigger disease symptoms, a correlation with severity of malaria outcome could not be undoubtedly assigned so far.¹⁴⁵⁻¹⁴⁹

1.13.2 Chondroitin sulfate A (CSA)

Chondroitin sulfate A (CSA) or chondroitin-4-sulfate is an extracellular membrane protein of the group glycosaminoglycans, present on a variety of cell types, especially of the brain and the placenta. Regarding malaria disease, CSA is predominantly related to pregnancy associated malaria, while expressed on syncytiotrophoblasts in the placenta, inducing it induces a firm adhesion of *P. falciparum* IE, mostly resulting in onset of malaria symptoms, both, affecting the mother and the child. Some recent investigations raise the thought that even though CSA is highly expressed on endothelial cells of various organs such as the brain, liver, lung and skin, CSA could also be involved in the clinical picture of SM and CM, yet proven evidences and correlations are still missing.¹⁵⁰⁻¹⁵³

1.13.3 Cellular adhesion molecules

> ICAM-1, VCAM1, PECAM-1, CD44 (H-CAM) and NCAM

ICAM-1, also called CD54 or intracellular adhesion molecule 1, is a single-pass transmembrane glycoprotein slightly but ubiquitously expressed on membranes of endothelial and immune cells, while a highly upregulation is induced by inflammation signals like IL6, IL1, TNFα or NFκB. VCAM1, CD106 or vascular cell adhesion molecule 1 is mainly expressed within the vascularity and on cytokine stimulated endothelial cells. ICAM-1 and VCAM1 mediate leucocyte adhesion and migration via interaction with integrins, a process thought to share many similarities with IE sequestration. In post mortem brain studies of CM patients, a co-localization of ICAM-1, VCAM1 and CD62-E together with IE within cerebral tissue was observed, while also IE of several field isolates inclined to preferentially bind to ICAM-1. Furthermore, capillaries with a higher level of ICAM-1 also have elevated levels of sequestered IE in SM patients, compared to UM malaria patients. However, a mutual correlation between ICAM-1 binding and SM or CM has not been unambiguously proven.^{148,154-160}

It should also be noted that platelet endothelial cell adhesion molecule 1, also called PECAM-1 or CD31, is likely involved in angiogenesis, integrin activation and also leucocyte recruitment and transmigration. It is of major importance in endothelium-to-endothelium interaction and can be found concentrated in cell-junctions, while being directed to the cell surface by inflammatory cytokines. Moreover, PECAM-1 is clearly stated as *P. falciparum* IE binding receptor on vascular endothelia with a pathological influence on rosetting and isolates from CM patients.¹⁶¹ The adhesion transmembrane protein CD44, or H-CAM, is characterized by alternative RNA splicing, resulting in multiple expressed isoforms and post-translational modifications. It is expressed on some endothelial cells, including the white matter of cerebral tissues, on all blood cells, except platelets, and mediate binding to hyaluronate. CD44 has a defined role in neutrophil attachment to endothelial cells, join a potential part in the attachment of hematopoietic stem cells to the stroma and is highly expressed in human carcinomas, indicating a likelihood of tumor progression. Regarding malaria disease, CD44 expressed on erythrocytes is decisive for *P. falciparum* merozoite of all strains, regarding attachment and invasion, as a deficiency in CD44 result in a significant reduction of parasitemia.¹⁶²⁻¹⁶⁵ The neural cell adhesion molecule, CD56, or NCAM is mainly expressed on the cerebellum and cerebral cortex, while mediating homophilic adhesion of neuronal cells. Furthermore, it is expressed on some immune cells and bone marrow residing macrophages, while lacking an expression on plasma cells. The non-polysialylated form, present on the surface of micro vessels, was determined as a receptor for *P. falciparum* IE sequestration.^{162,166}

1.13.4 Selectins

> CD62-E and CD62-P

The selectins family consist of 3 members: CD62-E (E-selectin), CD62-P (P-selectin) and CD62-L (L-selectin), while all share a conserved structure of a N-terminal lectin domain and an epidermal growth factor domain, followed by numerous short consensus repeats, a TM and a C-terminal cytoplasmic domain. Selectins mediate the initial steps (initial contact and rolling) of the leucocyte adhesion cascade on the endothelium. CD62-P is present on platelets, thrombocytes and endothelial cells, while it is stored in the cells after expression and presented to the cell surface after activation from granules in the platelets and from Weibel-Palade bodies within the endothelial cells. Whereas CD62-E is *de novo* synthesized after cellular activation.^{159,167-171} Therefore, an increased count of CD62-E and CD62-P is found on inflammation activated endothelial cells, CD62-L is constitutively expressed and active on leucocytes. Regarding malaria disease, CD62-P was described as IE receptor, while later PfEMP1 was termed as the interacting ligand. In the animal model of *P. berghei* ANKA infected mice, CD62-P deficiency on endothelial cells was described to protect from CM. Even selectins are barely expressed on healthy human brain endothelial cells. Previous investigation on elevated serum levels in SM patients and brain tissues of CM patients rose the possibility that also CD62-E could serve as receptor for IE.¹⁷²⁻¹⁷⁵ In patients with sickle cell anemia, due to vascular dysfunction and damage, circulating endothelial cells were predominantly CD36-positive, while also expressing ICAM-1, VCAM1, CD62-E and CD62-P.¹⁷⁶

1.13.5 Tetraspanins

The protein family of Tetraspanins contains about 33 members, while features a conserved structure of 4 transmembrane domains and 2 extracellular domains, lacking post-translational modifications. Tetraspanins are involved in numerous cellular processes such as proliferation, migration, cell fusion, adhesion, MHC multimerization, aggregation of thrombocytes as well as binding and processing pathogenic structures. Moreover, they are utilized in cellular attachment of bacteria and host cell entry by several viruses and *P. falciparum* sporozoites.^{177,178}

> CD9 and CD151

CD9 and CD151, in interaction with ICAM-1 and VCAM1 are described to convey firm leucocyte adhesion. As CD9 is also expressed on platelets, while associated with CD36, there is evidence that CD9 is involved in specific sequestration of *P. falciparum* IE and platelet-mediated clumping, while for CD151, no respective interacting PfEMP1 ligand could be described so far.^{146,175} Moreover, an interaction of IE with tetraspanins receptors could lead to a dysregulation of leucocyte transmigration, affecting the pathogenicity of a malaria infection.^{179–182}

> CD37 and CD81

Also, the cell surface glycoproteins CD37 and CD81 are described to complex with other tetraspanins and integrins. While the occurrence of CD37 is restricted to hematopoietic lineages and mature B-cells, CD81 is mostly detected on immune cells, like mature B-cells, while located on the membrane of various tissues, extracellular exosomes and immunological synapses, but not on erythrocytes or platelets. Both molecules play an important role in humoral and cellular immune response via T- and B-cell interactions and cell development. CD37, like CD81, acts as non-classical costimulatory molecule or directly influences antigen presentation via complex formation with MHC class II molecules.^{179,181} However, CD37 can build complexes with CD81, MHC, CD53 and CD82, while a murine deficiency of CD37, interacting with TSSC6, result in a rapid onset of hyper parasitemia when infected with *P. yoelii*.¹⁸³

The non-glycosylated CD81 is involved in cell transduction, development, activation, growth and motility, promotes muscle cell fusion and myotube maintenance as well as signal-transduction. It is located in a putative malignancy tumor-suppressor region. Moreover, CD81 constitutes an essential receptor for *Listeria* and HCV entry into hepatocytes, while regarding malaria disease, CD81 is also known to be used by *P. falciparum*, *P. vivax*, *P. yoelii* parasites to enter human or murine hepatocytes with formation of a parasitophorous vacuole, respectively, while being simultaneously essential for further differentiation into exoerythrocytic forms.^{182,184–186}

1.13.6 HRH1 – Histamine receptor 1

The histamine receptor 1, or HRH1, is a G-protein coupled multi-pass integral membrane protein, slightly expressed in the brain and peripheral tissues. It is sensitive to the ubiquitous messenger protein histamine. It mediates the increase in capillary permeability and the neurotransmission in the central nervous system. Moreover, it is

pathophysiological associated with allergic diseases, anaphylaxis, dermatitis and asthma. HRH1 were firstly part of previous investigations regarding binding capabilities of *P. falciparum* IE, while in the first course so far failed to induce initial binding.¹⁴⁶

1.13.7 CD55

CD55 is a GPI-anchored cell surface glycoprotein, coded by 14 exons and is mainly detected as single-pass membrane protein, but also available as soluble molecule. It is present on a broad range of tissues within the bone marrow, blood, brain, heart, as well as on white blood cells, epithelial cell linings, extracellular compartments and within most of the body fluids. Levels of CD55 decrease with increasing age of erythrocytes.¹⁸⁷ Together with the complement receptor CR1, or CD35, also CD55 is known to regulate the human complement cascade by accelerating the decay of complement-related proteins via binding them, thus preventing the damage of host cells. Moreover, CD55 is a prominent entry receptor for various viral and bacterial pathogens, while a deficiency leads to severe anemia, a hyperactivation of the complement, resulting in autoimmune, complement-driven hemolysis and protein-losing enteropathy, or also called CHAPLE syndrome. Regarding malaria, CD55 described to be a critical receptor for *Plasmodium* merozoite committed attachment and invasion to host erythrocytes, promoting severe anemia, while genetic variants in the CD55 gene did not affect the susceptibility of (severe) malaria.¹⁸⁸⁻¹⁹³

1.13.8 MDR1 / CD243 – Multidrug resistance protein 1

The MDR1 is a multi-pass membrane transporter protein composed of 6 TM, a functional cytoplasmic ATP-binding-cassette domain, followed by another 6 TM and an ATP binding site. This complex structure hosts several binding sites for various, e.g. hypoxia-responsive, transcription factors. It is described to be crucial for eliminating numerous toxic compounds from cerebral tissues, and thus critical for neuroprotection and likely evolved as a defense mechanism to harmful substances. MDR1 is therefore detectable in a wide array of tissues and cell types, like the capillary endothelial cells defining the blood-brain-barrier or the blood-testis-barrier.¹⁹⁴ So far, MDR1 was described to mediate initial binding of *P. falciparum* IE from Ghanaian field isolates, while it was never outlined in attachment or invasion of pathogens. Albeit, an overexpression results in increased efflux of therapeutic agents, critical in e.g. cancer chemotherapy, while a MDR1 decrease is positively correlated with severity of the Alzheimer disease.^{146,195,196}

1.13.9 TNFR1 and TNFR2 – Tumor necrosis factors

TNF α is a key player in malaria disease and known to be produced and released by human immune cells after exposure to various malarial antigens. Cytokines, such as TNF α can alter neurological responses and modulate the overexpression of adhesive molecules, especially ICAM-1. Consequently, the TNF receptors TNFR1 (CD120a) and TNFR2 (CD120b) are most probably also involved in forming malaria disease related symptoms. The receptors are membrane glycoproteins, present on almost all cell types but not on erythrocytes, excluding the possibility of being involved in rosetting. Soluble

forms of the receptors are generated by cleavage from the membrane, floating within body fluids able to bind to TNF α ; in low concentrations promoting the stability of TNF α , while in high concentrations inhibiting by competition with other cell membrane receptors. On the one hand, TNFR1 seems to be important for resistance of most pathogens, like fungi, *Listeria*, *Toxoplasma* or *Leishmania*, while a mutation is linked with autosomal dominant periodic fever syndromes. On the other hand, TNFR2 seems to be more decisive in cerebral related manners, as deficient mice were protected from cerebral upregulation of ICAM-1 and CM manifestations. Also, it was recently shown that soluble forms of TNFR1 and TNFR2 are increased in the peripheral blood of pregnant women, while also, positively correlated with parasitemia.¹⁹⁷ So far, increased levels of TNF α and partly the upregulation of TNFR1 and TNFR2, were detected during CM, maybe able to affect fever periods, while being positively correlate with renal failure, albeit a clear association with severity or CM is still elusive.^{198–201} Also, a previous study evidenced the involvement of both, TNFR1 and TNFR2 proteins in specific sequestration of *P. falciparum* IE.¹⁴⁶

> Taken together, due to the conserved structure of some receptors or similar function in the human host, a potentially crucial role in CM, a comparable similar pathogenicity or potentially related cytoadhesion profile are anticipated, bringing them into the focus of malaria and sequestration-concerning investigations.

2 AIM OF THE THESIS

Malaria is still one of the main infectious diseases worldwide, while *P. falciparum* induces the most severe form, with a high potential of developing devastating clinical symptoms such as high anemia, obstruction of blood flow, critical and insufficient supply of organs as well as cerebral impairment and death.

Variable surface proteins, such as PfEMP1 and other VSA, are involved in the interaction between the malaria pathogen and its human host, while in particular, two mechanisms are important for the immune evasion and parasite survival. Thus, sequestration and antigenic variation are the major factors for the high pathogenicity of *P. falciparum*. By now, various human receptors are known to bind IE but only for a few of them, PfEMP1 is identified as the parasite ligand.

The overall aim of this work is to characterize the gene expression of knob related and variable surface proteins within the *P. falciparum* isolate IT4 in relation to its particular receptor sequestration.

- i. Here, the actual set of interacting receptors will be extended by putatively cerebral related and, so far, barely or undescribed human endothelial receptor, mediating an initial binding of IE. By investigating several *P. falciparum* culture and field isolates within static binding assays, their binding capability will be evaluated.
- ii. The selection of suitable human receptors, inducing a promising IE binding profile, revealed 6 promising candidates, namely MDR1, TNFR1, TNFR2, CD37, CD55 and CD81. The respective gene expression of the *var* multigene family will be further investigated via next generation RNA sequencing, while a comprehensive analysis of the whole transcriptomes will be performed in the same course.
- iii. The subsequent quantitative and comparative transmission electron microscopy analysis will provide an overall view of the morphology, appearance and versatility of distinct *P. falciparum* populations. While exhibiting a definite binding profile towards the particular human receptors as well as cultivated under various febrile conditions, the appearance and distribution of knob formations will be focused on. Moreover, a comparison of various *P. falciparum* field isolates will be performed.

3 MATERIALS

3.1 Stocks & Solutions

| RPMI-HS | |
|--|------------|
| <i>Plasmodium</i> complete growth medium with human serum | 1 L |
| RPMI 1640; dissolved in 800 ml dH ₂ O | 16.4 g |
| Hypoxanthine; dissolved in 50 ml dH ₂ O | 0.05 g |
| heat inactivated human serum A ⁺ | 100 ml |
| 7.5% NaHCO ₃ | 30 ml |
| Gentamicin 40 mg/ml | 500 µl |
| ad dH ₂ O to total volume | |
| set pH with NaOH | 7.4 |
| sterile filtration (0.22 µm) | |
| store at 4°C for maximum 4 weeks | |

| RPMI-ALB | |
|--|------------|
| <i>Plasmodium</i> complete growth medium with AlbuMAX | 1 L |
| RPMI 1640 | 16.4 g |
| NaHCO ₃ | 1 g |
| AlbuMAX II | 0.5% |
| Glucose; H ₂ O-free | 2 g |
| Hypoxanthine | 0.028 g |
| Gentamycine; 40 mg/ml | 0.2 g |
| ad dH ₂ O to total volume | |
| set pH with NaOH | 7.2 |
| sterile filtration (0.22 µm) | |
| store at 4°C for maximum 4 weeks | |

| Binding medium | |
|--------------------------------------|------------|
| static binding assay | 1 L |
| RPMI 1640 | 16.4 g |
| Glucose; H ₂ O-free | 20 g |
| ad dH ₂ O to total volume | |
| set pH with NaOH | 7.4 |
| sterile filtration (0.22 µm) | |
| store at 4°C for maximum 4 weeks | |

| 5% D-Sorbitol | |
|--|------------|
| <i>Plasmodium</i> synchronization | 1 L |
| D-Sorbitol | 50 g |
| ad dH ₂ O to total volume | |
| sterile filtration (0.22 µm) | |
| store at 4°C | |

| | |
|--|---------------|
| Malaria Freezing Solution (MFS) cryogenic conserved stocks | 1 L |
| D-Sorbitol | 3 g |
| NaCl | 0.65 g |
| ad dH ₂ O to total volume | |
| sterile filtration (0.22 µm) | |
| Glycerol; autoclaved | 28 ml |
| store at 4°C | |
| Malaria Thawing Solution (MTS) re-culturing of cryogenic conserved stocks | 1 L |
| NaCl | 35 g |
| ad dH ₂ O to total volume | |
| sterile filtration (0.22 µm) | |
| store at 4°C | |
| Gelatine solution coating culturing plates for adherent cells | 100 ml |
| 2% Gelatine solution; 37°C prewarmed | 50 ml |
| ad PBS | 50 ml |
| sterile filtration (0.22 µm) | |
| store at -20°C in 50 ml aliquots | |
| 10% Giemsa Plasmodium blood smear staining or static binding assay | 100 ml |
| Giemsa solution | 10 ml |
| ad dH ₂ O (staining) or Weiser buffer (static binding assay) to total volume | 90 ml |
| store at RT for maximum 2 to 4 days | |
| Weiser-buffer Static binding assay | 1 L |
| Na ₂ HPO ₄ | 2.09 g |
| KH ₂ PO ₄ | 0.49 g |
| ad dH ₂ O to total volume | |
| store at RT | |
| Glutaraldehyde static binding assay fixation | 100 ml |
| Glutaraldehyde; 25% | 4 ml |
| ad PBS to total volume | |
| work immediately under hood at RT | |
| Percoll separating gradient solution for electron microscopy | |
| sterile filtration (0.22 µm) | each |
| store at 4°C | each |

| | | |
|---|--|--------------|
| 90% Percoll stock solution | | 50 ml |
| Percoll solution | | 5 ml |
| ad PBS to total volume | | |
| store at 4°C | | |
| 80% Percoll working solution | | 10 ml |
| 90% Percoll stock solution | | 8.9 ml |
| D-Sorbitol | | 0.8 g |
| ad RPMI culture medium to total volume | | 1.1 ml |
| store at 4°C | | |
| 60% Percoll working solution | | 10 ml |
| 90% Percoll stock solution | | 6.7 ml |
| D-Sorbitol | | 0.8 g |
| ad RPMI culture medium to total volume | | 3.3 ml |
| store at 4°C | | |
| 40% Percoll working solution | | 10 ml |
| 90% Percoll stock solution | | 4.4 ml |
| D-Sorbitol | | 0.8 g |
| ad RPMI culture medium to total volume | | 5.6 ml |
| store at 4°C | | |
| Ham's F12 CHO complete growth medium | | |
| Hams' F12 | | 500 ml |
| heat inactivated fetal calf serum | | 50 ml |
| Penicilline-Streptomycine | | 5 ml |
| store at 4°C for maximum 4 weeks | | |
| CHO freezing solution cryogenic conserved stocks | | |
| Hams' F12 | | 500 ml |
| DMSO | | 60 ml |
| vortex & sterile filtration (0.22 µm) | | |
| store at 4°C | | |
| HBEC-5i CGM HBEC-5i complete growth medium | | |
| DMEM/F12 | | 500 ml |
| endothelial growth factor supplement (ECGS); 30 µg/ml | | 15 mg |
| heat inactivated fetal calf serum | | 50 ml |
| gentamycin; 10 µg/ml | | 100 µl |
| store at 4°C for maximum 4 weeks | | |

| HBEC-5i freezing solution | |
|---|---------------|
| Cryogenic conserved stocks | |
| DMEM/F12 | 462.5 ml |
| DMSO | 37.5 ml |
| vortex & sterile filtration (0.22 µm) | |
| store at 4°C | |
| 10x CHO-PBS | |
| stock solution for cell culture | |
| | 1 L |
| NaCl | 80 g |
| KCl | 2 g |
| Na ₂ HPO ₄ | 14.4 g |
| KO ₂ PO ₄ | 2.4 g |
| ad dH ₂ O to total volume | |
| set pH with NaOH | 7.4 |
| autoclaved and stored at RT | |
| LB Medium | |
| bacterial complete growth medium | |
| | 1 L |
| LB medium | 20 g |
| ad dH ₂ O to total volume | |
| autoclaving at 121°C | |
| optional: add 1 ml ampicilline as antibiotal selection marker | |
| store at 4°C | |
| TBF I buffer | |
| competent bacterial cells | |
| | 500 ml |
| K-acetate; 30 mM | 1.47 g |
| MnCl ₂ - 4 H ₂ O; 50 mM | 4.49 g |
| RbCl ₂ ; 0.1 M | 6.01 g |
| CaCl ₂ ; 10 mM | 0.735 g |
| Glycerin; 100% | 75 ml |
| set pH with acetic acid | 5.8 |
| ad dH ₂ O to total volume | |
| store at 4°C or 30 ml aliquots at -20°C | |
| TBF I buffer | |
| competent bacterial cells | |
| | 500 ml |
| MOPS; 10 mM | 1.04 g |
| CaCl ₂ ; 75 mM | 5.5 g |
| RbCl ₂ ; 10 mM | 0.6 g |
| Glycerin; 100% | 75 ml |
| set pH with NaOH | 7.0 |
| ad dH ₂ O to total volume | |
| store at 4°C or 30 ml aliquots at -20°C | |

3.2 Chemicals

| chemicals | supplier |
|--|--|
| Accutase (500 – 720 U/ml) | GE Healthcare |
| AlbuMax II | Gibco/Invitrogen |
| Ampicilline | Roche |
| Biocoll (Ficoll) Seperating Solution | Biochrom |
| Bovine Serum Albumine (BSA) | Biomol |
| CoverSlips | Sarstedt |
| D-gucose | Merck |
| D-Sorbitol | Merck |
| Dako Cytomation Pen | DakoCytomation |
| Dako Mounting Medium | Agilent Technologies |
| Diamond Tween | Biozol |
| DMSO | Roth |
| dNTPs | Thermo Fisher |
| Epoxy resin (812) (EPON) | EMS |
| Ethanol | Merck |
| G-418-BC | Greiner |
| Gentamycin 40 | Hexal |
| Giemsa Solution | Merck |
| Glutaraldehyde 25% | Merck |
| Ham's F12 | PAN |
| Hoechst 33342 | Sigma-Aldrich |
| HPLC H ₂ O | Fresenius Kabi |
| Human Blood 0 ⁺ | UKE Hamburg |
| Human Serum A ⁺ | Interstate Blood Bank |
| Hypoxanthine (9636-5G) | Sigma-Aldrich |
| Methanol ≥ 99% | Roth |
| Osmium-(VIII)-Oxid in H ₂ O; 2% | EMS |
| Paraformaldehyde; 2.5% | EMS |
| Penicilline-Streptomycine (10.000 U/ml) | Life Technologies |
| Percoll Solution | Sigma-Aldrich |
| RNAse away | Roth |
| RPMI+L-Glutamine+25 mM HEPES-NaHCO ₃ | AppliChem |
| Sodium Cacodylate trihydrate buffer; 50 mM; pH 7.4 | EMS |
| Soluble CSA | Sigma |
| TRIzol | Invitrogen |
| Uranylacetate; 0.5 - 1% | EMS |
| Single use disposables | Roth, Merck, Sigma-Aldrich, Sarstedt, Greiner, Falcon, Eppendorf |

3.3 Enzymes

| enzymes & standards | supplier |
|---------------------------------|---------------|
| Fast Digest Restriction Enzymes | Fermentas |
| GeneRuler 100 bp DNA Ladder | Fermentas |
| GeneRuler 1 kb DNA Ladder | Fermentas |
| GoTaq Flexi Polymerase | Promega |
| Pwo DNA Polymerase | Sigma-Aldrich |

3.4 Kits

| kits | supplier |
|---|----------------------|
| Agilent RNA 6000 Pico Kit | Agilent Technologies |
| Fast Plasmid Mini | 5'Prime |
| NucleoBond | Macherey-Nagel |
| NucleoSpin Clean up | Macherey-Nagel |
| NucleoSpin Plasmid | Macherey-Nagel |
| Pure Link Total RNA Purification System | Invitrogen |
| Qiamp DNA Mini | 5'Prime |
| SuperScript III for RT-PCR | Invitrogen |
| TOPO TA Cloning | Invitrogen |

3.5 Devices

| devices | supplier |
|---|----------------------|
| Agilent 2100 Bioanalyzer | Agilent Technologies |
| Axioscope M1 | Zeiss |
| CO ₂ Incubator Function Line | Heraeus Instruments |
| EVOS Flauto | Thermo Fisher |
| EVOS XL | Thermo Fisher |
| FACS Ariall | BD Bioscience |
| HiSeq 4000 PE100 | BGI, HongKong |
| NanoDrop2000 | Thermo Scientific |
| Orca C4742-95 | Hamamatsu |
| pH-Meter CG840 | Sartorius |
| TEM Tecnai Spirit | FEI |
| Ultracut UC7 | Leica |

3.6 Software

| software & version | supplier |
|--------------------|----------------------|
| Agilent 2100, Exp. | Agilent Technologies |
| Axio Vision, 4.7 | Zeiss |
| EnzymeX, 3.3.3 | Mekentosj |
| Deseq, 2.0 | Bioconductor |
| FACS Diva, 6.1.3 | BD Bioscience |
| FlowJo, 10.4.2 | LLC |
| ImageJ, 1.52a | NIH |
| MacVector, 14.5.3 | MacVector |
| MySamples, 2.0 | mydata |
| NCBI, 12-2018 | www.ncbi.nlm.nih.gov |
| PlasmoDB, 40-2018 | www.plasmodb.org |
| PRISM, 6.0 | GraphPad |

3.7 Vectors & Genes

| accession | receptor | vector system |
|----------------|---------------------|---------------|
| Addgene-632469 | pAc-GFP-N1 | vector: GFP |
| Addgene-6085-1 | pEGFP Vektor | vector: GFP |
| P16671 | CD36 | pAcGFP1-N1 |
| P05362 | CD54/ICAM-1 | pAcGFP1-N1 |
| P21926 | CD9 | pEGFP_N1 |
| P48509 | CD151 | pEGFP_N1 |
| P16581 | CD63E | pAcGFP1-N1 |
| Q14242 | CD62P | pAcGFP1-N1 |
| P35367 | HRH1 | pAcGFP1-N1 |
| P19320 | CD106/VCAM1 | pAcGFP1-N1 |
| P08183 | CD243/MDR1 | pAcGFP1-N1 |
| P19438 | CD120a/TNFR1 | pAcGFP1-N1 |
| P20333 | CD120b/TNFR2 | pAcGFP1-N1 |
| P11049 | CD37 | pAcGFP1-N1 |
| P08174 | CD55 | pAcGFP1-N1 |
| P6003 | CD81 | pAcGFP1-N1 |
| P19235 | EPOR | pAcGFP1-N1 |
| P78423 | CX3CL1/Fralktalking | pAcGFP1-N1 |
| P16070 | CD44 | pAcGFP1-N1 |

3.8 Antibodies

| antibodies | | | | | |
|-------------------------|-------------------|-----------------|------------|-----------------|--------------------|
| host | reactivity | antibody | tag | supplier | accession # |
| first antibodies | | | | | |
| mouse | human | CD9 | PE | BioLegend | 312105 |
| mouse | human | CD36 | APC | BioLegend | 336207 |
| mouse | human | CD37 | APC | Thermo Fisher | 17-0379-41 |
| mouse | human | CD44 | APC | BioLegend | 338805 |
| mouse | human | CD44 | FITC | MyBiosource | MBS520132 |
| mouse | human | CD54/ICAM-1 | APC | BioLegend | 322712 |
| mouse | human | CD55 | APC | BioLegend | 311311 |
| mouse | human | CD56/NCAM | APC | BioLegend | 318309 |
| mouse | human | CD62E | APC | BioLegend | 3336011 |
| mouse | human | CD62P | APC | BioLegend | 304910 |
| mouse | human | CD81 | APC | BioLegend | 349509 |
| mouse | human | CD106/VCAM1 | none | Ancell | 327-020 |
| mouse | human | CD120a/TNFR1 | PE | BioLegend | 369903 |
| mouse | human | CD120b/TNFR2 | APC | BioLegend | 358405 |
| mouse | human | CD151 | APC | BioLegend | 350405 |
| mouse | human | CD243/ MDR1 | APC | Thermo Fisher | 12-2439-41 |
| mouse | human | CSA | PE | BD | 562415 |
| mouse | human | CX3CL1 | APC | R&D | IC365A |
| rabbit | human+mouse | EPO-R1 | APC | BioLegend | 35132 |
| mouse | human | HRH1 | none | R&D | 480045 |

| secondary antibodies | | | | | |
|-----------------------------|--------|-----------------|-------|---------------|---------|
| goat | mouse | Alexa Fluor 488 | green | Thermo Fisher | A-11001 |
| goat | rabbit | Alexa Fluor 488 | green | Thermo Fisher | A-11008 |
| goat | mouse | Alexa Fluor 594 | red | Thermo Fisher | A-11005 |
| goat | rabbit | Alexa Fluor 594 | red | Thermo Fisher | A-11002 |

| intercalating | | | | | |
|----------------------|-----|---------|------|-------------------|-------|
| all | DNA | DAPI | none | Thermo Scientific | 62247 |
| all | DNA | Hoechst | none | Thermo Scientific | 62249 |

4 METHODS

4.1 Cell lines

The following bacterial, rodent, human and parasitic cell lines were used in this thesis. Their origins and specifications are described in the next sections.

4.1.1 *E. coli* One Shot TOP10 (ATCC PTA-10989)

One Shot TOP10 chemically competent *E. coli* cells are ideal for high-efficiency cloning as they allow stable replication of high-copy number plasmids. They offer the feature of blue/white color screening of recombinant clones due to lacZ Δ M15 mutation.

4.1.2 Chinese hamster ovary (CHO) cell line (ATCC CRL-2242)

Adherent growing Chinese hamster ovary (CHO) epithelial cells belong to the most commonly used mammalian host cell line for long-term stable gene expression with high protein production rates. Initial CHO cells were obtained in 1957 during a biopsy from the ovary of the Chinese hamster *Cricetulus barabensis griseus*. CHO-K1 cell line arose as a direct subclone of the parental CHO cell line while CHO-pgsA (CHO-745) cell line was derived after treatment with mutagen ethylmethanesulfonate obtain spontaneous immortalization, with a subsequent screening for mutants defective in proteoglycan synthesis. The CHO cell line lacks catalytic function of xylosyltransferase I, so cells are deficient regarding biosynthesis of glycosaminoglycan chains. Also, these cells lack expression of placental adhesion receptor chondroitin-4-sulphate (CSA) on the surface that is known to bind *P. falciparum* infected human erythrocytes.

CHO cells were transfected with either pAc-GFP1-N1 or pEGFP-N1 plasmid, containing human endothelial receptors fused to the expression marker GFP. The receptor forms the extracellular part of the fusion protein whereas the GFP is located in the cytoplasm of the cell without affecting the extracellular domain. CHO-745/pAc-GFP1-N1 (mock) control cell line was solely transfected with the GFP-bearing expression vector, lacking any receptor sequence, consequently synthesizing cytosolic GFP only. An overview of all generated transgenic CHO cell lines is shown in **Table 2**.

Table 2. Overview of generated transgenic CHO cell lines.

| cell line | vector | receptor | accession # |
|---|-------------|----------------------|-------------|
| CHO-WT * | none | none | - |
| CHO-GFP * | pAc-GFP1-N1 | none | - |
| CHO-CD36 * | pAc-GFP1-N1 | CD36 | P16671 |
| CHO-ICAM-1 * | pAc-GFP1-N1 | CD54 (ICAM-1) | P05362 |
| CHO-CD9 * | pEGFP-N1 | CD9 (Tspan29) | 21926 |
| CHO-CD151 * | pEGFP-N1 | CD151 (Tspan24) | P48509 |
| CHO-CD62-E * | pAc-GFP1-N1 | CD62E (E-Selectin) | P16581 |
| CHO-CD62-P * | pAc-GFP1-N1 | CD62P (P-Selectin) | P16109 |
| CHO-MDR1 | pAc-GFP1-N1 | CD243 (MDR1) | P08183 |
| CHO-HRH1 * | pAc-GFP1-N1 | HRH1 | P35367 |
| CHO-VCAM1 * | pAc-GFP1-N1 | CD106 (VCAM1) | P19320 |
| CHO-TNFR1 | pAc-GFP1-N1 | CD120a (TNFR1) | P19438 |
| CHO-TNFR2 | pAc-GFP1-N1 | CD120b (TNFR2) | P20333 |
| CHO-CD37 | pAc-GFP1-N1 | CD37 (Tspan26) | P11049 |
| CHO-CD55 | pAc-GFP1-N1 | CD55 (CR, DAF) | P08174 |
| CHO-CD81 | pAc-GFP1-N1 | CD81 (Tspan28) | P60033 |
| CHO-EPOR | pAc-GFP1-N1 | EPOR | P19235 |
| CHO-CX3CL1 | pAc-GFP1-N1 | CX3CL1 (Fraktalkine) | P78423 |
| * CHO cell lines were kindly provided by the research group of Prof. Dr. Rolf Horstmann (Department of Molecular Medicine, BNITM, Hamburg). | | | |

4.1.3 Human brain endothelial cells (HBEC)-5i cell line

The human brain endothelial cell line (HBEC)-5i was derived from small fragments of cerebral cortexes, obtained from a pool of healthy male donors. The brains were devoid of any pathologic abnormalities. HBEC-5i cells were immortalized by the transfection with plasmid containing SV40 large T-antigen to receive a renewable source of human microvascular endothelial cells. HBEC-5i can be used for studies in cancer, tumor metastasis, endothelium function, cell trafficking, surface molecule interaction and microvascular changes of the brain caused by malaria. The cells express stable patterns of VE-Cadherin (CD144), von Willebrand factor VIII, occludin, ICAM-1 (CD54), tumor necrosis factor receptor (TNFR) superfamily 5 (CD120), chondroitin sulfate A (CSA) and show an upregulation of ICAM-1 and VCAM1 (CD106) upon TNF α activation.

4.1.4 *P. falciparum* clinical isolates

The *P. falciparum* clinical isolates were provided either by the Diagnostic Department of the Bernhard Nocht Institute for Tropical Medicine (BNITM) or the Bernhard Nocht Clinic of the University Hospital Eppendorf (UKE) in Hamburg, Germany. Previously, all patients agreed to the scientific use of their blood sample for research purposes.

4.1.5 *P. falciparum* field isolate NF54 and 3D7

The *P. falciparum* NF54 field isolate derived in 1981 from a patient who has never been in malaria-endemic areas but lived near Schiphol-Airport, Amsterdam in the Netherlands, suggesting the suspicion of an airport-malaria case. The clone 3D7 arose artificially from NF54 by limited dilution. Both *P. falciparum* isolates were directly adapted to cell culture handling and are chloroquine sensitive. MSP1 genotyping for NF54 and 3D7 show K - 203.

4.1.6 *P. falciparum* field isolate DD2

The *P. falciparum* strain Indochina III/CDC originate in 1980 from a patient in Laos, SEA. Clone W2 derived by sub-cloning the Indochina III/CDC; followed by 96 weeks of continuous culture with mefloquine, resulting in the mefloquine-resistant clone W2-mef. W2-mef was further sub-cloned, giving rise to DD2 isolate. MSP1 genotyping show Mad20 - 204.

4.1.7 *P. falciparum* field isolate MM

The *P. falciparum* field isolate MM derived of an initial mixture of 3 individual patient blood samples from Ghanaian children from Kumasi, West Africa. During cultivation, one genotype was lost over the time, resulting in the final *P. falciparum* MM isolate, including 2 genotypes. MSP1 genotyping show Mad20 - 222 and K - 212. While other isolates were long-term cultured over several years, the MM isolate never exceed culture periods over 6 months. (Ethic reference number CHRPE/01/11, Committee for Research, Publications and Ethics of the School of Medical Sciences, Kwame Nkrumah University of Science and Technology, Kumasi, Ghana)

4.1.8 *P. falciparum* field isolate FCR3/IT4

The *P. falciparum* field isolate FCR3/IT4, initially termed FMG, obtained in 1976 from the clinic at the Medical Research Council Laboratories in Fajara, The Gambia, West Africa. The isolate was diluted and shipped to New York City, USA for direct and continuously cell cultivation, giving rise to IT4/FCR3 strain. MSP1 genotyping show Mad20 - 186.

The IT4 isolate mainly used had following specifications:

IT4 – starting culture (ST)

IT4, initial population, constantly cultivated at 37°C

IT4 – 37°C *

IT4, constantly cultivated at 37°C, enriched over HBEC-5i with panning for 1.5 h at 37°C

IT4 – 40°C *

IT4, constantly cultivated at 37°C, enriched over HBEC-5i with panning for 1.5 h at 40°C

IT4 – 38.5°C *

IT4, constantly cultivated at febrile temperature of 38.5°C

IT4 – 40°C weekly *

IT4, constantly cultivated at 37°C with a weekly heat shock of 40°C for 1.5 h

IT4 – 7 h/40°C final *

IT4, initial population, constantly cultivated at febrile temperature of 38.5°C with a weekly heat shock of 40°C for 1.5 h and a final heat shock of 40°C for 7 h

IT4 – TNF α *

IT4, constantly cultivated at 37°C, with weekly TNF α stimulation

IT4 – Receptor

IT4, constantly cultivated at 37°C, enriched over transgene CHO cells, expressing the human receptor of interest, with preabsorbtion and panning at 37°C

- > WT*, CD36*, ICAM-1*, CD9*, CD151*, CD63E*, CD62P*, Gelafundin*
- > GFP, TNFR1, TNFR2, MDR1, CD37, CD55, CD81

IT4 – Receptor & Temperature

IT4, constantly cultivated at 37°C, enriched 7 times over transgenic CHO cells, with preabsorbtion and panning at 37°C.

Further enrichment over same receptor for 3 times, with preabsorbtion at either 37°C or 40°C and panning at 40°C

- > CD55-37p40°C, CD55-40p40°C
- > GFP-37p40°C, GFP-40p40°C (no preabsorbtion, but prewarming)

* Generation and cultivation of the marked conditions were performed in cooperation with other members of the Research group Protozoology.

4.2 Molecular biology

The following techniques and protocols were applied to process the molecular biological handling of the biological samples.

4.2.1 *P. falciparum* culturing

The following culture techniques and protocols were applied to cultivate the actual *P. falciparum* isolates.

4.2.2 *P. falciparum* thawing of cryogenic conserved stocks

In order to recapture *P. falciparum* cryogenic conserved isolates after freezing, the cryogenic tube was thawed with gentle shaking at 37°C in a water bath for about 2 min. The sample was transferred into a 15 ml reaction tube, filled with an equal

volume of 37°C prewarmed Malaria thawing solution (MTS). After centrifugation at 800 x g for 2 min, the supernatant was removed and the cell pellet was washed 3 times with 1 ml of MTS until the supernatant was clear. The erythrocyte pellet was resuspended with RPMI+HS complete growth medium and transferred into petri dishes with cams for further cultivation according to standard procedures.²⁰² Hematocrit was adjusted to 5% using erythrocytes of blood group 0⁺ derived from the blood bank of University Hospital Eppendorf, Hamburg.

4.2.3 P. falciparum freezing of cryogenic conserved stocks

In order to generate permanent cryogenic conserved stocks, synchronized *P. falciparum* culture with at least 1% ring stage parasites was centrifuged for 3 min at 800 x g. The supernatant was removed and the erythrocyte pellet was resuspended in a 4fold volume of Malaria freezing solution (MFS). The suspension was divided in aliquots of 1.5 ml into cryogenic tubes and immediately frozen. Using 'Mr. Frosti' freezing containers ensured the controlled and slow freezing with -1°C per minute for 2 h to -80°C. For long-term storage, the cryogenic tubes were transferred to the gas phase of a liquid nitrogen tank at -173°C.

4.2.4 P. falciparum culturing

The *in vitro* cultivation of *P. falciparum* was carried out in a volume of 10 ml with a 5% hematocrit, continuously adjusted with blood of blood group 0⁺ in petri dishes with cams using RPMI-1640 completed growth medium enriched with human serum of blood group A⁺ or with AlbuMAX II. The incubation was carried out in a vacuum container with a gas composition of 1% O₂, 5% CO₂ and 94% N₂ and a constant temperature of 37°C in the incubator. The medium was changed at least every third day, at a parasitemia of 5% or more daily.

4.2.5 P. falciparum Giemsa staining

To determine the parasitemia and parasitic development stages in the culture, thin blood smears were made on glass slides, using 4 µl of sedimented cell culture. The slides were air dried, fixed in 100% methanol for 2 min and transferred into 10% Giemsa staining solution for at least 5 min. The slides were rinsed with clear water, air dried and examined under a light microscope at 60x magnification using immersion oil. Parasitemia was calculated as percentage of IE per non-IE, counted in triplicates.

4.2.6 P. falciparum splitting

During regular cell cultivation, parasitemia was kept at 0.2% when medium was changed every second day and at 0.1% when medium was changed every third day. Otherwise, the parasitemia was adjusted by dilution with non-infected erythrocytes according to the required conditions of subsequent experiments.

4.2.7 *P. falciparum* synchronization via D-Sorbitol

A 5% D-sorbitol solution was used to synchronize *P. falciparum* culture containing at least 1% ring staged parasites. IE with adult staged parasites such as trophozoites and schizonts are lysed. Subsequently, the osmotically burst is due to the excessive uptake of D-sorbitol through the increased permeable membrane system of the erythrocyte. IE with ring staged parasites did not established those channel and pore system and thus remain intact, resulting in a synchronized cell culture with ring-staged parasitized erythrocytes.

For synchronization, IE culture was centrifuged for 5 min at 800 x g and the supernatant was removed. Erythrocyte pellet was resuspended in a 6fold volume of 5% D-sorbitol solution, incubated for 6 min in a water bath at 37°C with gentle shaking every 2 min. To remove the D-sorbitol solution, suspension was washed twice by centrifugation for 3 min at 800 x g, removing of supernatant and resuspension in 3 to 5 ml culture medium. The hematocrit was adjusted if necessary and erythrocyte pellet was transferred back into petri dishes for further cultivation. To keep the synchrony of the *Plasmodium* culture, procedure was carried out at least once a week. To achieve a highly synchronized parasite culture, procedure was carried out twice every day of ring stage, 2 times a week.

4.2.8 CHO and HBEC-5i culturing

The following culture techniques and protocols were applied to cultivate the actual CHO and HBEC-5i cell lines.

4.2.9 CHO thawing of cryogenic conserved stocks

Since the transient transgenic CHO cell lines expressed their respective human endothelial receptor on the surface for a period of about 3 weeks, new aliquots regularly had to be thawed and consequently also prepared.

The cryogenic tubes including the frozen cell samples of early passages were almost completely thawed in the water bath at 37°C with gentle shaking for about 2 min. The thawed cells were transferred to a 15 ml reaction tube and washed with completed culture medium, centrifuging at 250 x g. The cell pellet was resuspended in fresh culture medium, including neomycine (G418, 50 mg/ml) as selection marker in a final concentration of 0.7 mg/ml completed medium for transgenic CHO cell lines. The cell suspension was placed in a T25 or T57 cell culture flask for adherent cells and cultured at 37°C with a gas mixture including 5% CO₂. The medium, including neomycine selection marker for transgenic CHO cell lines, was changed at least every second day.

> **HBEC-5i:** Cryogenic conserved stocks were thawed identically, with the use of HBEC-5i completed culture medium respectively. Furthermore, the culture flask was coated with 0,1% gelatin solution for 45 min at 37°C and 5% CO₂ prior to further cultivation. Also, no selection marker was added.

4.2.10 CHO freezing of cryogenic conserved stocks

Cell suspension including detached cells of early passages deriving from a culture flask with at least 20% confluence were used to generate cryogenic conserved stocks. The cell number within the suspension was determined using a Neubauer counting chamber. The suspension was centrifuged for 5 min at 800 x g and cell numbers were adjusted to 1×10^6 cells/ml within freezing solution. Corresponding aliquots were transferred into cryogenic tubes and frozen using a 'Mr. Frosti' freezing container, ensuring controlled and slow freezing of the samples to -80°C for 2 h. For long-term storage, the cryogenic tubes were transferred to the gas phase of a liquid nitrogen tank at -172°C .

> **HBEC-5i:** Cryogenic conserved stocks were generated identically, with the use of HBEC-5i freezing solution instead of CHO freezing solution respectively.

4.2.11 CHO culturing

Cultivation of adherently growing cells were carried out in a volume of 5 ml or 15 ml of complete culture medium in T25 or T75 cell culture flasks for adherent cells respectively. 7 $\mu\text{l}/\mu\text{l}$ Neomycine was used for selection of transient transgenic CHO cell lines to ensure the surface expression of respective human endothelial receptor. The cells were incubated at a constant temperature of 37°C with a gas mixture of 5% CO_2 . The viability, vitality, mean fluorescence as well as the confluence of the cells was controlled and determined via an inverted fluorescence microscope. The medium and neomycine, if necessary, was changed at least every third day.

> **HBEC-5i:** Cultivation was carried out identically, with HBEC-5i completed culture medium respectively. Furthermore, no selection marker was added.

4.2.12 CHO splitting

To split the adherently growing cells, the culture medium was removed from the culture flask and the cells washed with 37°C prewarmed PBS. To detach the cells from the bottom of the culture flask, 400 μl of 37°C prewarmed accutase was added, followed by a 5 min incubation step at 37°C and 5% CO_2 . The complete detachment of all cells was achieved by gently tapping the culture flask and was controlled via an inverse light microscope. The enzymatic collagenolytic and proteolytic activity of the accutase was terminated by adding the 10fold volume of completed culture medium. The cell number within the suspension was being determined using a Neubauer counting chamber. Cells were diluted with adequate cell numbers into respective volumes of completed culture medium, including 7 $\mu\text{l}/\text{ml}$ neomycine if necessary. Further cultivation was carried out at 37°C and 5% CO_2 . To ensure viable cells and an adequate growth rate over several passages, cells were cultivated until a maximum confluence of 50 to 60% during regular cultivation.

> **HBEC-5i:** Cell splitting was carried out identically, with HBEC-5i completed culture medium respectively. Furthermore, the culture flask was coated with 0.1% gelatin solution for 45 min at 37°C and 5% CO_2 prior to further cultivation. Also, no selection marker was added.

4.2.13 *P. falciparum* isolation of genomic DNA (gDNA)

To obtain a hematocrit of 50%, 200 µl pellet of whole *P. falciparum* culture was resuspended with 200 µl D-PBS in a 1.5 ml reaction tube. Isolation of *P. falciparum* genomic DNA was performed at RT according to the 'QUIAGEN QIAamp DNA Mini Kit' manual. The sample was eluted in 2 times 25 µl DNase free H₂O and stored at -80°C.

4.2.14 Synthesis of complementary DNA

Human RNA of brain, liver, lung, arterial/venous blood vessel, testis or skin originates from either a pool of 5 male donors or 1 single male donor was purchased at BioChain. Total RNA was used for cDNA synthesis via reverse transcription, following the 'Thermo Fischer Maxima First Strand cDNA Synthesis Kit for RT-qPCR' manual. Total RNA from brain, arterial blood vessel and lung render the most promising cDNA. The received total of 20 µl cDNA was stored at -20°C for up to 7 days or long term stored at -70°C.

4.2.15 Polymerase chain reaction

The polymerase chain reaction (PCR) exponentially amplifies a given copy of a DNA segment by means of specific flanking primer sequences and polymerase enzymes. Following the 'Promega GoTaq® DNA Polymerase protocol, many different DNA amplifications were conducted by using a GOtaq/PWO polymerase enzyme mix. Particular thermocycler programs and times are listed below. The annealing temperature depends on the Primer melting temperature (T_m) and ranges from 45 to 68°C, following the (A) Mamur and Doty Rule.²⁰³ for primers less than 13 bp and the Wallace-Rule for longer primers:

$$(A) \quad T_m = (wA + xT) * 2 + (yG + zC) * 4$$

$$(B) \quad T_m = 64.9 + 41 * (yG + zC - 16.4) / (wA + xT + yG + zC)$$

| reagents | 50 µl |
|--|----------|
| DNA template | 1 - 2 µl |
| 5x GreenGO taq Flexi Buffer | 10 µl |
| MgCl ₂ (25 mM) | 5 µl |
| dNTP mix (2.5 mM each) | 2 µl |
| GO taq / PWO DNA polymerase mix (20 : 1) | 2 µl |
| Primer forward (10 mM) | 1 µl |
| Primer reverse (10 mM) | 1 µl |
| nuclease-free H ₂ O | ad 50 µl |

4.2.16 Thermocycler programs

Standard GOtaq/PWO PCR was used for amplification of receptor-encoded DNA, M13 colony PCR, and *Mycoplasma* PCR. RT PCR was used for cDNA synthesis. Genotyping via MSP1 was used to identify and confirm the amount and species of *P. falciparum* genotypes within isolates.

Standard – PCR

| | | |
|----------|-----------|----------------|
| 2' | 95°C | |
| 30" | 95°C | 30 - 40 cycles |
| 30" | 45 – 68°C | |
| 30" – 2' | 68°C | |
| 10' | 68°C | |
| hold | 4°C | |

RT – PCR

| | | |
|------|------|-----------|
| 2' | 95°C | |
| 30" | 95°C | 40 cycles |
| 30" | 45°C | |
| 2' | 68°C | |
| 10' | 72°C | |
| hold | 4°C | |

Genotyping MSP1

| | | |
|------|------------|-----------|
| 4' | 95°C | |
| 30" | 94°C | 8 cycles |
| 40" | 60 – 0,5°C | |
| 40" | 72°C | |
| 30" | 94°C | 30 cycles |
| 40" | 56°C | |
| 40" | 72°C | |
| 10' | 72°C | |
| hold | 4°C | |

Genotyping Mad20

| | | |
|------|------------|-----------|
| 4' | 95°C | |
| 30" | 94°C | 8 cycles |
| 40" | 60 – 0,5°C | |
| 40" | 72°C | |
| 30" | 94°C | 30 cycles |
| 40" | 56°C | |
| 40" | 72°C | |
| 10' | 72°C | |
| hold | 4°C | |

Genotyping RO33

| | | |
|------|------------|-----------|
| 4' | 95°C | |
| 30" | 94°C | 8 cycles |
| 40" | 60 – 0,5°C | |
| 40" | 72°C | |
| 30" | 94°C | 30 cycles |
| 40" | 56°C | |
| 40" | 72°C | |
| 10' | 72°C | |
| hold | 4°C | |

Genotyping K1

| | | |
|------|------------|-----------|
| 4' | 95°C | |
| 30" | 94°C | 8 cycles |
| 40" | 60 – 0,5°C | |
| 40" | 72°C | |
| 30" | 94°C | 30 cycles |
| 40" | 56°C | |
| 40" | 72°C | |
| 10' | 72°C | |
| hold | 4°C | |

4.2.17 Enzymatic restriction digest

DNA molecules can be cleaved at specific sites for identification, analysis, isolation and fragmentation by restriction endonucleases. The enzymes recognize particular and mostly palindromic short sequence of nucleotides within the genome or multiple cloning site (MCS). The restriction digest was performed for 15 min using FastDigest enzymes, following the 'Thermo Fischer Fast Digestion of DNA' manual.

4.2.18 Isolation of DNA – PCR clean up and gel extraction

The desired DNA, either a direct PCR product or cut out of an agarose gel under long-wave UV light (366 nm), was purified for further handling, following the 'Macherey-Nagel NucleoSpin Gel and PCR Clean-up' manual.

4.2.19 Chemically competent *Escherichia coli* (*E. coli*) cells

Competent bacteria cells are able to absorb disposable foreign DNA out of their environment through the membrane without losing the ability to proliferate and replicate their own and additionally the foreign DNA. *E. coli* cells are not competent by nature but a treatment with CaCl₂, MgCl₂, RbCl and a subsequent heat shock enable the uptake of the desired present DNA. For all transformation, *E. coli* TOP10 cells were used, following the 'Invitrogen One Shot TOP10 Competent Cells' manual.

4.2.20 Topoisomerase (TOPO) cloning

Due to *tqg*-induced 3'-A-overhangs, (purified) DNA fragments can be directly ligated into linearized pCRTM4-TOPO vector via topoisomerase I enzyme, following the 'Thermo Fischer Sticks ends TOPO-TA Cloning Kit' manual. The final construct was transformed into chemically competent *E. coli* TOP10 cells via 30 sec heat shock at 42°C. 2% 5-Brom-4-chlor-3-indoxyl-β-D-galactopyranosid (X-gal) dissolved in DMSO (w/v) was added. The cells were plated on LB^{amp} agar plates and incubated over night at 37°C. Positive bacterial colonies were selected via blue-white-screening.

4.2.21 Plasmid preparation

For extraction and purification of plasmid DNA, transformed TOP10 *E. coli* cells are cultured, harvested and further processed. For small amounts of DNA, the '5 Prime Fast Plasmid Mini Kit' and for larger amounts the 'Nucleo Bond Plasmid DNA Purification Kit' manual was followed.

4.2.22 Transfection of CHO cells

The gene for the desired human endothelial receptor of interest was cloned into the GFP containing vector system pAc-GFP-N1. CHO cells were transfected via lipofection. The transfection was carried out following the 'Lipofectamine2000' manual. Two days prior the transfection, 2x 10⁴ CHO-WT cells per well were seeded into 24-well plates and cultured in CHO completed culture medium, without G418. The lipofection

was conducted with a slightly higher volume of the recommended quantity of reagents, as the efficiency was increased several times, compared to the described procedure. Furthermore, after the lipofection, the well plate was centrifuged at 800 x g for 30 min at RT (RT) to enhance the transfection efficiency, also called spinoculation. The transfected cells were incubated over night at 37°C and 5% CO₂. On the next day, the culture medium was changed and G418 was added as selection marker with a final concentration of 0.7 mg/ml completed medium for transgenic CHO cell lines. Transgenic cells were cultured as usual until further use. As soon as the transfected cells reached a confluence of 30 to 50%, cells were collected and subjected to FACS sorting to achieve a homogenous population of double positive cells.

4.2.23 *P. falciparum* DNA sequencing

The sequencing of plasmids was performed by Eurofins – Barcode Economy Run Service. Received sequences were analyzed with current MacVector, version 14.5.3 and EnzymeX, version 3.3.3 software.

4.2.24 *P. falciparum* total RNA isolation with TRIzol reagent

To isolate parasitic RNA, *P. falciparum* cell culture was sedimented via centrifugation for 5 min at 800 x g. The erythrocyte pellet was resuspended in a 10fold volume of pre-warmed TRIzol reagent and incubated for 5 min at 37°C in a water bath. The RNA isolation was performed on ice, following the 'Invitrogen TRIzol Reagent Experimental protocol for DNA isolation' manual. Only the upper RNA containing aqueous phase was transferred carefully into a RNase free reaction tube, without disturbing the lower phenol-chloroform or the interphase, containing DNA, proteins and debris. The precipitated parasitic RNA was eluted twice with RNase free dH₂O in a total volume of 40 µl, following the 'Thermo Fischer PureLink RNA Mini Kit' manual. To minimize gDNA contamination, some samples were DNase treated, following the 'Thermo Fischer TURBO DNase Treatment and Removal' manual. An additional, magnetic beads-based RNA clean-up was performed following the 'Agencourt RNAClean XP' manual. RNA samples were either processed directly or stored at -80°C until further use.

4.2.25 *P. falciparum* RNA quality and quantity control

The RNA yield and purity were measured using NanoDrop2000 device at 260 nm and 280 nm, following the 'Thermo Fischer NanoDrop 2000/2000c Spectrophotometer' manual. At an optical density measured at 260 nm (OD 260) of 1, the concentration of double-stranded DNA is 50 ng/µl, or single-stranded RNA is 40 ng/µl. The absorption maximum of RNA and DNA is at 260 nm whereas proteins have their maximum at 280 nm. For RNA samples, a 260/280 ratio of 1.8 to 2.1 was accepted. RNA integrity was determined via a chip-based nucleic acid separation technique of a Bioanalyzer-System, following the 'Agilent 2100 Bioanalyzer System RNA 6000 Pico Kit' manual. Dye-intercalated RNA was separated according to its size and amount into mRNA, rRNA and fragmented RNA. The resulting virtual electrogram and the 'RNA integrity number' (RIN value) provides information about the RNA degradation. The RIN value ranges from '1' to '10', with '1' being highly degraded. RNA samples were stored at -80°C.

4.2.26 Next generation sequencing (NGS)

Transcriptome sequencing is used to reveal the presence, quantity and structure of RNA in a biological sample under specific conditions. The NGS sequencing of 'BGI Transcriptome Sequencing Services' is performed with the Illumina sequencing system detecting single bases while being incorporated during synthesis, resulting in a true base-by-base sequencing. All single nucleotides are reversibly labeled with a particular fluorochrome being detected as each dNTP is added and cleaved to allow incorporation of the next base subsequently. Paired-end approach ensures detection of genomic rearrangements, repetitive elements and novel transcripts. This 'sequencing by synthesis' method minimizes errors especially with repetitive sequences like the high Adenine-Thymine content within *P. falciparum* genomes. The RNA samples consist of highly synchronized *P. falciparum* ring staged parasites within a time-frame of 6 to 10 hpi of human erythrocytes as the highest peak of *var* gene expression is expected at that time of parasitic development. The library preparation, quality control and transcriptome sequencing were carried out via the 'Illumina HiSeq 4000 PE100' system of BGI Global Genomic Services in Hong Kong. The RNA samples comply with the requirements with a minimum concentration of 20 ng/ml, a minimum total mass of 200ng per sample and a RIN value above '7'. Samples with lower values were ranked as 'risky' – should be considered during analysis.

4.2.27 Bioinformatic analysis of *P. falciparum* transcriptomes

The bioinformatic analysis of the RNA sequencing raw data, derived from the NGS analysis performed by BGI in Hong King was kindly supported by Dr. Stephan Lorenzen (BNITM, Hamburg). Using RSEM Bowtie version 2, the retained reads were aligned to the IT4/FCR3 *P. falciparum* genome, obtained from the actual version 2018-38 of www.plasmodb.org.^{204,205} The reads were aligned and the transcript abundance estimated. Mostly, raw counts are not directly comparable within and between samples, differential expression analysis was performed by utilizing DEseq version 1.6.0 bioconductor package.²⁰⁶ Thereby, all counts were normalized by a scaling factor, suited to the complete data set. Over all, a pairwise comparison between the 2 controls, IT4-ST and IT4-GFP, were performed, to determine the differential expression of genes in the mock-transfected population, setting a baseline for further analysis. Second, a multiple comparison was performed, including both control population and each enriched population individually. Third, an overall comparison of all normalized data was performed, including both controls and all 6 receptors. Finally, the *p*-values were adjusted using Bonferroni-Holm method with a false detection rate of 10%.

4.2.28 Seeding of CHO and HBEC-5i cells

The cells were seeded 48 h before the respective experiment e.g. static binding assay, inhibition assay or enrichment via panning assays. For this purpose, a plastic coverslip with a diameter of 13mm was first placed in each well of a 24-well plate for adherently growing cells, using sterile forceps. The coverslips were coated with 37°C prewarmed 0.1% gelatin solution, dissolved in PBS, with a volume of 500 µl per well for 30 min at

37°C. The gelatin solution was removed and the respective cells were seeded at 3×10^4 cells per ml onto 3 coverslips as triplicates for each cell line and endothelial receptor, respectively. The cells were incubated for 48 h at 37°C and 5% CO₂ until the beginning of the according experiment, while a mean of 60 to 80% confluency was to be expected. Additionally, the preparation of T25 or T75 culture flasks with a confluency of 80 to 90% of wildtype or mock-transfected cells for experimental preabsorption steps was carried out identically.

4.2.29 *P. falciparum* static binding assay

The investigation of the binding capability of *P. falciparum* parasitized infected erythrocytes to human endothelial receptors was carried out by means of static binding experiments. For this purpose, 48 h before the beginning of the experiment, the CHO cells, expressing the corresponding human endothelial receptor, were seeded on plastic coverslips. The infected population of erythrocytes was synchronized to ring stages using sorbitol 48 h prior the trial.

On the day of the static binding assay, the *P. falciparum* culture was adjusted to a parasitemia of 5% with trophozoite staged parasites of 24 to 32 hpi and diluted to 1% hematocrit with 37°C prewarmed binding medium. The adaptation of the IE population to the binding medium was carried out for 30 min at 37°C and 5% CO₂. Meanwhile, the culture medium of culture flasks including mock-transfected CHO cells with a confluency of about 80% for preabsorption was removed. Cells were washed and incubated with binding medium for 15 min at 37°C and 5% CO₂. The IE suspension was added and incubated at 37°C and 5% CO₂ for 1 h with gentle circular shaking every 15 min to ensure the elimination of non-receptor-specific binding IE. Subsequently, the CHO cells within the 24-well plate were carefully washed and incubated for 5 min with binding medium. The preabsorbed IE suspension was carefully applied to the CHO cells on the coverslips in a volume of 500 µl per well and incubated for 1 h at 37°C and 5% CO₂. During the whole time, the 24-well plate was gently circular rotated every 15 min into every direction. Subsequently, the coverslips were removed individually from the wells, carefully dipped once in 37°C prewarmed binding medium and transferred with the cell-grown side upside down to a new 24-well plate, containing 600 µl of 37°C prewarmed binding medium. The well plate was placed for 45 min at RT at an angle of 45°, thus enabling all unbound erythrocytes to gravitationally sink down to the bottom of the well. The fixation of the CHO cells with the bound IE was carried out in 1% glutaraldehyde, dissolved in PBS at RT for at least 30 min under a hood. Subsequently, the cells were stained with a 10% Giemsa staining solution, dissolved in Weiser-Buffer and filtrated by paper for 15 min at RT. The coverslips were washed 3 times with clean water and were air-dried subsequently. Finally, triplicated coverslips were mounted with cell-side down on a glass slide and allowed to dry overnight at RT.

For the evaluation, 500 CHO cells as well as the bound IE were counted for every coverslip 3 times in independent fields of vision using a 40x magnification of a light microscope, resulting in mean values of 9fold counted setups.

4.2.30 Cytoadhesion inhibition assay with specific antibodies

To determine the specificity of the achieved binding of distinct *Plasmodium* isolates to respective human ligands on cell surfaces, a cytoadhesion inhibition assay with specific antibodies was carried out. For this experimental setup, 48 h before the beginning of the experiment, the CHO cells were seeded on plastic coverslips within a 24-well plate and cultured as usual until further use. The highly synchronized IE population was adjusted to a parasitemia of 5% with trophozoite staged parasites of 22 to 28 hpi. Furthermore, the specific antibody to the respective CHO cell line, dissolved in DPBS, were added to the CHO cell containing wells in required concentrations. As negative control, a suspension including DPBS only was processed and used identically. The cells were incubated for 30 min at RT. Afterwards, the antibody suspension was removed and cells were washed 3 times. The preincubated IE suspension was carefully applied on the CHO cells on the coverslips in a volume of 500 µl per well. The well plate was incubated for 1 h at 37°C and 5% CO₂ with gently circular rotations every 15 min. All further steps were identically to the *P. falciparum* static binding assay.

4.2.31 Cytoadhesion inhibition assay with soluble CSA (sCSA)

To determine the specificity of IE binding towards CSA on cell surfaces, a cytoadhesion inhibition assay with soluble CSA (sCSA) was carried out. Here, the binding of differently cultivated IT4 isolates on HBEC-5i was focused in particular. For this experimental setup, 48 h before the beginning of the experiment, the HBEC-5i cells as well as CHO-CD36 cells were seeded on plastic coverslips within a 24-well plate and cultured as usual until further use. A highly synchronized IE population was adjusted to a parasitemia of 5% with trophozoite staged parasites of 22 to 28 hpi. The suspension was diluted in a reaction tube to a hematocrit of 1% with 37°C prewarmed DPBS. Furthermore, the sCSA, dissolved in DPBS, was added to the reaction tube in required concentrations. As negative control, a suspension including soluble BSA, dissolved in PBS was processed and used identically. The suspensions were incubated for 30 min at 37°C. Meanwhile, the culture medium of the HBEC-5i cells was removed and the cells were washed and incubated for 5 min with 37°C prewarmed DPBS. Afterwards, the preincubated IE/sCSA or IE/sBSA suspension was carefully applied on the HBEC-5i cells on the coverslips in a volume of 500 µl per well. The well plate was incubated for 1 h at 37°C and 5% CO₂ with gently circular rotations every 15 min. All further steps were identically to the *P. falciparum* static binding assay except the use of DPBS instead of binding medium, to avoid interference caused by the high sugar concentration.

4.2.32 Enriched *P. falciparum* populations via panning assays

In order to achieve sufficient amounts of a homogenous IE population, capable for specific binding of a distinct human endothelial receptor, it is necessary to enrich the parasite populations via a panning procedure.

Two days prior the enrichment, highly fluorescent CHO cells were seeded to a confluency of 80% on the day of the assay. Firstly, corresponding to every single

panning assay of every investigated *P. falciparum* strain, mock-transfected, CHO cells were seeded in a separate culture flask to perform adequate preabsorption steps to ensure the elimination of non-receptor-specific binding IE. Secondly, CHO cells, expressing the investigated human endothelial receptor were seeded in separated culture flasks for every panning experiment, to perform the actual enrichment. The enrichment was carried out with highly synchronized IE population of at least 10% trophozoite staged parasites at 24 to 32 hpi.

On the day of the panning enrichment, the culture medium of mock-transfected CHO cells for preabsorption was removed. Cells were washed and incubated with binding medium for 15 min at 37°C and 5% CO₂. The parasite culture was centrifuged for 3 min at 800 x g and resuspended in 15 ml of 37°C prewarmed binding medium. Undiluted IE suspension was added to preabsorption culture flask and incubated at 37°C and 5% CO₂ for 1 h with gentle circular shaking every 15 min to ensure the elimination of non-receptor-specific binding IE. Meanwhile, the culture medium of CHO cells, expressing the receptor of interest was removed and cells were washed and incubated for 15 min with 37°C prewarmed binding medium. The preabsorbed IE suspension was added into the culture flask of the receptor expressing CHO cells and incubated for 30 min at 37°C and 5% CO₂ with gentle circular shaking every 15 min. Afterwards, supernatant including unbound IE was carefully removed by washing the culture flask in an upright position for 5 to 7 times with 37°C prewarmed binding medium. The remaining firmly bound IE were examined under an inverted light microscope. Ultimately, the culture flask was filled with 15 ml of *Plasmodium* completed culture medium (RPMI+HS) and 300 to 500 µl uninfected blood. The specific panned *Plasmodium* population remains within the culture flask to enhance the new infection of erythrocytes within the next round of replication. The IE suspension was incubated in a vacuum container with a gas mixture of 1% O₂, 5% CO₂ and 94% N₂ and a constant temperature of 37°C for about 20 to 26 h.

> **GFP:** For IT4 populations, enriched over mock-transfected CHO cells, (GFP) the preabsorption step was not necessary.

> **Knob-induction:** For knob-induction experiments, the preabsorption step was carried out for CD55 only

4.2.33 IE harvest for using Biocoll separating solution

Different cell types can be separated due to their different densities from another by density gradient centrifugation using Biocoll separating solution. For further cultivation, this method was used about 20 to 24 h post panning experiments, for the separation of ring staged IE and CHO cells after each round of enrichment. Biocoll separation solution contains the hydrophilic polymer polysucrose with a molecular weight of about 400 kDa, that can be used to generate aqueous solutions with a density up to 1.1 g/ml. CHO cells have an average density of 1.05 g/ml, while the average density of erythrocytes is 1.1 g/ml. Thus, during centrifugation, the IE migrate down through the Biocoll separation solution while the CHO cells remain floating on top of the Biocoll solution.

After every round of enrichment, the supernatant of the culture flask was collected in a 15 ml reaction tube, including IE, non-IE, CHO cells, debris and other particles from

cell culture. The suspension was centrifugated for 5 min at 800 x g while 7 ml of Biocoll separating solution was placed in another 15 ml reaction tube. The supernatant of the suspension was removed and the pellet was resuspended in 7 ml of 37°C prewarmed *Plasmodium* completed culture medium. Then, the suspension was pipetted dropwise and very carefully at the edge of the reaction tube, layered on top of the Biocoll separating solution, so the both liquids did not mix. Subsequently, the gradient was centrifuged for 20 min at 1300 x g without centrifugal breaks. After centrifugation, the supernatant was removed and the pellet was washed 3 times with 5 ml of 37°C prewarmed *Plasmodium* completed culture medium, with centrifugations at 800 x g for 3 min. Finally, the pellet was resuspended and the parasitemia was determined for further cultivation, using Giemsa staining. The hematocrit was adjusted according to experimental requirements.

4.2.34 *P. falciparum* harvest for RNA isolation using TRIzol

P. falciparum IE harvest can be carried out either with a highly synchronized and highly ring staged parasitized culture or subsequently after a round of enrichment, yielding a sufficient amount of ring staged parasitized IE. The chemical with the brand name TRIzol is also known as guanidinium-thiocyanate-phenol-chloroform-extraction due to its ingredients. During disruption and breaking down of cells and cell compartments as well as the inactivation of RNases and other enzymes, the RNA integrity remain intact and dissolves within the phenol phase.

To harvest cells for RNA isolation, the parasite culture was transferred to centrifuge tubes and centrifuged at 1000 x g for 5 min. The supernatant was removed, the pellet was quickly resuspended in the 20fold volume of 37°C prewarmed TRIzol reagent and incubated for 5 min in a 37°C water bath. The resuspension was carried out rapidly with juddered movements under a hood to ensure a rapid and evenly distribution of the reagent. Afterwards, the sample can be used immediately for RNA isolation. For long-term storage, the reaction tube containing the sample was quickly frozen at -80°C until further use.

4.2.35 IFA – Immunofluorescence assay

> *P. falciparum*

For immunofluorescence analyzes, a *Plasmodium* culture, containing high trophozoite and schizont staged parasitized IE was used. Thin blood smears were prepared by thinly spread 10 µl of *Plasmodium* sedimented culture on a glass slide. The slide was air dried and fixed for 10 min in -20°C, already precooled 100% absolute methanol. Afterwards, the glass slides were air dried, carefully stored in thin, lint-free paper towels and additionally wrapped in aluminum foil. The slides were stored at -20°C until further use.

> Adherent cells

One glass coverslip was placed within a well of a 24 well plate by using sterile forceps. If required, each coverslip was coated with 0.1% gelatin and incubated for 30 min at 37°C. The coating solution was removed and adequate number of about

1x 10⁶ cells/ml of cells, dissolved in respective amount of completed growth medium were seeded 48 h prior the assay. Further handling was carried out with one cell-grown glass coverslip instead of one square, mentioned below.

The immunofluorescence assay was carried out at RT. For the handling with glass slides, a silicon distributing DakoPen was used to draw 6 to 8 squares on top of the dry glass slide containing the fixed thin blood smear. To rehydrate the squares, *Plasmodium*-PBS was carefully pipetted in each square and incubated for 5 min at RT. The rehydration was carried out 3 times subsequently. Afterwards, the first antibody was diluted in PBS/1% BSA and 50 µl were loaded within the respective square. The slide was incubated for 2 h at RT within a humid dark box.

Following this, the antibody solution was completely removed and each square was washed and incubated 5 times with *Plasmodium*-PBS for 5 min at RT. Meanwhile, the second antibody has been dissolved in PBS/1% BSA and one of the core/DNA-dye Hoechst or DAPI was added in a respective dilution. Next, 50 µl of the antibody-dye suspension were added to the respective square. The slide was incubated for 2 h at RT within a humid dark box. Again, the antibody solution was completely removed and each square was washed and incubated 5 times with *Plasmodium*-PBS for 5 min at RT. The slide was air dried and embedded with some drops of Moviol mounting solution, carefully placed dropwise on every square, lidded with a large rectangular glass coverslip, avoiding air bubbles between the layers. The antibody stained blood smears were air dried over night at RT and analyzed using a 60x magnification of a fluorescence microscope. As negative control, one square was stained only with the second antibody, performing the same steps as mentioned above with a 0.1% PBS/BSA solution instead of the first antibody solution.

4.3 Biotechnical methods

The following techniques and protocols were applied to process the biological samples within the FACS and TEM procedures.

4.3.1 FACS analysis for further cultivation

CHO cells, expressing their respective human endothelial receptor on their surface, were analyzed and if necessary enriched, by the mean of flow cytometry to increase the proportion of fluorescent positive cells. By the use of the FACS Aria III device via fluorescence activated cell sorting, cells can be enumerated and separated according to several characteristics, such as viability, shape, structure and fluorescence appearance. Using flow cytometry, cell can be analyzed at high speed by passing an electrical voltage and laser beams. Thus, CHO cells, negative in auto-fluorescence or antibody staining can be sorted out from CHO cells, expressing the respective surface protein and the fused marker protein, visible as auto-fluorescence or detectable specific by non-permeabilizing and fluorochrome conjugated antibody staining. This procedure was carried out periodically when the microscopically

determined fluorescence level of CHO cells dropped under 80% or shortly before experimental setups.

Here, this method is explained exemplarily with the CHO-CD36 cell line. The CHO cells are transiently transfected with the pAc-GFP-N1 vector, additionally carrying the sequence of the human endothelial receptor CD36. This construct result in a produced fusion protein of CD36::GFP. As the CD36 protein is presented on the surface of the transgenic CHO cell, it can be detected by a specific non-permeabilizing conjugated antibody. The antibodies derive from the host species mouse and is reactive against human CD36 epitopes. It is conjugated with the far-red emitting fluorophore APC (allophycocyanin), exhibiting a peak emission at 660 nm after an activation with 594 nm to 633 nm laser and Cy5 filter set. The GFP of the fusion protein is located intracellular within the CHO cell cytoplasm, resulting in a bright-green auto-fluorescence of the cell. This auto-fluorescence can be detected with a 488 nm laser line and a FITC filter set, exhibiting a maximum emission at 525 nm. Due to these specifications, cells double-positive (+/+) for expression of the reporter marker protein GFP as well as the human endothelial receptor protein on the surface can be detected and specifically selected.

Furthermore, PE (phycoerythrin) was used as conjugated to second antibodies, as well as Alexa Fluor 488 and Alexa Fluor 594 (artificial dyes) as conjugated second antibodies.

4.3.2 FACS staining procedure

For FACS analysis, it is very important to collect the CHO cells in Ham's F12 medium, without, or at least in amounts below 1% iFCS as the serum can cause clogging of the nozzle and pipe system within the FACS Aria III device. Designated FACS puffer can be used if the analyzed cells are disposed afterwards. For further cultivation approaches, regular culture medium is recommended. Furthermore, it is essential to minimize contaminations, as the FACS Aria III device as well as the handling is only semi sterile and not feasible under clean bench conditions. To ensure a stable and consistent sort performance, the FACS Aria III device needs some lead time, so it is advisable to start the device and set all required temperatures at least 1 h in advanced.

Meanwhile, CHO cells were detached from the culture flask using accutase and transferred into a 15 ml reaction tube. Cell number was calculated using a Neubauer counting chamber. For the regular review of the cell and fluorescence integrity, a cell number of 1×10^6 cells/ml was sufficient. For experimental setup or enrichment of double-positive cell populations, all detached cells can be used for sorting. Cells are separated into individual reaction tubes, designated for FACS approaches. One tube was used for one distinct staining approach and was centrifuged for 2 min at $800 \times g$. The supernatant was removed and cells were resuspended and incubated for 30 min on ice in dark within the respective amount of the first antibody dilution.

If necessary, a second antibody can be used. Therefore, the cell suspension containing the first antibody was washed 5 times with 1 ml PBS and centrifuged at $800 \times g$ for 2 min. The supernatant was removed and cells were resuspended and incubated for 30 min on ice in the dark within the respective amount of the second antibody dilution.

Afterwards, the cell suspension containing the antibody dilution was washed 5 times with 1 ml PBS and centrifuged at 800 x g for 2 min. The supernatant was removed completely and cells were resuspended in up to 3 ml of Ham's medium without iFCS. Cells were stored as short as possible at +4°C in the dark, until further use.

4.3.3 FACS sorting procedure

For FACS approach with subsequent sorting of the designated cell population, the cell suspension was filtered through CellTrics FACS filters with a mesh size of 30 or 50 µm, to separate cell accumulations and to minimize the risk of pipe clogging. The filtered cell suspension was inserted into the FACS Aria III device and processed with the 85µm nozzle. The speed was set to a maximum of level '6' with a maximum of 3.000 events per second. The cells were sorted within the 37°C prewarmed setup for 6- or 24-well plate-sorting, adjusted by the far-left stream calibration. Laser and filter sets were selected and calibrated as required. The selection for the individual sort layout was set to purity sorting up to a previously determined average counted cell number, usually 500.000 cells per well. According to the experimental setup, the selected cell population was collected in a 37°C prewarmed 6- or 24-well plate, containing Ham's F12 completed culture medium, including iFCS and, if necessary, 7 µl/ml G418 as selection marker. The sorted cells were cultivated as usual with a daily change of medium and selection for the first 3 days after sorting.

4.3.4 FACS gating strategy

To ensure the collection of only double positive, viable CHO cells, gating strategy was carried out under consideration of the consecutive stepwise hierarchy of the individual gating. Unstained WT or mock-transfected CHO cells served as negative control and were used to set an adequate baseline of auto-fluorescence and non-fluorescence areas. The usual gating strategy is shown in **Figure 11**.

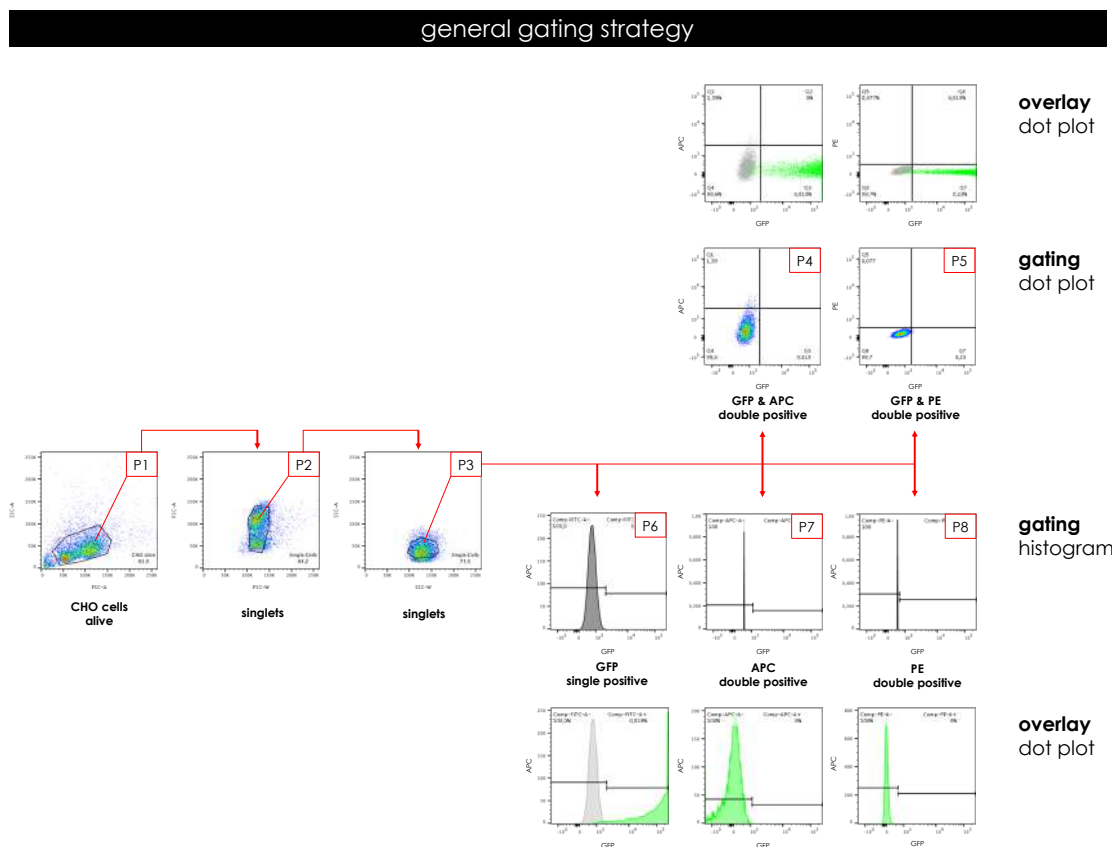


Figure 11. General gating strategy to sort double positive CHO cell populations using the FACSAriaIII device. Transgenic CHO cells were resuspended in CHO culture medium, lacking iFCS, sorted by the use of the FACSAriaIII device with an 85 μm nozzle and a medium flow velocity, while analyzed simultaneously with the FACSdiva software. The CHO cells were sorted for viability, GFP marker fluorescence as well as surface receptor specific and non-permeabilizing antibody staining using APC or PE, respectively. The following gating was applied for all cell lines: **P1**: living CHO cells; **P2**: singlets by forward scattering; **P3**: singlets by sideward scattering. All following gates emerge from P3. **P4**: double positive cells by plotting GFP against APC; **P5**: double positive cells by plotting GFP against PE. **P6**: GFP histogram for single positive cells; **P7**: APC histogram, emerging from P6 for double positive cells; **P8**: PE histogram, emerging from P6 for double positive cells. The overlay of 2 or more particular gates discriminate different cell population visually.

Gate P1 select for living and viable cells via granularity, size and shape. Gate P2 and P3 select for singlets (single cells) by forward and sideward scattering. Gate P4 and P5 emerge from P3 and select for double positive cells by plotting the GFP channel against the APC or PE channel respectively. Cells appearing in the 2 right quadrants are GFP positive, cells appearing in the 2 top quadrants are APC or PE positive. Thus, the top right quadrant selects for double positive, while the down left quadrant selects for double negative cells. So, the top left and bottom right quadrant select for only single positive cells.

Another gating strategy is the use of histograms instead of scattered dot plots. Here, gate P6 show GFP single positive cells, emerging from singlets, selected by P3. Gate P7 or P8 select for APC or PE positive cells respectively, emerging directly from P6 and thereby each of both histograms show double positive cells. Exemplarily, unstained

CHO WT cells are plotted to show the general gating strategy as well as to set the general baseline for further gating and sort approaches.

To compare 2 or more populations, dot plot or histogram gates can be overlaid for a visualization more clearly. Here, unstained CHO-WT cell, exhibiting no fluorescence and CHO-GFP cells, exhibiting GFP fluorescence could be discriminated due to the overlay of the 2 particular gates. Via pseudo coloring, CHO-WT population still appears in grey, while CHO-GFP population appears in green. Within all overlaid plots, the grey color indicates CHO WT population, exhibiting no fluorescence at all. The green color indicates unstained CHO cell populations, only expressing cytosolic GFP. The red color indicates stained CHO cells, either with APC or PE labeled antibodies, unique for the sorted receptor, appearing in red. The cyan color indicates a cell population, stained with a FITC antibody, usually appearing also in green.

The evaluation of the data was carried out using FACS Diva software, version 6.1.3.

4.3.5 *P. falciparum* separation using Percoll gradient solution

The separation of the parasite stages can also be carried out on the basis of a density gradient centrifugation using Percoll gradient solution. The preparation of a Percoll gradient with differently concentrated Percoll solutions and centrifugation allows separation between parasitized IE of different stages as well as other cell culture particles. Non-IE and ring staged IE have an average density of 1.1 g/ml and sediment on the bottom of the gradient, below the 80% Percoll solution. Trophozoite staged IE, with an average density of 1.062 g/ml float at the lower of the 2 middle phases, between the 80% and 60% Percoll solution, with a density of 1.082 and 1.061 g/ml, respectively. The schizont staged IE have a mean density of 1.075 g/ml and float on the upper of the 2 middle phases of 60% and 40% Percoll solution. Those stages are clearly visible as brownish rings, floating between clear phases. Merozoites, cell debris and other cellular particles float on top of the 40% Percoll solution, above a density of 1.046 g/ml.

Here, trophozoite and schizont staged IE were isolated, using Percoll density gradient centrifugation. The Percoll gradient consist of 3 layers of different densities. For this purpose, 1 ml of 80% was pipetted into a 15 ml reaction tube. 1 ml of 60% and subsequently 40% Percoll solution was pipetted dropwise and very carefully on top of the previous solution. The *Plasmodium* culture was centrifuged for 3 min at 800 x g. While the supernatant was removed, the pellet was resuspended in 1 ml PBS and layered dropwise and very carefully on top of the Percoll gradient stacks. The whole gradient was centrifuged for 5 min at maximum speed. Afterwards, the trophozoite staged IE, located within the circular brownish layers, floating in the middle of the reaction tube were carefully collected by pipetting. The acquired sample was washed 3 times with 1 ml of 37°C prewarmed PBS and centrifugation for 2 min at 800 x g. For electron microscopy, the pellet was resuspended in 700 µl of fixation solution, containing 2.5% glutaraldehyde and 2.5% paraformaldehyde in PBS at pH 7.2.

4.3.6 Transmission electron microscopy (TEM)

In order to investigate various *Plasmodium* isolates, cultured under distinct conditions, transmissive electron microscopy was conducted within the core facility of the BNITM, accompanied by Dr. Katharina Höhn. The phenotypical appearance of IE in general and the occurrence of knob structures on the surface in particular was focused. Therefore, trophozoite and schizont staged IE were prepared according to experimental requirements, while the fixated IE pellets were kept as brief as possible at 4°C prior further chemical embedding procedures.

For every single procedure, it is important to wear a **new** double layer of nitrile gloves to avoid direct contact with the highly toxic chemicals.

For sample preparation, the 20 to 32 hpi trophozoite and schizont staged, Percoll-enriched IE cells were fixed with a fixative containing 2.5% glutaraldehyde and 2.5% paraformaldehyde. The sample was transferred into 1.5 ml reaction tubes with safe locks and subsequently centrifuged for 5 min at 800 x g. Afterwards, the fixative supernatant as well as the pipette tips were removed and disposed into an extra waste container. The pellet was resuspended and washed twice with 50 mM Cacodylate trihydrate buffer at a pH of 7.4, with intermediate incubation times for 5 min at RT. The supernatant as well as the pipette tips were removed and disposed into an extra waste container. This step is crucial to avoid micro-precipitations on thin sections, maybe occurring with the handling of phosphate buffers, if the sample is not rinsed very well between pre- and post-fixation.

The supernatant was removed except a thin layer to keep the sample covered. The pellet was resuspended and post-fixed in 2% Osmium-(VIII)-Oxid (OsO_4), dissolved in H_2O and incubated for 45 min in the dark on ice. Afterwards, the sample was washed 3 times with dH_2O and centrifuged for 2 min at 1000 x g. The supernatant as well as the pipette tips were removed and disposed into an extra waste container.

The pellet was resuspended and heavy metal stained in the smallest possible volume of 1% uranyl acetate and incubated for 45 min in the dark at RT. Afterwards, the sample was washed 3 times with dH_2O and centrifuged for 2 min at 1000 x g. The supernatant as well as the pipette tips were removed and disposed into an extra waste container.

The pellet was resuspended for dehydration of the remaining dH_2O in an ethanol series with stepwise increasing alcohol concentrations. The pellet was incubated for 5 min and centrifuged at 1000 x g for every individual step: 1x 50% ethanol, 1x 70% ethanol, 1x 80% ethanol, 2x 95% ethanol and 3x 100% ethanol. If necessary, the sample was divided into several specimens, while 20 to 30 μl pellet per sample was considered as optimal.

Epoxy resin 812 (EPON) is stored at -20°C and was thawed at RT about 30 min prior the next step. The supernatant of the pelleted sample was removed except 10 to 20 μl of 100% ethanol to keep the sample covered. An equivalent volume of 100% EPON was poured on the pellet and the sample was resuspended by gentle pipetting. The suspension was incubated overnight at RT with open lid under the hood to allow the evaporation of the remaining ethanol.

On the next day, the sample was centrifuged several times for 3 min at 800 x g to

sediment the IEs. The supernatant as well as the pipette tips were removed and disposed in an extra waste container. The pellet was covered with 200 to 400 μ l of 100% EPON and incubated for at least 3 h at RT under the hood. Afterwards, the supernatant as well as the pipette tips were removed and disposed in an extra waste container. The pellet was covered with 200 to 500 μ l EPON and incubated for 1 to 3 days at 60°C in a designated oven under the hood to ensure constant and even polymerization of the EPON embedded sample pellet. Thereafter, the sample was pulled out of the reaction tube and stored at RT until further use.

In order to get an even and flatly shaped sample surface, the EPON cone, containing the IE pellet at the bottom tip was trimmed by the use of a sharp razor blade. The cone was clamped in a designated bracket of the Leica Ultracut UC7 microtome. Several ultrathin cuts of the sample were processed with a cutting size of 55 to 65 nm. The sections were collected by the use of a 'Perfect Loop' tool and placed on 80 mesh sized copper grids. The grids were stored at RT until further use.

The analysis and picture taking was conducted with the Tecnai Spirit transmission electron microscope, operated at an accelerated voltage of 80 kV. At least 100 cells per grid were examined and a representative number of adequate pictures were taken for further evaluation, using ImageJ software, version 1.52a.

5 RESULTS

5.1 Physiological relevance of a chosen human receptor set

Proof of concept – to decide for a physiological relevant set of receptors, to be investigated within this thesis, the cell surface composition of human brain endothelial cell line (HBEC-5i) was characterized by the use of transcriptomics; additionally, a staining panel of 18 specific and non-permeabilizing antibodies with subsequent FACS analysis was performed, shown in **Figure 12**.

The course of disease in the most physiological but still practicable way was simulated by cultivation of the cell line using 3 different culture conditions. Firstly, the HBEC-5i cells were constantly cultivated at 37°C; results are shown in blue. Secondly, HBEC-5i cells were constantly cultivated at 37°C with at least 3 periods of heat shocks at 40°C for 1.5 h, to mime reoccurring fever conditions in the febrile phase of the disease within the human body; the results are shown in red. Thirdly, HBEC-5i cells were constantly cultivated at 37°C and additionally stimulated with TNF α to simulate the host immune reaction and trigger cellular immune response; the results are shown in green. The upper section shows FACS results, while height of the bars represents the percentage of positively stained cell populations compared to the whole cell population detected. The lower section shows the RNA expression level of selected genes after analyzing NGS transcriptome data, normalized to the respective read counts.

The presence of various receptors could be detected with both methods, while the results correlate with each other. CD9, CD151, TNFR1, CD55, CD81 and EPCR are highly represented within human brain endothelial cells on the transcriptome level and were also highly detectable using FACS analysis. The expression level of CD44 was significantly (p ***; 0.0046) increased in the transcriptome of the TNF α stimulated HBEC-5i cells. This is in correlation with the high amounts of CSA, detectable in the FACS analysis as the macromolecule is bound to proteins as part of the proteoglycan within the Golgi apparatus. CD62-E, CD62-P, MDR1, TNFR2, CD37, CX3CL1, EPOR and NCAM1 are barely represented within the transcriptomes and consequently only detectable by antibody staining in less than 25% of the cell population. However, also CD36 is barely expressed on human brain endothelial cells, albeit it plays a key role in cytoadhesion of IE. Hence, and in line with those findings, receptors barely expressed on HBEC-5i are also chosen for further investigations due to their potential relevance in IE adhesion and (severe) malaria disease. Furthermore, the levels of ICAM-1 are significantly elevated (p ****; 0.0004) after stimulation with TNF α in the transcriptome, while also in the FACS analysis, a clear tendency is obvious. This is in physiological consensus, as the usual host immune response also trigger an intense upregulation of ICAM-1 by about 50%.

> Taken together, the set of human endothelial receptors to be investigated within this thesis are either already described to bind *P. falciparum* IE within previous studies or tend to be crucial for severe and cerebral malaria disease due to their localizations within the human brain. Therefore, it is reasonable to investigate those potentially

(new) interaction partners, playing a key role in *falciparum* malaria infection in general, and within the febrile and immunogenic phase of the infection in particular.

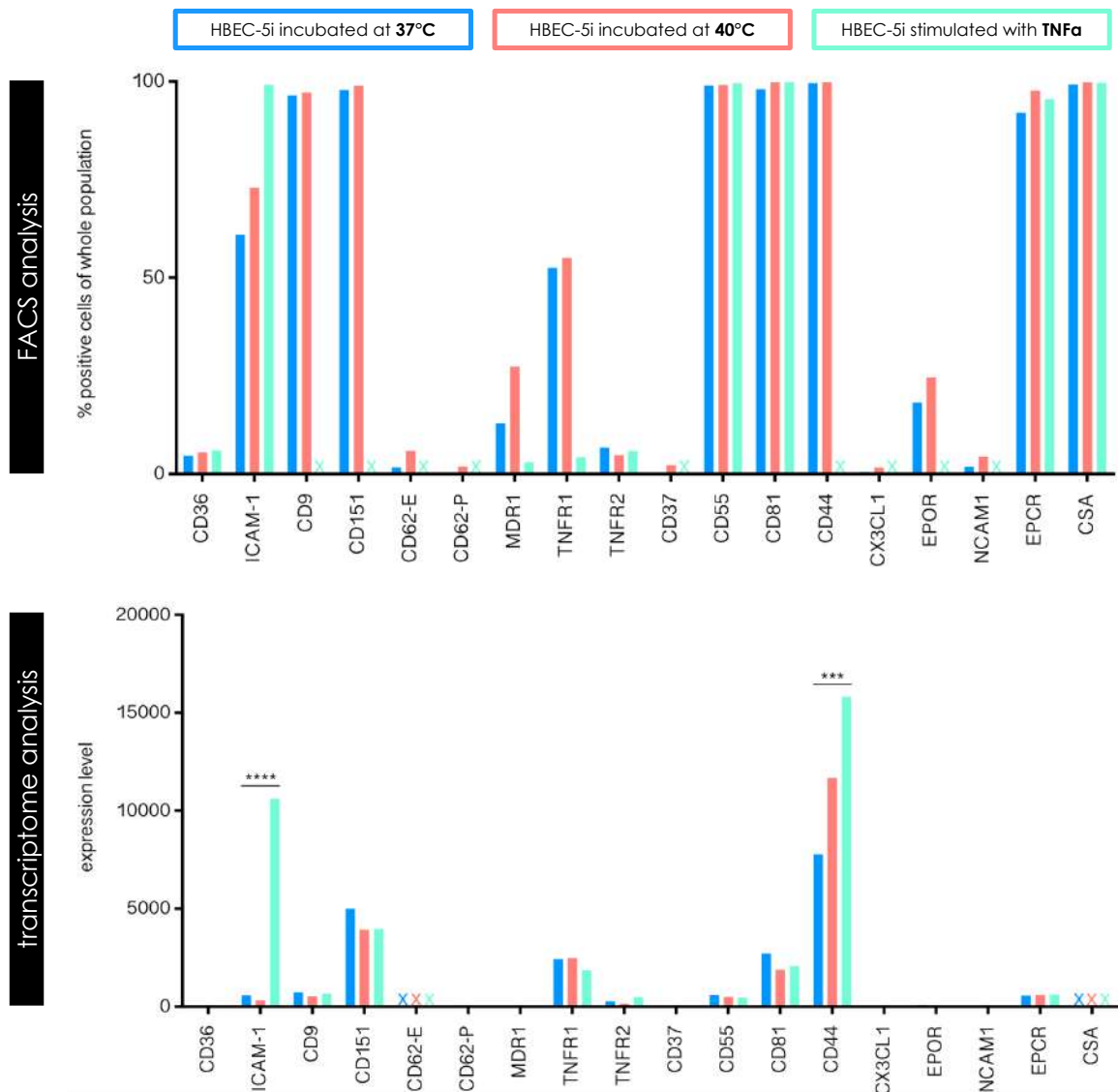


Figure 12. FACS analysis and transcriptome analysis* of HBEC-5i cells, incubated at either 37°C, 40°C or stimulated with TNFa. HBEC-5i cells were characterized by the use of specific non-permeabilizing antibody staining and subsequent FACS analysis and transcriptomics, as 3 different culture conditions were tested. The upper section shows FACS results, while height of the bars represents the percentage of positively stained cell population compared to the whole cell population detected. The lower section shows the RNA expression level of selected genes after analyzing NGS transcriptome data, normalized to the respective read counts. The red bars indicate HBEC-5i cells, constantly cultivated 37°C. The blue bars show HBEC-5i, constantly cultivated at 37°C with repetitive heat shocks at 40°C for 1.5 h. The green bars indicate HBEC-5i, constantly cultivated at 37°C and additionally stimulated with TNFa. For crossed samples, data are not available. Statistical significance was calculated by a two-way ANOVA with a Tukey correction for multiple comparisons and a 95% CI with **** $p \leq 0.0001$; *** $p \leq 0.005$. Transcriptome data from the HBEC-5i cells were subjected by another project within the Bruchhaus-Laboratory.

5.2 CHO repertoire, FACS data & fluorescence microscopy

In order to generate transient transfected CHO cells, expressing a specific human endothelial receptor on their surface, CHO cells were transfected with either pAc-GFP1-N1 or pEGFP-N1 plasmid, containing one specific human endothelial receptor fused to the expression marker GFP. The receptor forms the extracellular part of the fusion protein whereas the GFP is located in the cytoplasm of the cell without affecting the extracellular domain. CHO-pAc-GFP1-N1 (mock) control cell line was solely transfected with the GFP-bearing expression vector, lacking any receptor sequence, consequently synthesizing cytosolic GFP only. In total, 16 transgenic cell lines could be generated: CHO-WT, CHO-GFP, CHO-CD36, CHO-ICAM-1, CHO-CD9, CHO-CD151, CHO-CD62-E, CHO-CD62-P, CHO-VCAM1, CHO-HRH1, CHO-MDR1, CHO-TNFR1, CHO-TNFR2, CHO-CD37, CHO-CD55 and CHO-CD81.

To ensure that all CHO cell lines were transfected successfully and that human endothelial receptors are expressed and detectable by specific antibodies on their surface, a flow cytometric analysis was performed, following the general gating strategy, mentioned above. Furthermore, the fluorescence pattern of the cytosolic marker protein GFP was investigated by fluorescence microscopy with living cells. In the following, **Figure 13.1** and **Figure 13.2** show the individual microscopic images as well as the FACS results of the transgenic CHO cell lines.

The percentages of particular cell populations, compared to the previous gate, are given in any section. Thereby, the percentage of GFP single positive cells include the APC or PE antibody stained and therefore double positive cell population. In the shown graphic, the black labels comprise the CHO-WT and CHO-GFP cell lines, serving as negative controls. The CHO-WT cell line does not express any marker fluorescence and could not be stained with the specifically used antibodies. Thereby, CHO-WT cells appear only within the double negative gates, providing the general baseline for further gating and sort approaches. The CHO-GFP cell line only expresses the cytosolic marker protein GFP (89.1% GFP single positive), thus appearing within the GFP positive gates, while remains negative for receptor specific APC or PE staining. The white labels indicate transgenic CHO cell lines, expressing a specific human endothelial receptor on their surface, known to bind *P. falciparum* infected erythrocytes.

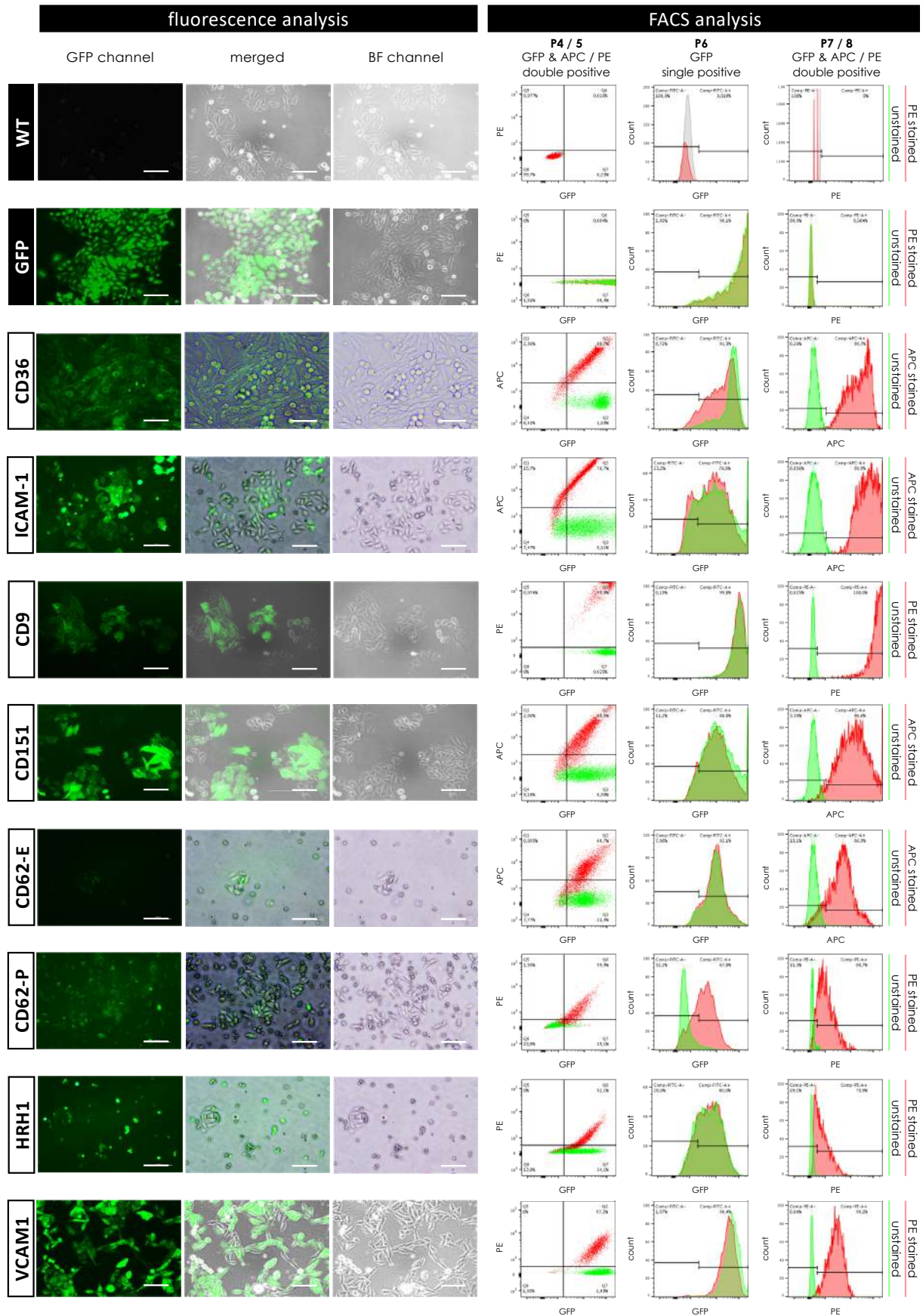


Figure 13.1 (to be continued). Fluorescence analysis and FACS analysis of transgenic CHO cells, expressing human endothelial receptors.

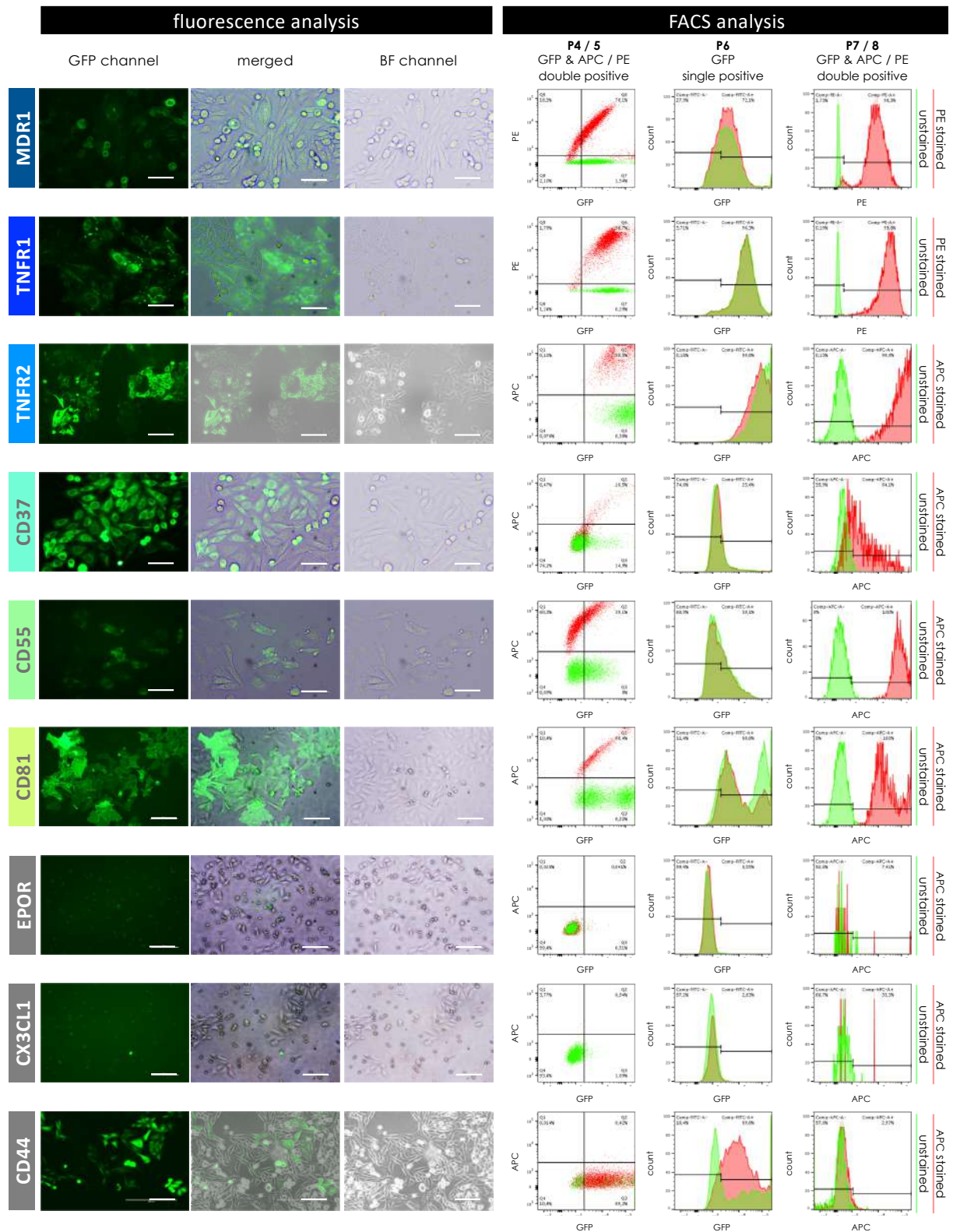


Figure 13.2 (continued). Fluorescence analysis and FACS analysis of transgenic CHO cells, expressing human endothelial receptors. The black labels indicate the CHO cell lines, serving as negative controls: non-transfected WT cells and mock-transfected (GFP) cell. The white labels indicate transgenic CHO cell lines, expressing a human endothelial receptor on their surface, known to bind *P. falciparum* infected erythrocytes. Those cell lines were used in several experimental setups. The 6 blue and green labels indicate transgenic CHO cell lines, expressing a human endothelial receptor, potentially bind *P. falciparum* IE, that were especially focused

within this thesis. The grey labels indicate transgenic CHO cell, expressing potential IE binding receptors, while the final establishment of the cell lines failed. The left section shows individual fluorescence images, recorded with EVOS FLauto fluorescence microscope at a 40x magnification. Green fluorescence, recorded via the GFP channel indicates the expression of cytosolic marker protein GFP in a distinct pattern. In the brightfield (BF) channel, cells were recorded with transmitted light. Both images were merged subsequently. Scale bar: 50 μm . The right section shows the results of the FACS analysis of the transgenic CHO cell lines, following the general gating strategy. Unstained GFP expressing cells are plotted in green, while APC and PE surface stained cells are plotted in red, as stated on the right side of the graph. The left section shows the individual microscopic images, taken by the EVOS FLauto fluorescence microscope, with a 40x magnification. Green fluorescence, recorded via the GFP channel indicates the expression of cytosolic marker protein GFP in a distinct pattern. In the brightfield (BF) channel, cells were recorded with transmitted light. Both channels were recorded separately and images were merged together subsequently, with a scale bar of 50 μm . In the right section, the FACS gates show the actual cell population via an overlay view that merges the same individual gate of the respective cell line. Unstained CHO cells are plotted together with specifically stained CHO cells of the same parental population. Here, the grey color indicates unstained CHO-WT cell populations with no fluorescence exhibited. The green color indicates unstained CHO cells, expressing cytosolic GFP only. The red color indicates CHO cell populations, expressing a specific human endothelial receptor on their surface, additionally stained with the red appearing APC or PE antibody, respectively.

The white label comprising CHO-CD36 (91.3% GFP and 99.7% GFP & APC positive), CHO-ICAM-1 (76.8% GFP and 99.9% GFP & APC positive), CHO-CD9 (99.8% GFP and 100% GFP & PE positive), CHO-CD151 (88.8% GFP and 96.6% GFP & APC positive), CHO-CD62-E (92.1% GFP & 86.9% GFP & APC positive), CD62-P (67.8% GFP and 88.7% GFP & PE), CHO-HRH1 (80.0% and 70.9% GFP & PE) and CHO-VCAM1 (98.4% GFP and 99.2% GFP & PE) cell lines, used in several experimental setups subsequently. The grey labels combine the transgenic cell lines CHO-EPOR (0.55% GFP & 7.41% GFP & APC), CHO-CX3CL1 (2.83% GFP and 33.3% GFP & APC) and CHO-CD44 (89.6% GFP and 2.97% GFP & APC), expressing potential IE binding receptors, while the final establishment of the cell lines failed. Eventually, it was either not possible to detect a sufficient number of cells, expressing GFP, or detected cells lacking specific surface antibody staining with APC or PE respectively. However, the transgenic cell lines CHO-MDR1 (72.1% GFP and 98.3% GFP & PE), CHO-TNFR1 (96.3% GFP and 99.8% GFP & PE), CHO-TNFR2 (99.8% GFP and 99.9% GFP & APC) belong to the dark blue label, are also known to bind *P. falciparum* IE and were particularly focused within this thesis. Furthermore, the light blue label includes CHO-CD37 (25.4% GFP and 64.1% GFP & APC), CHO-CD55 (39.1% GFP and 100% GFP & APC) and CHO-CD81 (88.6% GFP and 100% GFP & APC) cell lines, potentially able to bind *P. falciparum* IE in a pertinent manner. Also, those cells lines were especially focused within this thesis.

> Taken together, it was possible to establish 16 out of 19 transgenic CHO cell lines with a reliable level of detectable human endothelial receptor protein expression on the cell surface.

5.3 Specific cytoadhesion of IE to transgenic CHO cells

To determine the specificity of the observed binding of *P. falciparum* IE towards transgenic CHO cell lines, expressing a specific human receptor, a fluorescence analysis was performed. The intention was to investigate the appearance of IE cluster on GFP fluorescent, rather than on non-fluorescent CHO cells during a static binding assay. In **Figure 14**, the proof of concept is shown via the example of IT4 parasitized IE specifically bound to CHO-CD81 or CHO-CD55.

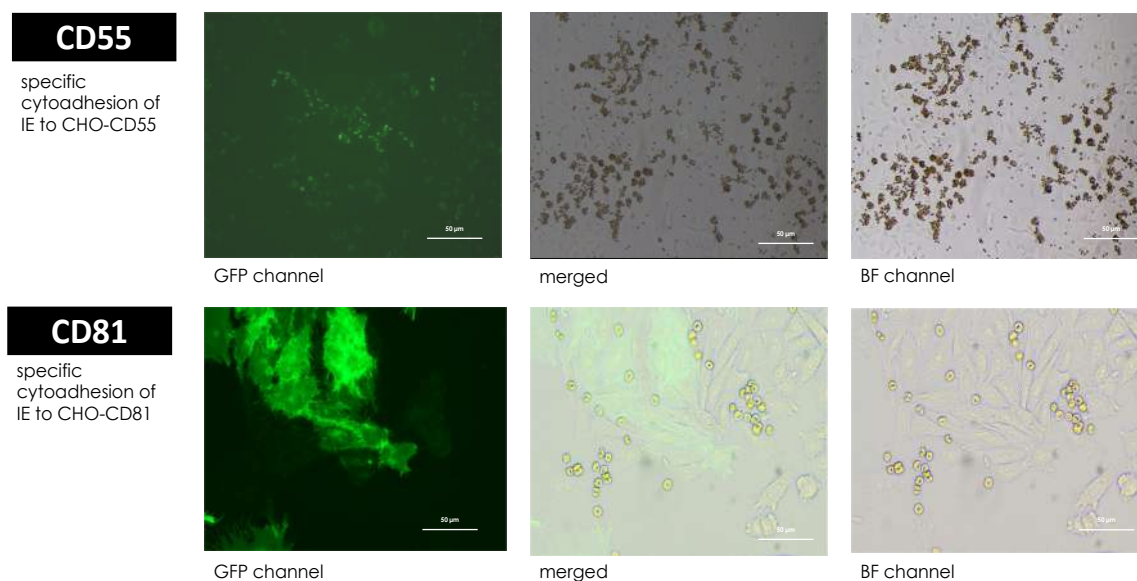


Figure 14. Specific cytoadhesion of *P. falciparum* IT4 parasitized IE towards transgenic CHO-CD81 and CHO-CD55 cells during a static binding assay. During a static binding assay, IT4 parasitized IE were co-incubated with CHO-CD81 or CHO-CD55 cells respectively. An increase of IE cluster on fluorescent cells is rather observed than on non-fluorescent cells. The fluorescence analysis was performed by the use of the EVOS FLauto fluorescence microscope with a 40x magnification and a scale bar of 50 µm.

In each case, the IE cluster almost exclusively on fluorescent cells, indicating a specific binding phenotype towards the actual human endothelial receptor. Within the static binding assay, as well as in further experiments like the sCSA inhibition assay or during rounds of enrichment via panning assays, the IE bind to the fluorescent CHO cells, indicating a specific binding behavior towards the expressed human receptors on the CHO cell surface. Those results are consistent with the binding patterns using all other transgenic CHO cell lines.

> Taken together, the specificity of cytoadhesion of *P. falciparum* parasitized IE towards the respective double positive transgenic CHO cells was evidenced.

5.4 Static binding assays

The intention of the static binding assays setup was to determine the initial binding capacity of various *P. falciparum* isolates towards a distinct set of human endothelial receptors. Here, CD36 and ICAM-1 served as positive controls due to an increased initial binding capability of most of all known field and clinical isolates. The initial aim was to eventually identify another human endothelial receptor, acting as putative PfEMP1 ligand, similar to CD36 or ICAM-1. Further aims of the assays were the investigation whether the amount of specifically bound IE was sufficient for total RNA isolation or, if not, the specifically bound population was enrichable over the respective receptor. As shown in **Figure 15.1** and **Figure 15.2**, in total, 19 different cell lines (CHO-WT, CHO-GFP, CHO-CD9, CHO-CD151, CHO-CD62-E, CHO-CD62-P, CHO-HRH1, CHO-VCAM1, CHO-MDR1, CHO-TNFR1, CHO-TNFR2, CHO-CD37, CHO-CD55, CHO-CD81, CHO-EPOR and HBEC-5i), each expressing one kind of specific human endothelial receptors on the surface of transgenic CHO cells, fused to cytosolic GFP as marker protein, as well as the HBEC-5i cell line, were screened against 16 different *P. falciparum* clinical and field isolates. Uninfected blood with blood group A⁺, originating from the same blood bank and also used for corresponding cell cultivation served as negative control (BB neg.) and baseline for the calculation of statistical significance. The IT4-ST and the IT4 parasite population, specifically enriched via panning, over mock-transfected CHO cells, IT4-GFP, served as controls. The respectively enriched IT4 population, IT4-CD62-P, IT4-TNFR1, IT4-CD55, IT4-37°C, IT4-40°C, as well as IT4-7 h final, NF54, 3D7 Australia, 3D7 BNI, DD2, MM, Patient 1, Patient 2, Patient 3) were analyzed likewise.

The binding assays were performed at least in triplicates and repeated at least twice, while the average number of firmly bound IE were calculated per 100 CHO or HBEC-5i cells, respectively.

The binding capacity towards **CHO-WT** cells was generally low for all isolates except IT4-CD62-P with a mean of 21.7 bound IE per 100 CHO cells ($p \leq 0.0001$). **CHO-GFP** triggered an expected initial binding capability of the GFP enriched *P. falciparum* culture isolate IT4-GFP, with a mean of 35.1 bound IE per 100 CHO cells ($p \leq 0.0001$). Furthermore, the IT4-CD62-P (mean 9.9 IE / 100 CHO; $p \leq 0.0025$) and DD2 (mean 10.4 IE / 100 CHO; $p \leq 0.0065$) isolates show also significant amounts of bound IE towards the mock transfected CHO cell line. The positive control **CHO-CD36** caused a significant higher initial binding capability of almost all tested isolates. The maximum mean was observed for IT4-TNFR1 (375.8 IE / 100 CHO; $p \leq 0.0001$). All other isolates show lower, but mostly significant initial binding capability with IT4-ST (239.7 IE / 100 CHO; $p \leq 0.0001$), IT4-GFP (288.3 IE / 100 CHO; $p \leq 0.0001$), IT4-CD62-P (143.1 IE / 100 CHO; $p \leq 0.0001$), IT4-CD55 (99.1 IE / 100 CHO; $p \leq 0.01$), IT4-37°C (19.5 IE / 100 CHO; $p = \text{ns}$), IT4-40°C (5.1 IE / 100 CHO; $p = \text{ns}$), IT4-7 h final (75 IE / 100 CHO; $p = \text{ns}$), NF54 (110.6 IE / 100 CHO; $p \leq 0.005$), 3D7 Australia (84.1 IE / 100 CHO; $p \leq 0.01$), 3D7 BNI (155.0 IE / 100 CHO; $p \leq 0.0001$), DD2 (215.0 IE / 100 CHO; $p \leq 0.0001$), MM (63.9 IE / 100 CHO; $p \leq 0.05$), Patient 1 (109.7 IE / 100 CHO; $p \leq 0.01$) and Patient 2 (1.9 IE / 100 CHO; $p = \text{ns}$).

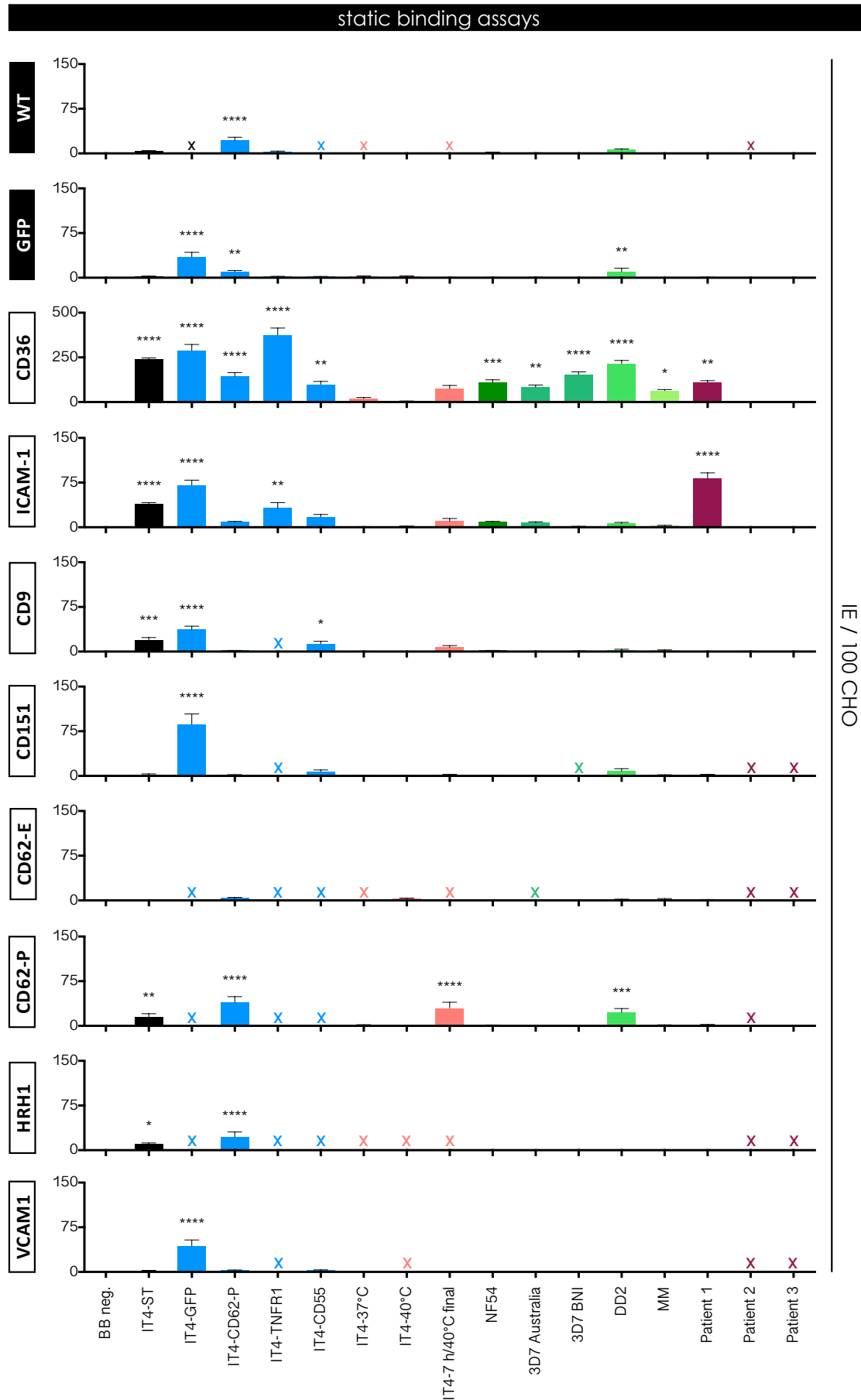


Figure 15.1 (to be continued). Static binding assays of various isolates over the complete human endothelial receptor set.

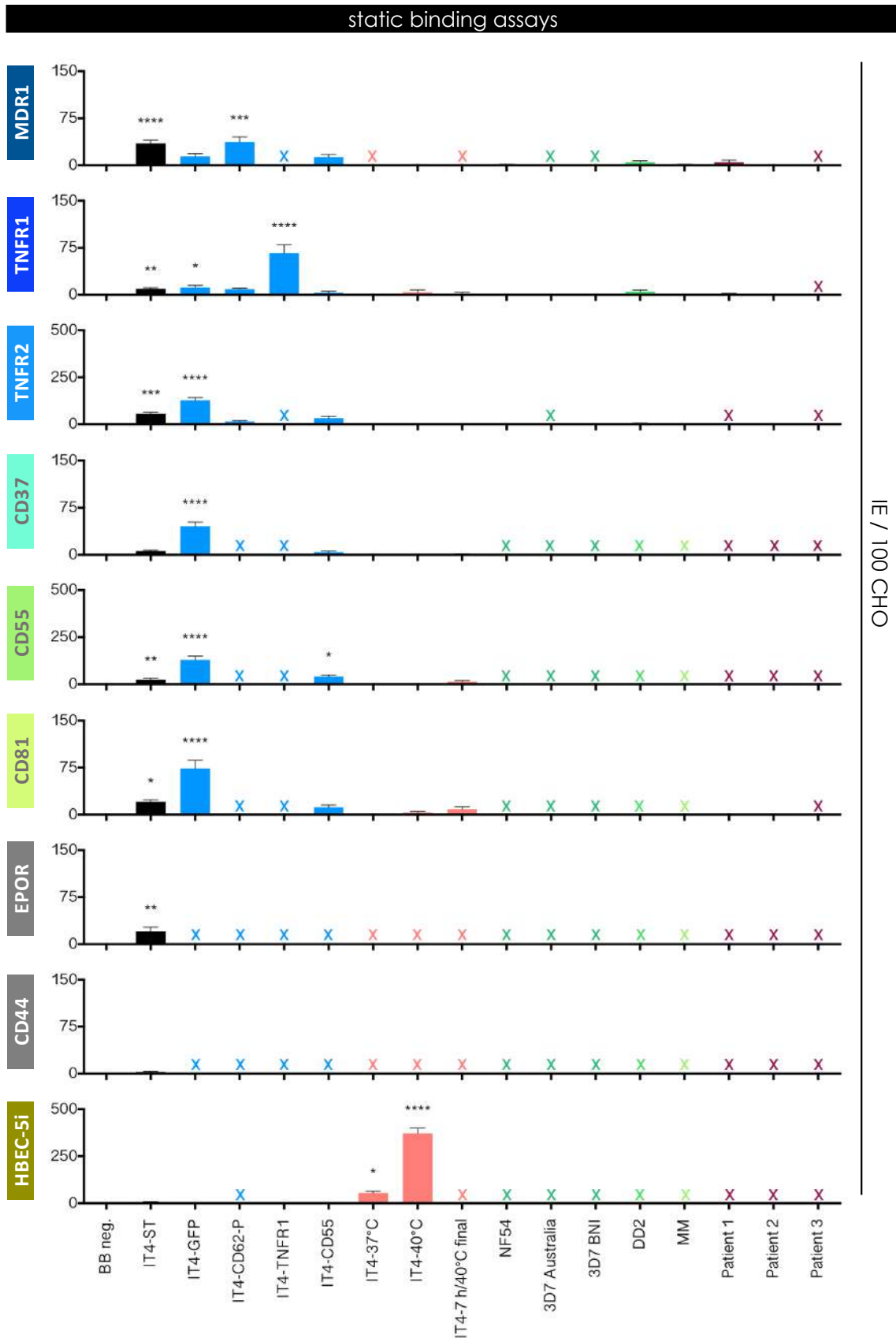


Figure 15.2 (continued). Static binding assays of various isolates over the complete human endothelial receptor set. To investigate the initial binding capability, a negative control, only containing respective uninfected A⁺ blood, as well as 16 distinct *P. falciparum* field and clinical isolates, as well as a negative control (x-axis: BB neg., IT4-St, IT4-GFP, IT4-CD62-P, IT4-TNFR1, IT4-CD55, IT4-37°C, IT4-40°C, IT4-7 h final, NF54, 3D7 Australia, 3D7 BNI, DD2, MM, Patient 1, Patient 2, Patient 3,

Patient 2, Patient 3) were screened over a set of the HBEC-5i cell line, as well as over 18 CHO cell lines, expressing a specific human endothelial receptor (sections: CHO-WT, CHO-GFP, CHO-CD9, CHO-CD151, CHO-CD62-E, CHO-CD62-P, CHO-HRH1, CHO-VCAM1, CHO-MDR1, CHO-TNFR1, CHO-TNFR2, CHO-CD37, CHO-CD55, CHO-CD81 and CHO-EPOR). The binding assays were performed at least in triplicates and repeated at least twice, while the average number of firmly bound IE were calculated per 100 CHO or HBEC-5i cells, respectively. For crossed samples, data are not available. Statistical significance was calculated by a one-way ANOVA with a Fisher's LSD test and a 95% CI with **** $p \leq 0.0001$; *** $p \leq 0.005$; ** $p \leq 0.01$; * $p \leq 0.05$, always compared to the BB neg. control. * The static binding assays for IT4-37°C in combination with HBEC-5i cells were performed in cooperation with Finn Fürstenwerth (Bruchhaus-Laboratory).

The **CHO-ICAM-1** cell induced a significant binding capability of IT4-ST (39.0 IE / 100 CHO; $p \leq 0.0001$), IT4-GFP (70.7 IE / 100 CHO; $p \leq 0.0001$), IT4-TNFR1 (32.1 IE / 100 CHO; $p \leq 0.01$) and Patient 1 (82.0 IE / 100 CHO; $p \leq 0.0001$). The following results of the **CHO-CD9** cell line, IT4-ST (19.0 $p \leq 0.005$), IT4-GFP (37.3 $p \leq 0.0001$) and IT4-CD55 (13.0 $p \leq 0.05$) show significant levels of bound IE and were in line with previous results.^{146,175} For the **CHO-CD151** cells, only IT4-GFP (86.7 IE / 100 CHO; $p \leq 0.0001$) and for **CHO-CD62-E**, no significant amount of bound IE was detected. Consistently with previous results, **CHO-CD62-P** induced firmly bound IE at a significant level for IT4-ST (15.4 IE / 100 CHO; $p \leq 0.01$), IT4-CD62-P (39.4 IE / 100 CHO; $p \leq 0.01$), IT4-7 h/40°C final (30.0 IE / 100 CHO; $p \leq 0.0001$) and DD2 (22.6 IE / 100 CHO; $p \leq 0.005$).¹⁷⁵ For **CHO-HRH1** only IT4-ST (9.9 IE / 100 CHO; $p \leq 0.05$) and IT4-CD62-P (22.3 IE / 100 CHO; $p \leq 0.0001$) while for **CHO-VCAM1** only IT4-GFP (43.4 IE / 100 CHO; $p \leq 0.0001$) and for **CHO-MDR1** only IT4-ST (35.0 IE / 100 CHO; $p \leq 0.0001$) and IT4-CD62-P (37.2 IE / 100 CHO; $p \leq 0.005$) show elevated amounts of bound IEs. The **CHO-TNFR1** cell line induced IT4-ST (9.6 IE / 100 CHO; $p \leq 0.01$), IT4-GFP (11.6 IE / 100 CHO; $p \leq 0.05$) as well as the isolate IT4-TNFR1 (66.3 IE / 100 CHO; $p \leq 0.0001$) to a significant level, while **CHO-TNFR2** only triggered IT4-ST (55.8 IE / 100 CHO; $p \leq 0.005$) and IT4-GFP (127.7 IE / 100 CHO; $p \leq 0.0001$) significantly. For the **CHO-CD37** cell line, a significant increase of bound IE was detected for the IT4-GFP (45.4 IE / 100 CHO; $p \leq 0.0001$) isolate. The **CHO-CD55** cell line induced IT4-ST (24.3 IE / 100 CHO; $p \leq 0.01$), eGFP (129.9 IE / 100 CHO; $p \leq 0.0001$) and eCD55 (40.3 IE / 100 CHO; $p \leq 0.05$). For **CHO-CD81** a significant level was measured for IT4-ST (20.9 IE / 100 CHO; $p \leq 0.05$) and IT4-GFP (73.6 IE / 100 CHO; $p \leq 0.0001$). While for **CHO-EPOR** and **CHO-CD44** only IT4-ST was measured, only the first show a significant increased level of bound IE (20.7 IE / 100 CHO; $p \leq 0.01$) towards the CHO-EPOR cell line. For the human brain endothelial cell line **HBEC-5i**, highly significant levels of bound IE were induced for the IT4-37°C (55.1 IE / 100 CHO; $p \leq 0.05$) and IT4-40°C (371.1 IE / 100 CHO; $p \leq 0.0001$) isolates.

> Taken together, in most instances, IT4 isolates, already enriched over respective CHO cell lines show significant increased levels of firmly bound IE towards the screened transgenic CHO cell lines. Furthermore, the IT4-ST isolate also shows a significance in most of the assays. While CHO-CD36 serves as a positive control, it was expected that almost all, except the temperature-related isolates, interact in a significant manner. Prominent values were observed for the Patient 1 isolate in connection with CHO-ICAM-1. Furthermore CHO-CD62-P cell lines triggered a significant effect for the

DD2 field isolate as well as for the IT4 isolate, cultivated with weekly heat shocks at 40°C for 1.5 h and a final heat shock at 40°C for 7 h. Finally, and in accordance with parallel findings within the Bruchhaus-Laboratory, HBEC-5i cells induced highly significance binding capability within the IT4 isolates, constantly cultivated and enriched over HBEC-5i cells, at either 37°C or 40°C.

5.5 Inhibition assay to unknown surface structures

Actual and previously performed static binding assays revealed, that IE can bind in small numbers to amorphous or non-fluorescent CHO cells. As rodent CD44 is an omnipresent structure, covering the whole surface of CHO cells, a specific, non-permeabilizing antibody staining was performed to determine the spreading pattern of the protein. Additionally, the presence of CD44 was also accounted for the surface of CHO-WT cells by the use of FACS analysis. To investigate whether the described phenomenon could be inhibited by the addition of specific antibodies against rodent CD44, respective inhibition assays were performed.

In the upper left section of **Figure 16**, the fluorescence analysis is shown for CHO-WT cells, stained with a specific and non-permeabilizing antibody against rodent CD44, primary labeled with FITC. Recorded pictures within the GFP channel and the BF channel were merged subsequently. The FITC labeled antibody appear within the GFP channel in bright green and is omnipresent on all CHO cell surfaces. The results of the consecutively performed FACS analysis are shown in the upper right section. A proportion of 99.7% FITC positive stained CHO-WT cells were recorded as sub population (petrol) out of the total screened CHO-WT population in comparison with 0% stained sub population within the non-stained CHO-WT cells (grey). Next, the binding capability of diverse IT4 isolates towards amorphous or non-fluorescent cells was attempted to be inhibited by addition of specific antibodies. The results are shown in the lower section. Within an experimental setup, similar to a static binding assay, the cytoadhesion was tried to inhibit. Consistently, uninfected erythrocytes of blood group A+ (BB neg.) as well as the IT4-ST isolate in combination with the respective CHO cell line served as negative controls. The IT4 isolates, individually enriched over the investigated CHO cell lines (IT4-GFP (back), IT4-TNFR1 (blue) and IT4-CD55 (green) were set as positive control and baseline for the calculation of statistical significance. To test if the observed binding phenotype of the isolate towards the particular CHO cell line could be inhibited, rodent specific α CD44 antibody (red frames) was added for 30 min at RT, previous to the pouring of IE on the CHO monolayer.

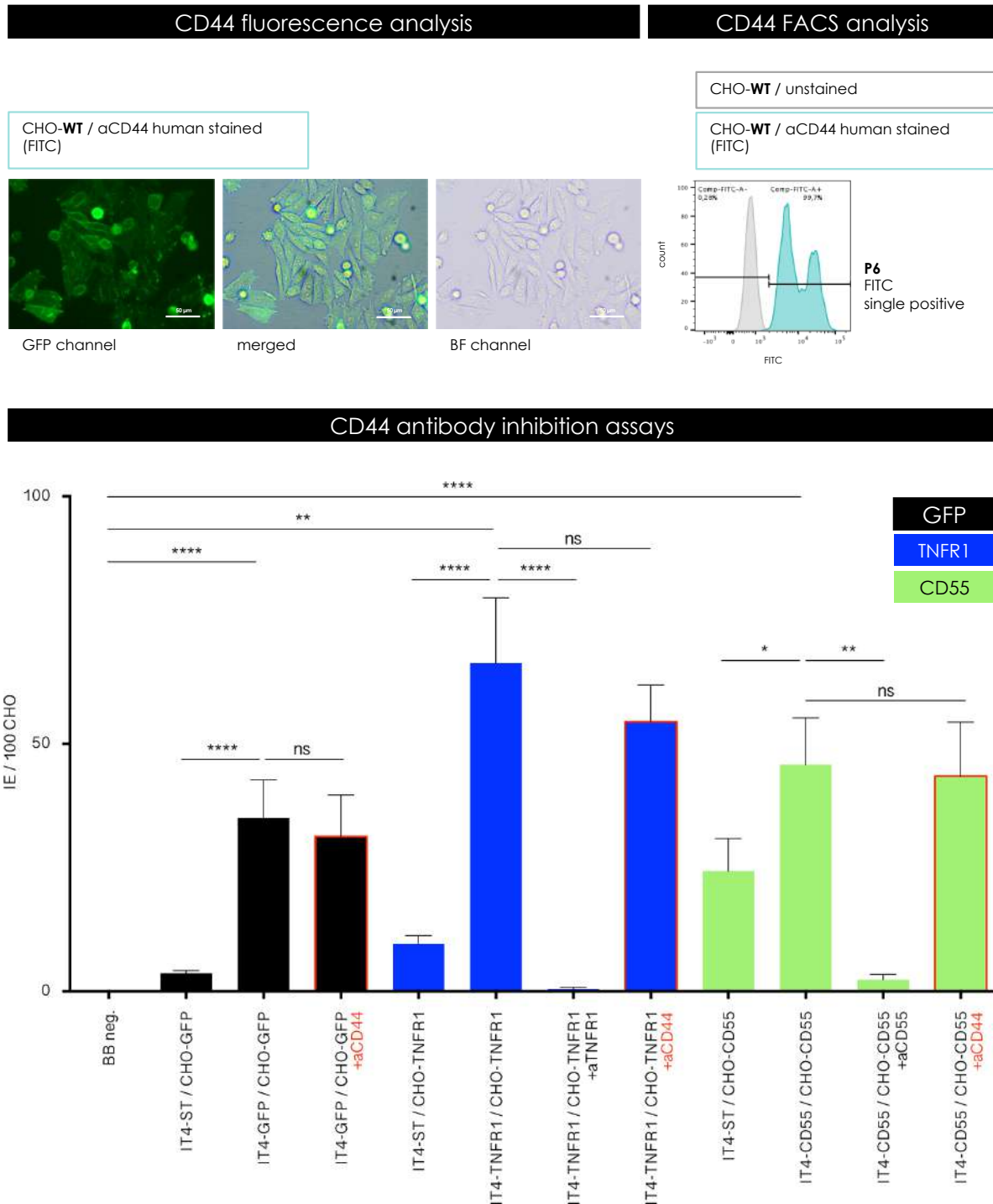


Figure 16. Cytoadhesion inhibition assay with specific antibodies. To determine the specificity of the observed cytoadhesion of various *P. falciparum* isolates towards transgenic CHO cell lines, fluorescence microscopy (upper left section), FACS analysis (upper right section) and cytoadhesion inhibition assays by the use of specific antibodies (lower section) were performed. The analyses also rule out the influence of the evidenced rodent CD44 protein structure, omnipresent on the CHO cell surface. The microscopic fluorescence analysis showed an overall spreading pattern of specifically stained rodent CD44 on the surface of almost all detected CHO-WT cells, appearing in bright green within the GFP channel. The microscopic pictures were recorded with the EVOC FLauto fluorescence microscope at a 40x magnification with a scale bar of 50 μm . The subsequent FACS analysis recorded a sub population of 99.7% of rodent specific αCD44 -FITC positive surface-stained CHO-WT cells. Transgenic CHO cells

were resuspended in CHO culture medium, lacking iFCS, recorded by the use of the FACS AriaIII device with an 85 μm nozzle and a medium flow velocity, while analyzed simultaneously with the FACSDiva software. The results of the cytoadhesion inhibition assay by the use of antibodies emerge a highly significant inhibition of individually enriched IT4 populations in combination with the respective antibodies against the human surface proteins, when assayed over the particular transgenic CHO cell line. An inhibition due to the rodent specific αCD44 antibody could not be observed. Statistical significance was calculated by a one-way ANOVA with a Fisher's LSD test and a 95% CI with **** $p \leq 0.0001$; *** $p \leq 0.005$; ** $p \leq 0.01$; * $p \leq 0.05$, compared either to the BB neg. or the IT4-ST control.

As a second positive control and proof of concept, specific antibodies for the actual CHO-TNFR1 and CHO-CD55 cell line were added in a separate approach while treated equally.

As expected, the IT4-ST isolate show a slight increase of bound IE towards the CHO-GFP, CHO-TNFR1 and CHO-CD55 cells. A significant increase was observed if the individually enriched IT4 isolates were examined in combination with the respective CHO cell line. Here, the IT4-GFP isolate induced a mean of 35.1 bound IE per 100 CHO-GFP cells ($p \leq 0.0001$), while the IT4-TNFR1 triggered a mean of 66.3 bound IE per 100 CHO-TNFR1 cells ($p \leq 0.0001$) and the IT4-CD55 induced a mean of 24.3 bound IE per 100 CHO-CD55 cells ($p \leq 0.01$). The specific receptor-IE inhibition using particular antibodies against the human TNFR1 and CD55 surface proteins resulted in significant decreases of bound IE numbers for the IT4-TNFR1 (0.4 IE / 100 CHO; $p \leq 0.0001$) and the IT4-CD55 (2.3 IE / 100 CHO; $p \leq 0.01$) isolate proving the general specific inhibitability by the use of antibodies. The addition of rodent specific αCD44 antibody did not show any effect on the observed binding phenotype of each tested IT4 isolate. The amount of bound IE towards the particular CHO cell line was almost similar to the results without antibody addition.

> Taken together, the cytoadhesion of individually enriched IT4 isolates towards their particular CHO cell line could be inhibited by the use of respective antibodies in a highly significant manner, verifying the specificity of cytoadhesion. However, the observed cytoadhesion could not be inhibited by the use of rodent specific αCD44 antibodies.

5.6 Cytoadhesion inhibition assay with sCSA

P. falciparum parasitized erythrocytes, enriched over human endothelial cell line 5i (HBEC-5i) at 40°C demonstrate a very high interaction affinity towards chondroitin sulfate A. These macromolecular structures are part of proteoglycans and omnipresent on most of human cell types. Also, it is found in high numbers on the placenta, giving rise to the pregnancy associated malaria (PAM), a very dangerous, severe and widespread form of the disease. Within the most experimental setups, CHO cells were used, as this cell line lacking CSA on the surface due to a mutation causing a defect in glycosaminoglycan biosynthesis.

During the static binding assays, it was observed that the *P. falciparum* IT4 isolate show

highly significant elevated binding capacities towards HBEC-5i, after repetitive enrichment under febrile conditions of 40°C. This phenotype was constant over various rounds of enrichment and is most likely due to the extensive expression of the *var2csa*-*var* gene within the IT4 population. The investigation of this phenotype and behavior were performed at the same time within the Bruchhaus-Laboratory, but were focus of a different project. The PfEMP1 'VAR2CSA' is very well known in connection with PAM and therefore studied in detail. So far, the fact that a similar phenotype can be observed during the contact of IE and human brain endothelial cells in conjunction with an enrichment at febrile temperature is barely described. To prove the general binding capability of the *P. falciparum* IT4 isolate towards this surface structure, the CSA expressing HBEC-5i was utilized within binding assays and electron microscopy. To investigate whether the resulting binding capacity of the IT4 isolate and CSA is of specific nature and related to the febrile enrichment procedure, a cytoadhesion inhibition assay was performed. Within this assay, it was tested if the binding capability of the IT4-St, IT4-37°C and IT4-40°C isolates was directed towards the CSA on the surface of the HBEC-5i cells and if this interaction could be inhibited by sCSA. Furthermore, the concentration of sCSA was decreased stepwise, to determine the gradual inhibition limit. The assay was performed at least in triplicates and repeated at least twice, while the average number of firmly bound IE were calculated per 100 HBEC cells; the results are shown in **Figure 17**.

The 3 different IT4 isolates were assayed over either HBEC-5i cells (light green) or CHO-CD36 cells (dark green) as control. Prior to the assay, the *P. falciparum* IE were incubated for 30 min at 37°C, with respective amounts of sCSA, dissolved in D-PBS. As negative control, the IE were also incubated with sBSA, also dissolved in D-PBS at the highest amount used within the assay (10 µg/ml) to rule out unspecific inhibition of cytoadhesion by a non-relevant soluble protein. Furthermore, as a second negative control and to set a baseline to compare the subsequent results, the IE were incubated in D-PBS only. All samples were treated equally, independent from the combination of incubation.

The left section shows the results for the IT4-37°C isolate. The combination with the HBEC-5i sample, serving as negative control by the use of D-PBS only, shows a mean of 6.4 bound IE per 100 HBEC-5i cells. The results for the incubation of HBEC-5i cells in combination with sBSA were similar (9.2 IE / 100 HBEC-5i). The inhibition with 10 µg/ml sCSA (0.8 IE / 100 HBEC-5i; $p \leq 0.05$) as well as with 1 µg/ml sCSA (0.6 IE / 100 HBEC-5i; $p \leq 0.05$) significantly reduced the binding capability of the IT4-37°C isolate towards the HBEC-5i cell line. The observed findings for the IT4-37°C isolate in combination with CHO-CD36 and D-PBS only (21.6 IE / 100 HBEC-5i) were in line with previous results of static binding assays. Also, the combination with the additives in concentrations of 10 µg/ml sBSA (37.5 IE / 100 HBEC-5i) and 1 µg/ml sBSA (22.3 IE / 100 HBEC-5i) did not change the general range of the binding capability.

The right section gives the results for the IT4-40°C isolate, mimicking febrile conditions within the infected human host. The negative control, IE incubated with D-PBS only shows a mean of 332.3 bound IE per 100 HBEC-5i cells. The addition of 10 µg/ml sBSA (367.5 IE / 100 HBEC-5i) did not change the range of the binding potential. Both conditions were set as baseline for statistical calculations of the subsequent inhibition

approaches. The addition of either 10 µg/ml sCSA (0.2 IE / 100 HBEC-5i; $p \leq 0.0001$), 1 µg/ml sCSA (64.4 IE / 100 HBEC-5i; $p \leq 0.0001$) or even 0.1 µg/ml sCSA (187.5 IE / 100 HBEC-5i; $p \leq 0.0001$) decreased the binding capability of the IT4-40°C isolate significantly. Furthermore, the results proved a stepwise inhibition in correlation with the added concentration of sCSA. Strikingly, the concentration dependent inhibition of firmly bound IE towards HBEC-5i could be proven by the use of sCSA up to 1 µg/ml. Here, a nearly complete inhibition of 99.9% was observed for the highest concentration of 10 µg/ml sCSA, while the 1 µg/ml sCSA inhibited the binding of IE by 81.6% and the addition of 0.1 µg/ml still performed an inhibition of 46.4%. As expected and in line with previously results during static binding assays, the binding ability of the IT4-40°C isolate towards CHO-CD36 was in the range of 40 bound IE per 100 HBEC-5i and did not change significantly with the addition of the sBSA or sCSA solution.

Also, as anticipated, the results for the IT4-ST isolate (data not shown) exhibit nearly no binding potential when assayed with HBEC-5i, independent of the incubation with D-PBS only (7.6 IE / 100 HBEC-5i), 10 µg/ml sBSA (0.5 IE / 100 HBEC-5i) or 10 µg/ml and 1 µg/ml sCSA (0.5 and 1.8 IE / 100 HBEC-5i), respectively. The range of the amounts of bound IE towards the CHO-CD36 cells in combination with D-PBS only (250.6 IE / 100 HBEC-5i) is in line with previously performed static binding assays and did not vary significantly by the use of 10 µg/ml sBSA (193.3 IE / 100 HBEC-5i) and 1 µg/ml sCSA (199.0 IE / 100 HBEC-5i).

> Taken together, the addition of various concentrations of sCSA inhibited the binding capability of the *P. falciparum* IT4-40°C and IT4-37°C isolates in a highly significant and concentration dependent manner.

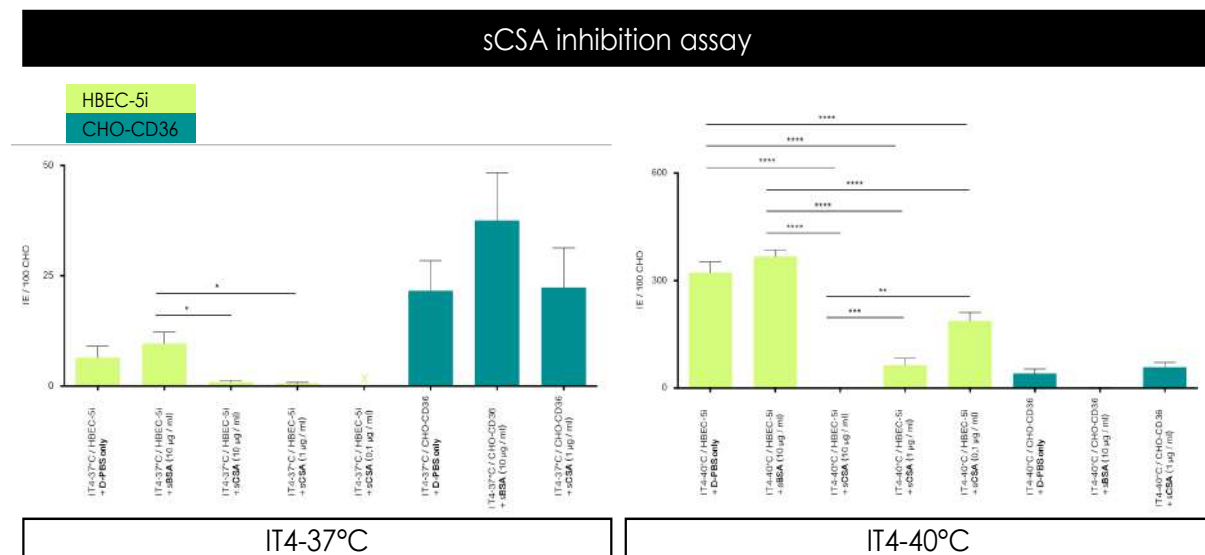


Figure 17. Cytoadhesion inhibition assay of specific IE binding towards HBEC-5i with sCSA. The cytoadhesion inhibition assay by the use of HBEC-5i and CHO-CD36 in combination with D-PBS only, 10 µg/ml sBSA and 10, 1 and 0.1 µg/ml sCSA was performed to determine the general binding capability and the gradual inhibition limit of *P. falciparum* IT4-37°C, IT4-40°C and IT4-ST isolates towards the omnipresent expressed cell surface structure CSA. IT4-37°C and IT4-40°C isolates showed a highly significant decrease in the binding potential of up to 99.9%, when co-incubated with sCSA. The inhibition is graduated, depending on the added sCSA

concentration. The IT4-ST isolate did not show an obvious binding phenotype towards the HBEC-5i cell line. Furthermore, the assays in combination with CHO-CD36 were in line with previously findings and the range of bound IE did not changed when sBSA or sCSA were added. The assay was performed at least in triplicates and repeated at least twice, while the average number of firmly bound IE were calculated per 100 HBEC cells; the results are shown in **Figure 17**. For crossed samples, data are not available. Statistical significance was calculated by a one-way ANOVA with a Tukey correction for multiple comparisons and a 95% CI with **** $p \leq 0,0001$; *** $p \leq 0,005$; ** $p \leq 0,01$; * $p \leq 0,05$ and compared as indicated within the graph.

5.7 Enrichment via multiple rounds of panning assays

Within this thesis, 6 human endothelial receptors were chosen for further investigations, acting as putative interaction partner for PfEMP1 or at least being very crucial in the process of cytoadhesion and sequestration as well as concerning the clinical symptomatic of cerebral malaria disease. Even if CHO-MDR1, CHO-TNFR1, CHO-TNFR2, CHO-CD37, CHO-CD55 and CHO-CD81 show promising results regarding initial binding capability of the IT4-ST isolate within static binding assays, the amount of firmly bound IE was not sufficient for total RNA isolation and subsequent NGS analysis. Therefore, the particular parasite populations were individually enriched via multiple rounds of enrichment via panning assays. In parallel, the same IT4-ST isolate as well as the IT4 isolate, separately enriched over CHO-GFP cell line, were processed and treated equally to serve as control and baseline for the subsequent NGS analysis. The finally enriched populations were harvested and processed for total RNA sequencing at the BGI facility in Hong Kong.

In **Figure 18**, the microscopical images for the initial binding capability (not enriched) of the IT4 isolate in combination with the respective transgenic CHO cell line are shown in comparison with the binding potential after several rounds of enrichment via panning assays (enriched). The specifically bound IE population was harvested at ring stage directly within the next cycle of development to ensure a faithful representation of the genetic background of the actual enriched *P. falciparum* population. After RNA isolation, the condition was measured with the Bioanalyzer Agilent 2000 subsequently. The results of RNA content and integrity are shown for each population in the respective section separately.

As for the IT4-ST isolate, no enrichment procedures were carried out, only the bioanalyzer data are shown. For each enriched *P. falciparum* population, an enormous and extensive increase of the amount of firmly bound IE towards the respective transgenic CHO cell line was observed and is shown in each rightmost microscopic picture, marked as enriched. For each population, 4 biological replicates from consecutive rounds of enrichment were processed for further analysis. The RNA integrity was calculated as RIN value within each electrogram for each sample and the level of degradation was visualized in the electrophoresis gel-like image, individually compared to the marker band containing the actual RNA ladder. The RNA samples comply with the requirements with a minimum concentration of 20ng/ml, a minimum total mass of 200 ng per sample and a RIN value above '7'. Samples with lower values were ranked as 'risky' and should be considered during analysis.

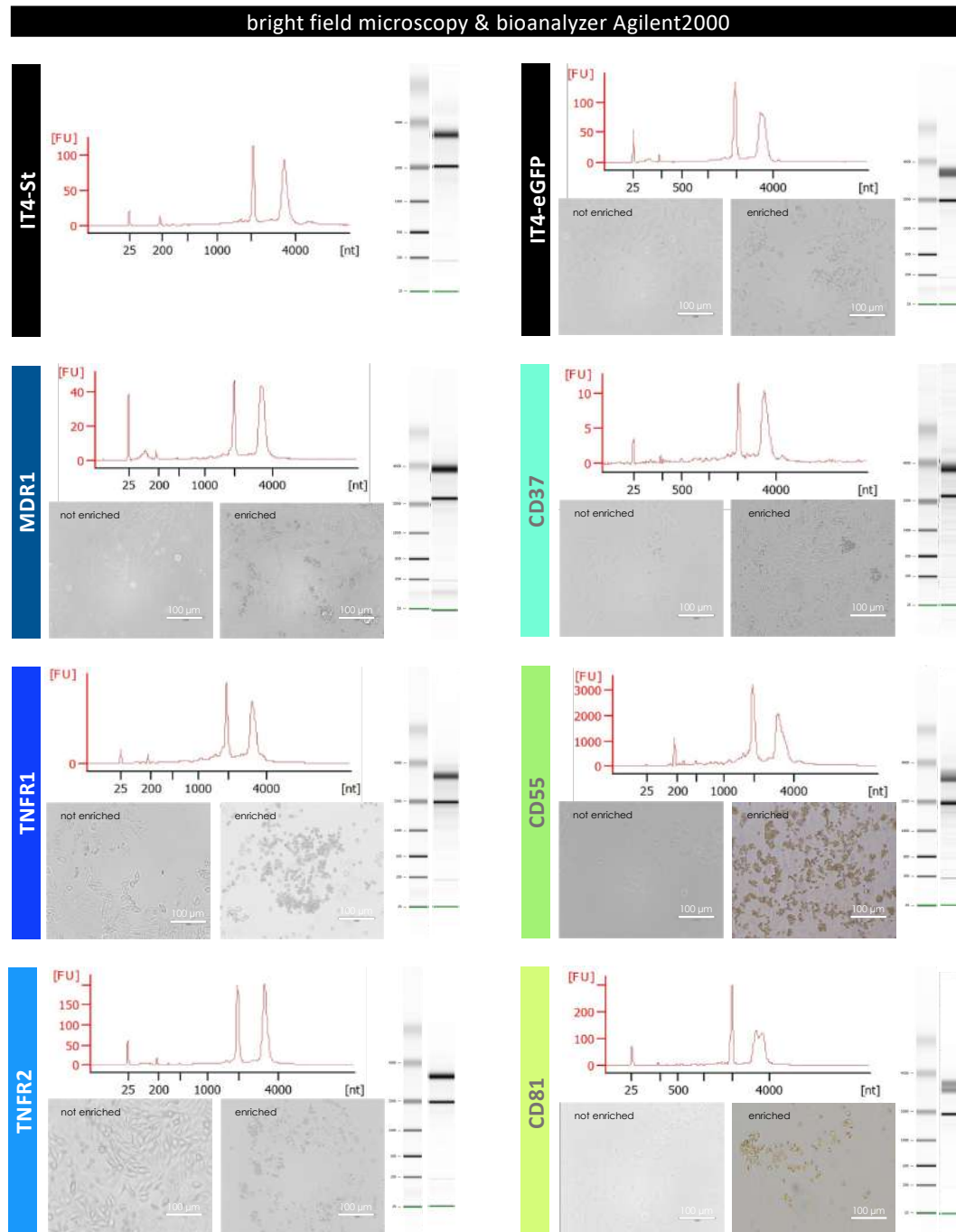


Figure 18. Enrichment via multiple rounds of panning assays to generate a homogenous population of *P. falciparum* IE specifically interact to a human endothelial receptor. The IT4 isolate was enriched over 6 particular transgenic CHO cell lines, each expressing a particular human endothelial receptor. The IT4-ST isolate and IT4-GFP enriched isolate served as control and baseline for subsequent NGS analysis. The IE were enriched via multiple rounds of panning assays to generate a homogenous parasite population interacting specifically with the receptor of interest. For each enriched population, an extensive increase of firmly bound IE was observed (enriched) in comparison to the not enriched cultures prior the panning assays. Ring staged parasites were harvested directly in the next round of development and RNA content and integrity were tested by the bioanalyzer Agilent 2000 device and shown as electrograms and electrophoresis gel-like results for the respective *P. falciparum* population in each section. The fluorescence analysis was performed by the use of the EVOS FLauto fluorescence microscope with a 20x magnification and a scale bar of 100 μm .

5.8 NGS analysis: comparison of gene expression levels

The NGS analysis of ring stage parasitized IE was performed to determine the differential gene expression of the *P. falciparum* isolate IT4 after interaction and enrichment over 6 different human endothelial receptors compared to IT4, enriched over mock-transfected CHO-GFP cells and the IT4-ST population.

To focus expression levels, altered in a considerable, tendency related manner, the following **cutoff criteria** were chosen for the mean values, received from the whole multiple comparison approach of all biological replicates: The expression level of the IT4-receptor enriched population (IT4-REC) should reach at least a value of 50, while being at least 2fold higher than the expression level of the control population (IT4-ST) as well as being higher as the expression level of the second control population (IT4-GFP). Additionally, the calculated significant p and p_{adj} values with $p < 0.05$ were considered as well and stated below the mean values, while significances are indicated in red. Albeit on average between 2700 to 3100 genes have a differentially upregulated expression level, only a few (36 to 334) of them are subject to the cutoff criteria. The comprehensive data are listed in **Annex I**, while the main data are shown in **Figures 19**, **Figure 20.1** and **Figure 20.2**.

5.8.1 Comparison of var gene expression levels

Focusing on the *var* genes, **Figure 19** shows in the left section the comparison of the actual mean values, while the right section shows the percentage of each *var* gene in relation to the whole gene set.

To evaluate the *var* gene expression levels of the specifically enriched IT4 population over the 6 respective human endothelial receptors, the mean values of IT4-MDR1 (dark blue), IT4-TNFR1 (indigo), IT4-TNFRF2 (light blue), IT4-CD37 (green), IT4-CD55 (light green) and IT4-CD81 (yellow) were compared individually with the mean of the two control populations.

Within the **IT4-GFP** population, B_var32A (56.1%) and B_var32B (34.3%) met the cutoff and were significantly upregulated, dominating the expression profile and additionally, while B_var14 and B_var29 only met the cutoff criteria. The circular charts show clearly that the **IT4-ST** population is dominated by the expression of the C_var34 gene (69.3%) then only followed by the C_var23 (6.7%). All other *var* genes exhibited an expression of less than 3% each in the particular comparison.

> Further procedure of analysis

The actual mean values of the whole *var* gene set, the p and p_{adj} values ($p < 0.05$, red font) as well as the maximal values of the respective population, in which the mean value peaks, are summarized in **Table 3**,

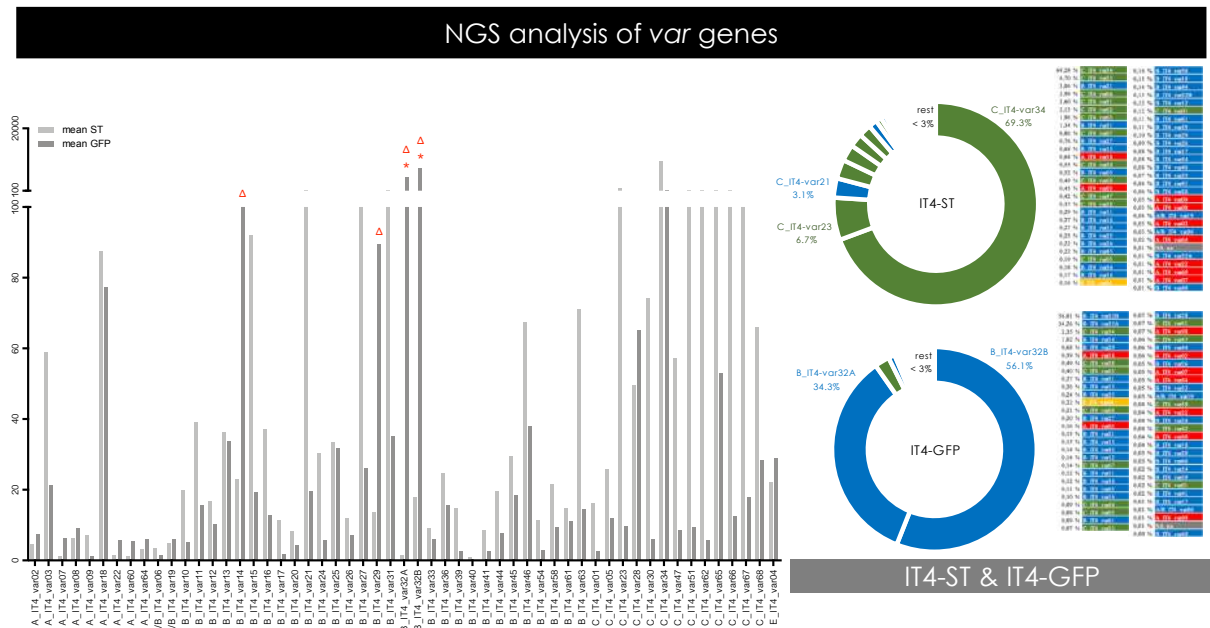


Figure 19. Comparison of var gene expression levels of IT4-ST and IT4-GFP population. The left section shows the actual mean expression values, while the right section shows the percentage of each var gene in relation to the whole gene set. For IT4-GFP, B_var32A (56.1%) and B_var32B (34.3%) were significantly upregulated and met the cutoff, while B_var14 and B_var29 met the cutoff criteria, compared to IT4-ST. For IT4-ST the C_var34 gene dominate the expression composition with (69.3%) then only followed by the C_var23 (6.7%). All other var genes exhibited an expression of less than 5% each in the proportional comparison, respectively for each analysis. Significances ($p < 0.05$) are marked with red asterisks, values meeting the cutoff criteria were marked with red triangles.

To analyze the expression changes, related to the interaction with the respective receptors, all values peaking in IT4-ST (B_var10, B_var15, B_var16, B_var17, B_var21, B_var27, B_var31, B_var33, B_var54, B_var58, B_var63, C_var01, C_var23, C_var28, C_var30, C_var34, C_var47, C_var51, C_var62, C_var65, C_var66 and C_var67) and IT4-GFP (A_var07, A_var60, B_var14, B_var29, B_var32A and B_var32B) were excluded, respectively. The resulting percentages of expressed var genes, compared to the remaining gene set (exclusion of the IT4-ST and IT4-GFP peaking var genes) are shown in the right sections for each population individually as circular chart.

The overall analysis, comparing the whole var gene set of IT4-ST, IT4-GFP and the individual enriched IT4-Receptor population, is shown in the left sections as bar graphs, in **Figure 20.1** and **Figure 20.2**.

Table 3. Overview of NGS data for control and enriched IT4 population with mean values and respective p- and padj-values focusing on var genes.

| # | ID | mean ST | mean GFP | | mean MDR1 | | mean TNFR1 | | mean TNFR2 | | mean CD37 | | mean CD55 | | mean CD81 | | name | peak | | | | | | | |
|----|----------------|---------|----------|------|-----------|--------|------------|------|------------|------|-----------|---------|-----------|------|-----------|------|------|--------|------|------|-------------|------|------|---------------|-------|
| | | | pval | padj | pval | padj | pval | padj | pval | padj | pval | padj | pval | padj | pval | padj | | | | | | | | | |
| 1 | PFIIT_bin08900 | 4,54 | 7,50 | 0,34 | 1,00 | 2,29 | 0,11 | 0,48 | 7,24 | 0,65 | 0,97 | 2,23 | 0,05 | 0,59 | 0,05 | 0,25 | 0,56 | 0,81 | 0,56 | 0,86 | A_IT4_var02 | CD81 | | | |
| 2 | PFIIT_bin02700 | 58,97 | 21,34 | 0,20 | 1,00 | 15,09 | 0,69 | 0,92 | 132,31 | 0,05 | 0,19 | 84,69 | 0,12 | 0,68 | 44,40 | 0,54 | 0,86 | 87,24 | 0,02 | 0,13 | 111,29 | 0,00 | 0,06 | A_IT4_var03 | TNFR1 |
| 3 | PFIIT_bin06100 | 3,50 | 1,50 | 0,36 | 1,00 | 3,64 | 0,31 | 0,73 | 5,03 | 0,26 | 0,89 | 4,29 | 0,21 | 0,76 | 3,23 | 0,40 | 0,77 | 5,83 | 0,09 | 0,31 | 13,04 | 0,01 | 0,09 | A/B_IT4_var06 | CD81 |
| 4 | PFIIT_1300100 | 1,32 | 6,22 | 0,02 | 1,00 | 1,44 | 0,09 | 0,44 | 2,94 | 0,12 | 0,65 | 1,13 | 0,03 | 0,54 | 0,46 | 0,07 | 0,33 | 2,78 | 0,22 | 0,51 | 5,13 | 0,77 | 0,93 | A_IT4_var07 | GFP |
| 5 | PFIIT_1150900 | 6,34 | 9,10 | 0,55 | 1,00 | 7,95 | 0,77 | 0,95 | 8,80 | 0,96 | 1,00 | 6,47 | 0,52 | 0,90 | 1,80 | 0,12 | 0,43 | 8,56 | 0,87 | 0,97 | 13,73 | 0,56 | 0,86 | A_IT4_var08 | CD81 |
| 6 | PFIIT_1400200 | 7,23 | 1,25 | 0,02 | 0,91 | 5,75 | 0,04 | 0,32 | 5,87 | 0,05 | 0,28 | 11,57 | 0,06 | 0,19 | 6,53 | 0,06 | 0,28 | 10,23 | 0,00 | 0,02 | 19,57 | 0,00 | 0,02 | A_IT4_var09 | CD81 |
| 7 | PFIIT_bin10900 | 87,55 | 77,46 | 0,86 | 1,00 | 59,02 | 0,29 | 0,71 | 78,48 | 0,94 | 1,00 | 58,66 | 0,27 | 0,80 | 69,49 | 0,64 | 0,90 | 118,16 | 0,16 | 0,42 | 123,06 | 0,32 | 0,73 | A_IT4_var18 | CD81 |
| 8 | PFIIT_bin09600 | 4,86 | 6,02 | 0,60 | 1,00 | 6,06 | 0,93 | 0,99 | 6,46 | 1,00 | 1,00 | 3,82 | 0,41 | 0,87 | 4,66 | 0,43 | 0,80 | 4,53 | 0,62 | 0,84 | 3,89 | 0,65 | 0,89 | A/B_IT4_var19 | TNFR1 |
| 9 | PFIIT_bin01000 | 1,45 | 5,84 | 0,03 | 1,00 | 2,20 | 0,22 | 0,65 | 3,28 | 0,40 | 0,95 | 2,24 | 0,16 | 0,73 | 1,79 | 0,20 | 0,57 | 2,78 | 0,25 | 0,55 | 10,39 | 0,54 | 0,85 | A_IT4_var22 | CD81 |
| 10 | PFIIT_bin06900 | 1,34 | 5,57 | 0,08 | 1,00 | 1,53 | 0,16 | 0,58 | 3,82 | 0,57 | 0,97 | 2,17 | 0,20 | 0,76 | 0,00 | 0,01 | 0,09 | 4,34 | 0,69 | 0,88 | 4,88 | 0,81 | 0,94 | A_IT4_var60 | GFP |
| 11 | PFIIT_0710900 | 3,16 | 6,06 | 0,18 | 1,00 | 6,02 | 0,93 | 0,99 | 10,21 | 0,50 | 0,96 | 6,32 | 0,96 | 1,00 | 6,16 | 0,67 | 0,91 | 10,97 | 0,37 | 0,67 | 8,40 | 0,70 | 0,90 | A_IT4_var64 | CD55 |
| 12 | PFIIT_0800100 | 19,81 | 5,16 | 0,17 | 1,00 | 12,31 | 0,38 | 0,77 | 6,03 | 0,99 | 0,72 | 7,36 | 0,72 | 0,94 | 7,44 | 0,54 | 0,86 | 15,48 | 0,19 | 0,46 | 14,50 | 0,20 | 0,60 | B_IT4_var10 | ST |
| 13 | PFIIT_0500100 | 39,09 | 15,77 | 0,02 | 1,00 | 43,79 | 0,01 | 0,11 | 38,76 | 0,11 | 0,62 | 35,23 | 0,04 | 0,58 | 45,20 | 0,08 | 0,36 | 64,26 | 0,00 | 0,00 | 86,53 | 0,03 | 0,20 | B_IT4_var11 | CD81 |
| 14 | PFIIT_bin00400 | 16,66 | 10,24 | 0,25 | 1,00 | 41,50 | 0,01 | 0,05 | 15,49 | 0,58 | 0,97 | 44,74 | 0,02 | 0,54 | 24,73 | 0,06 | 0,30 | 28,06 | 0,01 | 0,09 | 54,75 | 0,04 | 0,23 | B_IT4_var12 | CD81 |
| 15 | PFIIT_0411400 | 36,18 | 33,85 | 0,88 | 1,00 | 18,06 | 0,19 | 0,61 | 27,96 | 0,55 | 0,97 | 25,23 | 0,35 | 0,85 | 25,70 | 0,37 | 0,75 | 20,55 | 0,23 | 0,51 | 50,47 | 0,48 | 0,83 | B_IT4_var13 | CD81 |
| 16 | PFIIT_bin07000 | 23,03 | 133,92 | 0,03 | 1,00 | 20,35 | 0,07 | 0,39 | 26,43 | 0,05 | 0,28 | 26,69 | 0,03 | 0,54 | 24,63 | 0,03 | 0,18 | 21,75 | 0,04 | 0,17 | 27,80 | 0,03 | 0,20 | B_IT4_var14 | GFP |
| 17 | PFIIT_bin10700 | 91,98 | 19,31 | 0,12 | 1,00 | 33,01 | 0,64 | 0,89 | 25,49 | 0,81 | 0,99 | 36,08 | 0,48 | 0,89 | 28,24 | 0,71 | 0,93 | 20,68 | 0,98 | 1,00 | 28,93 | 0,71 | 0,90 | B_IT4_var15 | ST |
| 18 | PFIIT_bin09100 | 37,08 | 12,82 | 0,29 | 1,00 | 1,89 | 0,15 | 0,56 | 9,12 | 0,61 | 0,97 | 2,15 | 0,08 | 0,64 | 5,44 | 0,41 | 0,78 | 3,85 | 0,25 | 0,54 | 4,98 | 0,33 | 0,74 | B_IT4_var16 | ST |
| 19 | PFIIT_bin07600 | 11,32 | 1,71 | 0,05 | 1,00 | 7,59 | 0,09 | 0,45 | 4,36 | 0,36 | 0,94 | 7,21 | 0,09 | 0,64 | 4,49 | 0,20 | 0,57 | 4,42 | 0,29 | 0,58 | 3,77 | 0,28 | 0,70 | B_IT4_var17 | ST |
| 20 | PFIIT_bin10800 | 8,31 | 4,30 | 0,24 | 1,00 | 5,08 | 0,82 | 0,96 | 6,54 | 0,73 | 0,98 | 7,48 | 0,36 | 0,86 | 10,87 | 0,18 | 0,54 | 9,16 | 0,17 | 0,44 | 11,05 | 0,15 | 0,51 | B_IT4_var20 | CD81 |
| 21 | PFIIT_bin10500 | 415,16 | 19,58 | 0,01 | 0,40 | 110,14 | 0,13 | 0,52 | 49,04 | 0,40 | 0,95 | 76,98 | 0,19 | 0,75 | 82,94 | 0,15 | 0,49 | 55,64 | 0,34 | 0,64 | 63,88 | 0,27 | 0,68 | B_IT4_var21 | ST |
| 22 | PFIIT_bin07650 | 30,46 | 5,83 | 0,05 | 1,00 | 22,73 | 0,09 | 0,44 | 17,12 | 0,17 | 0,75 | 20,94 | 0,07 | 0,64 | 26,97 | 0,03 | 0,17 | 24,41 | 0,03 | 0,15 | 34,94 | 0,05 | 0,25 | B_IT4_var24 | CD81 |
| 23 | PFIIT_0537600 | 33,37 | 31,69 | 0,91 | 1,00 | 54,93 | 0,13 | 0,53 | 29,80 | 0,79 | 0,98 | 46,68 | 0,43 | 0,87 | 24,62 | 0,48 | 0,83 | 43,21 | 0,41 | 0,71 | 42,61 | 0,70 | 0,90 | B_IT4_var25 | MDR1 |
| 24 | PFIIT_1400100 | 11,88 | 7,16 | 0,25 | 1,00 | 13,97 | 0,18 | 0,60 | 9,97 | 0,41 | 0,95 | 10,64 | 0,48 | 0,89 | 16,97 | 0,10 | 0,40 | 19,24 | 0,04 | 0,18 | 37,72 | 0,03 | 0,18 | B_IT4_var26 | CD81 |
| 25 | PFIIT_0411500 | 103,84 | 26,13 | 0,06 | 1,00 | 41,50 | 0,60 | 0,88 | 46,15 | 0,41 | 0,95 | 54,68 | 0,26 | 0,80 | 39,34 | 0,55 | 0,86 | 24,59 | 0,90 | 0,98 | 32,54 | 0,79 | 0,94 | B_IT4_var27 | ST |
| 26 | PFIIT_bin02100 | 13,62 | 89,63 | 0,01 | 0,36 | 3,91 | 0,08 | 0,36 | 12,36 | 0,07 | 0,30 | 7,53 | 0,00 | 0,19 | 3,63 | 0,00 | 0,01 | 2,73 | 0,00 | 0,00 | 6,85 | 0,00 | 0,04 | B_IT4_var29 | GFP |
| 27 | PFIIT_bin02200 | 181,80 | 35,12 | 0,12 | 1,00 | 106,90 | 0,27 | 0,69 | 63,62 | 0,53 | 0,97 | 43,18 | 0,86 | 0,97 | 25,93 | 0,75 | 0,94 | 37,29 | 0,99 | 1,00 | 55,37 | 0,65 | 0,89 | B_IT4_var31 | ST |
| 28 | PFIIT_bin00100 | 1,47 | 4518,56 | 0,00 | 0,00 | 13,11 | 0,00 | 0,00 | 273,84 | 0,00 | 0,00 | 88,84 | 0,00 | 0,00 | 12,23 | 0,00 | 0,00 | 0,31 | 0,00 | 0,00 | 13,02 | 0,00 | 0,00 | B_IT4_var32A | GFP |
| 29 | PFIIT_bin00900 | 18,06 | 7386,00 | 0,00 | 0,00 | 34,18 | 0,00 | 0,00 | 473,23 | 0,00 | 0,00 | 141,57 | 0,00 | 0,00 | 42,09 | 0,00 | 0,00 | 20,44 | 0,00 | 0,00 | 37,03 | 0,00 | 0,00 | B_IT4_var32B | GFP |
| 30 | PFIIT_bin04200 | 9,07 | 6,03 | 0,65 | 1,00 | 5,88 | 0,93 | 0,99 | 4,91 | 0,70 | 0,97 | 5,64 | 0,85 | 0,97 | 0,90 | 0,10 | 0,40 | 6,23 | 1,00 | 0,94 | 6,23 | 0,94 | 0,98 | B_IT4_var33 | ST |
| 31 | PFIIT_0100100 | 24,63 | 15,63 | 0,36 | 1,00 | 23,58 | 0,40 | 0,78 | 21,25 | 0,38 | 0,95 | 13,70 | 0,87 | 0,98 | 17,28 | 0,97 | 1,00 | 31,22 | 0,08 | 0,27 | 27,59 | 0,33 | 0,74 | B_IT4_var36 | CD55 |
| 32 | PFIIT_1240000 | 14,73 | 2,75 | 0,10 | 1,00 | 19,85 | 0,10 | 0,17 | 8,50 | 0,18 | 0,78 | 10,35 | 0,09 | 0,65 | 9,25 | 0,09 | 0,38 | 10,41 | 0,12 | 0,36 | 5,56 | 0,43 | 0,80 | B_IT4_var39 | MDR1 |
| 33 | PFIIT_0900100 | 8,60 | 2,60 | 0,04 | 1,00 | 7,37 | 0,09 | 0,46 | 9,63 | 0,05 | 0,40 | 8,28 | 0,06 | 0,63 | 16,34 | 0,06 | 0,29 | 7,29 | 0,10 | 0,32 | 16,18 | 0,01 | 0,11 | B_IT4_var41 | CD37 |
| 34 | PFIIT_1151000 | 19,64 | 7,67 | 0,08 | 1,00 | 15,54 | 0,20 | 0,63 | 18,65 | 0,08 | 0,54 | 14,42 | 0,23 | 0,78 | 23,08 | 0,02 | 0,14 | 15,46 | 0,15 | 0,41 | 33,91 | 0,05 | 0,28 | B_IT4_var44 | CD81 |
| 35 | PFIIT_bin04300 | 29,42 | 18,60 | 0,27 | 1,00 | 38,81 | 0,06 | 0,36 | 39,35 | 0,07 | 0,36 | 37,25 | 0,08 | 0,64 | 58,79 | 0,01 | 0,08 | 53,67 | 0,00 | 0,02 | 99,83 | 0,04 | 0,24 | B_IT4_var45 | CD81 |
| 36 | PFIIT_bin11000 | 67,37 | 38,09 | 0,10 | 1,00 | 36,11 | 0,77 | 0,95 | 53,12 | 0,40 | 0,95 | 36,94 | 0,79 | 0,96 | 68,83 | 0,14 | 0,47 | 67,13 | 0,07 | 0,26 | 69,22 | 0,26 | 0,67 | B_IT4_var46 | CD81 |
| 37 | PFIIT_bin09200 | 11,30 | 2,79 | 0,12 | 1,00 | 6,33 | 0,37 | 0,77 | 4,52 | 0,69 | 0,97 | 3,59 | 0,81 | 0,97 | 3,21 | 0,54 | 0,86 | 4,40 | 0,60 | 0,83 | 2,91 | 0,98 | 1,00 | B_IT4_var54 | ST |
| 38 | PFIIT_0411350 | 21,49 | 9,41 | 0,39 | 1,00 | 3,50 | 0,33 | 0,74 | 11,98 | 0,78 | 0,98 | 3,18 | 0,17 | 0,74 | 11,61 | 0,99 | 1,00 | 4,22 | 0,36 | 0,66 | 11,65 | 0,80 | 0,94 | B_IT4_var58 | ST |
| 39 | PFIIT_0835600 | 14,91 | 11,23 | 0,46 | 1,00 | 17,74 | 0,34 | 0,75 | 18,65 | 0,53 | 0,97 | 13,56 | 0,76 | 0,96 | 6,02 | 0,48 | 0,83 | 8,34 | 0,50 | 0,77 | 15,74 | 0,57 | 0,86 | B_IT4_var61 | MDR1 |
| 40 | PFIIT_1219000 | 71,17 | 14,47 | 0,09 | 1,00 | 21,07 | 0,74 | 0,93 | 28,70 | 0,41 | 0,95 | 19,36 | 0,77 | 0,96 | 24,09 | 0,54 | 0,86 | 24,45 | 0,58 | 0,82 | 38,52 | 0,24 | 0,65 | B_IT4_var63 | ST |
| 41 | PFIIT_0616500 | 16,35 | 2,63 | 0,12 | 1,00 | 3,68 | 0,82 | 0,96 | 9,22 | 0,19 | 0,84 | 6,04 | 0,37 | 0,86 | 2,71 | 0,76 | 0,95 | 11,91 | 0,71 | 0,89 | 6,23 | 0,30 | 0,71 | C_IT4_var01 | ST |
| 42 | PFIIT_1240400 | 25,71 | 12,01 | 0,04 | 1,00 | 53,36 | 0,05 | 0,21 | 37,13 | 0,05 | 0,41 | 66,04 | 0,04 | 0,59 | 23,15 | 0,12 | 0,45 | 33,25 | 0,01 | 0,06 | 34,37 | 0,05 | 0,28 | C_IT4_var05 | TNFR2 |
| 43 | PFIIT_0411000 | 910,14 | 9,73 | 0,00 | 0,10 | 7,46 | 0,82 | 0,96 | 17,32 | 0,66 | 0,97 | 9,16 | 0,93 | 0,99 | 69,20 | 0,12 | 0,44 | 7,85 | 0,84 | 0,95 | 14,81 | 0,76 | 0,92 | C_IT4_var23 | ST |
| 44 | PFIIT_0711000 | 49,70 | 65,06 | 0,32 | 1,00 | 815,39 | 0,05 | 0,41 | 560,34 | 0,05 | 0,41 | 1251,38 | 0,00 | 0,13 | 309,26 | 0,00 | 0,05 | 168,75 | 0 | | | | | | |

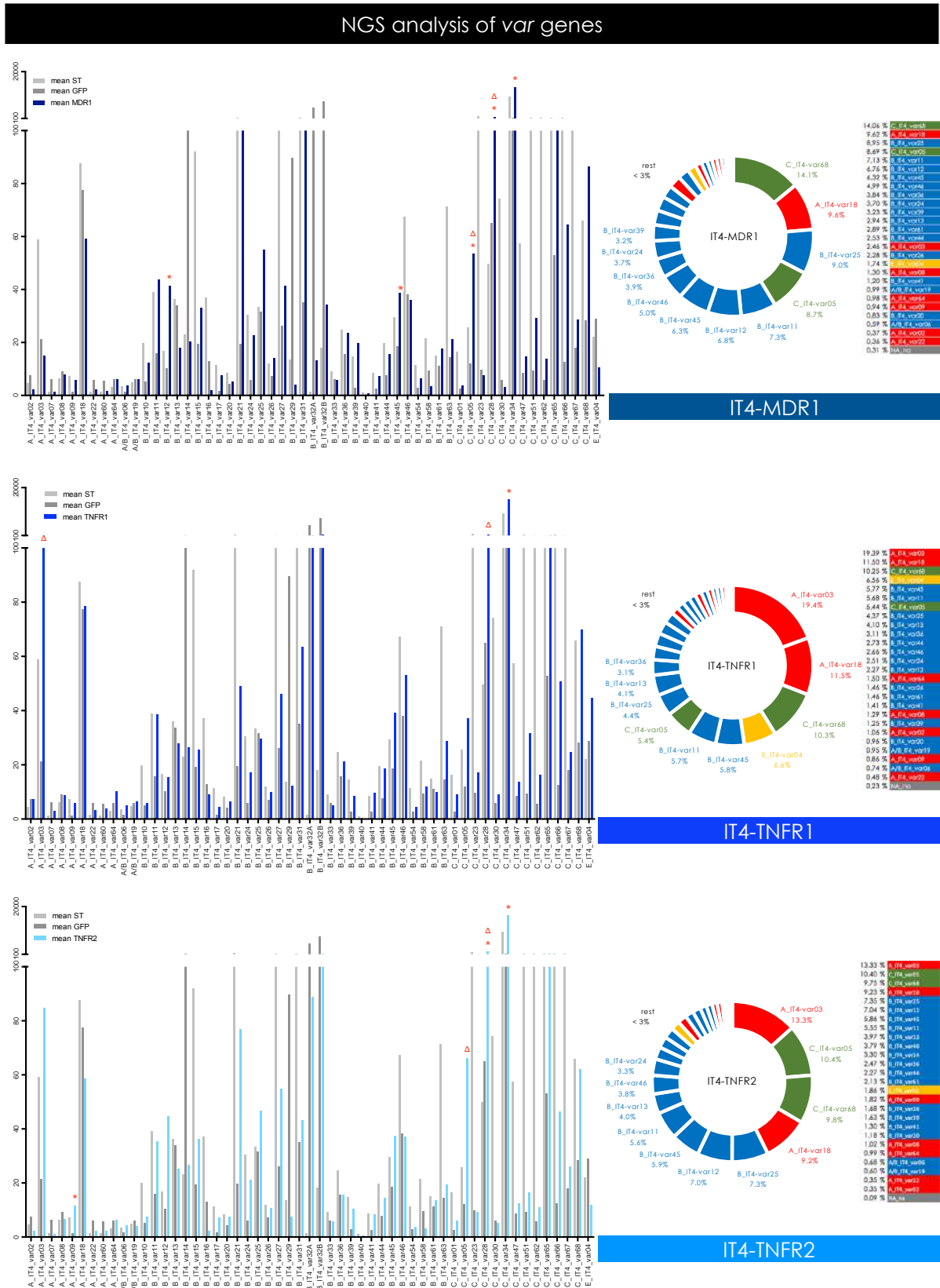


Figure 20.1 (to be continued). Comparison of var gene expression levels of IT4-MDR1, IT4-TNFR1 and IT4-TNFR2.

NGS analysis of var genes

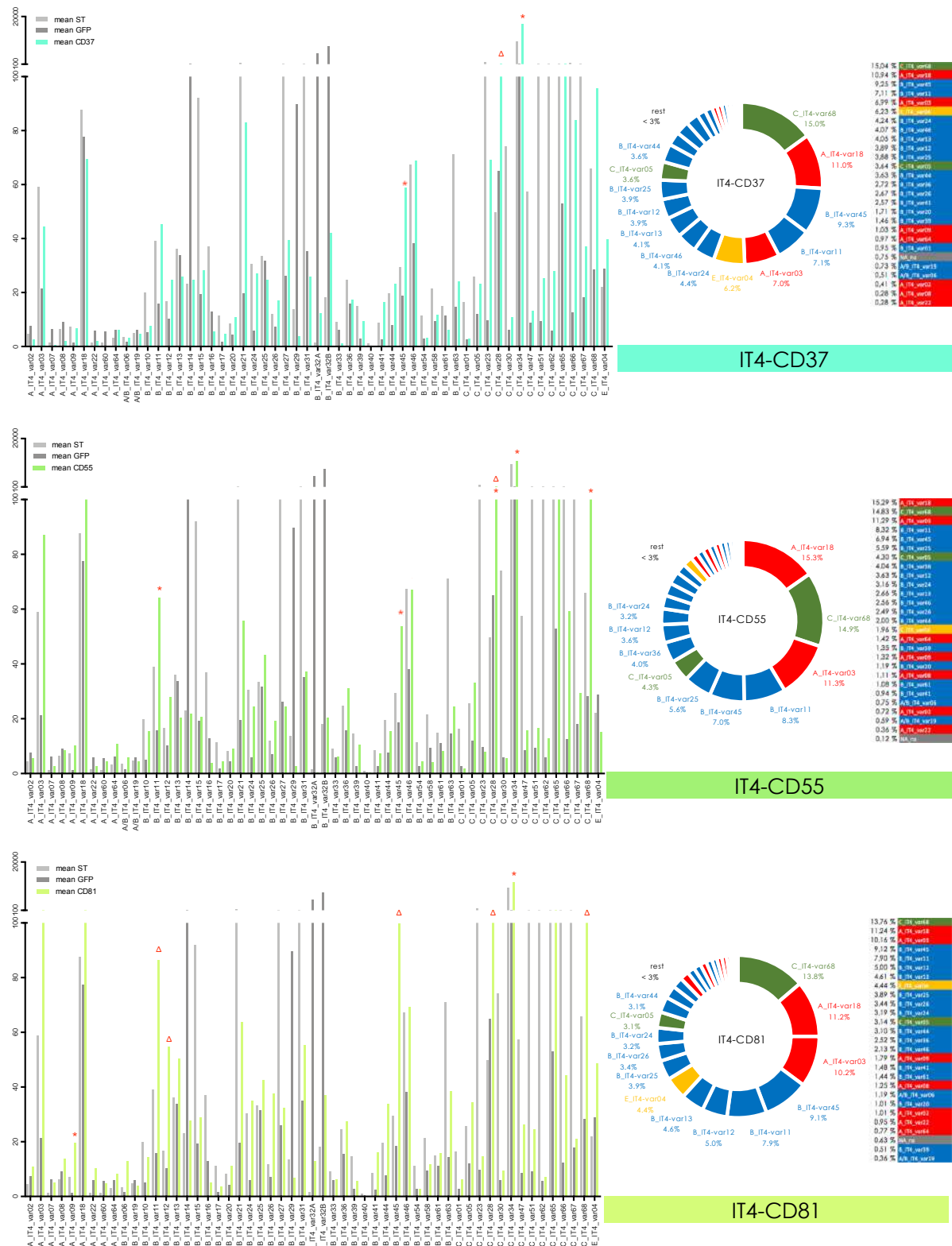


Figure 20.2 (continued). Comparison of var gene expression levels of IT4-CD37, IT4-CD55 and IT4-CD81. The left section shows the actual mean expression values, the right section shows the percentage of each var gene in relation to the whole gene set. IT4-MDR1 upregulation: B_var12, B_var46, C_var05; percentage distribution: C_var68 (14.1%), A_var18 (9.6%), B_var25 (9.0%), C_var05 (8.7%) and B_var11 (7.3%). IT4-TNFR1 upregulation: A_var03; percentage distribution: A_var03 (19.4%), A_var18 (11.5%) and C_var68 (10.3%). IT4-TNFR2 upregulation

A_var09; percentage distribution: A_var03 (13.3%), C_var05 (10.4%), C_var68 (9.8%), A_var18 (9.2), B_var25 (7.3%) and B_var12 (7.0%). IT4-CD37 upregulation: A_var03, B_var45; percentage distribution: C_var68 (15.0%), A_var18 (11.0%), B_var45 (9.3%), B_var11 (7.1%) and A_var03 (7.0%). IT4-CD55 upregulation: B_var11, B_var46, and C_var68; percentage distribution: A_var18 (15.3%), C_var68 (14.9%), A_var03 (11.3%), B_var11 (8.3%) and B_var45 (7.0%). IT4-CD81 upregulation: A_var09, B_var11, B_var12, B_var45; percentage distribution: C_var68 (13.8%), A_var18 (11.2%), A_var03 (10.2%), B_var45 (9.1%) and B_var11 (7.9%). All other *var* genes exhibited an expression of less than 7% each in the proportional comparison, respectively for each analysis. Significances ($p < 0.05$) are marked with red asterisks, values meeting the cutoff criteria were marked with red triangles.

For **IT4-MDR1** the actual expression values indicate a significant upregulation in the gene expression levels of 3 *var* genes (B_var12, B_var46 and, C_var05), while C_var05 additionally exceeded the cutoff. The proportional distribution within the remaining *var* gene set is led by C_var68 (14.1%), A_var18 (9.6%), B_var25 (9.0%), C_var05 (8.7%) and B_var11 (7.3%). All other *var* genes exhibited an expression of less than 7% each in the particular comparison.

For **IT4-TNFR1** the compared *var* gene expression levels show only an upregulation for A_var03 exceeding the cutoff criteria and show a clear and strong tendency of receptor specific regulation. Considering 3 of 4 biological readings by excluding 1 outlier, the mean expression value for A_var03 would also be significant by general calculation. Accordingly, within the proportional distribution of the remaining *var* gene set, A_var03 leads the list (19.4%), followed by A_var18 (11.5%) and C_var68 (10.3%). All other *var* genes exhibited an expression of less than 7% each.

For **IT4-TNFR2** the comparison showed a significant upregulation of the gene expression levels of A_var09; while C_var05 surpassed the cutoff criteria. Within the proportional comparison, A_var03 (13.3%), C_var05 (10.4%), C_var68 (9.8%), A_var18 (9.2), B_var25 (7.3%) and B_var12 (7.0%) were the most prevalent genes. All other *var* genes showed an expression of less than 7% each.

For **IT4-CD37** the actual expression values indicate a significant upregulation of A_var03 and B_var45. Within the proportional distribution of the remaining *var* gene set, C_var68 (15.0%), A_var18 (11.0%), B_var45 (9.3%), B_var11 (7.1%) and A_var03 (7.0%) were the most prevalent genes. All other *var* genes exhibited an expression of less than 7% each.

For **IT4-CD55** 3 genes showed a significant upregulation within the compared expression analysis, namely B_var11, B_var46 and C_var68. The circular chart state A_var18 (15.3%), C_var68 (14.9%), A_var03 (11.3%), B_var11 (8.3%) and B_var45 (7.0%) as most prevalent within the percentage distribution of the remaining *var* gene set, while all other did not reach a value of 7% each.

For **IT4-CD81** the comparison showed a significant upregulation of the gene expression levels of A_var09, B_var11, B_var12, B_var45 and C_var68 surpassing the cutoff criteria. The proportional distribution indicated C_var68 (13.8%), A_var18 (11.2%), A_var03 (10.2%), B_var45 (9.1%) and B_var11 (7.9%) as leading *var* genes. All other *var* genes exhibited an expression of less than 7% each.

5.8.2 Comparison of overall gene expression levels

Aside the var gene expression profile, also the overall picture of differentially expressed genes of the whole *P. falciparum* IT4 control and enriched isolates were compared, utilizing the same cutoff criteria as mentioned above.

The comparison of IT4-St and IT4-GFP showed a total of 2473 genes with upregulated expression levels, while 127 met the cutoff criteria. For IT4-MDR1 enriched population, 2868 genes were upregulated, while 205 reached the cutoff. For TNFR1 and TNFR2, 2711 and 2971 upregulated genes were detected, while 55 and 334 surpass the cutoff, respectively. For CD37, CD55 and CD81 a total of 2773, 2700 and 3123 genes were differentially upregulated, while 36, 96 and 362 genes met the cutoff criteria, respectively. In **Table 4.1** and **Table 4.2** an overview of 72 upregulated genes is shown, selected according to the criteria and relevance of this thesis. Values surpassing the cutoff criteria appear in red boxes, while significant *p* and *padj* values < 0.05 are indicated below in red font color.

Table 4.1 (to be continued.). Overview of NGS data for control and enriched IT4 population with mean values and respective *p*- and *padj*-values.

| # | ID | IT4-St | IT4-GFP | IT4-MDR1 | IT4-TNFR1 | IT4-TNFR2 | IT4-CD37 | IT4-CD55 | IT4-CD81 | name | function |
|----|---------------|----------|----------|-------------------------|-------------------------|-------------------------|-------------------------|-------------------------|-------------------------|-------------------------------------|--------------------------------------|
| | | | | <i>pval</i> <i>padj</i> | <i>pval</i> <i>padj</i> | <i>pval</i> <i>padj</i> | <i>pval</i> <i>padj</i> | <i>pval</i> <i>padj</i> | <i>pval</i> <i>padj</i> | | |
| 1 | PFIT_0801900 | 540.64 | 1000.42 | 772.80 0.25 0.67 | 723.02 0.58 | 756.80 0.32 0.94 | 1406.75 0.23 0.60 | 1008.69 0.92 0.98 | 1180.22 0.81 0.94 | acyl-CoA synthetase | knobs |
| 2 | PFIT_1149200 | 77.80 | 91.03 | 134.98 0.32 0.73 | 120.13 0.79 0.55 | 598.45 0.11 0.66 | 79.55 0.62 0.89 | 38.78 0.03 0.14 | 410.60 0.20 0.61 | AG 332, DBL-like protein | knobs |
| 3 | PFIT_0302400 | 2155.17 | 506.74 | 1381.80 0.08 0.43 | 1470.15 0.08 0.43 | 817.44 0.39 0.86 | 3438.93 0.00 0.03 | 3464.03 0.00 0.00 | 8014.72 0.02 0.17 | CLAG 3.1 | knobs |
| 4 | PFIT_1474300 | 386.46 | 377.56 | 935.38 0.11 0.17 | 533.52 0.97 0.41 | 978.52 0.13 0.69 | 505.75 0.44 0.80 | 493.94 0.19 0.47 | 473.94 0.62 0.88 | DnaJ protein, putative | trafficking, membrane & cytoskeleton |
| 5 | PFIT_1355800 | 21.41 | 27.85 | 59.69 0.14 0.30 | 39.32 0.56 0.31 | 51.30 0.10 0.66 | 30.92 0.74 0.94 | 61.20 0.13 0.38 | 31.37 0.78 0.93 | DnaJ protein, putative | trafficking, membrane & cytoskeleton |
| 6 | PFIT_0826700 | 78.36 | 110.23 | 129.23 0.71 0.92 | 99.90 0.32 0.52 | 198.73 0.21 0.77 | 75.45 0.16 0.52 | 110.25 0.93 0.99 | 137.08 0.62 0.88 | DnaJ protein, putative | trafficking, membrane & cytoskeleton |
| 7 | PFIT_0201000 | 4.93 | 0.00 | 15.05 0.00 0.00 | 6.64 0.00 0.00 | 1.07 0.01 0.58 | 564.31 0.00 0.00 | 27.26 0.00 0.00 | 8.13 0.00 0.01 | DnaJ protein, putative | knobs |
| 8 | PFIT_1300800 | 1326.48 | 299.04 | 943.03 0.01 0.11 | 601.52 0.00 0.07 | 590.78 0.11 0.66 | 1710.01 0.01 0.08 | 1837.83 0.00 0.00 | 4217.86 0.03 0.17 | EBA-140 | merozoites & invasion |
| 9 | PFIT_0730400 | 5542.69 | 1538.69 | 4382.58 0.01 0.01 | 2955.00 0.00 0.06 | 2694.41 0.11 0.66 | 8901.27 0.00 0.06 | 9441.50 0.00 0.00 | 21327.92 0.04 0.22 | EBA-175 | merozoites & invasion |
| 10 | PFIT_0101000 | 582.69 | 169.72 | 559.61 0.00 0.00 | 304.06 0.00 0.00 | 373.06 0.01 0.57 | 959.98 0.01 0.07 | 1209.00 0.00 0.00 | 2339.97 0.04 0.21 | EBA-181 | merozoites & invasion |
| 11 | PFIT_0535800 | 10067.47 | 13777.11 | 19650.37 0.24 0.67 | 14847.83 0.34 0.90 | 28344.76 0.00 0.04 | 16877.37 0.46 0.82 | 13959.47 0.02 0.99 | 13417.94 0.84 0.95 | ETRAMPS | trafficking, membrane & cytoskeleton |
| 12 | PFIT_1032600 | 148.10 | 188.81 | 240.69 0.32 0.73 | 213.36 0.46 0.78 | 841.79 0.18 0.75 | 183.09 0.82 0.96 | 192.62 0.97 1.00 | 342.35 0.16 0.54 | ETRAMPI0.2 | trafficking, membrane & cytoskeleton |
| 13 | PFIT_1038200 | 674.61 | 935.23 | 1459.33 0.13 0.53 | 983.88 0.26 0.98 | 1813.46 0.30 0.83 | 594.60 0.07 0.31 | 837.83 0.61 0.84 | 1013.56 0.92 0.98 | FIKK, serine/threonine kinase | trafficking, membrane & cytoskeleton |
| 14 | PFIT_0101100 | 107.12 | 97.07 | 84.72 0.52 0.84 | 81.80 0.92 0.37 | 236.08 0.20 0.75 | 74.12 0.22 0.60 | 65.34 0.11 0.34 | 118.83 0.70 0.90 | FIKK, serine/threonine kinase | trafficking, membrane & cytoskeleton |
| 15 | PFIT_0703400 | 63.03 | 15.41 | 46.17 0.00 0.06 | 55.28 0.00 0.00 | 30.47 0.08 0.64 | 96.88 0.01 0.10 | 95.65 0.00 0.00 | 126.84 0.00 0.00 | FIKK, serine/threonine kinase, put. | trafficking, membrane & cytoskeleton |
| 16 | PFIT_0808000 | 313.24 | 113.36 | 351.60 0.00 0.05 | 171.77 0.00 0.32 | 182.80 0.23 0.78 | 414.22 0.04 0.22 | 467.86 0.00 0.00 | 642.75 0.06 0.29 | gamete release protein, put. | gametogenesis |
| 17 | PFIT_1300400 | 215.36 | 248.27 | 648.86 0.00 0.00 | 287.66 0.69 0.73 | 502.75 0.10 0.66 | 255.42 0.99 1.00 | 405.58 0.30 0.59 | 302.78 0.69 0.90 | glycophorin binding protein | knobs |
| 18 | PFIT_0408000 | 579.61 | 1108.10 | 1185.04 0.95 1.00 | 1009.43 0.01 0.53 | 1191.62 0.94 0.99 | 1012.00 0.68 0.91 | 1039.61 0.68 0.87 | 1025.33 0.74 0.92 | HSP40 | trafficking, membrane & cytoskeleton |
| 19 | PFIT_1015100 | 130.73 | 162.28 | 176.34 0.94 1.00 | 191.36 0.76 0.79 | 433.27 0.19 0.75 | 108.00 0.25 0.63 | 132.59 0.61 0.83 | 260.55 0.40 0.79 | HSP60 | trafficking, membrane & cytoskeleton |
| 20 | PFIT_1134700 | 1538.20 | 3921.77 | 3557.32 0.57 0.87 | 3404.12 0.00 0.39 | 4753.54 0.60 0.91 | 2770.80 0.14 0.48 | 3015.37 0.30 0.59 | 3109.81 0.44 0.81 | HSP70 | trafficking, membrane & cytoskeleton |
| 21 | PFIT_0201300 | 19.63 | 0.65 | 302.56 0.00 0.00 | 23.52 0.00 0.00 | 20.41 0.00 0.00 | 3096.87 0.00 0.00 | 341.39 0.00 0.00 | 230.64 0.02 0.14 | KAHRP | knobs |
| 22 | PFIT_0201100 | 1.69 | 0.00 | 29.87 0.00 0.00 | 2.38 0.00 0.00 | 0.67 0.00 0.54 | 400.29 0.00 0.00 | 31.03 0.00 0.00 | 8.84 0.00 0.00 | knob associated HSP40 | knobs |
| 23 | PFIT_1369300 | 11122.21 | 20566.00 | 24773.28 0.64 0.89 | 21696.68 0.06 0.97 | 26997.31 0.40 0.87 | 18655.82 0.64 0.90 | 17675.87 0.58 0.82 | 12650.89 0.14 0.49 | MAHRP1 | trafficking, membrane & cytoskeleton |
| 24 | PFIT_0930500 | 6925.09 | 951.19 | 4437.32 0.00 0.00 | 3448.97 0.00 0.00 | 2674.56 0.02 0.52 | 10115.42 0.00 0.02 | 8632.89 0.00 0.00 | 18402.89 0.01 0.10 | MSP1 (and others) | merozoites & invasion |
| 25 | PFIT_0500900 | 266.72 | 69.21 | 277.32 0.09 0.45 | 336.00 0.32 0.07 | 799.56 0.06 0.62 | 195.61 0.13 0.46 | 180.34 0.23 0.51 | 811.13 0.04 0.23 | PFEMP2/MESA | knobs |
| 26 | PFIT_0201200 | 1.68 | 0.00 | 17.38 0.00 0.00 | 4.28 0.30 0.06 | 4.24 0.00 0.41 | 103.63 0.00 0.00 | 17.19 0.01 0.07 | 30.68 0.01 0.11 | PFEMP3 | knobs |
| 27 | PFIT_1102000 | 11.75 | 3.28 | 9.03 0.36 0.76 | 11.16 0.41 0.22 | 53.00 0.07 0.64 | 5.89 0.83 0.96 | 0.96 0.30 0.59 | 32.65 0.06 0.29 | PFMC-2TM | VSA |
| 28 | PFIT_0423100 | 299.43 | 145.95 | 438.62 0.00 0.01 | 253.43 0.00 0.04 | 268.86 0.01 0.58 | 914.07 0.00 0.00 | 401.60 0.00 0.00 | 317.15 0.06 0.29 | PHIST_a, unknown function | knobs |
| 29 | PFIT_bin01500 | 84.54 | 54.98 | 99.31 0.09 0.44 | 57.04 0.41 0.91 | 81.44 0.26 0.79 | 230.38 0.00 0.00 | 85.62 0.16 0.43 | 79.59 0.38 0.77 | PHIST_a, unknown function | VSA |
| 30 | PFIT_0835200 | 22.68 | 59.74 | 34.36 0.11 0.49 | 35.23 0.00 0.05 | 121.44 0.44 0.88 | 16.03 0.00 0.02 | 21.40 0.01 0.06 | 43.33 0.51 0.84 | PHIST_a, unknown function | VSA |
| 31 | PFIT_0732300 | 16.80 | 86.66 | 64.99 0.42 0.80 | 81.12 0.80 | 87.80 0.90 0.98 | 17.11 0.00 0.01 | 68.01 0.54 0.80 | 61.48 0.45 0.81 | PHIST_a, unknown function | VSA |
| 32 | PFIT_0400700 | 105.27 | 42.82 | 120.16 0.20 0.62 | 154.45 0.59 0.18 | 443.92 0.08 0.44 | 54.45 0.73 0.94 | 46.92 0.94 0.99 | 341.77 0.04 0.29 | PHIST_a, unknown function | VSA |
| 33 | PFIT_0536100 | 372.54 | 900.86 | 1718.52 0.17 0.22 | 958.18 0.07 0.97 | 2658.65 0.25 0.79 | 427.91 0.00 0.05 | 879.62 0.79 0.93 | 1191.60 0.75 0.92 | PHIST_b - lysine-rich | knobs |
| 34 | PFIT_0423000 | 381.76 | 98.10 | 260.88 0.00 0.00 | 178.39 0.00 0.00 | 149.11 0.18 0.75 | 804.52 0.00 0.00 | 280.33 0.00 0.00 | 197.97 0.11 0.42 | PHIST_b, unknown function | knobs |
| 35 | PFIT_0701000 | 891.70 | 296.31 | 1004.66 0.00 0.00 | 477.83 0.00 0.20 | 581.34 0.09 0.64 | 1920.52 0.01 0.07 | 848.55 0.00 0.01 | 1704.13 0.06 0.30 | PHIST_b, unknown function | VSA |
| 36 | PFIT_1477300 | 89.13 | 97.43 | 328.21 0.00 0.00 | 101.72 0.91 0.97 | 792.88 0.14 0.70 | 31.94 0.00 0.04 | 53.10 0.13 0.38 | 291.02 0.38 0.77 | PHIST_b, unknown function | VSA |

Table 4.2 (continued.). Overview of NGS data for control and enriched IT4 population with mean values and respective *p*- and *padj*-values.

| # | ID | IT4-ST | IT4-GFP | IT4-MDR1 | | IT4-TNFR1 | | IT4-TNFR2 | | IT4-CD37 | | IT4-CD55 | | IT4-CD81 | | name | function | | | | | | |
|----|---------------|----------|----------|----------|----------|-----------|----------|-----------|-----------|----------|------|----------|------|----------|------|------|----------|------|------|--------------------------------------|--------------------------------|---|--------------------------------------|
| | | | | pval | padj | pval | padj | pval | padj | pval | padj | pval | padj | pval | padj | | | | | | | | |
| 37 | PFIT_1478600 | 142.48 | 393.32 | 598.20 | 351.02 | 919.90 | 252.39 | 218.12 | 365.94 | 0.17 | 0.59 | 0.01 | 0.47 | 0.30 | 0.82 | 0.11 | 0.43 | 0.01 | 0.09 | 0.84 | 0.95 | PHIST_b, unknown function | VSA |
| 38 | PFIT_0730200 | 97.29 | 165.47 | 204.82 | 146.19 | 438.82 | 58.99 | 120.87 | 184.76 | 0.56 | 0.87 | 0.08 | 0.44 | 0.22 | 0.77 | 0.00 | 0.02 | 0.29 | 0.58 | 0.93 | 0.98 | PHIST_b, unknown function | VSA |
| 39 | PFIT_0536000 | 6058.94 | 9924.00 | 15919.32 | 8984.27 | 20666.63 | 5375.95 | 8084.13 | 8851.06 | 0.10 | 0.48 | 0.06 | 0.50 | 0.21 | 0.77 | 0.01 | 0.10 | 0.48 | 0.75 | 0.70 | 0.90 | PHIST_b, unknown function | VSA |
| 40 | PFIT_1200700 | 331.21 | 132.23 | 245.12 | 319.00 | 1046.13 | 129.55 | 113.04 | 610.32 | 0.47 | 0.82 | 0.46 | 0.24 | 0.07 | 0.64 | 0.96 | 1.00 | 0.80 | 0.93 | 0.16 | 0.53 | PHIST_b, unknown function | VSA |
| 41 | PFIT_0833900 | 11.15 | 17.73 | 32.79 | 10.86 | 68.84 | 4.27 | 18.85 | 32.02 | 0.22 | 0.64 | 0.44 | 0.29 | 0.23 | 0.78 | 0.06 | 0.31 | 0.95 | 0.99 | 0.40 | 0.78 | PHIST_b, unknown function | VSA |
| 42 | PFIT_0400500 | 557.07 | 521.88 | 1088.94 | 750.30 | 4192.25 | 463.22 | 312.95 | 1040.68 | 1.11 | 0.15 | 0.98 | 0.36 | 0.11 | 0.66 | 0.61 | 0.89 | 0.08 | 0.29 | 0.08 | 0.36 | PHIST_b, unknown function | VSA |
| 43 | PFIT_1148900 | 1181.29 | 2627.32 | 4244.68 | 2418.88 | 4930.37 | 964.38 | 2510.67 | 2469.93 | 0.10 | 0.46 | 0.09 | 0.56 | 0.28 | 0.82 | 0.00 | 0.00 | 0.82 | 0.94 | 0.82 | 0.95 | PHIST_c, unknown function | VSA |
| 44 | PFIT_0422200 | 60.01 | 65.61 | 43.88 | 72.30 | 240.78 | 47.14 | 68.71 | 100.77 | 0.16 | 0.57 | 0.80 | 0.92 | 0.14 | 0.71 | 0.37 | 0.75 | 0.98 | 1.00 | 0.32 | 0.73 | PHIST_c, unknown function | VSA |
| 45 | PFIT_0501300 | 301.25 | 320.58 | 490.59 | 440.94 | 1143.68 | 263.99 | 309.17 | 535.71 | 0.16 | 0.58 | 0.85 | 0.35 | 0.10 | 0.66 | 0.45 | 0.81 | 0.83 | 0.95 | 0.38 | 0.77 | PIESP2 | trafficking, membrane & cytoskeleton |
| 46 | PFIT_0401000 | 1719.79 | 439.36 | 2624.56 | 836.38 | 1112.59 | 3165.50 | 4200.28 | 7893.80 | 0.00 | 0.00 | 0.00 | 0.00 | 0.00 | 0.26 | 0.01 | 0.09 | 0.00 | 0.00 | 0.02 | 0.15 | (and others) | reticulu binding protein, RBP |
| 47 | PFIT_0100700 | 51328.40 | 34753.27 | 50344.34 | 30016.50 | 30269.86 | 94089.89 | 87394.99 | 106013.36 | 0.21 | 0.64 | 0.30 | 0.38 | 0.50 | 0.89 | 0.01 | 0.09 | 0.00 | 0.00 | 0.20 | 0.60 | RESA | knobs |
| 48 | PFIT_0200900 | 1.27 | 0.60 | 5.03 | 3.46 | 8.87 | 81.42 | 6.09 | 2.07 | 0.04 | 0.31 | 0.70 | 0.18 | 0.81 | 0.96 | 0.00 | 0.00 | 0.01 | 0.08 | 0.31 | 0.72 | RESA-like protein 1 with PHIST_b domain | knobs |
| 49 | PFIT_1200800 | 43.05 | 26.45 | 90.78 | 66.83 | 413.31 | 15.29 | 30.91 | 166.11 | 0.09 | 0.23 | 0.21 | 0.07 | 0.64 | 0.20 | 0.57 | 0.78 | 0.92 | 0.15 | 0.51 | RESA-like, with PHIST and DnaJ | knobs | |
| 50 | PFIT_1411400 | 1735.32 | 162.18 | 683.00 | 736.11 | 388.69 | 1753.36 | 1724.47 | 3535.55 | 0.07 | 0.39 | 0.04 | 0.24 | 0.79 | 0.00 | 0.02 | 0.00 | 0.00 | 0.01 | 0.08 | (and others) | rhopty-associated protein 1 | |
| 51 | PFIT_0500200 | 44.41 | 98.26 | 71.06 | 109.84 | 109.21 | 59.06 | 78.72 | 110.33 | 0.22 | 0.65 | 0.81 | 0.82 | 0.97 | 0.06 | 0.30 | 0.38 | 0.68 | 0.91 | 0.97 | RIFIN A-type | VSA | |
| 52 | PFIT_0835500 | 122.29 | 21.10 | 135.56 | 127.19 | 791.20 | 28.59 | 38.65 | 258.84 | 0.10 | 0.47 | 0.29 | 0.09 | 0.03 | 0.55 | 0.81 | 0.96 | 0.65 | 0.86 | 0.10 | 0.40 | RIFIN A-type | VSA |
| 53 | PFIT_bin04600 | 49.95 | 4.68 | 24.48 | 25.60 | 33.69 | 83.94 | 110.27 | 100.11 | 0.03 | 0.26 | 0.03 | 0.09 | 0.01 | 0.51 | 0.02 | 0.17 | 0.00 | 0.00 | 0.00 | 0.00 | RIFIN A-type | VSA |
| 54 | PFIT_0800300 | 27.81 | 29.86 | 24.30 | 204.84 | 167.16 | 35.51 | 27.21 | 44.17 | 0.49 | 0.83 | 0.95 | 0.00 | 0.09 | 0.64 | 0.79 | 0.96 | 0.73 | 0.90 | 0.46 | 0.82 | RIFIN B-type | VSA |
| 55 | PFIT_0424300 | 1.66 | 0.00 | 12.04 | 1.07 | 0.75 | 233.86 | 18.05 | 4.42 | 0.00 | 0.00 | 0.13 | 0.20 | 0.08 | 0.64 | 0.00 | 0.00 | 0.00 | 0.00 | 0.00 | 0.07 | RIFIN NA-type | knobs |
| 56 | PFIT_0501400 | 21872.82 | 33377.12 | 40658.10 | 35407.14 | 37417.83 | 44357.21 | 36689.29 | 28661.04 | 0.58 | 0.87 | 0.26 | 0.96 | 0.80 | 0.96 | 0.29 | 0.68 | 0.82 | 0.94 | 0.58 | 0.86 | SBP1 | knobs |
| 57 | PFIT_0111500 | 4.00 | 4.49 | 3.37 | 3.99 | 5.07 | 3.37 | 1.58 | 63.44 | 0.66 | 0.91 | 0.94 | 0.92 | 0.91 | 0.99 | 0.58 | 0.88 | 0.22 | 0.50 | 0.27 | 0.69 | SURFIN 1.1 | VSA |
| 58 | PFIT_0111200 | 50.46 | 101.28 | 88.89 | 74.65 | 66.59 | 112.77 | 115.92 | 108.52 | 0.65 | 0.86 | 0.06 | 0.25 | 0.11 | 0.66 | 0.79 | 0.96 | 0.73 | 0.90 | 0.99 | 1.00 | SURFIN 1.2 | VSA |
| 59 | PFIT_0400900 | 243.52 | 76.93 | 135.33 | 158.38 | 189.65 | 421.10 | 372.33 | 602.38 | 0.21 | 0.64 | 0.03 | 0.08 | 0.07 | 0.54 | 0.01 | 0.06 | 0.03 | 0.16 | 0.01 | 0.11 | SURFIN 4.1 | VSA |
| 60 | PFIT_0834000 | 12.89 | 19.90 | 48.15 | 20.48 | 60.26 | 5.06 | 46.70 | 90.52 | 0.07 | 0.33 | 0.48 | 0.85 | 0.08 | 0.63 | 0.01 | 0.06 | 0.14 | 0.40 | 0.26 | 0.68 | SURFIN 8.1 | VSA |
| 61 | PFIT_0833700 | 28.04 | 16.04 | 118.58 | 32.94 | 99.21 | 36.31 | 78.72 | 110.33 | 0.00 | 0.00 | 0.35 | 0.10 | 0.07 | 0.64 | 0.03 | 0.20 | 0.00 | 0.00 | 0.17 | 0.55 | SURFIN 8.2 | VSA |
| 62 | PFIT_1301000 | 10.60 | 14.28 | 25.20 | 17.11 | 17.45 | 28.74 | 16.12 | 149.57 | 0.30 | 0.71 | 0.70 | 0.89 | 0.69 | 0.93 | 0.15 | 0.50 | 0.84 | 0.95 | 0.24 | 0.65 | SURFIN 13.1 | VSA |
| 63 | PFIT_0818700 | 255.37 | 84.78 | 208.54 | 167.61 | 250.38 | 313.45 | 301.59 | 582.08 | 0.03 | 0.06 | 0.03 | 0.09 | 0.02 | 0.52 | 0.00 | 0.01 | 0.00 | 0.00 | 0.00 | 0.01 | VSP 9, putative | trafficking, membrane & cytoskeleton |
| 64 | PFIT_1250500 | 51.69 | 23.93 | 65.26 | 54.44 | 104.57 | 40.14 | 49.12 | 86.04 | 0.09 | 0.09 | 0.07 | 0.00 | 0.06 | 0.62 | 0.13 | 0.46 | 0.03 | 0.15 | 0.00 | 0.06 | VSP 26, putative | trafficking, membrane & cytoskeleton |
| 65 | PFIT_1111300 | 98.24 | 156.28 | 200.28 | 146.82 | 244.89 | 159.00 | 148.25 | 196.45 | 0.48 | 0.83 | 0.16 | 0.63 | 0.16 | 0.73 | 0.95 | 1.00 | 0.78 | 0.92 | 0.61 | 0.87 | VSP 35, putative | trafficking, membrane & cytoskeleton |
| 66 | PFIT_0725900 | 82.91 | 180.27 | 225.98 | 192.45 | 233.45 | 153.82 | 205.70 | 198.09 | 0.53 | 0.85 | 0.01 | 0.91 | 0.29 | 0.82 | 0.50 | 0.84 | 0.69 | 0.88 | 0.89 | 0.97 | VSP 53, putative | trafficking, membrane & cytoskeleton |
| 67 | PFIT_0936800 | 81.88 | 84.66 | 189.95 | 107.25 | 583.50 | 36.24 | 53.10 | 224.40 | 0.03 | 0.28 | 0.95 | 0.72 | 0.12 | 0.67 | 0.05 | 0.27 | 0.32 | 0.62 | 0.40 | 0.79 | exp. protein (HYP11), unknown funct. | VSA |
| 68 | PFIT_1300600 | 679.66 | 1754.10 | 3985.84 | 1705.57 | 4933.59 | 505.87 | 1774.87 | 2312.97 | 0.00 | 0.08 | 0.06 | 0.85 | 0.25 | 0.79 | 0.00 | 0.00 | 0.97 | 1.00 | 0.74 | 0.92 | exp. protein (HYP12), unknown funct. | VSA |
| 69 | PFIT_1000600 | 25.35 | 9.70 | 44.11 | 15.99 | 83.23 | 1.80 | 8.87 | 102.36 | 0.14 | 0.54 | 0.63 | 0.65 | 0.13 | 0.69 | 0.25 | 0.63 | 0.91 | 0.98 | 0.15 | 0.51 | exp. protein (HYP12), unknown funct. | VSA |
| 70 | PFIT_1478100 | 73.10 | 133.68 | 723.06 | 230.05 | 1074.34 | 68.95 | 186.07 | 508.82 | 0.00 | 0.00 | 0.00 | 0.00 | 0.11 | 0.66 | 0.02 | 0.15 | 0.42 | 0.71 | 0.40 | 0.79 | exp. protein (HYP17), unknown funct. | VSA |
| 71 | PFIT_0802300 | 54.00 | 153.42 | 827.58 | 187.46 | 1310.70 | 62.91 | 191.66 | 478.11 | 0.06 | 0.74 | 0.12 | 0.68 | 0.00 | 0.05 | 0.68 | 0.88 | 0.43 | 0.81 | exp. protein (HYP17), unknown funct. | VSA | | |
| 72 | PFIT_0217000 | 83.43 | 152.24 | 274.40 | 198.83 | 256.94 | 156.96 | 212.60 | 196.35 | 0.00 | 0.34 | 0.36 | 0.12 | 0.67 | 0.92 | 0.99 | 0.32 | 0.62 | 0.57 | 0.86 | (and others) | conserved, protein, unknown funct. | |

5.8.2.1 Knob related genes

Regarding knob formation and the knob structure itself, 17 genes were upregulated within at least one of the enriched IT4 population. The main actors of knob formation, like **KAHRP** (PFIT_0201300), is about 163fold upregulated in IT4-CD37, while also being highly upregulated in IT4-MDR1 (~16fold), IT4-CD55 (~18fold) and IT4-CD81 (~12fold). The **knob associated HSP40** (PFIT_0201100, ~200fold) and **PfEMP3** (PFIT_0201200, ~65fold) gene expression levels are upregulated in IT4-CD37 only. The knob associated gene for an **acyl-CoA synthetase** (PFIT_0801900) was ~3fold upregulated in IT4-CD37 and ~2fold in IT4-CD81. The knob structure related **glycophorin binding protein** (PFIT_1300400) surpassed the cutoff for IT4-MDR1 (~3fold) and IT4-TNFR2 (~2fold). Interestingly, genes, highly upregulated in the IT4 population, enriched over HBEC-5i cells at 40°C as well, show elevated levels solely in the IT4-CD37 enriched population, like **DnaJ** (PFIT_0201000, ~115fold), **NA-type RIFIN** (PFIT_0424300, ~140fold), **PHIST_a**

(PFIT_0423100, ~3fold), **PHIST_b** (PFIT_0423000, ~2fold), the **RESA-like protein 1 with PHIST_b domain** (PFIT_0200900, ~65fold) and **SBP1** (PFIT_0501400, ~2fold). The **DBL-like antigen332** (PFIT_1149200) met the cutoff criteria within the IT4-TNFR2 (~8fold) and IT4-CD81 (~5fold) population. The expression level for **PfEMP2/MESA** (PFIT_0500900) was elevated about 3fold for IT4-TNFR2 and IT4-CD81 each. The **RESA-like protein with PHIST and DnaJ domains** (PFIT_1200800) surpass the cutoff for IT4-MDR1 (~2fold), IT4-TNFR2 (~10fold) and IT4-CD81 (~4fold). Moreover, the **CLAG 3.1** gene (PFIT_0302400, ~4fold) and the **RESA** gene (PFIT_0100700, ~2fold) were differentially upregulated for IT4-CD81 solely. The gene for the **lysine-rich membrane-associated PHISTb protein** (PFIT_0536100) met the cutoff in all populations, except IT4-CD37 and IT4-CD55.

5.8.2.2 Trafficking, membrane & cytoskeleton related genes

Genes, coding for proteins, putatively involved in protein trafficking, membrane rigidity, cytoskeleton formation or related functions within the IE met the cutoff criteria in various populations. The expression levels for the 3 other **DnaJ** genes (PFIT_1474300; PFIT_1355800; PFIT_0826700) were below the cutoff level for IT4-CD81 but met the criteria for the other populations, respectively. The **HSP40** gene (PFIT_0408000) was ~2fold enhanced in the IT4-MDR1 population, while all 3, including **HSP60** (PFIT_1015100) and **HSP70** (PFIT_1134700) genes were ~2 to 3fold elevated for the IT4-TNFR2 population. While the **MAHRP** gene (PFIT_1369300) was about 2fold elevated within the IT4-MDR1 and IT4-TNFR2 population, respectively; the **PIESP2** gene (PFIT_0501300) met the cutoff about 4fold for IT4-TNFR2 solely. Appurtenant gene expression levels for **ETRAPP5** (PFIT_0535800) and **ETRAPP10.2** (PFIT_1032600) were ~2 to 4fold elevated for IT4-TNFR2 and IT4-CD81; levels for the 3 **FIKK serine/threonine kinase** family members, were about 2fold increased for IT4-MDR1 (PFIT_1038200), IT4-TNFR2 (PFIT_1038200, PFIT_0101100) and IT4-CD81 (PFIT_0703400), each. The expression levels of 4 **vacuolar protein sorting-associated protein** members (PFIT_0818700, PFIT_1250500, PFIT_1111300, PFIT_0725900) were mainly elevated about 3fold each within the IT4-MDR1 and IT4-TNFR2 population. Albeit the level for the **VSP53** gene (PFIT_0725900) was increased in 5, while in general, none VSP gene was enriched within the IT4-CD37 population.

5.8.2.3 VSA genes

Conspicuously, within the IT4-TNFR2 population, most expression levels from genes coding for **PHIST** proteins were upregulated. In general, 3 of 5 highly expressed genes, coding for **PHIST_a** (PFIT_0835200, PFIT_0732300; both ~5fold; PFIT_0400700, ~4fold) topped the cutoff in the IT4-TNFR2 population, while only the last one also did about 3fold in IT4-CD81. The other genes, coding for **PHIST_a** (PFIT_0423100, PFIT_bin01500, ~3fold each) exhibited an elevated expression level solely for the IT4-CD37 population. Including all selected genes coding for **PHIST_b**, 2 were elevated solely within the IT4-CD37 (PFIT_0701000, PFIT_0423000, ~2fold), while for IT4-CD81 only 2 genes (PFIT_0536100, PFIT_1477300; both ~3fold) and for IT4-TNFR1 only the first (~2.5fold) met the cutoff criteria. Within the IT4-MDR1 and IT4-TNFR2 population, 5 of 10 (PFIT_0536100, ~5 and 7fold; PFIT_1477300, ~4 and 9fold; PFIT_1478600, ~4 and 8fold; PFIT_0730200, ~2

and 5fold; PFIT_0536000, ~3 and 4fold) were over the cutoff, while 3 gene expression levels (PFIT_1200700, ~3fold; PFIT_0833900, ~6fold; PFIT_0400500, ~8fold) were over the cutoff for IT4-TNFR2 solely. Both **PHIST_c** (PFIT_1148900, PFIT_0422200) gene expression levels met the cutoff within the IT4-TNFR2 population, while only the first did within the IT4-MDR1, at about 4fold in each case.

Regarding selected members of other multigene families, only 2 **PfMC-2TM** gene (PFIT_1102000) exhibited an about 4fold increased expression level within the IT4-TNFR2 population.

All 3 **RIFIN A-type** genes (PFIT_0500200, PFIT_0835500, PFIT_bin04600) met the cutoff criteria by ~2fold or 6fold, except within the IT4-MDR1 and IT4-CD37 population. However, the expression level of only 1 **RIFIN B-type** gene (PFIT_0800300) was differentially upregulated about ~7.5fold and 6fold, in both, IT4-TNFR1 and IT4-TNFR2, respectively.

It is remarkably that all 6 upregulated **SURFIN** coding genes (PFIT_0111500, ~16fold; PFIT_0112000, ~2fold; PFIT_0400900, ~2fold; PFIT_0834000, ~4fold; PFIT_0833700, ~4fold; PFIT_1301000, ~15fold) were detected within the IT4-CD81 population and none SURFIN gene exhibited an upregulated expression level within the IT4-CD37 population. While for IT4-MDR1 and IT4-CD55, the SURFIN 8.2 (~4fold and ~3fold) and for IT4-TNFR2, the SURFIN 8.1 (~9fold) and the SURFIN 8.2 (~4fold) genes surpassed the cutoff, the level for SURFIN 1.2 was elevated within IT4-CD37, IT4-CD55 and IT4-CD81 about 2fold in each case.

Members of the, in total 17 annotated exported **HYP** multigene families with unknown functions, have been detected above the cutoff for all population, surprisingly except IT4-CD37. The HYP11 gene (PFIT_0936800) exhibited elevated expression levels in IT4-MDR1 (~2fold), IT4-TNFR2 (~7fold), IT4-CD81 (~3fold), while one HYP12 (PFIT_1300600) was elevated in IT4-MDR1 (~6fold), IT4-TNFR2 (~7fold), IT4-CD55 and IT4-CD81 (~3fold each) and another HYP12 (PFIT_1000600) showed an upregulated expression level in IT4-TNFR2 (~3fold) and IT4-CD81 (~4fold). A remarkable upregulation of the genes for HYP17 (PFIT_1478100) and HYP17 (PFIT_0802300) was observed for IT4-TNFR2 (~15fold and ~24fold), as well as IT4-MDR1 (~10fold and ~15fold), as IT4-TNFR1, IT4-CD55 (~3fold each) and IT4-CD81 (~7fold and ~9fold) surpassed lower.

5.8.2.4 Merozoites & invasion related genes and others

Due to a slight time shift in early harvesting of IE of the IT4-CD81 population, differentially upregulated expression levels of invasion associated and merozoite ascribed genes were detectable. This can be identified by the elevated levels of different EBA (PFIT_1300800, PFIT_0730400, PFIT_0101000), MSP (PFIT_0930500, and others), RBP (PFIT_0401000, and others) and rhoptry associated genes (PFIT_1411400, and others). Interestingly, the gene for the **gamete release protein** (PFIT_0808000) exhibited an about 2fold upregulation within the IT4-CD81 population.

5.8.2.5 Conserved genes with unknown function

Both differentially expressed genes of the HYP17 (PFIT_1478100, PFIT_0802300) met the cutoff for IT4-MDR1 (~10fold and ~15fold), IT4-TNFR1 (~3fold and ~4fold), IT4-TNFR2

(~15fold and ~24fold), IT4-CD55 (~3fold and ~4fold) and IT4-CD81 (~7fold and ~9fold) but did not for IT4-CD37. As the function for a large number of genes is not determined so far, many are termed as **conserved membrane proteins with unknown function**, while 22 of them were differentially upregulated in IT4-MDR1, IT4-TNFR2 and IT4-CD81 populations, but surprisingly only 3 gene expression levels hit the cutoff in IT4-CD55, albeit not at all within the IT4-TNFR1 and the IT4-CD37 population. For general **conserved Plasmodium proteins with unknown function**, 189 genes were above the cutoff, but also here, only 6 of them were also upregulated within the IT4-CD37 population.

> Taken together, the obtained results evidenced a differentially upregulation in IT4-MDR1 for the C_var05; in IT4-TNFR1 for the A_var03; in IT4-CD55 for the B_var11 and in IT4-CD81 for the A_var09, B_var11 and B_var12 genes. Furthermore, diverse gene clusters, associated with knob formation on the surface of IE were cumulatively detected in IT4-MDR1, IT4-TNFR2, IT4-CD37 and IT4-CD81. The gene, coding for the major knob associated histidine rich protein (KAHRP), was found to be extensively upregulated in the IT4-CD37 population, while also being present at considerable levels in IT4-MDR1, IT4-CD55 and IT4-CD81.

5.9 Knob presence mediated by a combination of heat and sequestration

The actual *P. falciparum* IT4 isolate used, is characterized by a stable knobless phenotype since years of cultivation. As the previous TEM analysis of IE cultivated under different conditions revealed that an enrichment of IE over HBEC-5i cells at febrile temperatures of 40°C resulted in knobby IE. Here, the aim was to investigate whether cytoadhesion at febrile temperature to human receptors, expressed on CHO cells, or even to CHO-mock transfected itself, is capable to promote the presence of surface expressed knob structures, resulting in a knobby IT4 phenotype. The protein expression and presentation on the IE surface was detected via IFA, by utilizing a specific α KAHRP antibody. The staining pattern was qualified by the comparison with a positive and negative control of knobless IT4-ST IE (neg. control) and knobby 3D7 isolate (pos. control) as a general baseline as well as an individual control by using samples, lacking the α KAHRP antibody, while still being stained with the labeled secondary antibody, to evaluate the background signals.

Initially, both the IT4-CD55 and the IT4-GFP populations, were enriched 7 times on the respective human CD55 receptor and the mock-transfected CHO-GFP cells at 37°. The same culture was split for further experiments. The IT4-CD55 line underwent the preabsorbtion at either 37°C (IT4-CD55-37p40°C) or 40°C (IT4-CD55-40p40°C), followed by the actual panning at 40°C. For the IT4-GFP population, no preabsorbtion was appropriate, so the populations were prewarmed for the time of preabsorbtion at either 37°C (IT4-GFP-37p40°C) or 40°C (IT4-GFP-40p40°C), followed by the actual panning at 40°C.

The results, shown in **Figure 21** shows that both, the IT4-CD55-37p40°C and IT4-GFP-37p40°C, clearly show KAHRP positively stained cells within the examined field of view. For the 40°C preabsorbed or prewarmed condition, only a strong background was detectable, respectively.

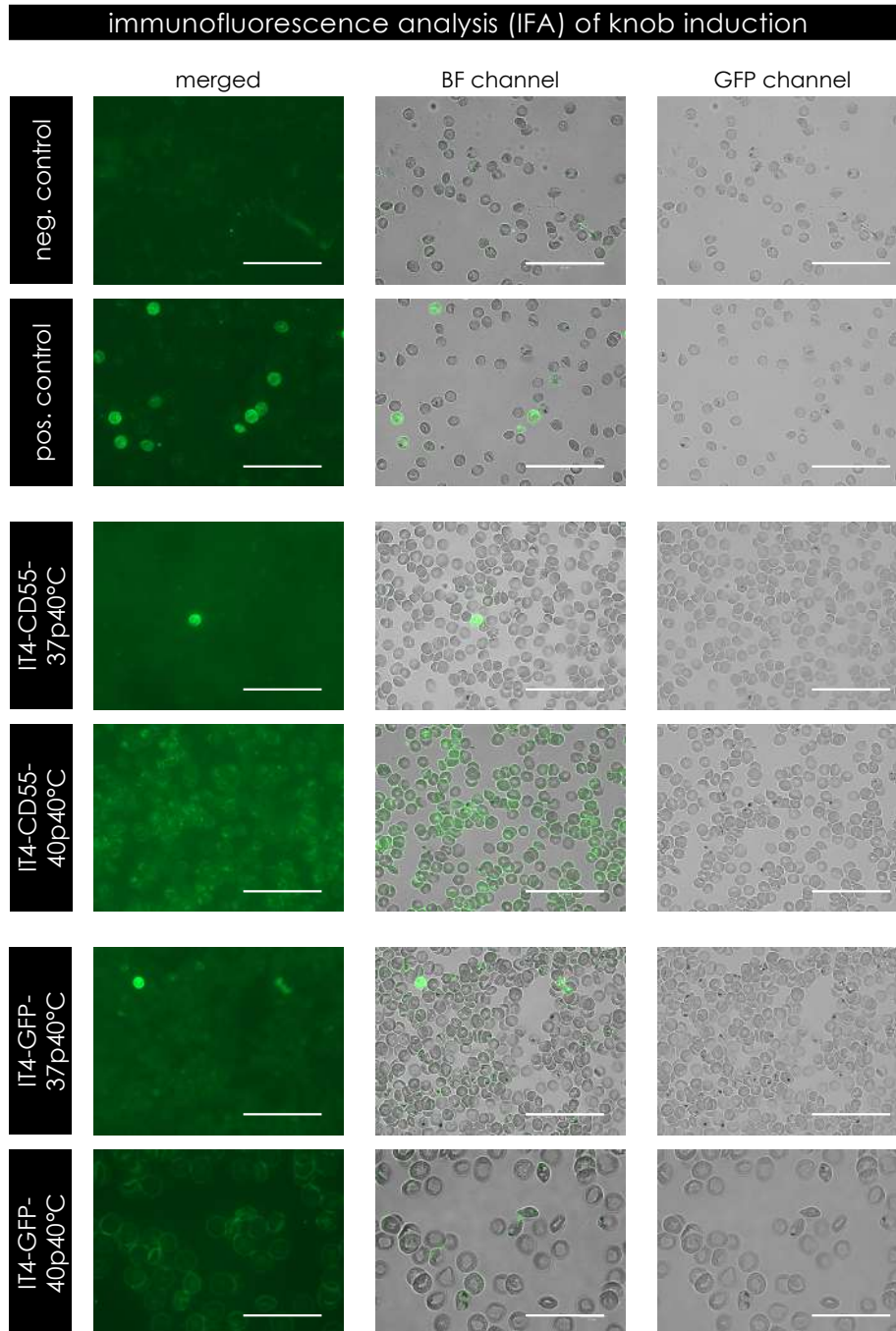


Figure 21. Immunofluorescence analysis: knob induction of the knobless IT4 isolate via cytoadhesion at febrile temperatures. Negative control is the IT4-ST culture, positive control is the knobby *P. falciparum* isolate 3D7. Initially knobless IT4-CD55 and IT4-GFP were enriched 7 times prior the experiment. Each culture was split for preabsorption at either 37°C (IT4-CD55-37p40°C) or 40°C (IT4-CD55-40p40°C), followed by the actual panning at 40°C. IT4-GFP was prewarmed for the time of preabsorption at either 37°C (IT4-GFP-37p40°C) or 40°C (IT4-GFP-40p40°C), followed by the actual panning at 40°C. A specific primary aKAHRP

antibody was used to stain the samples. Both, the IT4-CD55-37p40°C and IT4-GFP-37p40°C, clearly show KAHRP positively stained cells within the examined field of view. For the 40°C prewarmed and preabsorbed condition, only a strong background was detectable, respectively. Fluorescence images were recorded with EVOS FLauto at a 40x magnification, while GFP and BF channel were merged subsequently. Scale bar: 50 µm for all and 10 µm for IT4-GFP-40p40°C.

5.10 Transmission electron microscopy analysis

By utilizing transmissive electron microscopy (TEM), the phenotypical differences of the IT4 culture isolate was investigated at different conditions, focusing on the overall knob appearance and distribution.

The results for the comparison of different *P. falciparum* field isolates, including various culturing time and culture medium, are presented in **Figure 22**. For each condition regarding the IT4 culture isolate, at least 100 IE were analyzed, while, due to the restricted sample size, for the field isolates, all IE possibly detected have been considered.

The results pertaining to the IE of the *P. falciparum* IT4 control culture, the knob positive control after Gelafundin enrichment as well as the IT4 populations after enrichment over various human endothelial receptors, are shown in **Figure 21.1**. The results regarding IE of the IT4 culture isolate, enriched over human brain endothelial cells and/or cultivated at different febrile temperatures over an extended timespan or else, treated with the TNF α stimulant, are shown in **Figure 21.2**.

Quite in contrast to the IT4 isolate, all of the investigated the *P. falciparum* field isolates had knob structures on their surfaces, as shown in **Figure 22**. Different culture conditions were considered, as the BNI060616_long (top right) and BNI220616_HS (third right) isolate were handled with RPMI culture medium, completed with human serum A⁺, while the BNI220616_ALB (second right) was cultivated with RPMI, completed with AlbuMAX. All 3 isolates were in culture about 2 months. The BNI130716 (bottom left), BNI010916 (top right), BNI090916_1 (second right) and BNI090916_2 (third right) were handled under general culture conditions prior to TEM analysis about 14 days, while the BNI111216 (bottom right) isolate was processes already 2 days after cultivation.

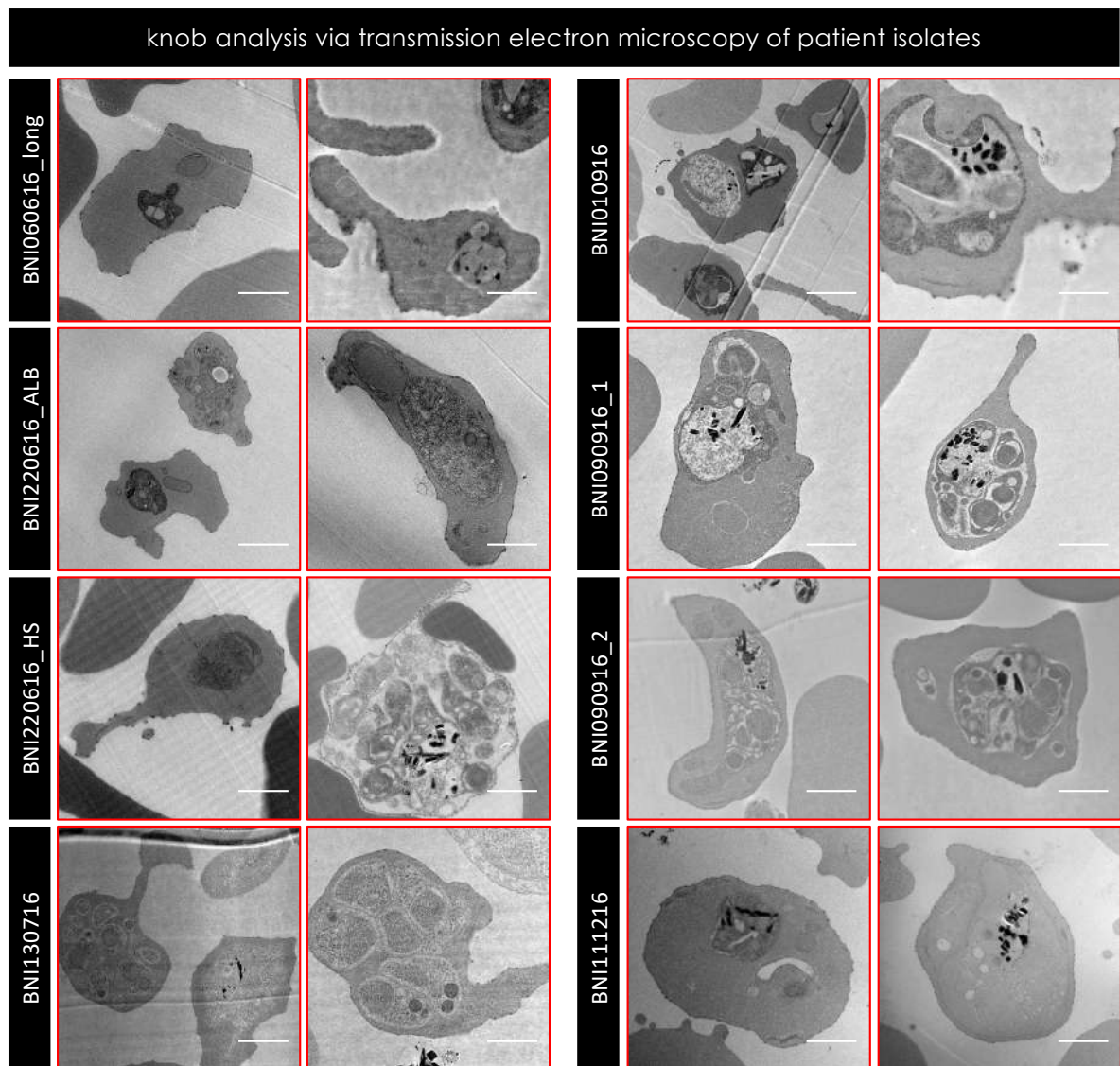


Figure 22. Transmission electron microscopy: analysis of knob appearance of *P. falciparum* field isolates. For investigating distinct *P. falciparum* field isolates, different culture conditions were considered. The BNI060616_long (top right) and BNI220616_HS (third right) isolate were handled with RPMI culture medium, completed with human serum A⁺, while the BNI220616_ALB (second right) was cultivated with RPMI, completed with AlbuMAX. All 3 isolates were in culture about 2 months. The BNI130716 (bottom left), BNI010916 (top right), BNI090916_1 (second right) and BNI090916_2 (third right) were handled under general culture conditions prior to TEM analysis for about 14 days, while the BNI111216 (bottom right) isolate was processed already 2 days after cultivation. Knob positive populations are marked with a red frame, scale bar is 1 μ m.

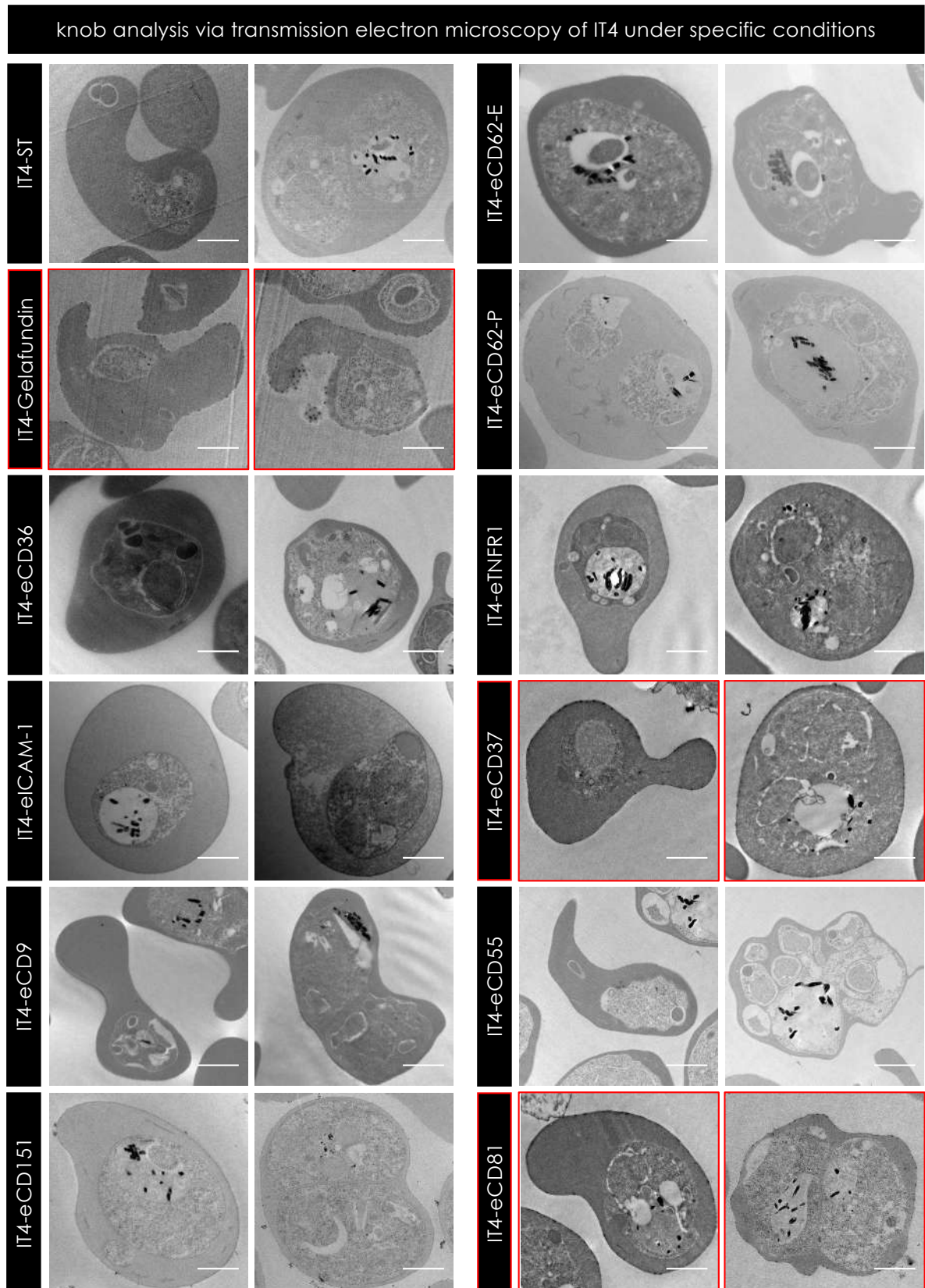


Figure 23.1 (to be continued). Transmission electron microscopy: analysis of knob appearance of the *P. falciparum* IE, enriched over human endothelial receptors.

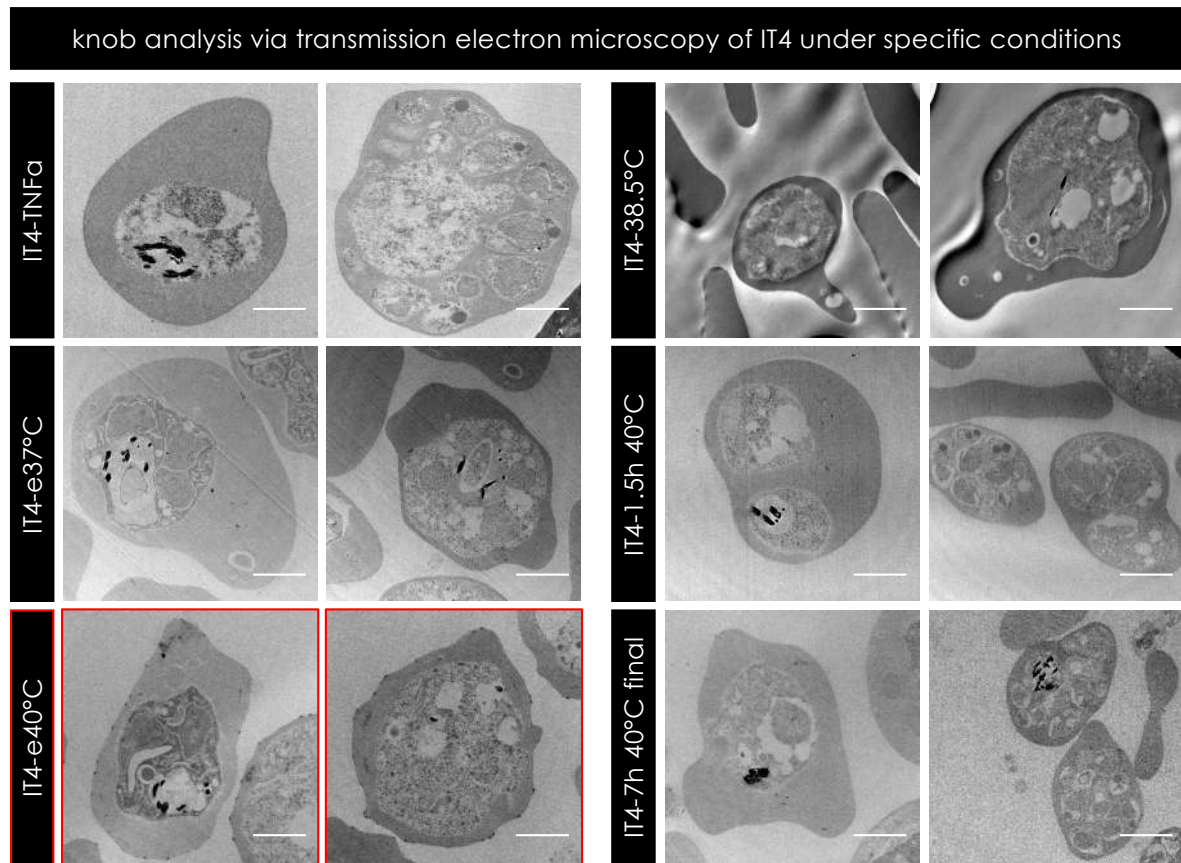


Figure 23.2 (continued). Transmission electron microscopy: analysis of knob appearance of the *P. falciparum* IE, treated with TNF α , as well as enriched and/or cultivated over HBEC-5i at febrile temperatures. IE of the *P. falciparum* IT4 control culture (IT4-ST), the positive, knobby control after Gelafundin enrichment (IT4-Gelafundin), as well as the IT4 populations after enrichment over 10 different human endothelial receptors are shown in **Figure 21.1**. The IE, enriched over human brain endothelial cells and/or cultivated at different febrile temperatures over an extended timespan or else, treated with the TNF α stimulant, are shown in **Figure 21.2**. Overall, only IE from the IT4-CD37 (Fig. 21.1, fourth right), IT4-CD81 (Fig. 21.1, bottom right), as well as IT4-40°C (Fig. 21.2, bottom left), population exhibited knob structures on the IE surface. Knob positive populations are marked with a red frame, scale bar is 1 μ m.

Figure 23.1 and **Figure 23.1** show the TEM analysis of the specifically enriched IT4 populations. By investigating the IT4-ST (top left) population, it became obvious that no IE exhibited any knob structure on the surface, as more than 6 different IT4-ST samples were analyzed individually. The IE within the IT4-Gelafundin (second left) enriched population served as a positive control, since it should be ensured that the enrichment actually leads to the accumulation of knobby IE. In general, only 2 of the 10 enriched IT4 population, namely the IT4-CD37 (fourth right) and IT4-CD81 (bottom right), exhibited definite knob structure on the IE surface. For all other populations, no knobby IE was found within the complete sample set, neither in early or late trophozoite stages, nor in early or late schizont staged parasitized erythrocytes. Considering the IT4 population, weekly treated with TNF α (top left), mimicking an inflammation-like environment, also no knob structures could be observed. Moreover, the cultivation of the IT4 isolate permanently exposed to elevated temperatures of 38.5°C (top right), also did not induce knob formation. By cultivating the IE

permanently at 37°C with a weekly heat shock of 40°C for 1.5 h (middle right), even after 9 weeks, no knob structures were found; eventually also not in week 10, after a final heat shock at 40°C for 7 h (bottom right). By investigating IT4 IE, enriched over human brain endothelial cells HBEC-5i at 37°C (middle left), at none of the erythrocytes, knobs were induced, unlike the IE, enriched over HBEC-5i at 40°C (bottom left), that clearly exhibited authentic knob protrusions on the IE surface.

5.11 Morphological analysis of knob appearance

While the single TEM pictures give a selected overview for each population investigated, the comprehensive data of the morphological appearance analysis are summarized in **Figure 24**. The percentages below the graph give the proportion of knob-positive cells within the analyzed set, while the ratio of knobs per μm is indicated as bars within the graph for each positive population individually.

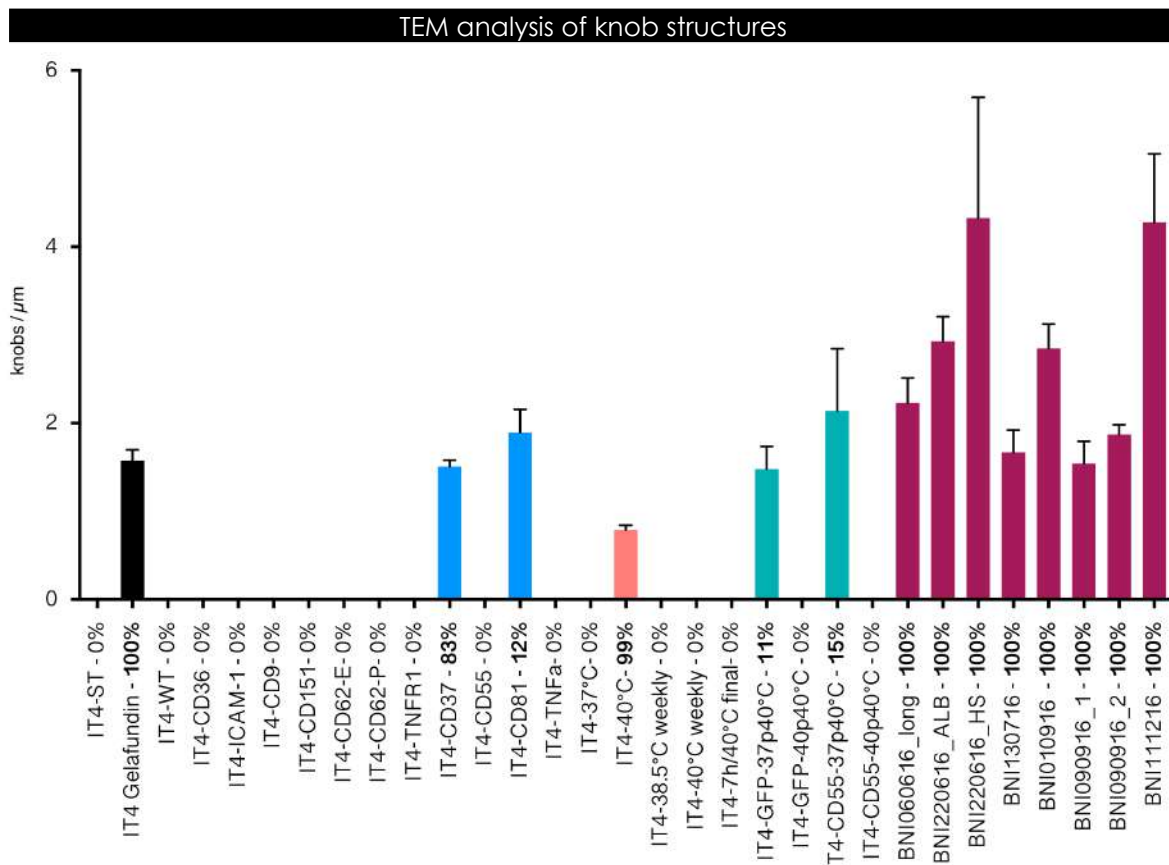


Figure 24. TEM analysis of knob structure focusing on the morphological appearance. The Gelafundin enriched population served as positive, knobby control, accordingly 100% of investigated IE exhibited knob structures, with a ratio of 1.6 ± 0.9 knobs per μm . Also, for the IT4-CD37 (83% knobby, 1.5 ± 0.6 knobs/ μm), IT4-CD81 (12% knobby, 1.9 ± 0.9 knobs/ μm) and IT4-40°C (100% knobby, 0.8 ± 0.3 knobs/ μm), knob structures were detected in the listed proportion of investigated IE. Consequently, in every field isolate, 100% of the investigated IE exhibited knobs. While all isolates had a ratio between 1.7 and 2.9 knobs per μm , the BNI220616_HS (4.3 ± 2.4 knobs/ μm) as well as the BNI111216 (4.3 ± 1.6 knobs/ μm), showed a slightly higher ratio.

The Gelafundin enriched population served as knobby control, accordingly 100% of investigated IE exhibited knob structures, with a ratio of 1.6 ± 0.9 knobs per μm . Also, for the IT4-CD37 (83% knobby, 1.5 ± 0.6 knobs/ μm), IT4-CD81 (12% knobby, 1.9 ± 0.9 knobs/ μm) and IT4-40°C (100% knobby, 0.8 ± 0.3 knobs/ μm), knob structures were detected in the listed proportion of investigated IE. Consequently, in every field isolate, 100% of the investigated IE exhibited knobs. While all isolates had a ratio between 1.7 and 2.9 knobs per μm , the BNI220616_HS (4.3 ± 2.4 knobs/ μm) as well as the BNI111216 (4.3 ± 1.6 knobs/ μm), showed a slightly higher ratio.

> Taken together, the TEM analysis revealed a knob positive phenotype apparent within the IT4-CD37 and the IT4-CD81 population. Additionally, the sequestration towards human endothelial brain cells at febrile temperature manifested knob positive IE. Surprisingly, this phenotype was also achieved within particular IT4 populations, specifically sequestered to mock-transfected CHO-GFP cells as well as to human receptor protein expressing CHO-CD55, in combination with short periods of febrile temperatures.

6 DISCUSSION

So far, only a handful of involved receptor proteins or surface molecules, interacting with the IE are described, while only few of them are deeply investigated and described to convey sequestration via defined structures, such as *PfEMP1*. Furthermore, the relevance of knob formation on the IE surface, as well as the cellular and adhesive alterations, due to phases of febrile temperatures come to the fore little by little.

To support this movement, and to extend the previous investigated set of receptors involved in *falciparum* malaria, this thesis focusses on 6 known and unknown human endothelial receptors, as well as on the possibility of knob induction via sequestration under febrile temperatures.

6.1 Physiological relevance of a chosen human receptor set

The comparison of the surface composition of HBEC-5i cells was performed, to evaluate the presence of various human endothelial receptors within cerebral tissues. As many receptors, definitely mediating cytoadhesion of IE, like CD36, ICAM-1, CD9, EPCR and CSA, also structures, less well described should be accommodated, such as MDR1, TNFR1, TNFR2, CD37, CD55 and CD81, comprising the main components of this investigations. To generate the most physiological picture, analyzing the surface composition, 3 states of cultivation of HBEC-5i were chosen. First, the cultivation at 37°C, constituting the general body temperature in non-febrile phases. Second the incubation at 37°C with reoccurring heat shocks of 40°C for 1.5 h, mimicking fever conditions within the febrile phase. Third, a constant cultivation at 37°C and additionally stimulation with TNF α to imitate the host immune reaction and trigger cellular immune response. HBEC-5i were analyzed via RNA sequencing as well as via specific antibody staining.

While most of the focused receptors are, if at all, only detectable at low levels within the transcriptomes, TNFR1 and CD81 display similar levels like CD151. Only CD44 is constitutively transcribed on elevated levels, while also additionally ICAM-1 displays a significant higher expression level after the TNF α stimulation. The upregulation of ICAM-1 after TNF α stimulation is well described, while also the generally low expression levels of CD36 within brain tissues are in line with previous studies.^{207,208} The recently focused EPCR protein is described to mediate the link of cerebral *PfEMP1* sequestration and severity of disease, while also being barely detectable within the transcriptome data.^{209,210} Thus, a high detected RNA or protein level is not mandatory to induce SM or CM. Furthermore, as almost all detected cells exhibit an equivalent presence of ICAM-1, CD9, EPCR, CSA among with CD55 and CD81, those receptors are chosen to be focused within this thesis. Also, up to half of the detected HBEC-5i population showed an expression for MDR1, TNFR1 and TNFR2, similar or more than for CD36, those receptors were also chosen. Additionally, an initial binding capability of IE of field and culture isolates was described in further studies for the first time, justifying further research.¹⁴⁶ Within the human host, the pro-inflammatory, cellular immune response

follows an acute malaria infection. Due to the upregulated production of TNF α , potentially captured by the TNFR1 and TNFR2 receptors, cellular death programs are activated, inducing the upregulation of inflammatory proteins and adhesins. Thus, the levels of ICAM-1, VCAM1, CD62-E and other endothelial adhesins increase in various tissues, contributing to an enhanced potential of further cytoadhesion of IE.²¹¹ This is evidenced in post-mortem immunohistochemistry analyses of cerebral tissues of CM patients, where the presence of parasitized erythrocytes was highly significantly associated with an elevated expression of the mentioned adhesins.^{6,212} Also, it was recently shown that soluble forms of TNFR1 and TNFR2 are increased in the peripheral blood of pregnant women, while also, positively correlated with parasitemia.¹⁹⁷ While the upregulation of ICAM-1 was clearly detectable on transcriptomes and FACS analysis, no suitable antibody for VCAM1 was just not available, but the transcriptomes showed a significant increase.

All received results, both, at the RNA and the protein level, are in line with general detected levels by further studies.²¹³

> However, is it important to remember, the HBEC-5i is not a primary, but an immortalized cell line, not displaying the absolute physiological constitution of human brain tissue cells, noticeable by the highly increased levels of CSA and CD44.

A possible improvement of the physiology and nature of protein interaction, primary cell lines should be considered as objectives for further experiments. Also, other tissues, involved in the severe course of disease could be implemented, such as lung, liver and kidney, also to include the clinical picture of SM in adults.

6.2 CHO repertoire, FACS data & fluorescence microscopy

Generating a suitable experimental setup investigating binding capability and protein interaction of living cells is challenging. The well-established procedure of mammalian cell-based protein expression include CHO cells, genetically manipulated to express human endothelial proteins on their surface. Albeit it is artificial and not closely bound to the human physiology, due to advanced technologies and precise genetical tools, it still gives us a handle *in vitro* model for profound experiments. Here, 16 different transgenic CHO cell lines could be generated, reliable in protein expression and cell integrity. Regarding the generation of CHO-EPOR, CHO-CX3CL1 and CHO-CD44, the transfection of the CHO-WT was possible and resulted in few fluorescence positive cells, albeit they were not capable for enrichment via sorting.

For the CHO-EPOR, CHO-CX3CL1, the fluorescence signal disappeared after about 72 h of cultivation within the respective cell population, indicating an exclusion or loss of the introduced plasmid. Therefore, a sustainable cell sorting was not possible.

For CHO-CD44, a sufficient amount of GFP positive cells could be generated, while the detection of the presence on the cell surface via within the specific antibody staining was not possible. A reason could be an impaired transportation towards the membrane, or an altered folding of the protein itself. As CD44 is characterized by numerous expressed isoforms, as the chosen, also most abundant form could be either

not processed on the surface, mislocated exported, not correctly produced within a foreign organism, or the epitope, detected by the antibody could be not present or reachable.²¹⁴

Moreover, a stable transfection model was attempted to be established, by utilizing a lentiviral transfection method. However, in the first steps, the so called LentiGO-system made use of human embryonic kidney (HEK) cells, bridging the artificial cell culture more to the human physiology. The HEK cells were used to generate infectious viral particles to further infect and introduce the gene of interest permanently into the genome of CHO cells. The resulting CHO cell lines were less stable in their expression of protein, as also the fluorescence was more diffuse and fainter. The subsequent initial binding assays of the stable transfected CHO cells, in comparison with the transient cell lines exhibited a significant reduced binding capability by up to 80%. The experimental results for culture isolate IT4 and 3D7, comparing the initial binding capability of IE towards stable (LeGO) and transient transfected CHO cell lines, expressing either human CD36 or ICAM-1 on their surface, are shown in **Annex II**. Due to those discrepancies, for all experiments, the already established setup, including transient transfected CHO cells was used.

Regarding the present receptor set, it could be interesting to include other members of the tetraspanins family, as the already tested, show promising findings related with malaria disease. Other receptors, involved in invasive processes, general cell-cell, or pathogen-cell adhesion, or molecules, similar to already described molecules could be considered for further experiments. Receptors, integrins or related molecules, mediating adhesion and being present on endothelial cells are for example: CD102/ICAM-2, exhibiting similarities to CD54/ICAM-1 and is expressed on vascular endothelial cells; CD56/NCAM, the neural cellular adhesion molecule or CD146/MCAM, potential adhesion molecule, associated with cell-cell interaction and expressed at distinct endothelial cells, as well as in the cerebellum. Also, CD15, CD34 (expressed on capillary endothelium), CD47, CD92, CD93 are expressed on numerous endothelial cells, strongly associated with adhesion. CD2 is associated with erythrocytic rosetting, while CD141 and CD142 are expressed on vascular and endothelial cells, strongly associated with agglutination of erythrocytes. CD66f is specifically expressed during pregnancy within placental tissues, indicating a putative involvement in PAM. The integrins CD41 and CD51 are expressed on megakaryocytes, similar to CD151, indicating cytoadhesive interactions with *P. falciparum* IE, while CD104 and CD109 are associated with adhesion. The lectin CD62-L share similarities to CD62-E and CD62-P, already described to interact with *P. falciparum* IE. Proteins, clustering and complexing with CD81 are CD19, CD21 and CD216, constituting a putative involvement in CD81 function and performance. Furthermore, CD97 can bind CD55, which is highly distinct on a broad variety of tissues and hematopoietic cells and erythrocytes, being a putative receptor for IE. Similar to CD120a and b/TNFR1 and TNFR2, binding TNF α and TNF β , CD119 is described as receptor for INF γ . CD144/VE-Cadherin is expressed on endothelial cells, organizing the adherent junctions, putatively involved in sequestration. CD236/GYPC and maybe other members of the glycoporphin family, are involved in IE adhesion and are thought to act as putative receptor for *P. falciparum* parasites. However, the Duffy antigen/receptor for chemokines/CD234 is traded as receptor for *P. vivax* and *P. knowlesi*, therefore also

potentially involved in *P. falciparum*. Regarding the upregulation of CD230, in patients with a variety of cognitive disorder and neurodegenerative symptoms of e.g. Alzheimer's or Creutzfeldt–Jakob disease, this receptor could also play a role in CM. Also, receptor for viral infections, such as CD46 for measles or CD155 for Polio could be considered as well. Moreover, CD53, CD63, CD82 are member of the tetraspanins family (total of 33 members), sharing similarities to already malaria-involved receptors, such as CD9. Furthermore, CD206 binds mannose structures of pathogens, raising the question if *Plasmodium* parasites can alter the mannose processing or phosphorylation of erythrocytes to its favor.¹⁶²

> A possible improvement of generating transfected CHO cell lines, harboring new, undiscovered receptors, could be an adaptation of the transfection protocol, as altering the ratio of introduced genetic material, the timing and amount of selection marker or the procedure of transfection, including an obligate spinoculation step. Also, utilizing the genic CRISPR/Cas9 tool, a very distinct insertion of the gene of interest into the target cell genome would be possible, improving the mass of the produced protein and determine the conditions of activation by placing the gene in a suitable promoter region.²¹⁵

6.3 Specific cytoadhesion of IE to transgenic CHO cells

Regarding the utilized system, including CHO-pgsa-C745 cells may pose difficulties for some reasons. The CHO-pgsa-C745 culture is a spontaneously immortalized cell line with subsequent mutagenesis and a deficiency in the production of proteoglycan, originating in the Chinese hamster *Cricetulus griseus*. The cell line does not express any of the known *P. falciparum* receptor proteins on the surface validated via specific antibody staining and FACS analysis of CHO-WT and mock-transfected CHO-GFP cells. Albeit the cytoadhesion of IE took place mostly on fluorescent, and therefore human protein expressing CHO cells, an adhesion of IE towards non-fluorescent cells could be observed as well. An explanation could be a degradation or miss production of the GFP marker protein, resulting anyway in the expression of uncoupled human surface proteins, as partly detected within FACS analysis. More probable, however, is the adhesion of IE towards a so far unknown surface structure, present on both, CHO-WT and transfected CHO cells. Though, the problem is a familiar one, as this phenomenon was already observed in previous studies.^{175,216,217}

The observation of apparent non-IE binding towards fluorescent CHO cells could be explained by a scarcely investigated phenomenon, describing the adhesion of early ring-infected erythrocytes, potentially mediated by ring-infected erythrocyte surface antigen/RSP1 and RSP2 (PFIT_1149400 and PFIT_1149700), within this study termed as pseudogenes, while the expression level was just slightly increased in IT4-CD37, IT4-CD55 and IT4-CD81, compared to IT4-ST and mock-enriched IT4-GFP.^{218,219}

It was also perceivable, that IE accumulate in enhanced clusters on senescent, amorphous or morphological suspicious cells, indicating an attraction of IE by maybe CHO apoptosis or stress-related cell signals and (surface) proteins or cellular secrets. In

general, senescent cells are defined to be unable for further replication while still being metabolic active. As a result, it is possible that the protein synthesis is altered and dysfunctional, evidenced in the elevated upregulation of endogenous CD44 on the cell surface.^{220–222} A recent study revealed that beside the 3 known trigger-dependent apoptotic pathways, also a non-induced apoptotic progression of cells was described, occurring in prolonged cell cultures, regardless of the cell types. Here, 40 differentially expressed proteins, including cytoskeleton-, metabolism- and folding-associated, as well as chaperones were described, altering the cell morphology and membrane integrity.²²³

A possible strategy to eliminate such dying cells could be a specific staining and subsequent sorting, whereas the occurrence of other apoptotic populations is highly probable. As the actual surface constitution of CHO cells is not fully described, and only available as a conglomerate of a CHO-K1 reference sequence and Chinese hamster assemblies, the present constitution of the CHO-pgsa-C745 cell line remain elusive.²²⁴

By the use of human, instead of other mammalian cell lines, setups face the problem of various surface structures, involved and already described in the field of IE sequestration. Many cell lines, e.g. a schwannoma line, expressing CSA can be utilized in PAM studies, while other common receptors, like CD36, VCAM1, ICAM.1 and CD62-E are absent. The cleavage of CSA leaves a system, potentially suitable for studies with recombinantly (over)expressed adhesion receptors.²¹⁹ The use of recombinant proteins out of e.g. *E. coli* systems, for example coated on plastic surfaces or respective beads are even less physiological, while the correct processing and folding within those lyophilized biomolecules are not ensured. The generation of recombinant proteins within eukaryotic expression system could lead to more physiological processed and folded proteins, albeit the effort, feasibility and the scaling should not be underestimated.

Fixating protein expressing cells, to generate a durable, comparable and more handle system, waiving the need for active cell culture – with all its demands on constant environmental conditions, possible contaminations and undefined difficulties – could be a promising approach. On the other hand, fixatives, such as paraformaldehyde and/or glutaraldehyde are not properly suitable, as the cross-linking negatively affect the binding capabilities. (data not shown)

Another challenge is the determination of the protein level of actual presented protein on the cell surface, as the performed FACS analysis gives only information of the presence but not of the quantity. By loading a defined amount of recombinant protein on suitable beads and a stepwise comparison with the used cell lines would help by estimating the expressed protein amount, as well as classical western blotting or extracted membrane fractions.^{225,226}

In times of 3D printing of biomaterial, the most unconventional approach to generate a defined matrix, including a certain amount of membrane proteins would be an artificial membrane system. An outstanding approach was proceeded by 3D printing a physiological model, mimicking the microenvironment of the placenta barrier structure, the so-called placenta-on-a-chip, with human endothelial cells.^{227,228}

> A possible improvement for further transgenic expression experiments would be the use of human cell lines, suitable for the individual investigated receptor set, or maybe primary cell lines, instead of immortalized ones. Additionally, the actual quantity of expressed surface proteins should be evaluated in advanced to ensure comparable starting situations and reproducibility.

6.4 Static binding assays

To evaluate the initial binding capability of various *P. falciparum* strains, also cultivated at different conditions and field isolates, static binding assays were performed. The results were compared, regarding the respective amount of bound IE per individual transgenic CHO cell line, expressing the human endothelial receptor of interest.

Setting the baseline, 3 controls were applied. By using only non-infected erythrocytes (BB neg), deriving from the same source as the blood used for general cultivation, an unspecific binding towards HBEC-5i, CHO-WT or transfected cells was excluded. The CHO-WT and CHO-GFP cell line served as negative control, as no known *P. falciparum* receptor is expressed on the surface, therefore no initial binding capability was expected for any of the parasitic isolates.

Regarding the isolate IT4-ST, mainly focused within this thesis, a significant initial binding capability was observed towards CHO cell lines, expressing CD36, ICAM-1, CD9, CD62-P, HRH1, MDR1, TNFR1, TNFR2, CD55, CD81 and EPOR, including a tendency to bind also to CD37. As the binding towards already and well described receptors, such as the first 4, the positive results for the remaining rose the hope for finding putative new interacting partner.

The mock-enriched population of IT4-GFP exhibited initial capabilities towards the respective positive control of CHO-GFP, but also towards all other tested endothelial receptors. By retrospection of the described phenomenon of IE binding towards unknown surface structures on CHO cells, this result is explainable, as exactly this population was specifically enriched. The promiscuous binding profile of IT4-CD62-P could result in the differential upregulation of A_var02 and A_var07 genes, as already described in a recent study.¹⁷⁵

Enriched population of IT4-TNFR1 and IT4-CD55 did show an enhanced binding towards CD36 and ICAM-1, CD9, as well as towards the respective CHO control of CD55 and TNFR1. As it is not possible to generate a complete homogenous population of enriched IE, a promiscuous binding profile within the same experimental setup is expectable by performing cross-binding studies.

However, for IT4-37°C and IT4-40°C, the binding profiles of the temperature related populations show a significant binding capability to their respective HBEC-5i cell line. Other than the IT4 population, that was weekly heat shocked, with a final phase of 7 h at 40°C (IT4-7 h/40°C final), which initially bind towards CD62-P in a significant manner, with a slight enhancement for CD36 and ICAM-1. It is well known, that human cells of various tissues change their surface composition during fever and immune stress. Therefore, it is conceivable that also the parasites and/or erythrocytes change their composition or binding profile during such phases, adapted to the upregulated

adhesive molecules on the endothelial surfaces, such as ICAM-1 and CD62-P.^{148,173,207,229} While this effect was not in primary cultured endothelial micro- and macrovascular cells.²³⁰

All the other culture isolates, namely NF54, 3D7 Australia, 3D7 BNI and DD2 show significant initial binding capability towards CD36, underpinning the fact that about 80% of all detected PfEMP1 proteins hosting a CD36 binding domain, enable nearly all *P. falciparum* isolates to bind to this specific receptor. While no isolate show elevated proportions of bound IE towards any tested receptor set, it was noticeable that DD2 in fact exhibited significant levels of initial binding towards CHO-CD62-P but also to CHO-GFP. This phenomenon could be explained by an involved *var* gene or specific binding domain towards the CD62-P protein, or else, towards unknown surface structures of CHO cells themselves. The fact, that no specific binding towards other tested receptors was observed, there is a strong suspicion that the DD2 isolate mediate a preferential binding towards CD62-P. By performing inhibition assays, utilizing α CD62-P antibodies or recombinant CD62-P, competing for the IE binding, the specificity could easily be determined.

Considering the 3 field isolates, named Patient 1, Patient 3 and Patient 3, an initial binding capability was only detectable for Patient 1, towards CD36 and ICAM-1, moreover significant. The IE of Patient 2 and Patient 3, surprisingly did not exhibit any binding profile, not even towards CD36. The reason could be mis-performed static binding assay, albeit it would be puzzling if only those assays contain errors, as the assays were conducted on 3 independent attempts, together with other, correctly working assays, while also the batch of used CHO cells were identical. Another explanation could be that at least 20% of detected PfEMP1 do not contain a CD36 binding domain. Given that the mutually exclusive expression mechanism is still intact in fresh field isolates, such as Patient samples, compared to long term cultivated ones, it might be possible that at the given time point of the experiments, no CD36-binding PfEMP1 was expressed within the used populations.⁶⁷

> To investigate the specificity of the observed binding characteristics, further studies are needed. An inhibition assay with specific antibodies or respective soluble recombinant proteins, applied in a concentration dependent manner could be easily used.

Another idea to improve the analysis of static assays would be the IE counting via machine learning tools. There are many possibilities to program respective features, while the ImageJ plugin, described in a recent study seems appropriate for the requested requirements.²³¹

To determine the sole interaction of IE and endothelial receptor, a coating of recombinant proteins on suitable and FACS-detectable beads would be conceivable, while also, GFP expressing parasites could be detected via FACS.²³² The detection of firmly bound IE would be more precise than the manual counting via a light microscope. On the other hand, weak interactions could be disrupted during the detection within the stream of the cytometer. Also, parasitic proteins, either recombinantly expressed or extracted from respective population could be used to determine surface interaction with e.g. endothelial cells. Albeit the production of total PfEMP1 proteins is challenging, individual domain structures could be used.²²⁶

To investigate whether the observed phenotypes and binding profiles are in relevance of CM or sequestration in brain tissues, the static binding assays could be conducted with HBEC-5i. However, this immortalized cell line presents a broad mass of CSA on the surface, a known receptor for the *var2csa* *var* gene. A solution could be the cleavage of the CSA via e.g. CSase or the selection of a primary cell line. Also, other cell types, with a lack in CSA could be considered, maybe to focus on other affected sites and tissues during severe infections, like lung, kidney, liver and heart. Comparable experiments were performed by the use of specific PfEMP1 domains, but if ever, not with whole PfEMP1 or specifically enriched IE population.¹¹²

For a more physiological insight and to determine possible changes in the nature of the IE adhesion, binding assays could be conducted under flow conditions, mimicking the human blood circulation and a physiological moving environment.^{141,233}

Furthermore, it would be interesting to apply the used Patient isolates together with a complete and broader receptor set, to reveal initial binding profiles. Also, the comparison with more Patient isolates, altering in number and composition of genotypes, parasitemia, site of infection, host gender and previous infection, as well as changes in binding profiles and switching present a particular exciting experimental setup.

6.5 Cytoadhesion inhibition assay to unknown surface structures

To validate the specificity of the observed binding of 2 enriched IT4 populations, the binding nature was investigated by using specific antibodies against TNFR1 and CD55, respectively. As the initial binding capability of the IT4-ST population was relatively low, it increased significantly after several rounds of enrichment. This enhanced binding profile could be almost completely blocked by the antibody incubation of the individual CHO cell line prior to the assay, also, in a highly significant manner. Therefore, it is conceivable that the received enrichment is specifically attained, maybe mediated by an upregulated *var* gene and a particular PfEMP1 expression. (discussed later in detail)

> Nevertheless, due to given circumstances, this experiment was carried out only once, so the results should be considered with caution. Further repetitions of the assay are mandatory to receive reliable results. Furthermore, the concentration dependency should be tested by diluting the antibodies in a serial manner. Additionally, other enriched IT4 populations have not been implemented in this inhibition assay, although this will have to be specified in the future.

With regards to the omnipresence of the adhesin CD44 on the complete surface of CHO cells, and its relevance within the human system in cell-cell interactions and merozoite invasion, the idea rose that CD44 could be the unknown surface structure, mediate adhesion of IE towards CHO-GFP cells. To evaluate the influence of rodent CD44 within static binding assays, a cytoadhesion inhibition assay was performed, utilizing an α -hamsterCD44 antibodies blocking the CHO monolayers. The α CD44

antibody could not inhibit any binding of enriched IE population, towards their respective cell line, tested for IT4-GFP, IT4-TNFR1 and IT4-CD55. It can therefore be concluded, that the rodent CD44 allocated on the whole CHO surface does not interfere the binding capability of IE towards the expressed human endothelial receptors. As this approach still did not reveal the unknown surface structure, other rodent specific antibodies should be tested. A recent study observed CHO-WT cells to independently co-stimulate T-cell activation and IL-2 production. Via monoclonal antibody studies, immunoprecipitation and recombinant expression, capable hamster homologues of CD21, CD44, CD54/ICAM-1, CD63, CD87, CD147, and a so far undefined 80 to 90 kDa protein were revealed on the CHO surface. Further experiments clarified, that hamster CD54/ICAM-1, heterologous expressed on COS cells was able fulfill the independent co-stimulation in the same manner.²³⁴ Moreover, a recent study determined CD56, or NCAM as putative *P. falciparum* receptor, while the protein seems to be also present on CHO cells.¹⁶⁶

> With respect to the crucial role of human ICAM-1 within the sequestration of IE, the hamster homologue presents an extremely promising candidate for the unknown surface structure. Also, the rodent form of NCAM should be considered to possibly interfering the specific IE-receptor binding. Immunofluorescence assays and FACS analysis could reveal the abundance and the surface distribution of the protein, while antibody inhibition assays could determine the level of IE binding interference.

6.6 Cytoadhesion inhibition assay with sCSA

During the static binding assays, it was observed that the *P. falciparum* IT4 isolate show highly significant elevated binding capacities towards HBEC-5i, after repetitive enrichment under febrile conditions of 40°C, albeit not at 37°C. This phenotype was constant over various rounds of enrichment and is most likely due to the extensive expression of the *var2csa-var* gene within the IT4 population. To investigate whether the resulting binding capacity of the IT4 isolate and CSA is of specific nature and related to the febrile enrichment procedure, a cytoadhesion inhibition assay was performed, utilizing the soluble form of CSA as no suitable specific antibody was reachable in the required scale or concentration. The actual experimental setup was inspired by prior described assays.²³⁵⁻²³⁷

The inhibition of the binding capability towards CSA on the surface of HBEC-5i monolayers was tested for IT4-ST as control, IT4-40°C as the affected population, as well as for IT4-37°C to determine a general involvement of febrile conditions and as second negative control. Furthermore, the concentration of sCSA was decreased stepwise, to determine the gradual inhibition limit.

Albeit the IT4-37°C population exhibit only a restricted binding capability towards HBEC-5i, a complete inhibition was achieved by both, 10 µg/ml and 1 µg/ml, while an incubation with sBSA did not alter the profile. The binding affinity towards CD36 was not modified, neither by sBSA nor sCSA. The same results were seen for IT4-40°C population, although in a more extended way. The highly increased ability of IT4-40°C

to bind HBEC-5i, was also complete reversed by a preincubation with sCSA at the highest concentration of 10µg/ml. A stepwise and concentration dependent inhibition was observed for 1µg/ml and even 0.1µg/ml. While sBSA did not alter the general binding profile, also, the overall picture of CD36 binding was not modified.

A recent study revealed that cytoadhesion of CSA binding IE inhibited the cytoadhesion of CD36 binding IE. Furthermore, CD44 was determined as signal receptor for cytoadhesion of CSA binding IE, providing the first evidence that some IE population can downregulate the IE cytoadhesion profile of another phenotype, by modifying endothelial cells via signaling pathways, relating CD44 to CD36.²³⁸

> Keeping this in mind and considering the FACS analysis of the HBEC-5i surface composition, a preceding block of human CD44 on the HBEC-5i surface would be advisable to rule out the overall enrichment of *var2csa* expressing IE populations, when enriching over HBEC-5i or other CSA containing cell lines. Additionally, to determine the final inhibition limit, further dilutions of sCSA would be necessary.

6.7 Enrichment via multiple rounds of panning assays

The amount of initial bound IE towards the respective human endothelial receptor is generally small, so the specific population was enriched via various rounds of panning assays. Even a few interacting IE are sufficient to start an enrichment, as is was seen for IT4-GFP, IT4-MDR1, IT4-TNFR1 and IT4-CD37, relatively big clusters were found in after first rounds for IT4-TNFR2, IT4-CD55 and IT4-CD81.

It seems like the receptors, previously described to mediate parasite invasion are also more potent in capturing IE from the blood in the first course. Here, the enrichment was performed for several rounds, until a coverage of about 70 to 80% bound IE per detected CHO cells were reached. The ring staged IE were harvested within the next cycle of replication, directly following the last enrichment. As the amount of IE per 23 mm culture dish was still not enough for one biological replicate, several dishes were prepared in the same approach, while being fixated in TRIzol and subsequently stored at -80°C. An improvement would be the cultivation in a bigger scale, as the 4 biological replicates needed could be collected at once, giving a more accurate picture of the actual transcriptomes.

Albeit, *var* genes can switch in every cycle, at least in naturally infected patients (approx. switching rate of 18%), the *var* expression, in general, is relatively stable over the course of time within long term cultivated isolates (approx. switching rate of 0.3 to 2%). By working with fresh field isolates, the higher switching rate should be considered, so the harvest of the first generation is advisable.^{133,239,240} Thus, the harvest of the ring staged IE could be done in the subsequent cycle of replication, as the expression profile seems to be stable. This approach also gives the opportunity to synchronize the IE population tightly via D-sorbitol or MACS, prior the RNA isolation, as well as generating more biomass to process.

The RNA purification was performed subsequently via phenol/chloroform extraction, while a subsequent treatment with TurboDNase and magnetic beads was omitted. To

generate more clear RNA and receive more specific read counts of NGS, those additional purifications should be performed.

> An improvement for further experimental setups would be the upscaling of the respective cultivation, the harvest of IE in the second generation of replication and the immediate processing of the token samples, avoiding several freeze and thaw cycles. The more biomass is harvested, the better are the possibilities of RNA purification, definitely required by working with 3 different cell types.

6.8 NGS analysis – comparison of gene expression levels

The differential gene expression levels of the collected IT4 samples, obtained by NGS analysis give a still image, or a frozen picture of the actual composition and interplay of the whole genome, dispersed on a mostly homogenous population. By comparing the individual picture of differentially cultivated IT4 population, some changes in gene expression are expected. Albeit the overall picture of cell function, metabolism and interaction is thought to be similar, a deviation in particular clusters are considered as specific for the performed receptor binding. As PfEMP1 proteins are described to act as key player within IE sequestration, the first analysis was focusing the PfEMP1 coding *var* genes, present in the IT4 isolate. The extremely high AT content of *Plasmodium* genomes of up to 80% in coding and even up to 90% in non-coding regions, is the top recorded among any other organism, whose DNA has been characterized.^{241,242} Due to this, as well as to the highly polymorphic nature and numerous repetitive elements within *var* gene sequences across isolates and even parasitic members of the same strain, the unambiguous assignment of *var* gene borders are not clearly defined and hard to assign.

6.9 Analyzing the *var* transcriptome

Regarding the distribution of *var* gene expression levels, it is striking that, by far, C_var34, B_var32A and B_var32B overwhelm within all analyzed populations. This phenomenon was already observed within previous studies and could be traced back to the inapplicable mutually exclusive model towards those particular genes, promoted by the long-term cultivation of the IT4 isolate.^{175,217,243} Moreover, it seems that the presence of human serum within the cultivation medium promote the transcription of the C_var34 gene of the IT4 isolate, in comparison with AlbuMAX completed medium.¹⁴² Such constantly activated genes could serve as a diversity archive, like the surface glycoproteins in *Trypanosoma*.^{132,244}

Other *var* genes, such as A_var18, B_var29, B_var12, B_var25, B_var45, C_var28, C_var65 and C_var68 could be equally exempted, as they were equally high expressed within all 6 populations, as seen in the bar diagram and the circular graphs of **Figure 20.1** and **Figure 20.2**.









> Taking to account, that the transcriptional alterations, triggered by the sequestration towards the 6 investigated endothelial receptors MDR1, TNFR1, TNFR2, CD37, CD55 and CD81 show a profile, different from the initial IT4-ST population, all *var* genes, with a peaking expression level within the IT4-ST population have been excluded in further calculations. Furthermore, the general procedure of enrichment, as well as the binding towards undefined surface structures on CHO cells result most likely also in alternated profiles, *var* genes peaking in the IT4-GFP population were equally excluded. Those prerequisites ensure a more distinct and clearer view of the altered gene expression levels, mediated by the respective surface proteins. On the other hand, if a distinct upregulation of any of the excluded *var* genes is by chance specifically mediated or triggered by the receptor interaction, it would not be detectable within this attempt.

6.10 Analyzing the whole transcriptome

Even though, in average between 2700 to 3100 genes of 5600 existing genes have slightly differentially upregulated expression levels, only a few (36 to 334) of them are subject to the chosen cutoff criteria. For each enriched population, the expression levels for various genes are discussed, that have been selected according to the focus of this thesis.

> Comparison of the NGS analysis

Shortly recapitulating the results of the NGS analysis, the 6 transcriptomes give a comparable picture, regarding the *var* gene expression levels, while some genes are differentially upregulated in a significant manner or above a particular cutoff. The following color code was assigned:

| | |
|---|---|
|  | CD36 binding domain ²⁴⁵ |
|  | ICAM-1 binding domain ²⁴⁶ |
|  | DC4 cluster ²⁴⁷ |
|  | DC9 ^{145,247} |
|  | DC3 ¹⁴⁵ |
|  | found in group upsA <i>var</i> genes ¹⁴⁵ |
|  | not associated with SM ²⁴⁸ |
|  | no clinical importance or function described so far |

6.10.1 IT4-GFP

For **IT4-GFP** enriched population and after excluding the ubiquitous expressed *var* genes, only B_var14 stands out as highly upregulated.

B_var14

| | | | | | | |
|-------------------|-----------------|---------------|----------------|-----------------|----------------|---------------|
| DBL α 0.23 | CIDR α 5 | DBL β 5 | DBL δ 1 | CIDR γ 2 | DBL γ 3 | DBL ζ 4 |
|-------------------|-----------------|---------------|----------------|-----------------|----------------|---------------|

Strikingly, this *var* gene is not differentially expressed in any of the other 6 tested populations. However, B_var14 was already been described as differentially upregulated within specifically enriched IT4-WT, IT4-CD62-E and IT4-CD151 populations in a former study.¹⁷⁵ However, this gene contains the general CD36 binding domain as head structure, followed by an ICAM-1 binding domain, mediating a relatively low binding profile towards endothelial cells of various tissues.²⁴⁹ While for CIDR γ 2 no actual relevance was described so far, the C terminal domains are determined as DC9. This particular DC9 is described as the most abundant one, upregulated in SM, but not as single transcript, indicating that DC9 do not mediate relevance in SM alone. It is expressed at least as high in SM as the EPCR binding domain CIDR α 1, while the CIDR α 1 itself is not present within the same PfEMP1.²⁴⁷

Other genes

Applying the cutoff criteria, for the IT4-GFP enriched population, HSP70, 2 different PHIST_a, a PHIST_b, as well as the knob related lysine-rich PHIST_b, a PHIST_C, a A-type RIFIN, the surface adhesion associated SURFIN1.2, VSP53, a HYP12 and a HYP17 coding gene surpassed the threshold.²⁵⁰ This sparse picture indicates the small changes regarding the selected genes, mediated by the binding towards the mock-transfected CHO-GFP cell line. Also, almost no knob relevant or sequestration linked genes are differentially upregulated, compared to the IT4-ST population, evidencing a stable knobless phenotype.

6.10.2 IT4-MDR1

For **IT4-MDR1**, by applying the chosen cutoff criteria, only B_var05 reached a considerable level.

C_var05

| | | | |
|------------------|-------------------|----------------|----------------|
| DBL α 0.5 | CIDR α 2.3 | DBL δ 1 | CIDR β 1 |
|------------------|-------------------|----------------|----------------|

The C_var05 contain the general head structure, indicating a CD36 binding domain, followed by domains, mainly found in DC4. While the DBL domain, usually found in DC4 related structures, most recent studies assigned the rear tandem structure with SM.^{247,251,252} Moreover, this tandem is widely present in many *var* genes, while also within the upregulated, regarding CHO-WT and CHO-GFP cells (B_var14 (partly), B_var29, B_var32A, B_var32B and C_var28).^{145,217} The B_var05 is also differentially upregulated in IT4-TNFR2. As the MDR1 involvement in sequestering IE was already assessed in a prior study, the concentration dependent inhibition by receptor specific antibodies was proven for IT4 and the MM field isolate.¹⁴⁶ Nevertheless, a repetition of this experiment would reveal also the specificity obtained within this study.

Other genes

Regarding the selected gene set of the IT4-MDR1 population, an upregulation over the cutoff was detected for several genes, strongly related with knob formation and protein trafficking towards the IE membrane. Summarizing, 2 DnaJ genes, a FIKK kinase, GYP binding protein, HSP40, MAHRP1, 5 PHIST_b, including the knob related lysine-rich PHIST_b, while especially the expression level of KAHRP was notably upregulated. Additionally, some genes putatively related genes are also affected, such as 1 PHIST_c, a RESA-like (involved in KAHRP self-assembling), SURFIN8.2, VSP35 and VSP53 and both HYP17 genes. The overall view draws a picture of a putatively knobby parasite population, with an upregulated protein trafficking towards the IE membrane. This aspect gives credence to the hypothesis that the specific binding of MDR1 proteins does alter the genomic and morphologic appearance towards a sequestration related profile. It could seem like the profile draw less respect of the surface presentation of knob related proteins but more to the general knob formation process and anchoring membrane modifications. This is evidenced by the upregulated gene expression levels of up to 22 different conserved membrane proteins with unknown function. However, the evaluation of the received results underpin the relevance of this receptor, as it was, so far, only been described once in association with IE sequestration.¹⁴⁶

6.10.3 IT4-TNFR1

Within the **IT4-TNFR1** population, after excluding the ubiquitous expressed genes, only the A_var03 lead the list.

A_var03

| | |
|---------|-------|
| DBLα1.3 | DBLε8 |
|---------|-------|

The A_var03 represents the unique DC3 on its own, while being strongly conserved across 5 of 7 analyzed genomes.¹⁴⁵ A recent study on the 3D7 isolate revealed 3 conserved small A_var03 genes with a very strict temporal transcription profile, while the proteins could be detected in late trophozoite and schizont stages.²⁵³ For A_var03, no binding to the complement component gC1qR, but is associated with SM, investigated with static binding assays and qPCR, while 3D7 transcripts are not associated with SM.^{254,255} Moreover, it was shown that isolates of patients with CM transcribed significant higher levels of A_var03, compared to UM patients.²³⁵ This indicates a clinical relevance of A_var03 for SM and CM malaria disease, as primers targeting A_var03 showed significantly higher transcript abundance in SM than in UM samples and a trend of higher transcript abundance with increased severity of disease.²⁵⁶ Also, A_var03 was better recognized than var genes of the upsB group, by IgG from children who were hospitalized with malaria.²⁵⁷ In general, upsA group var genes are strongly associated to the process of rosetting and crucial for SM and CM forms of malaria.^{113,145,258-260} The TNFR1 specify of sequestering IE, involved in sequestration of IE was already determined in a concentration dependent manner, by utilizing inhibitory antibodies during static binding assays of IT4 and the MM field isolate.¹⁴⁶ Moreover, the same results were obtained within this study, albeit only one trial was performed, also, with only one antibody concentration.

Other genes

Applying the cutoff criteria on the selected gene set, only a few shows a differentially upregulated gene expression level. For IT4-TNFR1, only the lysine-rich PHIST_b, a A-type and B-type RIFIN, as well as VSP53 and both HYP17 coding genes were upregulated. Except for the lysine-rich PHIST_b, no knob related or particular protein trafficking associated genes were affected. Moreover, only about 3 genes coding for conserved membrane proteins with unknown function surpassed the cutoff. However, a previous study evidenced the involvement of both, TNFR1 and TNFR2 proteins in specific sequestration of *P. falciparum* IE. Furthermore, the binding capability was inhibited in a concentration dependent manner, by utilizing specific antibodies against the surface proteins in a static binding assay.¹⁴⁶ The obtained results for IT4-TNFR1, expressing the upsA group A_var03, are in line with previous studies, regarding the indicated correlation of TNFR1 in severe courses of disease as well as in CM patients.^{198,201} Moreover, the block of the TNFR1 receptor in a murine model reduced the severity of disease, while increasing the transmission rate and the gametocyte density.²⁶¹

6.10.4 IT4-TNFR2

For **IT4-TNFR2** a similar profile as IT4-MDR1 was seen. While for A_var09 a significant upregulation was calculated, while also, here, only C_var05 met the cutoff.

C_var05

| | | | |
|---------|----------|-------|--------|
| DBLa0.5 | CIDRa2.3 | DBLδ1 | CIDRβ1 |
|---------|----------|-------|--------|

See description for IT4-MDR1 above.

A_var09

| | | | | | |
|---------|--------|--------|-------|-------|--------|
| DBLa1.6 | CIDRγ3 | DBLγ15 | DBLε1 | DBLδ1 | CIDRβ1 |
|---------|--------|--------|-------|-------|--------|

A_var09 is one of the about 20% of *var* genes, not harboring a CD36 binding head structure. However, regarding the first domain, DBLa1.6 is not associated with SM.²⁴⁸ As for CIDRγ3 no clinical importance was described, the tandem structure of DBLγ15 and DBLε1 can be found in group upsA type *var* genes, generally associated with SM and CM.¹⁴⁵ Additionally, A_var09 is also differentially upregulated in IT4-CD9 enriched population.¹⁷⁵ During flow cytometry binding assays and bead-associated binding assays towards endothelial cell types of various tissues, A_var09 bound at very low or negligible levels and displayed low and patchy binding to different.²⁴⁹ The B_var09 is also differentially upregulated in IT4-CD81. Also, here, the TNFR2 involvement sequestration was already described and proven by specific antibodies inhibition of IE of the IT4 and the MM field isolate.¹⁴⁶ Nevertheless, a repetition of this experiment would reveal also the specificity obtained within this study.

Other genes

For IT4-TNFR2 quiet a lot of genes exhibit a differential upregulated expression level, surpassing the chosen cutoff criteria. Regarding the overall picture, genes involved in knob formation processes and protein transport towards the IE membrane surface are of particular interest, such as the *PfEMP1* trafficking associated AG 332, 3 DnaJ, both

ETRAMP, the GYP binding protein and 2 FIKK kinases, all 3 HSP coding genes, as well as MAHRP1, PfEMP2/MESA, almost all PHIST coding genes of all subgroups, 3 RIFIN, RESA-like (involved in KAHRP self-assembling), SURFIN8.1 and SURFIN8.2, as well as all members of the VSP and HYP family. This intense conglomerate of related proteins gives a strong indication of sequestration assignment of IT4-TNFR2 binding IE. The enhanced activation of transport, trafficking and membrane alteration seems to be additionally evidenced by the upregulated gene expression levels of up to 22 different conserved membrane proteins with unknown function. TNFR2 was investigated in the same course as TNFR1 and determined as putative interaction partner of *P. falciparum* IE, while also being associated with CM in patients.^{146,198,200,201}

6.10.5 IT4-CD37

For **IT4-CD37**, B_var11 and E_var04, or var2csa show a slight tendency of regulation, albeit below the cutoff criteria.

Other genes

Albeit no unique upregulated var gene could be detected within the IT4-CD37 enriched population, the results of the whole transcriptome give a striking evidence of knob formation processes, mediated by IE binding towards the CD37 protein. The highly elevated levels of the acyl-CoA synthetase, 2 PHIST_a, the RESA-like PHIST and 2 PHIST_b, SBP1 and the surface adhesion associated SURFIN1.2 give a hint of an excited protein trafficking towards the IE membrane and their modification.²⁵⁰ Strikingly, the knob determined DnaJ (~115fold), KAHRP (163fold) and the knob associated HSP40 (~200fold), PfEMP3 (~65fold) and the knob associated NA-type RIFIN are of remarkably interest, due to their extended upregulation, compared to the IT4-ST population. This overall view strongly suggests and underpins the presence of knobs on the IE surface. Also, here, only a few genes, coding for conserved membrane proteins with unknown function were detected above the cutoff. Regarding the effect associated within the rodent malaria *P. yoelii* and as CD37 can build complexes with CD81, an interaction of those proteins or even a synergistic effect regarding sequestration is quite possible.¹⁸³

6.10.6 IT4-CD55

Regarding **IT4-CD55**, a significant upregulated expression level was calculated for B_var11.

B_var11

| | | | | |
|------------------|-------------------|----------------|----------------|----------------|
| DBL α 0.3 | CIDR α 2.4 | DBL β 10 | DBL δ 1 | CIDR β 1 |
|------------------|-------------------|----------------|----------------|----------------|

The CD36 binding head structure is followed by a, so far, barely determined DBL β 10 domain and the DC4 clustered tandem domain, already described above for IT4-MDR1. The B_var11 is also differentially upregulated in IT4-CD81. The specificity of the CD55 involvement of sequestering IE was determined by utilizing specific antibodies against CD55, prior a static binding assay, albeit only one trial was

performed. Nevertheless, a repetition of this experiment, additionally with various antibody concentrations, would affirm the obtained results.

Other genes

Applying the cutoff criteria for the IT4-CD55 enriched population, only few genes exhibited an expression level over the chosen cutoff, such as a DnaJ, a A-type RIFIN, the surface adhesion associated SURFIN1.2, VSP53, a HYP12 and both HYP17 and just a few conserved membrane proteins with unknown function hit the level.²⁵⁰ Nevertheless, within the IT4-CD55 enriched population, also KAHRP was differentially upregulated, giving a hint towards the presence of knob structures on the IE surface, albeit no other related genes surpassed the cutoff. Unexpectedly, also invasion and merozoite associated genes were differentially affected within this population, such as EBA-181 and members of the RBP family. This phenomenon could rather be traced back to a certain amount of merozoites within the processed sample, than to a physiological reason, regarding the actual CD55 binding. As CD55 is described to be a critical receptor for *Plasmodium* merozoite committed attachment and invasion to host erythrocytes, those results could be misleading. While no correlation of the observed genes was drawn to IE sequestration, nor was the protein expression abundant in the mid-trophozoites stages. Nevertheless, it is possible that proteins, expressed in merozoites can be injected or introduced into the host erythrocyte. If not destroyed or degraded, they can be stored or traverse to the IE membrane, exercising a second function, like a task related to later staged parasitized IE. This phenomenon could be already shown for STEVOR variants and other proteins, like RIFIN and the rhoptry-derived antigen. This may contribute significantly to the long-term survival of the parasite by an efficient management of the natural resources.^{96,124,262–265} Even not relevant within this study, this thought could be considered regarding further experiments.

6.10.7 IT4-CD81

For **IT4-CD81**, a significant upregulation was calculated for A_var09, while B_var11 and B_var12 reached the cutoff.

A_var09

| | | | | | |
|---------|--------|--------|-------|-------|--------|
| DBLa1.6 | CIDRγ3 | DBLγ15 | DBLε1 | DBLδ1 | CIDRβ1 |
|---------|--------|--------|-------|-------|--------|

See description for IT4-TNFR2 above.

B_var11

| | | | | |
|---------|----------|--------|-------|--------|
| DBLa0.3 | CIDRa2.4 | DBLβ10 | DBLδ1 | CIDRβ1 |
|---------|----------|--------|-------|--------|

See description for IT4-CD55 above.

B_var12

| | | | | |
|----------|--------|-------|-------|--------|
| DBLa0.18 | CIDRa6 | DBLβ4 | DBLδ1 | CIDRβ1 |
|----------|--------|-------|-------|--------|

The CD36 binding head structure is followed by α, so far, barely determined DBLβ4 domain and the DC4 clustered tandem domain, already described above for

IT4-MDR1. Interestingly, the B_var12 is additionally differentially upregulated in a significant manner in IT4-MDR1, while not surpassing the cutoff level.

Other genes

For IT4-CD81, some merozoite and invasion assigned genes surpassed the cutoff criteria, indicating a certain amount of merozoites within the processed samples. Those genes comprise the EBA, MSP and RBP members. Furthermore, the gamete release protein also exceeded the cutoff, maybe giving a hint on elevated levels of gametocytes or sexually committed parasites, albeit no further evidence was found. Interestingly, and in somehow similar to the profile of IT4-CD37, most of the knob related genes show a differentially upregulated gene expression level, such as the acyl-CoA synthetase, the *PfEMP1* trafficking associated AG 332, the lysine-rich PHIST_b and RESA. Moreover, also, ETRAMP10.2, a FIKK kinase, *PfEMP2/MESA*, the RESA-like (involved in KAHRP self-assembling), 2 PHIST and 3 RIFIN, 2 VSP and – solely within this population – CLAG 3.1 exhibited elevated levels. Surprisingly, completely all 6 SURFIN and all members of the HYP family were differentially upregulated, while they do not share the premise of mutually exclusive expression.^{124,125} However, only the SURFIN13.1 also showed a differentially upregulation in IT4-CD9 and IT4-CD62-P of within a prior study.¹⁷⁵ CD81 is also known to be used by *P. falciparum*, *P. vivax*, *P. yoelii* parasites to enter human or murine hepatocytes with formation of a parasitophorous vacuole.^{182,184} However, no correlation of sequestering IE was drawn so far, leaving the hypothesis of similar activated genes in two different stages of the parasitic life cycle, where some proteins can outlast the whole 48 h cycle and undertake a task related to cytoadhesion or membrane modifications at later stages. Matching, up to 22 genes for conserved membrane proteins with unknown function are differentially upregulated within the IT4-CD81 population. Also, an interesting theoretical hypothesis was triggered by a recent study, regarding the likelihood of activated *var* genes.¹³² Here, it was described that no *var* gene is in a determined active state, all have the same probability of being activated. This status is valid at the point in the life cycle, when parasites first exit the infected liver. When merozoites firstly circulating within the blood flow, random *var* gene activation by each individual ensure an antigenically diverse population. Examination of experimental human infections have detected activation of all *var* genes immediately after parasite leave the liver, consistent with this model. Moreover, here, it was indicated that in cultures representing the first generation of parasites after hepatic release, all *var* genes were transcribed, but *upsA* group *var* genes were transcribed at the lowest levels. However, cultures established from second or third generation blood stage parasites expressing specific *var* genes, mainly belonging to group *upsA* and *upsB*, therefore being more effectively in vivo compared to parasites expressing other *var* genes.²⁶⁶ As CD81 represent a prominent invasion receptor for *P. falciparum* parasites into human hepatocytes, the binding towards this protein could trigger a change in *var* gene expression, also in blood stage parasites. A rearrangement in *var* gene expression hierarchy could be triggered, maybe by changing the 'molecular memory' archive by e.g. the alteration of specific histone modifications via particular activation of methyltransferases. The modification due to sirtuin-like *PfSIR2* proteins is not likely, as the respective genes do not exhibit any altered expression level. (data not shown) As also CD55 is determined as invasion

receptor, it is assigned to merozoite invasion and not hepatocyte attachment. The even though slight enhanced expression levels of upsA group var genes is only observed within the IT4-CD81 population, may give a hint towards this theory.

6.11 Operational matters

Concerning the overall analysis of the NGS data and the obtained results, some thought need to be kept in mind. As the analysis of the NGS data were aligned to the IT4/FCR3 *P. falciparum* genome, obtained from the actual version 2018-38 of www.plasmodb.org, some of the results need to be reviewed as the most recent version 2019-42 is available since march 2019. Within the newest releases, some annotations were clarified and unambiguously matched sequences improved. Moreover, due to small amounts of biomass, the depth of read counts was not as high as possible, while also some contaminations with human and rodent RNA was detected. A further filter to exclude those interfering signals will improve the quality of the data set and maybe trigger some small changes regarding the chosen cutoff levels and significance calculations. However, those improvements will not change in general the overall picture of the obtained data.

To validate the received results, it would be an idea to generate a qPCR panel or array studies, including primers for the var genes, present in the IT4 isolate.^{108,118,267,268} Although the performed experimental setup aimed the harvest of ring staged parasites at 6 to 8 hpi, focusing the peak in var gene expression, a comprehensive analysis of other multicopy gene families was given at this point. The extension of the setup to other time points, or in general a broader time frame, would allow a more distinct view towards e.g. knob related gene, other VSA members or transport associated genes, whose expressions or peaks in later timepoints. As many genes are expressed not only in the early phase of the life cycle, the presence could be determined by specific (permeabilizing) immunofluorescence assays, wester blotting or FACS analysis. Also, here, further results can be achieved by implementing the respective genes in a qPCR panel and testing harvested populations at various development stages.

Moreover, the usage of *P. falciparum* isolates with a knobby phenotype, such as 3D7 would also be an interesting object to compare the obtained results and the relation to knob related genes and the maybe altered presence of knobs on the IE surface. The most physiological approach would be the usage of fresh field isolates, just shortly adapted to artificial culture. This would also avoid the common genomic alteration of long-term cultivated isolates, as the deletion of chromosomal parts and the adaption to non-immunogenic environments without immune cells, selection pressure and interacting host cells.²⁶⁹ Furthermore, the use of AlbuMAX completed medium could be considered, as the C_var34 gene expression of the IT4 isolate seems to be promoted in the presence of human serum.¹⁴²

A recent study presented an interesting method, the so-called selection-linked integration (SLI), enable the functional analyzation of targets at gene and protein levels by permitting mislocalization, or knock sideways, or native proteins.^{270,271} This

would enable the generation of parasitic population, just being able to express one specific *var* gene at a time, bypassing the defective mutually exclusive premise, termed for long-term culture isolates. (in preparation, projects of Spielman-Laboratory, BNITM Hamburg) This would be a potent approach to investigate particular binding profiles and respective expression levels of particular *var* genes individually.

6.12 TEM analysis of knob appearance of the *P. falciparum* IE

The performed TEM analysis aimed the phenotypical differences of the IT4 culture isolate, cultivated at different conditions, focusing the overall knob appearance and distribution. The comparison with various field isolates completed the picture regarding the physiology of natural infections.

6.12.1.1 Field isolates

Here, distinct **field isolates** were analyzed, also including the cultivation with RPMI, complemented with human serum and AlbuMAX. As expected, all isolated exhibited a knobby phenotype, which is common in natural infections. Albeit, a recent study could show the appearance of knobless IE within field isolates, here, no knobless IE were detected in any sample. Moreover, the shown cultivation, either in the presence of human serum or AlbuMAX did not alter the number of detected knobs on IT4 IE, while significantly within 3D7 isolate.¹⁴² Here, the differential cultivation induced no significance change in knob appearance. However, as the field isolate BNI111216 was already processed 2 days after cultivation, it serves as baseline for physiological statements, regarding the number of detected knobs. Surprisingly, both, the BNI220616_HS and BNI220616_ALB isolate reached comparable levels, while being in culture for about 2 months. While the BNI060616_long isolate, cultivated for a similar time span, exhibited a fewer ratio of detected knobs per μm . While only being adapted for about 14 days, the other isolates show a clearly smaller number of detected knobs, while only the BNI010916 still reach the physiological baseline. The numbers of detected knobs on the IE surface for culture isolates were slightly higher, but in the same range and thus in line with prior findings.¹⁴²

6.12.1.2 Culture isolate IT4

Regarding the **culture isolate IT4**, cultivated at different temperatures and conditions or enriched over various endothelial receptors, the results differ from those of field isolates. While the IT4-St population exhibit a stable knobless phenotype, as evidenced by several samples and time points, there are some conditions, promoting the detection of knobby IE within the populations. By artificial selection for knobby IE via enrichment by Gelafundin, 100% of the population present a knobby surface, already after the first round of enrichment. The IT4 populations, after enrichment over human endothelial receptors were compared. As almost no receptor binding result in the presence of a knobby phenotype, it was somewhat surprising that IT3-CD37 and IT4-CD81 show knob structures on the IE surface. Following the claim that KAHRP is the

key marker protein for knobby phenotypes, the transcription levels should be elevated in knob positive, while almost undetectable in knob negative populations. By comparing former NGS analysis of the IT4 isolate, enriched over WT, CD36, ICAM-1, CD9, CD151, CD62-E and CD62-P and similarly processed as the actual experimental setup, the expression levels for KAHRP were concerned.¹⁷⁵ Thus, the levels, detected in the IT4-WT and IT4-CD151 population range in with the levels for IT4-MDR1, IT4-CD55 and IT4-CD81. The levels for IT4-CD36, IT4-CD9 and IT4-CD62-P were in the same range as IT4-TNFR1 and IT4-TNFR2. The outstanding expression level of IT4-CD37 is positively related to the knob appearance, visible in the TEM analysis, while 83% of the population exhibit a knobby phenotype. As also 12% of the IT4-CD81 population display knobs, while KAHRP being in the same range as other enriched, but knobless population, it is logical to assume that not KAHRP alone mediate knob formation on IE surfaces. Therefore, also, IT4-WT and IT4-CD151 IE should have at least some detectable knobby IE within their population, while they don't.

Comparing the results for the temperature dependent experimental setups, it was striking that only the IT4-40°C IE, enriched over HBEC-5i at 40°C, exhibited a knobby phenotype, even in 100% of the population. Otherwise, IT4-37°C, enriched over HBEC-5i at 37°C did not. Moreover, IT4 cultivated at elevated temperatures, experienced reoccurring febrile heat shocks or a treatment with TNF α exhibited no knobby phenotypic IE at all.

Therefore, my question rose, if the process of sequestration, compared with febrile temperatures is a decisive model to generate knobby phenotypes within IE populations. To test the newly set thesis, 2 enriched IT population should be compared regarding their phenotypic expression after experiencing sequestration and febrile temperatures. To rule out the involvement of HBEC-5i cells, triggering the expression, sequestration was induced towards mock-transfected CHO-GFP cells, and CHO-CD55 cells, expressing the respective human endothelial receptor. Therefore, the equally enriched IT4-GFP population, as well as the IT4-CD55 population was co-incubated or rather preabsorbed by either 37°C or 40°C, followed by the actual panning at 40°C. Within this setup, also the time frame of febrile temperatures was adjusted, to see if an abrupt temperature change (37°C to 40°C) or a continuous temperature (40°C to 40°C) is more favorable. By immunofluorescence analysis utilizing a specific α KAHRP antibody, knobby IE could be detected for both, the IT4-GFP and IT4-CD55 population, within the temperature changing approach. Consequently, these results could also be validated in the TEM analysis. (data not shown) Otherwise, the continuous elevation of the temperature prior and at the panning, was proved not to be successful.

Taking to account that long-term cultivated isolates are capable of chromosomal deletions and genomic alterations, experimental setups could be established, using adapted field isolates that have lost or reduced their knobby phenotype over the time. Also, analyzing the genomic background of the individual population could be easily tested with particular qPCR panels, focusing knob related genes. The possibility that only knobby IE were positively selected via the enrichment procedure is given, albeit not likely. The initial knobless IT4-CD55 population does express KAHRP in the same range as the knobby IT4-CD81 population, until enrichment at febrile temperature, where knobby IE can be detected.

Moreover, it would be interesting if the initial knobby phenotype of IT4-CD37 and IT4-CD81 could be altered into a knobless one by enrichment over other human endothelial receptors e.g. TNFR1, which enriched populations do not exhibit knob structures, such as IT4-TNFR1. A former study showed that knobless IT4 populations, expressing A_var60 can switch to a knobby phenotype, when enriched for E_var04 (low knob density) or B_var32B (high knob density) expression, and vice versa. Here, the theory rose that the differential expression of a particular *var* gene alter the knob related phenotypic appearance.¹³⁹ However, those findings are not applicable to the actual experiments, as all enriched population highly express the B_var32B gene, while consequently being knobless. The only exemptions are IT4-CD37, while no particular differential upregulated *var* genes was found; and IT4-CD81, differentially expressing A_var09, B_var11 and B_var12; also found in other populations. However, it could be of interest to validate if the expression profile is still the same before and after an enrichment at febrile temperatures of 40°C. There might be the possibility, that some *var* genes are more favored to be expressed at elevated temperatures, coupled with endothelial sequestration.

> As these experiments were only carries out one, a repetition is clearly needed. Also, further controls could be the implementation of a knobby isolate, such as 3D7, to evaluate if also there, the overall amount or the density of knobs increase. As the gene expression level for KAHRP is nearly not detectable for the enriched IT4-GFP population, for IT4-CD55, it was in the same range as the initially knobby IT4-CD81 population. Similar levels are detected for IT4-MDR1, while no TEM analysis or IFA is available. This would be a potential condition investigating the knob appearance as well. Also, other enriched population could be further processed at 40°C panning assays, evaluating the possibility of generating knobby phenotypes in distinct population, or if the appearance is restricted to the sequestration of few selected receptor proteins. Therefore, it would be interesting to utilize other cell lines, such as HEK cells or primary cell lines to draw a more physiological picture and to determine if the effect can be restored with unspecific binding as well.

> To clarify the involvement of particular genes in the formation of knob structures, it would be advisable to compare whole NGS analysis of the general knobless isolate IT4 and the partly knobby isolate 3D7. As the data for both isolates are available and include the starting population, as well as the enriched populations, a comparison of all knob related and maybe so far undetermined genes could be drawn. This would give a high impact on understanding and evaluating the available expression levels, at relatively low further costs and effort.

CONCLUSION

The overall aim of this work was to characterize the gene expression of knob related and variable surface proteins within the *P. falciparum* isolate IT4 in relation to its particular receptor sequestration.

Within this thesis, the initial binding capability of various *P. falciparum* culture and field isolates was evaluated. It was possible to generate 16 transient transfected CHO cell lines, expressing particular human endothelial receptors on the surface. The performance of static binding assays was carried out with, in total, 19 different cell lines (CHO-WT, CHO-GFP, CHO-CD9, CHO-CD151, CHO-CD62-E, CHO-CD62-P, CHO-HRH1, CHO-VCAM1, CHO-MDR1, CHO-TNFR1, CHO-TNFR2, CHO-CD37, CHO-CD55, CHO-CD81, CHO-EPOR and HBEC-5i).

It was revealed that almost all populations are capable to bind CD36, except 2 field isolates, while no binding was detected towards the mock-transfected control. This validates the integrity of the overall performance of IE sequestration within the experimental setup. Moreover, initial binding profiles as well as the compositional surface analyses of human brain endothelial cells, allow the selection of 6 distinct human endothelial receptors, relevant for further investigation, namely MDR1, TNFR1, TNFR2, CD37, CD55 and CD81.

By cytoadhesion inhibition assays, using specific antibodies or soluble CSA, the characteristic binding could be specifically inhibited, likewise in a concentration dependent manner. These experiments were carried out for IT4-CD55, IT4-TNFR1, IT4-37°C and IT4-40°C, while for others, it still needs to be accomplished.

Regarding the already described phenomenon of IE sequestration towards mock-transfected or CHO-WT cells, a so far unknown structure on the surface of CHO cells is thought to be responsible. By cytoadhesion inhibition assays, the ubiquitously dispersed rodent surface protein CD44 could be ruled out as the interfering receptor by using specific antibodies.

The selection of suitable human receptors, inducing a promising IE binding profile, revealed 6 promising candidates, namely MDR1, TNFR1, TNFR2, CD37, CD55 and CD81. The respective gene expression profiles were determined by next generation RNA sequencing of ring staged parasites. Regarding the individually enriched IT4 populations and after bioinformatical analysis of the whole transcriptomes, various genes exhibited differentially upregulated expression levels. Some ubiquitous expressed *var* genes were excluded from further evaluation, as their premise of mutually exclusivity was not given any more.

For **IT4-GFP**, the B_var14, some PHIST, RIFIN and SURFIN as well as a few protein transport related genes, were observed to be differentially upregulated.

For **IT4-MDR1**, the C_var05 as well as several genes, strongly related with knob formation, surpassed the chosen cutoff criteria, including KAHRP and KAHRP-assembling associated genes.

For **IT4-TNFR1**, the A_var03 gene showed a differentially upregulated expression level, while only few other relevant genes were affected.

For **IT4-TNFR2**, the C_var05 and A_var09 genes were differentially upregulated. Also, many protein trafficking genes, like HSP and FIKK kinases as well as knob formation genes, such as MAHRP1, PfEMP2/MESA and (RESA-like) PHISTs, together with few RIFIN and SURFIN, VSP and HYP coding genes were affected.

For **IT4-CD37**, no particular *var* gene was detected at a considerable level, while strikingly, upregulations were evidenced regarding knob formation and protein trafficking genes. This includes genes for the knob determined DnaJ, KAHRP and the knob associated HSP40, PfEMP3 and the knob associated NA-type RIFIN gene.

For **IT4-CD55**, the B_var11 gene was found to be differentially expressed, together with some considerable levels of knob related genes.

For **IT4-CD81**, the A_var09, B_var11 and B_var12 gene as well as most of the knob related genes show a differentially upregulated gene expression level.

Nevertheless, albeit partly low parasitic relevant read counts, the revealed results are reliable but need further bioinformatical processing for a more stringent picture.

By performing transmissive electron microscopic analysis, it was revealed that only some proportions of the IT4-CD37 and the IT4-CD81 population exhibited a knob positive phenotype, albeit within the physiological range of comprehensively tested *P. falciparum* field isolates. Furthermore, the analysis showed an overall knob positive phenotypic IE within the IT4-40°C population, after sequestration towards human brain endothelial cells at febrile temperatures of 40°C. All of the remaining IT4 populations, either specifically sequestered or after experiencing various febrile phases were detected as knob negative.

Surprisingly, the combination of sequestration and febrile temperature evidenced a knob positive phenotype, tested for IT4-GFP and IT4-CD55, also within the physiological range of knob formation.

Summarizing, the yet described set of human receptors interacting with *P. falciparum* infected erythrocytes can be extended, while also a hint towards the interacting PfEMP1 proteins has been revealed. Eventually, the influence of febrile temperatures coupled with sequestration, must be noted. The obtained findings open up new possibilities for further investigations regarding major factors of the high pathogenicity of *P. falciparum*.

Final Summary

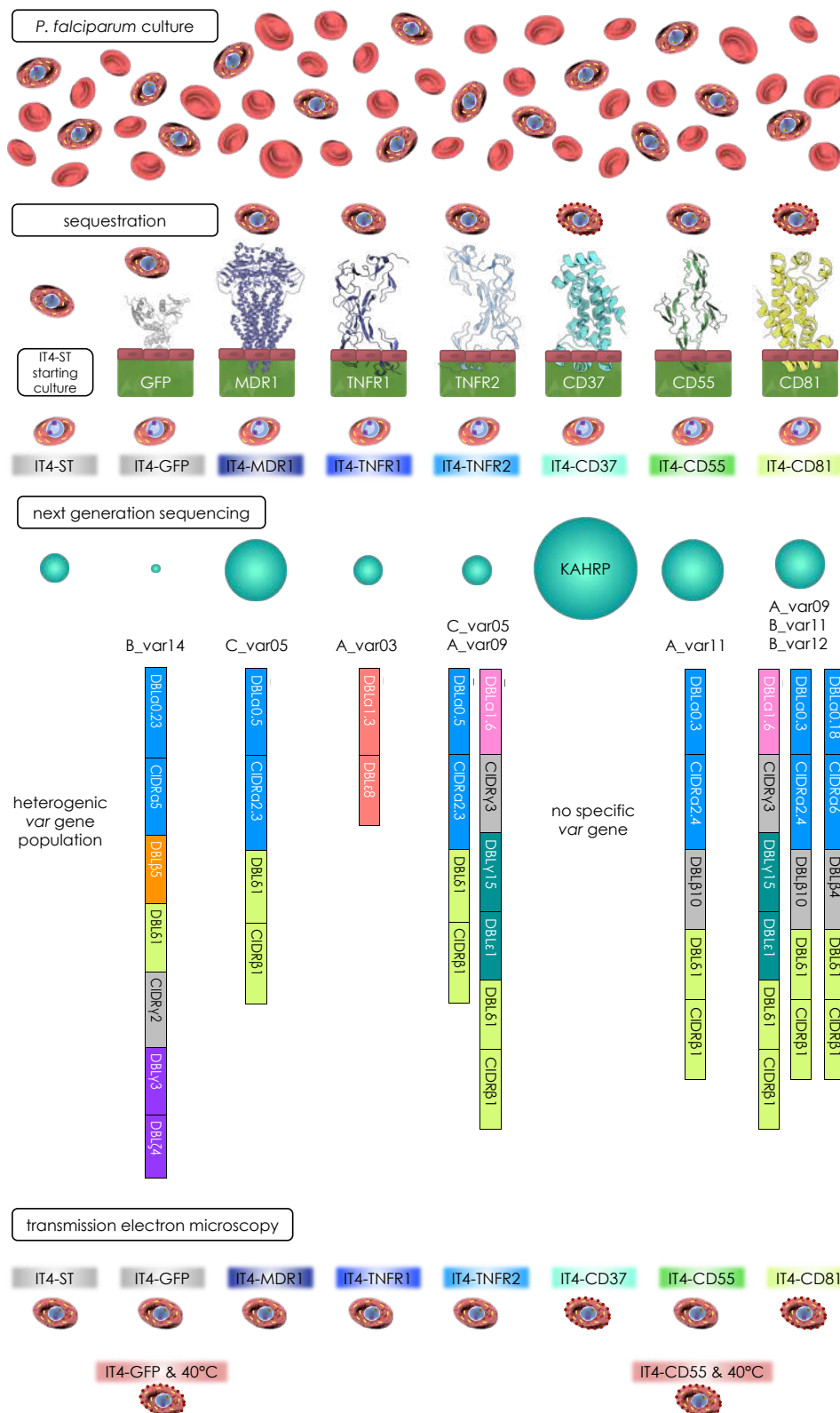


Figure 25. Overview of the experimental setup and obtained results. Trophozoite staged IE of the *P. falciparum* IT isolate sequester to specific, transgenically expressed human endothelial receptors. The next generation RNA sequencing revealed differential upregulations of particular *var* genes for most of the enriched IT4 populations. The knob associated protein KAHRP was found at a highly increased expression level in IT4-CD37. The TEM analysis evidenced, that the initially knobless IT4-ST population exhibited knob structures, directly after sequestration for IT4-CD37 and IT4-CD81. Additionally, a knob positive phenotype appeared in IT4-GFP and IT4-CD55 after sequestration, combined with febrile temperatures of 40°C.

LITERATURE

1. WHO. *World Malaria Report. World Malaria Report* (2018). doi:ISBN 978 92 4 1564403
2. Loew, H. & Meigen, J. W. *Systematische Beschreibung der bekannten europäischen zweiflügeligen Insekten*. (Bei Friedrich Wilhelm Forstmann : Gedrukt bei Beaufort Sohn, 1820). doi:10.5962/bhl.title.65747
3. Sutamihardja, A., Muth, S., Barcus, M. J., Wongsrichanalai, C. & Wernsdorfer, W. H. A Review of Malaria Diagnostic Tools: Microscopy and Rapid Diagnostic Test (RDT). *Am. J. Trop. Med. Hyg.* **77**, 119–127 (2018).
4. Wangai, L. N. *et al.* Sensitivity of microscopy compared to molecular diagnosis of *P. Falciparum*: Implications on malaria treatment in epidemic areas in Kenya. *African J. Infect. Dis.* **5**, 1–6 (2011).
5. The Nigeria Centre for Disease Control (NCDC). MALARIA. (2016). Available at: <https://ncdc.gov.ng/diseases/info/M>. (Accessed: 17th March 2019)
6. Wassmer, S. C. *et al.* Investigating the pathogenesis of severe malaria: A multidisciplinary and cross-geographical approach. *Am. J. Trop. Med. Hyg.* **93**, 42–56 (2015).
7. Arama, C. & Troye-Blomberg, M. The path of malaria vaccine development: Challenges and perspectives. *J. Intern. Med.* **275**, 456–466 (2014).
8. Alphey, L. *et al.* Sterile-insect methods for control of mosquito-borne diseases: an analysis. *Vector Borne Zoonotic Dis.* **10**, 295–311 (2010).
9. Yoshida, S. *et al.* Hemolytic C-type lectin CEL-III from sea cucumber expressed in transgenic mosquitoes impairs malaria parasite development. *PLoS Pathog.* **3**, 1962–1970 (2007).
10. Hughes, G. L., Rivero, A. & Rasgon, J. L. *Wolbachia* can enhance *Plasmodium* infection in mosquitoes: implications for malaria control? *PLoS Pathog.* **10**, e1004182 (2014).
11. Gomes, F. M. *et al.* Effect of naturally occurring *Wolbachia* in *Anopheles gambiae s.l.* mosquitoes from Mali on *Plasmodium falciparum* malaria transmission. *Proc. Natl. Acad. Sci.* **114**, 12566–12571 (2017).
12. Hoffman, S. L., Vekemans, J., Richie, T. L. & Duffy, P. E. The march toward malaria vaccines. *Vaccine* **33**, D13–D23 (2015).
13. Rieckmann, K. H., Beaudoin, R. L., Cassells, J. S. & Sell, K. W. Use of attenuated sporozoites in the immunization of human volunteers against falciparum malaria. *Bull. World Health Organ.* **57 Suppl 1**, 261–5 (1979).
14. Overstreet, M. G., Cockburn, I. A., Chen, Y.-C. & Zavala, F. Protective CD8⁺ T cells against *Plasmodium* liver stages: immunobiology of an 'unnatural' immune response. *Immunol. Rev.* **225**, 272–283 (2008).
15. Warburg, A. & Schneider, I. In Vitro Culture of the Mosquito Stages of *Plasmodium falciparum*. *Exp. Parasitol.* **76**, 121–126 (1993).
16. Rathore, D. *et al.* Molecular mechanism of host specificity in *Plasmodium falciparum* infection: role of circumsporozoite protein. *J. Biol. Chem.* **278**, 40905–10 (2003).
17. Reber-Liske, R., Salako, L. A., Matile, H., Sowunmi, A. & Stürchler, D. [NANP]19-5.1. A malaria vaccine field trial in Nigerian children. *Trop. Geogr. Med.* **47**, 61–3 (1995).
18. Miller, L. H., Baruch, D. I., Marsh, K. & Doumbo, O. K. The pathogenic basis of malaria. *Nature* **415**, 673–679 (2002).
19. Chen, Q. The naturally acquired immunity in severe malaria and its implication for a PfEMP-1 based vaccine. *Microbes Infect.* **9**, 777–783 (2007).
20. Makobongo, M. O., Keegan, B., Long, C. A. & Miller, L. H. Immunization of Aotus Monkeys with Recombinant Cysteine-Rich Interdomain Region 1a Protects against Severe Disease during *Plasmodium falciparum* Reinfection. *J. Infect. Dis.* **193**, 731–740 (2006).
21. Bannister, L. H. & Mitchell, G. H. The fine structure of secretion by *Plasmodium knowlesi* merozoites during red cell invasion. *J. Protozool.* **36**, 362–7 (1989).
22. Mota, M. M. *et al.* Migration of *Plasmodium* Sporozoites Through Cells Before Infection. *Science (80-)*. **291**, 141–144 (2001).
23. Mota, M. M., Hafalla, J. C. R. & Rodriguez, A. Migration through host cells activates *Plasmodium* sporozoites for infection. *Nat. Med.* **8**, 1318–1322 (2002).
24. Mota, M. M. & Rodriguez, A. Migration through host cells: The first steps of *Plasmodium* sporozoites in the mammalian host. *Cell. Microbiol.* **6**, 1113–1118 (2004).

25. Sidjanski, S. & Vanderberg, J. P. Delayed migration of Plasmodium sporozoites from the mosquito bite site to the blood. *Am. J. Trop. Med. Hyg.* **57**, 426–9 (1997).
26. Sibley, L. D. Toxoplasma gondii: perfecting an intracellular life style. *Traffic* **4**, 581–6 (2003).
27. Burda, P.-C., Caldelari, R. & Heussler, V. T. Manipulation of the Host Cell Membrane during Plasmodium Liver Stage Egress. *MBio* **8**, (2017).
28. Langreth, S. G., Jensen, J. B., Reese, R. T. & Trager, W. Fine structure of human malaria in vitro. *J. Protozool.* **25**, 443–52 (1978).
29. Preiser, P., Kaviratne, M., Khan, S., Bannister, L. & Jarra, W. The apical organelles of malaria merozoites: host cell selection, invasion, host immunity and immune evasion. *Microbes Infect.* **2**, 1461–77 (2000).
30. Cowman, A. F., Berry, D. & Baum, J. The cellular and molecular basis for malaria parasite invasion of the human red blood cell. *J. Cell Biol.* **198**, 961–971 (2012).
31. Zuccala, E. S. & Baum, J. Cytoskeletal and membrane remodelling during malaria parasite invasion of the human erythrocyte. *Br. J. Haematol.* **154**, 680–689 (2011).
32. Maier, A. G. *et al.* Exported Proteins Required for Virulence and Rigidity of Plasmodium falciparum-Infected Human Erythrocytes. *Cell* **134**, 48–61 (2008).
33. Planche, T. Molecular approaches to malaria. *J. Clin. Pathol.* **59**, 1228–1228 (2006).
34. Steiner, I. S. Beschreibung: Funktionalisierte Inhibitoren der New Permeability Pathways in malarieinfizierten Erythrozyten. (Philipps-Universität Marburg, 2016).
35. De Niz, M. *et al.* Progress in imaging methods: Insights gained into Plasmodium biology. *Nat. Rev. Microbiol.* **15**, 37–54 (2017).
36. Hanssen, E. *et al.* Targeted mutagenesis of the ring-exported protein-1 of Plasmodium falciparum disrupts the architecture of Maurer's cleft organelles. *Mol. Microbiol.* **69**, 938–953 (2008).
37. Spry, C. & Saliba, K. J. The Human Malaria Parasite Plasmodium falciparum Is Not Dependent on Host Coenzyme A Biosynthesis. *J. Biol. Chem.* **284**, 24904–24913 (2009).
38. Marti, M., Good, R. T., Rug, M., Knuepfer, E. & Cowman, A. F. Targeting malaria virulence and remodeling proteins to the host erythrocyte. *Science (80-.)*. **306**, 1930–1933 (2004).
39. Spielmann, T. *et al.* A cluster of ring stage-specific genes linked to a locus implicated in cytoadherence in Plasmodium falciparum codes for PEXEL-negative and PEXEL-positive proteins exported into the host cell. *Mol. Biol. Cell* **17**, 3613–24 (2006).
40. Maier, A. G., Cooke, B. M., Cowman, A. F. & Tilley, L. Malaria parasite proteins that remodel the host erythrocyte. *Nat. Rev. Microbiol.* **7**, 341–354 (2009).
41. Bannister, L. H., Hopkins, J. M., Fowler, R. E., Krishna, S. & Mitchell, G. H. A brief illustrated guide to the ultrastructure of Plasmodium falciparum asexual blood stages. *Parasitol. Today* **16**, 427–433 (2000).
42. Goldberg, D. E. Complex nature of malaria parasite hemoglobin degradation [corrected]. *Proc. Natl. Acad. Sci. U. S. A.* **110**, 5283–4 (2013).
43. Coronado, L. M., Nadovich, C. T. & Spadafora, C. Malarial hemozoin: From target to tool. *Biochim. Biophys. Acta - Gen. Subj.* **1840**, 2032–2041 (2014).
44. Gruenberg, J., Allred, D. R. & Sherman, I. W. Scanning electron microscope-analysis of the protrusions (knobs) present on the surface of Plasmodium falciparum-infected erythrocytes. *J. Cell Biol.* **97**, 795–802 (1983).
45. Kilejian, A. & Jensen, J. B. A histidine-rich protein from Plasmodium falciparum and its interaction with membranes. *Bull. World Health Organ.* **55**, 191–7 (1977).
46. Oh, S. S. *et al.* Plasmodium falciparum erythrocyte membrane protein 1 is anchored to the actin-spectrin junction and knob-associated histidine-rich protein in the erythrocyte skeleton. *Mol. Biochem. Parasitol.* **108**, 237–47 (2000).
47. Pei, X. *et al.* Structural and Functional Studies of Interaction between Plasmodium falciparum Knob-associated Histidine-rich Protein (KAHRP) and Erythrocyte Spectrin. *J. Biol. Chem.* **280**, 31166–31171 (2005).
48. Flick, K. & Chen, Q. var genes, PfEMP1 and the human host. *Mol. Biochem. Parasitol.* **134**, 3–9 (2004).
49. Gardner, J. P., Pinches, R. A., Roberts, D. J. & Newbold, C. I. Variant antigens and endothelial receptor adhesion in Plasmodium falciparum. *Proc. Natl. Acad. Sci. U. S. A.* **93**, 3503–8 (1996).
50. Kriek, N. *et al.* Characterization of the pathway for transport of the cytoadherence-mediating protein, PfEMP1, to the host cell surface in malaria parasite-infected

- erythrocytes. *Mol. Microbiol.* **50**, 1215–27 (2003).
51. Cowman, A. F. & Crabb, B. S. Invasion of red blood cells by malaria parasites. *Cell* **124**, 755–766 (2006).
 52. Gerald, N., Mahajan, B. & Kumar, S. Mitosis in the Human Malaria Parasite *Plasmodium falciparum*. *Eukaryot. Cell* **10**, 474–482 (2011).
 53. Beeson, J. G. *et al.* Merozoite surface proteins in red blood cell invasion, immunity and vaccines against malaria. *FEMS Microbiol. Rev.* **40**, 343–372 (2016).
 54. Grüning, C. *et al.* Development and host cell modifications of *Plasmodium falciparum* blood stages in four dimensions. *Nat. Commun.* **2**, 165 (2011).
 55. Bousema, T. & Drakeley, C. Epidemiology and infectivity of *Plasmodium falciparum* and *Plasmodium vivax* gametocytes in relation to malaria control and elimination. *Clin. Microbiol. Rev.* **24**, 377–410 (2011).
 56. Bruce, M. C., Alano, P., Duthie, S. & Carter, R. Commitment of the malaria parasite *Plasmodium falciparum* to sexual and asexual development. *Parasitology* **100 Pt 2**, 191–200 (1990).
 57. Horrocks, P. *et al.* PfEMP1 expression is reduced on the surface of knobless *Plasmodium falciparum* infected erythrocytes. *J. Cell Sci.* **118**, 2507–2518 (2005).
 58. Kafsack, B. F. C. *et al.* A transcriptional switch underlies commitment to sexual development in malaria parasites. *Nature* **507**, 248–252 (2014).
 59. Baker, D. A. Malaria gametocytogenesis. *Mol. Biochem. Parasitol.* **172**, 57–65 (2010).
 60. Shahabuddin, M. *Plasmodium* ookinete development in the mosquito midgut: a case of reciprocal manipulation. *Parasitology* **116 Suppl**, S83–93 (1998).
 61. Aly, A. S. I., Vaughan, A. M. & Kappe, S. H. I. Malaria parasite development in the mosquito and infection of the mammalian host. *Annu. Rev. Microbiol.* **63**, 195–221 (2009).
 62. Bull, P. C. *et al.* Parasite antigens on the infected red cell surface are targets for naturally acquired immunity to malaria. *Nat. Med.* **4**, 358–60 (1998).
 63. Douki, J.-B. L. Adhesion of normal and *Plasmodium falciparum* ring-infected erythrocytes to endothelial cells and the placenta involves the rhoptry-derived ring surface protein-2. *Blood* **101**, 5025–5032 (2003).
 64. Baruch, D. I. Adhesive receptors on malaria-parasitized red cells. *Baillieres. Best Pract. Res. Clin. Haematol.* **12**, 747–61 (1999).
 65. David, P. H. *et al.* Parasite sequestration in *Plasmodium falciparum* malaria: spleen and antibody modulation of cytoadherence of infected erythrocytes. *Proc. Natl. Acad. Sci.* **80**, 5075–5079 (1983).
 66. Ho, M. *et al.* Splenic Fc receptor function in host defense and anemia in acute *Plasmodium falciparum* malaria. *J. Infect. Dis.* **161**, 555–61 (1990).
 67. Kyes, S. A., Kraemer, S. M. & Smith, J. D. Antigenic Variation in *Plasmodium falciparum*: Gene Organization and Regulation of the var Multigene Family. *Eukaryot. Cell* **6**, 1511–1520 (2007).
 68. MacPherson, G. G., Warrell, M. J., White, N. J., Looareesuwan, S. & Warrell, D. A. Human cerebral malaria. A quantitative ultrastructural analysis of parasitized erythrocyte sequestration. *Am. J. Pathol.* **119**, 385–401 (1985).
 69. Bachmann, A. *et al.* Absence of erythrocyte sequestration and lack of multicopy gene family expression in *Plasmodium falciparum* from a splenectomized malaria patient. *PLoS One* **4**, e7459 (2009).
 70. Anyona, S. B., Schrier, S. L., Gichuki, C. W. & Waitumbi, J. N. Pitting of malaria parasites and spherocyte formation. *Malar. J.* **5**, 64 (2006).
 71. Schnitzer, B., Sodeman, T., Mead, M. L. & Contacos, P. G. Pitting function of the spleen in malaria: ultrastructural observations. *Science* **177**, 175–7 (1972).
 72. Wahlgren, M., Goel, S. & Akhouri, R. R. Variant surface antigens of *Plasmodium falciparum* and their roles in severe malaria. *Nat. Rev. Microbiol.* **15**, 479–491 (2017).
 73. Deans, A.-M. & Rowe, J. A. *Plasmodium falciparum*: Rosettes do not protect merozoites from invasion-inhibitory antibodies. *Exp. Parasitol.* **112**, 269–273 (2006).
 74. Pain, A. *et al.* Platelet-mediated clumping of *Plasmodium falciparum*-infected erythrocytes is a common adhesive phenotype and is associated with severe malaria. *Proc. Natl. Acad. Sci.* **98**, 1805–1810 (2001).
 75. David, P. H., Handunnetti, S. M., Leech, J. H., Gamage, P. & Mendis, K. N. Rosetting: a new cytoadherence property of malaria-infected erythrocytes. *Am. J. Trop. Med. Hyg.*

- 38**, 289–97 (1988).
76. Götz, A. *et al.* Atypical activation of dendritic cells by *Plasmodium falciparum*. *Proc. Natl. Acad. Sci. U. S. A.* **114**, E10568–E10577 (2017).
 77. Miller, L., Good, M. & Milon, G. Malaria Pathogenesis. *Science (80-.)*. **264**, 1878–1883 (1994).
 78. Roberts, D. J. *et al.* *Plasmodium falciparum*-infected erythrocytes modulate the maturation of dendritic cells. *Nature* **400**, 73–77 (1999).
 79. Ferreira, M. U., da Silva Nunes, M. & Wunderlich, G. Antigenic diversity and immune evasion by malaria parasites. *Clin. Diagn. Lab. Immunol.* **11**, 987–95 (2004).
 80. Gupta, S. & Day, K. P. A strain theory of malaria transmission. *Parasitol. Today* **10**, 476–481 (1994).
 81. Gupta, S., Snow, R. W., Donnelly, C. & Newbold, C. Acquired immunity and postnatal clinical protection in childhood cerebral malaria. *Proc. R. Soc. B Biol. Sci.* **266**, 33–38 (1999).
 82. Helms, G., Dasanna, A. K., Schwarz, U. S. & Lanzer, M. Modeling cytoadhesion of *Plasmodium falciparum*-infected erythrocytes and leukocytes-common principles and distinctive features. *FEBS Lett.* **590**, 1955–71 (2016).
 83. Sherling, E. S. & van Ooij, C. Host cell remodeling by pathogens: the exomembrane system in *Plasmodium*-infected erythrocytes. *FEMS Microbiol. Rev.* **40**, 701–21 (2016).
 84. Dasanna, A. K., Lansche, C., Lanzer, M. & Schwarz, U. S. Rolling Adhesion of Schizont Stage Malaria-Infected Red Blood Cells in Shear Flow. *Biophys. J.* **112**, 1908–1919 (2017).
 85. Davis, S. P. *et al.* *Plasmodium falciparum*-induced CD36 clustering rapidly strengthens cytoadherence via p130CAS-mediated actin cytoskeletal rearrangement. *FASEB J.* **26**, 1119–1130 (2012).
 86. Hiller, N. L. *et al.* A Host-Targeting Signal in Virulence Proteins Reveals a Secretome in Malarial Infection. *Science (80-.)*. **306**, 1934–1937 (2004).
 87. Kaur, J. & Hora, R. '2TM proteins': An antigenically diverse superfamily with variable functions and export pathways. *PeerJ* **2018**, (2018).
 88. Spielmann, T. *et al.* A Cluster of Ring Stage-specific Genes Linked to a Locus Implicated in Cytoadherence in *Plasmodium falciparum* Codes for PEXEL-negative and PEXEL-positive Proteins Exported into the Host Cell. *Mol. Biol. Cell* **17**, 3613–3624 (2006).
 89. Spielmann, T. & Gilberger, T. W. Protein export in malaria parasites: do multiple export motifs add up to multiple export pathways? *Trends Parasitol.* **26**, 6–10 (2010).
 90. Proellocks, N. I., Coppel, R. L., Mohandas, N. & Cooke, B. M. *Malaria Parasite Proteins and Their Role in Alteration of the Structure and Function of Red Blood Cells. Advances in Parasitology* **91**, (Elsevier Ltd, 2016).
 91. Spielmann, T. & Gilberger, T.-W. Critical Steps in Protein Export of *Plasmodium falciparum* Blood Stages. *Trends Parasitol.* **31**, 514–525 (2015).
 92. Sam-Yellowe, T. Y. *et al.* A *Plasmodium* gene family encoding Maurer's cleft membrane proteins: structural properties and expression profiling. *Genome Res.* **14**, 1052–9 (2004).
 93. Maier, A. G., Cooke, B. M., Cowman, A. F. & Tilley, L. Malaria parasite proteins that remodel the host erythrocyte. *Nat. Rev. Microbiol.* **7**, 341–354 (2009).
 94. Spillman, N. J., Beck, J. R. & Goldberg, D. E. Protein Export into Malaria Parasite-Infected Erythrocytes: Mechanisms and Functional Consequences. *Annu. Rev. Biochem.* **84**, 813–841 (2015).
 95. Leech, J. H., Barnwell, J. W., Aikawa, M., Miller, L. H. & Howard, R. J. *Plasmodium falciparum* malaria: Association of knobs on the surface of infected erythrocytes with a histidine-rich protein and the erythrocyte skeleton. *J. Cell Biol.* **98**, 1256–1264 (1984).
 96. Blythe, J. E., Suretheran, T. & Preiser, P. R. STEVOR - A multifunctional protein? *Mol. Biochem. Parasitol.* **134**, 11–15 (2004).
 97. Cheng, Q. *et al.* *stevor* and *rif* are *Plasmodium falciparum* multicopy gene families which potentially encode variant antigens. *Mol. Biochem. Parasitol.* **97**, 161–76 (1998).
 98. Kyes, S. A., Kraemer, S. M. & Smith, J. D. Antigenic variation in *Plasmodium falciparum*: gene organization and regulation of the var multigene family. *Eukaryot. Cell* **6**, 1511–20 (2007).
 99. Fernandez, V., Hommel, M., Chen, Q., Hagblom, P. & Wahlgren, M. Small, clonally variant antigens expressed on the surface of the *Plasmodium falciparum*-infected erythrocyte are encoded by the *rif* gene family and are the target of human immune responses. *J.*

- Exp. Med.* **190**, 1393–404 (1999).
100. Makhtar Niang, Amy Kristine Bei, Kripa Gopal Madnani, Shaaretha Pelly, Selasi Dankwa, Usheer Kanjee, Karthigayan Gunalan, Anburaj Amaladoss, K. P. Y. & Ndeye Sakha Bob, Benoit Malleret, , Manoj Duraisingh, and P. R. P. The variant STEVOR protein of *Plasmodium falciparum* is a red cell binding protein important for merozoite invasion and rosetting. *Cell Host Microbe* **16**, 81–93 (2014).
 101. Lavazec, C., Sanyal, S. & Templeton, T. J. Hypervariability within the Rifin, Stevor and Pfmc-2TM superfamilies in *Plasmodium falciparum*. *Nucleic Acids Res.* **34**, 6696–6707 (2006).
 102. Gardner, M. J. *et al.* Genome sequence of the human malaria parasite *Plasmodium falciparum*. *Nature* **419**, 498–511 (2002).
 103. Kyes, S. A., Rowe, J. A., Kriek, N. & Newbold, C. I. Rifins: a second family of clonally variant proteins expressed on the surface of red cells infected with *Plasmodium falciparum*. *Proc. Natl. Acad. Sci. U. S. A.* **96**, 9333–8 (1999).
 104. Bultrini, E. *et al.* Revisiting the *Plasmodium falciparum* RIFIN family: From comparative genomics to 3D-model prediction. *BMC Genomics* **10**, 445 (2009).
 105. Bachmann, A. *et al.* A comparative study of the localization and membrane topology of members of the RIFIN, STEVOR and PfMC-2TM protein families in *Plasmodium falciparum*-infected erythrocytes. *Malar. J.* **14**, (2015).
 106. Baruch, D. I. *et al.* Cloning the *P. falciparum* gene encoding PfEMP1, a malarial variant antigen and adherence receptor on the surface of parasitized human erythrocytes. *Cell* **82**, 77–87 (1995).
 107. Rowe, J. A. & Kyes, S. A. The role of *Plasmodium falciparum* var genes in malaria in pregnancy. *Mol. Microbiol.* **53**, 1011–9 (2004).
 108. Albrecht, L. *et al.* Var gene transcription and PfEMP1 expression in the rosetting and cytoadhesive *Plasmodium falciparum* clone FCR3S1.2. *Malar. J.* **10**, 1–9 (2011).
 109. Kraemer, S. M. & Smith, J. D. A family affair: var genes, PfEMP1 binding, and malaria disease. *Curr. Opin. Microbiol.* **9**, 374–380 (2006).
 110. Su, X. zhuan *et al.* The large diverse gene family var encodes proteins involved in cytoadherence and antigenic variation of *plasmodium falciparum*-infected erythrocytes. *Cell* **82**, 89–100 (1995).
 111. Smith, J. D., Subramanian, G., Gamain, B., Baruch, D. I. & Miller, L. H. Classification of adhesive domains in the *Plasmodium falciparum* Erythrocyte Membrane Protein 1 family. *Mol. Biochem. Parasitol.* **110**, 293–310 (2000).
 112. Avril, M., Brazier, A. J., Melcher, M., Sampath, S. & Smith, J. D. DC8 and DC13 var Genes Associated with Severe Malaria Bind Avidly to Diverse Endothelial Cells. *PLoS Pathog.* **9**, 1–14 (2013).
 113. Singh, V., Gupta, P. & Pande, V. Revisiting the multigene families: *Plasmodium* var and vir genes. *J. Vector Borne Dis.* **51**, 75–81 (2014).
 114. Lavstsen, T., Salanti, A., Jensen, A. T. R., Arnot, D. E. & Theander, T. G. Sub-grouping of *Plasmodium falciparum* 3D7 var genes based on sequence analysis of coding and non-coding regions. *Malar. J.* **2**, 27 (2003).
 115. Bachmann, A. Etablierung einer Methode zur Analyse der var - Genexpression bei *Plasmodium falciparum* (Welch , 1897) isoliert aus Malaria-Patienten. (2006).
 116. Joannin, N., Abhiman, S., Sonnhammer, E. L. & Wahlgren, M. Sub-grouping and sub-functionalization of the RIFIN multi-copy protein family. *BMC Genomics* **9**, 1–14 (2008).
 117. Petter, M., Bonow, I. & Klinkert, M. Q. Diverse expression patterns of subgroups of the rif multigene family during *Plasmodium falciparum* gametocytogenesis. *PLoS One* **3**, (2008).
 118. Bachmann, A. *et al.* Temporal expression and localization patterns of variant surface antigens in clinical *Plasmodium falciparum* isolates during erythrocyte schizogony. *PLoS One* **7**, e49540 (2012).
 119. Abdel-Latif, M. S., Khattab, A., Lindenthal, C., Kremsner, P. G. & Klinkert, M. Q. Recognition of variant rifin antigens by human antibodies induced during natural *Plasmodium falciparum* infections. *Infect. Immun.* **70**, 7013–7021 (2002).
 120. Saito, F. *et al.* Immune evasion of *Plasmodium falciparum* by RIFIN via inhibitory receptors. *Nature* **552**, 101–105 (2017).
 121. Naissant, B. *et al.* *Plasmodium falciparum* STEVOR phosphorylation regulates host

- erythrocyte deformability enabling malaria parasite transmission. *Blood* **127**, e42–e53 (2016).
122. Frech, C. & Chen, N. Variant surface antigens of malaria parasites: functional and evolutionary insights from comparative gene family classification and analysis. *BMC Genomics* **14**, 427 (2013).
 123. Cabral, F. J., Fotoran, W. L. & Wunderlich, G. Dynamic Activation and Repression of the *Plasmodium falciparum* rif Gene Family and Their Relation to Chromatin Modification. *PLoS One* **7**, e29881 (2012).
 124. Winter, G. *et al.* SURFIN is a polymorphic antigen expressed on *Plasmodium falciparum* merozoites and infected erythrocytes. *J. Exp. Med.* **201**, 1853–63 (2005).
 125. Mphande, F. A. *et al.* SURFIN4.1, a schizont-merozoite associated protein in the SURFIN family of *Plasmodium falciparum*. *Malar. J.* **7**, 116 (2008).
 126. Watermeyer, J. M. *et al.* A spiral scaffold underlies cytoadherent knobs in *Plasmodium falciparum*-infected erythrocytes. *Blood* **127**, 343–351 (2016).
 127. Gitaka, J. N. *et al.* Selections, frameshift mutations, and copy number variation detected on the surf 4.1 gene in the western Kenyan *Plasmodium falciparum* population. *Malar. J.* **16**, 98 (2017).
 128. Quintana, M. del P. *et al.* Antibodies in children with malaria to PfEMP1, RIFIN and SURFIN expressed at the *Plasmodium falciparum* parasitized red blood cell surface. *Sci. Rep.* **8**, 3262 (2018).
 129. Joannin, N. Antigenic Variation in *Plasmodium Falciparum*: Understanding the Rifin Protein Family. *Diss.Kib.Ki.Se* (2010).
 130. Dzikowski, R. *et al.* Mechanisms underlying mutually exclusive expression of virulence genes by malaria parasites. *EMBO Rep.* **8**, 959–965 (2007).
 131. Roberts, D. J., Biggs, B.-A., Brown, G. & Newbold, C. I. Protection, pathogenesis and phenotypic plasticity in *Plasmodium falciparum* malaria. *Parasitol. Today* **9**, 281–286 (1993).
 132. Dzikowski, R. & Deitsch, K. W. Active Transcription is Required for Maintenance of Epigenetic Memory in the Malaria Parasite *Plasmodium falciparum*. *J. Mol. Biol.* **382**, 288–297 (2008).
 133. Scherf, A., Lopez-Rubio, J. J. & Riviere, L. Antigenic Variation in *Plasmodium falciparum*. *Annu. Rev. Microbiol.* **62**, 445–470 (2008).
 134. Voss, T. S. *et al.* A var gene promoter controls allelic exclusion of virulence genes in *Plasmodium falciparum* malaria. *Nature* **439**, 1004–1008 (2006).
 135. Ralph, S. A., Scheidig-Benatar, C. & Scherf, A. Antigenic variation in *Plasmodium falciparum* is associated with movement of var loci between subnuclear locations. *Proc. Natl. Acad. Sci.* **102**, 5414–5419 (2005).
 136. Duraisingh, M. T. *et al.* Heterochromatin Silencing and Locus Repositioning Linked to Regulation of Virulence Genes in *Plasmodium falciparum*. *Cell* **121**, 13–24 (2005).
 137. Proellocks, N. I. *et al.* A lysine-rich membrane-associated PHISTb protein involved in alteration of the cytoadhesive properties of *Plasmodium falciparum*-infected red blood cells. *FASEB J.* **28**, 3103–3113 (2014).
 138. Goel, S. *et al.* Targeted disruption of a ring-infected erythrocyte surface antigen (RESA)-like export protein gene in *Plasmodium falciparum* confers stable chondroitin 4-sulfate cytoadherence capacity. *J. Biol. Chem.* **289**, 34408–34421 (2014).
 139. Subramani, R. *et al.* *Plasmodium falciparum*-Infected Erythrocyte Knob Density Is Linked to the PfEMP1 Variant Expressed. *MBio* **6**, 1–7 (2015).
 140. Lalchandama, K. *Plasmodium falciparum* erythrocyte membrane protein 1. *WikiJournal Med.* **4**, 1–8 (2017).
 141. Crabb, B. S. *et al.* Targeted gene disruption shows that knobs enable malaria-infected red cells to cytoadhere under physiological shear stress. *Cell* **89**, 287–296 (1997).
 142. Tilly, A. K. *et al.* Type of in vitro cultivation influences cytoadhesion, knob structure, protein localization and transcriptome profile of *Plasmodium falciparum*. *Sci. Rep.* **5**, 1–13 (2015).
 143. Gritzmacher, C. A. & Reese, R. T. Reversal of knob formation on *Plasmodium falciparum*-infected erythrocytes. *Science (80-.)*. **226**, 65–67 (1984).
 144. Arman, M., Adams, Y., Lindergard, G. & Rowe, J. A. A Method for Positive and Negative Selection of *Plasmodium falciparum* Platelet-Mediated Clumping Parasites and Investigation of the Role of CD36. *PLoS One* **8**, (2013).

145. Rask, T. S., Hansen, D. A., Theander, T. G., Pedersen, A. G. & Lavstsen, T. Plasmodium falciparum erythrocyte membrane protein 1 diversity in seven genomes - divide and conquer. *PLoS Comput. Biol.* **6**, (2010).
146. Esser, C. *et al.* Evidence of promiscuous endothelial binding by *Plasmodium falciparum* -infected erythrocytes. *Cell. Microbiol.* **16**, 701–708 (2014).
147. Robinson, B. A., Welch, T. L. & Smith, J. D. Widespread functional specialization of Plasmodium falciparum erythrocyte membrane protein 1 family members to bind CD36 analysed across a parasite genome. *Mol. Microbiol.* **47**, 1265–78 (2003).
148. Turner, G. D. *et al.* An immunohistochemical study of the pathology of fatal malaria. Evidence for widespread endothelial activation and a potential role for intercellular adhesion molecule-1 in cerebral sequestration. *Am. J. Pathol.* **145**, 1057–69 (1994).
149. Herricks, T., Avril, M., Janes, J., Smith, J. D. & Rathod, P. K. Clonal Variants of Plasmodium falciparum Exhibit a Narrow Range of Rolling Velocities to Host Receptor CD36 under Dynamic Flow Conditions. *Eukaryot. Cell* **12**, 1490–1498 (2013).
150. Hviid, L. & Salanti, A. VAR2CSA and protective immunity against pregnancy-associated Plasmodium falciparum malaria. *Parasitology* **134**, 1871–1876 (2007).
151. Fried, M. & Duffy, P. E. Adherence of Plasmodium falciparum to chondroitin sulfate A in the human placenta. *Science* **272**, 1502–4 (1996).
152. Reeder, J. C. *et al.* The adhesion of Plasmodium falciparum-infected erythrocytes to chondroitin sulfate A is mediated by P. falciparum erythrocyte membrane protein 1. *Proc. Natl. Acad. Sci. U. S. A.* **96**, 5198–202 (1999).
153. Clausen, T. M. *et al.* Structural and Functional Insight into How the Plasmodium falciparum VAR2CSA Protein Mediates Binding to Chondroitin Sulfate A in Placental Malaria. *J. Biol. Chem.* **287**, 23332–23345 (2012).
154. Armah, H. *et al.* Cytokines and adhesion molecules expression in the brain in human cerebral malaria. *Int. J. Environ. Res. Public Health* **2**, 123–131 (2005).
155. Lennartz, F. *et al.* Mapping the Binding Site of a Cross-Reactive Plasmodium falciparum PfEMP1 Monoclonal Antibody Inhibitory of ICAM-1 Binding. *J. Immunol.* **195**, 3273–83 (2015).
156. Ochola, L. B. *et al.* Specific Receptor Usage in Plasmodium falciparum Cytoadherence Is Associated with Disease Outcome. *PLoS One* **6**, e14741 (2011).
157. Ockenhouse, C. F., Klotz, F. W., Tandon, N. N. & Jamieson, G. A. Sequestrin, a CD36 recognition protein on Plasmodium falciparum malaria-infected erythrocytes identified by anti-idiotypic antibodies. *Proc. Natl. Acad. Sci. U. S. A.* **88**, 3175–9 (1991).
158. Ockenhouse, C. F. *et al.* Human vascular endothelial cell adhesion receptors for Plasmodium falciparum-infected erythrocytes: roles for endothelial leukocyte adhesion molecule 1 and vascular cell adhesion molecule 1. *J. Exp. Med.* **176**, 1183–9 (1992).
159. Silamut, K. *et al.* A Quantitative Analysis of the Microvascular Sequestration of Malaria Parasites in the Human Brain. *Am. J. Pathol.* **155**, 395–410 (1999).
160. Newbold, C. *et al.* Receptor-specific adhesion and clinical disease in Plasmodium falciparum. *Am. J. Trop. Med. Hyg.* **57**, 389–98 (1997).
161. Wahlgren, M. & Perlmann, P. *Malaria: molecular and clinical aspects.* (Harwood Academic, 1999).
162. Bain, B. J. & Gupta, R. *A-Z of haematology.* (Blackwell Pub, 2003).
163. Satchwell, T. J. Erythrocyte invasion receptors for Plasmodium falciparum: New and old. *Transfus. Med.* **26**, 77–88 (2016).
164. Koch, M. & Baum, J. The mechanics of malaria parasite invasion of the human erythrocyte - towards a reassessment of the host cell contribution. *Cell. Microbiol.* **18**, 319–29 (2016).
165. Kanjee, U. *et al.* CRISPR/Cas9 knockouts reveal genetic interaction between strain-transcendent erythrocyte determinants of Plasmodium falciparum invasion. *Proc. Natl. Acad. Sci.* **114**, E9356–E9365 (2017).
166. Pouvelle, B. *et al.* Neural Cell Adhesion Molecule, a New Cytoadhesion Receptor for Plasmodium falciparum-Infected Erythrocytes Capable of Aggregation. *Infect. Immun.* **75**, 3516–3522 (2007).
167. Keelan, E. T. *et al.* Imaging vascular endothelial activation: an approach using radiolabeled monoclonal antibodies against the endothelial cell adhesion molecule E-selectin. *J. Nucl. Med.* **35**, 276–81 (1994).

168. Kansas, G. S. Selectins and their ligands: current concepts and controversies. *Blood* **88**, 3259–87 (1996).
169. Yeo, T. W. *et al.* Greater Endothelial Activation, Weibel-Palade Body Release and Host Inflammatory Response to *Plasmodium vivax*, Compared with *Plasmodium falciparum* : A Prospective Study in Papua, Indonesia. *J. Infect. Dis.* **202**, 109–112 (2010).
170. Schofield, L. *et al.* Glycosylphosphatidylinositol toxin of *Plasmodium* up-regulates intercellular adhesion molecule-1, vascular cell adhesion molecule-1, and E-selectin expression in vascular endothelial cells and increases leukocyte and parasite cytoadherence via tyrosine kinase-dependent signal transduction. *J. Immunol.* **156**, 1886–96 (1996).
171. Perrin, A. J., Bartholdson, S. J. & Wright, G. J. P-selectin is a host receptor for *Plasmodium* MSP7 ligands. *Malar. J.* **14**, 238 (2015).
172. Ho, M. *et al.* Characterization of *Plasmodium falciparum*-infected erythrocyte and P-selectin interaction under flow conditions. *Blood* **91**, 4803–9 (1998).
173. Senczuk, A. M., Reeder, J. C., Kosmala, M. M. & Ho, M. *Plasmodium falciparum* erythrocyte membrane protein 1 functions as a ligand for P-selectin. *Blood* **98**, 3132–5 (2001).
174. Combès, V. *et al.* Pathogenic Role of P-Selectin in Experimental Cerebral Malaria: Importance of the Endothelial Compartment. *Am. J. Pathol.* **164**, 781–786 (2004).
175. Metwally, N. G. *et al.* Characterisation of *Plasmodium falciparum* populations selected on the human endothelial receptors P-selectin, E-selectin, CD9 and CD151. *Sci. Rep.* **7**, 4069 (2017).
176. Matsui, N. M. *et al.* *P-selectin mediates the adhesion of sickle erythrocytes to the endothelium.* (2001).
177. Levy, S., Todd, S. C. & Maecker, H. T. CD81 (TAPA-1): A MOLECULE INVOLVED IN SIGNAL TRANSDUCTION AND CELL ADHESION IN THE IMMUNE SYSTEM. *Annu. Rev. Immunol.* **16**, 89–109 (1998).
178. Yeung, L., Hickey, M. J. & Wright, M. D. The many and varied roles of tetraspanins in immune cell recruitment and migration. *Frontiers in Immunology* **9**, 1644 (2018).
179. Sheng, K.-C. *et al.* Tetraspanins CD37 and CD151 differentially regulate Ag presentation and T-cell co-stimulation by DC. *Eur. J. Immunol.* **39**, 50–55 (2009).
180. Wright, M. D. *et al.* Characterization of mice lacking the tetraspanin superfamily member CD151. *Mol. Cell. Biol.* **24**, 5978–88 (2004).
181. Charrin, S., Jouannet, S., Boucheix, C. & Rubinstein, E. Tetraspanins at a glance. *J. Cell Sci.* **127**, 3641–3648 (2014).
182. Chambrion, C. & le Naour, F. The tetraspanins CD9 and CD81 regulate CD9P1- induced effects on cell migration. *PLoS One* **5**, e11219 (2010).
183. Gartlan, K. H. *et al.* A Complementary Role for the Tetraspanins CD37 and Tssc6 in Cellular Immunity. *J. Immunol.* **185**, 3158–3166 (2010).
184. Silvie, O. *et al.* Expression of human CD81 differently affects host cell susceptibility to malaria sporozoites depending on the *Plasmodium* species. *Cell. Microbiol.* **8**, 1134–1146 (2006).
185. Foquet, L. *et al.* Anti-CD81 but not anti-SR-BI blocks *Plasmodium falciparum* liver infection in a humanized mouse model. *J. Antimicrob. Chemother.* **70**, 1784–7 (2015).
186. Tham, T. N. *et al.* Tetraspanin CD81 is required for *Listeria monocytogenes* invasion. *Infect. Immun.* **78**, 204–209 (2010).
187. Gwamaka, M., Fried, M., Domingo, G. & Duffy, P. E. Early and extensive CD55 loss from red blood cells supports a causal role in malarial anaemia. *Malar. J.* **10**, 386 (2011).
188. Egan, E. S. *et al.* A forward genetic screen identifies erythrocyte CD55 as essential for *Plasmodium falciparum* invasion. *Science (80-)*. **348**, 711–714 (2015).
189. Schuldt, K. *et al.* Lack of Association of CD55 Receptor Genetic Variants and Severe Malaria in Ghanaian Children. *G3ɪmp;#x27; Genes | Genomes | Genetics* **7**, 859–864 (2017).
190. Ozen, A. *et al.* CD55 Deficiency, Early-Onset Protein-Losing Enteropathy, and Thrombosis. *N. Engl. J. Med.* **377**, 52–61 (2017).
191. Coetzer, T. Deadly Malaria Parasites Hijack CD55 to Invad Erythrocytes. **12**, (2015).
192. Koch, M. & Baum, J. The mechanics of malaria parasite invasion of the human erythrocyte - towards a reassessment of the host cell contribution. *Cell. Microbiol.* **18**,

- 319–329 (2016).
193. Satchwell, T. J. Erythrocyte invasion receptors for *Plasmodium falciparum* : new and old. *Transfus. Med.* **26**, 77–88 (2016).
 194. Begley, D. J. ABC transporters and the blood-brain barrier. *Curr. Pharm. Des.* **10**, 1295–312 (2004).
 195. van Assema, D. M. *et al.* Blood-brain barrier P-glycoprotein function in healthy subjects and Alzheimer's disease patients: effect of polymorphisms in the ABCB1 gene. *EJNMMI Res.* **2**, 57 (2012).
 196. Jungsuwadee, P. & Vore, M. E. Efflux Transporters. *Compr. Toxicol.* 557–601 (2010). doi:10.1016/B978-0-08-046884-6.00426-7
 197. Thévenon, A. D. *et al.* Elevated levels of soluble TNF receptors 1 and 2 correlate with *Plasmodium falciparum* parasitemia in pregnant women: potential markers for malaria-associated inflammation. *J. Immunol.* **185**, 7115–22 (2010).
 198. Gimenez, F., De Lagerie, S. B., Fernandez, C., Pino, P. & Mazier, D. Tumor necrosis factor α in the pathogenesis of cerebral malaria. *Cell. Mol. Life Sci.* **60**, 1623–1635 (2003).
 199. Lucas, R. *et al.* Both TNF receptors are required for direct TNF-mediated cytotoxicity in microvascular endothelial cells. *Eur. J. Immunol.* **28**, 3577–86 (1998).
 200. Lucas, R. *et al.* TNF receptors in the microvascular pathology of acute respiratory distress syndrome and cerebral malaria. *J. Leukoc. Biol.* **61**, 551–558 (1997).
 201. Piguet, P. F., Kan, C. D. & Vesin, C. Role of the tumor necrosis factor receptor 2 (TNFR2) in cerebral malaria in mice. *Lab. Investig.* **82**, 1155–1166 (2002).
 202. Trager, W. & Jensen, J. B. Human malaria parasites in continuous culture. *Science* **193**, 673–5 (1976).
 203. Marmur, J. & Doty, P. Determination of the base composition of deoxyribonucleic acid from its thermal denaturation temperature. *J. Mol. Biol.* **5**, 109–118 (1962).
 204. Li, B. & Dewey, C. N. {{RSEM}}: Accurate Transcript Quantification from {{RNA}}-{{Seq}} Data with or without a Reference Genome. *BMC Bioinformatics* **12**, 323 (2011).
 205. Langmead, B. & Salzberg, S. L. Fast gapped-read alignment with Bowtie 2. *Nat. Methods* **9**, 357–9 (2012).
 206. Anders, S. & Huber, W. Differential expression analysis for sequence count data. *Genome Biol.* **11**, R106 (2010).
 207. Wong, D. & Dorovini-Zis, K. Upregulation of intercellular adhesion molecule-1 (ICAM-1) expression in primary cultures of human brain microvessel endothelial cells by cytokines and lipopolysaccharide. *J. Neuroimmunol.* **39**, 11–21 (1992).
 208. Szmítka, P. E. *et al.* New Markers of Inflammation and Endothelial Cell Activation. *Circulation* **108**, 1917–1923 (2003).
 209. Lavstsen, T. *et al.* *Plasmodium falciparum* erythrocyte membrane protein 1 domain cassettes 8 and 13 are associated with severe malaria in children. *Proc. Natl. Acad. Sci.* **109**, E1791–E1800 (2012).
 210. Turner, L. *et al.* Severe malaria is associated with parasite binding to endothelial protein C receptor. *Nature* (2013). doi:10.1038/nature12216
 211. Welty-Wolf, K. E. *et al.* Antibody to intercellular adhesion molecule 1 (CD54) decreases survival and not lung injury in baboons with sepsis. *Am. J. Respir. Crit. Care Med.* **163**, 665–673 (2001).
 212. Armah, H. *et al.* Cytokines and adhesion molecules expression in the brain in human cerebral malaria. *Int. J. Environ. Res. Public Health* **2**, 123–31 (2005).
 213. The Human Protein Atlas Project. The Human Protein Atlas. (2019). Available at: <https://www.proteinatlas.org>.
 214. Mackay, C. R. *et al.* Expression and modulation of CD44 variant isoforms in humans. *J. Cell Biol.* **124**, 71–82 (1994).
 215. Ghorbal, M. *et al.* Genome editing in the human malaria parasite *Plasmodium falciparum* using the CRISPR-Cas9 system. *Nat. Biotechnol.* **32**, 819–821 (2014).
 216. Andrews, K. T., Adams, Y., Viebig, N. K., Lanzer, M. & Schwartz-Albiez, R. Adherence of *Plasmodium falciparum* infected erythrocytes to CHO-745 cells and inhibition of binding by protein α in the presence of human serum. *Int. J. Parasitol.* **35**, 1127–1134 (2005).
 217. Metwally, N. Analyses of the transcriptome profiles of *Plasmodium falciparum* infected erythrocytes selected for binding to the human endothelial receptors (ICAM-1, P-selectin, E-selectin, CD9 and CD151). (2016).

218. Pouvelle, B., Buffet, P. A., Lépolard, C., Scherf, A. & Gysin, J. Cytoadhesion of Plasmodium falciparum ring-stage-infected erythrocytes. *Nat. Med.* **6**, 1264–1268 (2000).
219. Andrews, K. T. *et al.* A human schwannoma cell line supports the in vitro adhesion of Plasmodium falciparum infected erythrocytes to chondroitin-4-sulfate. *Parasitol. Res.* **89**, 188–93 (2003).
220. Hayflick, L. & Moorhead, P. S. The serial cultivation of human diploid cell strains. *Exp. Cell Res.* **25**, 585–621 (1961).
221. Campisi, J. & d'Adda di Fagagna, F. Cellular senescence: when bad things happen to good cells. *Nat. Rev. Mol. Cell Biol.* **8**, 729–740 (2007).
222. Mun, G. I. & Boo, Y. C. Identification of CD44 as a senescence-induced cell adhesion gene responsible for the enhanced monocyte recruitment to senescent endothelial cells. *Am. J. Physiol. Circ. Physiol.* **298**, H2102–H2111 (2010).
223. Wei, Y.-Y. C. *et al.* Proteomics analysis of chinese hamster ovary cells undergoing apoptosis during prolonged cultivation. *Cytotechnology* **63**, 663–77 (2011).
224. Vishwanathan, N. *et al.* Global insights into the Chinese hamster and CHO cell transcriptomes. *Biotechnol. Bioeng.* **112**, 965–976 (2015).
225. Hogg, K. *et al.* Quantification of proteins by flow cytometry: Quantification of human hepatic transporter P-gp and OATP1B1 using flow cytometry and mass spectrometry. *Methods* **82**, 38–46 (2015).
226. Smith, J. D. *et al.* Analysis of adhesive domains from the A4VAR Plasmodium falciparum erythrocyte membrane protein-1 identifies a CD36 binding domain. *Mol. Biochem. Parasitol.* **97**, 133–148 (1998).
227. Visser, C. W., Kamperman, T., Karbaat, L. P., Lohse, D. & Karperien, M. In-air microfluidics enables rapid fabrication of emulsions, suspensions, and 3D modular (bio)materials. *Sci. Adv.* **4**, 1–9 (2018).
228. Mandt, D. *et al.* Fabrication of biomimetic placental barrier structures within a microfluidic device utilizing two-photon polymerization. Fabrication of biomimetic placental barrier structures within a microfluidic device utilizing two-photon polymerization. *Int. J. Bioprinting* **4**, (2018).
229. Viebig, N. K. *et al.* Direct Activation of Human Endothelial Cells by Plasmodium falciparum-Infected Erythrocytes. *Society* **73**, 3271–3277 (2005).
230. Seon, B. *et al.* Cytokine and adhesion molecule expression in primary human endothelial cells stimulated with fever-range hyperthermia. *Int. J. Hyperth.* **18**, 534–551 (2003).
231. Falk, T. *et al.* U-Net: deep learning for cell counting, detection, and morphometry. *Nat. Methods* **16**, 67–70 (2018).
232. VanWye, J. D. & Halder, K. Expression of green fluorescent protein in Plasmodium falciparum. *Mem.Inst.Oswaldo Cruz (Rio Janeiro)* **92**, 163 (1997).
233. Cooke, B., Coppel, R. & Wahlgren, M. Falciparum Malaria: Sticking up, Standing out and Out-standing. *Parasitol. Today* **16**, 416–420 (2000).
234. Gaglia, J. L. *et al.* Characterization of Endogenous Chinese Hamster Ovary Cell Surface Molecules That Mediate T Cell Costimulation. *Cell. Immunol.* **213**, 83–93 (2002).
235. Almelli, T. *et al.* Cytoadherence phenotype of Plasmodium falciparum-infected erythrocytes is associated with specific pfemp-1 expression in parasites from children with cerebral malaria. *Malar. J.* **13**, 1–9 (2014).
236. Reeder, J. C., Hodder, A. N., Beeson, J. G. & Brown, G. V. Identification of Glycosaminoglycan Binding Domains in Plasmodium falciparum Erythrocyte Membrane Protein 1 of a Chondroitin Sulfate A-Adherent Parasite Identification of Glycosaminoglycan Binding Domains in Plasmodium falciparum Erythrocyte Membrane Prot. **68**, 1–5 (2000).
237. Scherf, A. *et al.* Antigenic variation in malaria: In situ switching, relaxed and mutually exclusive transcription of var genes during intra-erythrocytic development in Plasmodium falciparum. *EMBO J.* **17**, 5418–5426 (1998).
238. Jurzynski, C., Gysin, J. & Pouvelle, B. CD44, a signal receptor for the inhibition of the cytoadhesion of CD36-binding Plasmodium falciparum-infected erythrocytes by CSA-binding infected erythrocytes. *Microbes Infect.* **9**, 1463–1470 (2007).
239. Frank, M. *et al.* Strict Pairing of var Promoters and Introns Is Required for var Gene Silencing in the Malaria Parasite Plasmodium falciparum. *J. Biol. Chem.* **281**, 9942–9952

- (2006).
240. Bachmann, A. *et al.* Highly co-ordinated var gene expression and switching in clinical *Plasmodium falciparum* isolates from non-immune malaria patients. *Cell. Microbiol.* **13**, 1397–409 (2011).
 241. Weber, J. L. Analysis of sequences from the extremely A + T-rich genome of *Plasmodium falciparum*. *Gene* **52**, 103–109 (1987).
 242. Hamilton, W. L. *et al.* Extreme mutation bias and high AT content in *Plasmodium falciparum*. *Nucleic Acids Res.* **45**, 1889–1901 (2017).
 243. Lubiana, P. H. Charakterisierung der Interaktion zwischen *Plasmodium* infizierten Erythrozyten und humanen Endothelrezeptoren. (2017).
 244. Marcello, L. & Barry, J. D. Analysis of the VSG gene silent archive in *Trypanosoma brucei* reveals that mosaic gene expression is prominent in antigenic variation and is favored by archive substructure. *Genome Res.* **17**, 1344–1352 (2007).
 245. Hsieh, F. L. *et al.* The structural basis for CD36 binding by the malaria parasite. *Nat. Commun.* **7**, 1–11 (2016).
 246. Smith, J. D. *et al.* Identification of a *Plasmodium falciparum* intercellular adhesion molecule-1 binding domain: A parasite adhesion trait implicated in cerebral malaria. *Proc. Natl. Acad. Sci.* **97**, 1766–1771 (2000).
 247. Tonkin-Hill, G. Q. *et al.* The *Plasmodium falciparum* transcriptome in severe malaria reveals altered expression of genes involved in important processes including surface antigen-encoding var genes. *PLoS Biology* **16**, (2018).
 248. Jespersen, J. S. *et al.* *Plasmodium falciparum* var genes expressed in children with severe malaria encode CIDRa1 domains. *EMBO Mol. Med.* **8**, 839–850 (2016).
 249. Avril, M., Brazier, A. J., Melcher, M., Sampath, S. & Smith, J. D. DC8 and DC13 var Genes Associated with Severe Malaria Bind Avidly to Diverse Endothelial Cells. *PLoS Pathog.* **9**, e1003430 (2013).
 250. Oakley, M. S. M. *et al.* Molecular factors and biochemical pathways induced by febrile temperature in intraerythrocytic *Plasmodium falciparum* parasites. *Infect. Immun.* **75**, 2012–2025 (2007).
 251. Bengtsson, A. *et al.* A Novel Domain Cassette Identifies *Plasmodium falciparum* PfEMP1 Proteins Binding ICAM-1 and Is a Target of Cross-Reactive, Adhesion-Inhibitory Antibodies. *J. Immunol.* **190**, 240–249 (2012).
 252. Argy, N. *et al.* Preferential expression of domain cassettes 4, 8 and 13 of *Plasmodium falciparum* erythrocyte membrane protein 1 in severe malaria imported in France. *Clin. Microbiol. Infect.* **23**, 211.e1–211.e4 (2016).
 253. Zhang, Y. *et al.* The var3 genes of *Plasmodium falciparum* 3D7 strain are differentially expressed in infected erythrocytes. *Parasite* **21**, 19 (2014).
 254. Magallón-Tejada, A. *et al.* Cytoadhesion to gC1qR through *Plasmodium falciparum* Erythrocyte Membrane Protein 1 in Severe Malaria. *PLOS Pathog.* **12**, e1006011 (2016).
 255. Duffy, M. F. *et al.* Differences in PfEMP1s recognized by antibodies from patients with uncomplicated or severe malaria. *Malar. J.* **15**, (2016).
 256. Rottmann, M. *et al.* Differential Expression of var Gene Groups Is Associated with Morbidity Caused by *Plasmodium falciparum* Infection in Tanzanian Children. *Infect. Immun.* **74**, 3904–3911 (2006).
 257. Wang, C. W. *et al.* Evidence for in vitro and in vivo expression of the conserved VAR3 (type 3) *plasmodium falciparum* erythrocyte membrane protein 1. *Malar. J.* **11**, (2012).
 258. Bull, P. C. *et al.* *Plasmodium falciparum* Variant Surface Antigen Expression Patterns during Malaria. *PLoS Pathog.* **1**, e26 (2005).
 259. Kaestli, M. *et al.* Virulence of Malaria Is Associated with Differential Expression of *Plasmodium falciparum* var Gene Subgroups in a Case-Control Study. *J. Infect. Dis.* **193**, 1567–1574 (2006).
 260. Kyriacou, H. M. *et al.* Differential var gene transcription in *Plasmodium falciparum* isolates from patients with cerebral malaria compared to hyperparasitaemia. *Mol. Biochem. Parasitol.* **150**, 211–218 (2006).
 261. Long, G. H., Chan, B. H. K., Allen, J. E., Read, A. F. & Graham, A. L. Blockade of TNF receptor 1 reduces disease severity but increases parasite transmission during *Plasmodium chabaudi chabaudi* infection. *Int. J. Parasitol.* **38**, 1073–1081 (2008).
 262. Bachmann, A. *et al.* A comparative study of the localization and membrane topology

- of members of the RIFIN, STEVOR and PfMC-2TM protein families in Plasmodium falciparum-infected erythrocytes. *Malar. J.* **14**, 1–18 (2015).
263. Florens, L. *et al.* A proteomic view of the Plasmodium falciparum life cycle. *Nature* **419**, 520–526 (2002).
264. Douki, J.-B. L. *et al.* Adhesion of normal and Plasmodium falciparum ring-infected erythrocytes to endothelial cells and the placenta involves the rhoptry-derived ring surface protein-2. *Blood* **101**, 5025–5032 (2003).
265. Scholz, J. A. M. *Genexpression, Lokalisation und funktionelle Untersuchung der variablen Oberflächenproteinfamilie STEVOR des Malariaerregers Plasmodium falciparum (Welch, 1897).* (2017).
266. Lavstsen, T. *et al.* Expression of Plasmodium falciparum erythrocyte membrane protein 1 in experimentally infected humans. *Malar. J.* **4**, 1–9 (2005).
267. Subudhi, A. K. *et al.* A cross strain Plasmodium falciparum microarray optimized for the transcriptome analysis of Plasmodium falciparum patient derived isolates. *Genomics Data* **9**, 118–125 (2016).
268. Predehl, S. Funktionsanalysen der PfEMP1 Proteinfamilie von Plasmodium falciparum (Welch, 1897). (2010).
269. Biggs, B. A., Kemp, D. J. & Brown, G. V. Subtelomeric chromosome deletions in field isolates of Plasmodium falciparum and their relationship to loss of cytoadherence in vitro. *Proc. Natl. Acad. Sci. U. S. A.* **86**, 2428–32 (1989).
270. Spielmann, T. *et al.* Selection linked integration (SLI) for endogenous gene tagging and knock sideways in Plasmodium falciparum parasites. *Protoc. Exch.* (2017). doi:10.1038/protex.2017.022
271. Birnbaum, J. *et al.* A genetic system to study Plasmodium falciparum protein function. *Nat. Methods* **14**, 450–456 (2017).

ABBREVIATIONS

| | |
|-------------------|--|
| °C | grad Celsius |
| A, T, G, C | adenine, thymine, guanine, cytosine |
| AM | asymptomatic malaria |
| APC | allophycocyanin |
| ATCC | American Type Culture Collection |
| ATP | adenosintriphosphate |
| ATS | acidic terminal segment |
| BB | blood bank |
| BF | bright field |
| BNITM | Bernhard Nocht Institute for Tropical Medicine |
| bp | base pairs |
| BSA | bovine serum albumin |
| CD | cluster of differentiation |
| CHO | Chinese Hamster Ovary |
| CIDR | cysteine-rich interdomain region |
| CLAG | cytoadherence-linked asexual protein |
| CM | cerebral malaria |
| CO ₂ | carbon dioxide |
| CR1 | complement receptor 1 |
| CSA | chondroitin sulphate A |
| DBL | Duffy binding like |
| DC | domain cassette |
| dH ₂ O | distilled water |
| DNA | deoxyribonucleic acid |
| e.g. | for example |
| EPON | epoxy resin |
| ER | endoplasmic reticulum |
| FACS | fluorescent activated cell sorting |
| fikk | serine/threonine kinases |
| FITC | fluorescein isothiocyanate |
| GFP | green fluorescence protein |
| GPI | glycosyl-phosphatidyl-inositol |
| GYP | glycophorin |
| h | hours |
| H ₂ O | water |
| HBEC | human brain endothelial cell |
| HCAM | homing cell adhesion molecule |
| HCV | hepatitis C virus |
| hpi | hours post infection |
| HRH1 | histamine receptor H1 |
| HS | human serum |
| HSP | heat shock proteins |
| ICAM | Intracellular adhesion molecule |

| | |
|-----------------|---|
| IE | infected erythrocytes |
| iFCS | inactivated fetal calf serum |
| Kb | kilo base |
| kDa | kilo Dalton |
| L | liter |
| LB | lysogeny broth |
| MAHRP1 | membrane associated histidine rich protein 1 |
| MC | Maurer's Clefts |
| MCS | multiple cloning site |
| MDR1 | multidrug receptor 1 |
| MESA | mature parasite-infected erythrocyte surface antigen |
| MHC | major histocompatibility complex |
| min | minutes |
| ml | milliliter |
| mM | millimolar |
| MSP | merozoite surface protein |
| N ₂ | nitrogen |
| NCAM | neural cell adhesion molecule |
| NGS | next generation sequencing |
| nm | nanometer |
| NPP | new permeation pathways |
| NTS | N-terminal segment |
| O ₂ | oxygen |
| <i>P.</i> | <i>Plasmodium</i> |
| PAM | pregnancy associated malaria |
| PBS | phosphate-buffered saline |
| PCR | polymerase chain reaction |
| PE | phycoerythrin |
| PECAM | platelet endothelial cell adhesion molecule 1 |
| PEXEL | <i>Plasmodium</i> export element |
| <i>PfEMP</i> | <i>Plasmodium falciparum</i> erythrocyte membrane protein |
| <i>Pfmc-2tm</i> | <i>P. falciparum</i> Maurer's cleft – two transmembrane domains |
| PHIST | <i>Plasmodium</i> helical interspersed subtelomeric |
| PNEP | PEXEL negative exported proteins |
| PPM | parasite plasma membrane |
| PTA | protein transport aggregate |
| PV | parasitophorous vacuole |
| PVM | parasitophorous vacuole membrane |
| RESA | ring-infected erythrocyte surface antigen |
| REX1 | ring exported protein 1 |
| RhAG | rhesus antigen |
| RIFIN | repetitive interspersed family |
| RIN | RNA integrity number |
| RNA | ribonucleic acid |
| RT | room temperature |

| | |
|--------------|--|
| s | soluble |
| SBP1 | skeleton binding protein 1 |
| sec | seconds |
| SM | severe malaria |
| <i>spp.</i> | species |
| STEVOR | subtelomeric variant open reading frame |
| SURF | surface-associated interspersed proteins |
| TEM | Transmission electron microscopy |
| TLR | Toll-like receptor |
| TM | transmembrane |
| T_m | melting temperature |
| TNF α | tumor necrosis factor alpha |
| TNFR | tumor necrosis factor 1 |
| U | units |
| UKE | University Hospital Eppendorf |
| UM | uncomplicated malaria |
| ups | upstream |
| V | variable region |
| <i>var</i> | variant surface antigens |
| VCAM | vascular cell adhesion molecule 1 |
| VE-Cadherin | vascular endothelial cadherin |
| VSA | variant surface antigens |
| VTS | vacuolar transport signal |
| w/v | weight/volume |
| WT | wild type |
| x g | times gravity |
| μ | micro |

APPENDIX

Annex I

Comprehensive list of NGS analysis

Anex 1. Comprehensive list of NGS analysis.

| mean ST | mean GFP | mean MDR1 | mean TNFR1 | mean TNFR2 | mean CD37 | mean CD55 | mean CD81 | name | var description |
|--------------|----------|-----------|------------|------------|-----------|-----------|-----------|---------|---|
| PHT_0213200 | 20.69 | 17.49 | 36.16 | 21.29 | 50.35 | 16.85 | 24.89 | 19.05 | 10 kDa chaperonin |
| PHT_0204000 | 874.80 | 1413.06 | 1362.85 | 1871.85 | 1566.22 | 1935.56 | 1957.74 | 4147.84 | 18S ribosomal RNA |
| PHT_0307800 | 1598.97 | 1270.48 | 1038.90 | 2184.59 | 1050.12 | 3075.17 | 1559.84 | 3207.96 | 18S ribosomal RNA |
| PHT_0304900 | 46.55 | 70.21 | 44.90 | 46.39 | 38.08 | 43.46 | 70.21 | 100.84 | 2-oxalovalerate dehydrogenase subunit beta, mitochondrial, putative |
| PHT_0214500 | 162.15 | 342.77 | 311.36 | 254.83 | 372.78 | 180.22 | 192.84 | 235.88 | 20 kDa chaperonin |
| PHT_0107600 | 635.15 | 1044.64 | 1298.14 | 1082.57 | 1349.88 | 752.77 | 959.04 | 997.89 | 26S proteasome regulatory subunit RPNS3, putative |
| PHT_0205000 | 1550.08 | 1815.30 | 2808.61 | 3694.43 | 2168.86 | 4248.58 | 3603.14 | 9053.78 | 28S ribosomal RNA |
| PHT_0214000 | 262.21 | 318.80 | 362.17 | 468.45 | 367.93 | 568.50 | 533.71 | 1154.90 | 28S ribosomal RNA |
| PHT_0307900 | 489.96 | 932.19 | 413.29 | 510.29 | 525.77 | 675.95 | 487.91 | 1540.93 | 28S ribosomal RNA |
| PHT_0308000 | 937.71 | 570.67 | 975.15 | 1873.36 | 940.17 | 1554.00 | 1337.27 | 2685.42 | 28S ribosomal RNA |
| PHT_0101800 | 24.48 | 28.39 | 75.42 | 40.23 | 57.82 | 17.88 | 40.44 | 38.27 | 4-diphosphocytidyl-2-C-methyl-D-erythritol kinase, putative |
| PHT_0304600 | 127.88 | 54.90 | 110.04 | 102.97 | 114.14 | 219.76 | 186.30 | 317.34 | 50S ribosomal protein L28, apicoplast, putative |
| PHT_0215400 | 33.34 | 73.54 | 58.26 | 69.44 | 77.31 | 45.06 | 45.82 | 39.30 | 50S ribosomal protein L19, mitochondrial, putative |
| PHT_0207500 | 51.84 | 51.60 | 98.91 | 48.50 | 108.93 | 38.23 | 29.75 | 41.30 | 4-cysteine protein |
| PHT_0317000 | 97.86 | 79.09 | 117.77 | 116.47 | 186.51 | 99.54 | 131.34 | 235.72 | 60 kDa chaperonin |
| PHT_0215700 | 340.08 | 748.73 | 619.59 | 662.02 | 782.44 | 642.20 | 519.07 | 644.75 | AAA family ATPase, putative |
| PHT_0419800 | 213.92 | 345.29 | 479.44 | 361.11 | 588.89 | 192.97 | 318.47 | 429.06 | AAA family ATPase, putative |
| PHT_0201600 | 134.58 | 163.24 | 252.73 | 185.59 | 287.58 | 213.18 | 225.95 | 284.98 | ABC transporter B family member 4, putative |
| PHT_0203100 | 52.85 | 23 | 91.81 | 67.20 | 112.42 | 83.23 | 51.99 | 188.58 | ABC transporter F family member 1, putative |
| PHT_0217000 | 870.37 | 3890.88 | 1253.98 | 2350.14 | 1466.26 | 4649.45 | 4374.99 | 2533.78 | acyl-CoA synthetase |
| PHT_0216900 | 540.64 | 1000.42 | 772.80 | 923.02 | 756.80 | 1408.75 | 1008.69 | 1180.22 | acyl-CoA synthetase |
| PHT_0100400 | 32.07 | 15.08 | 66.97 | 16.93 | 84.44 | 22.46 | 30.65 | 73.76 | adaptor complex medium subunit family |
| PHT_0403300 | 353.61 | 574.67 | 836.66 | 672.82 | 843.47 | 517.59 | 725.62 | 574.10 | adenosuccinyl synthetase |
| PHT_0308300 | 294.73 | 139.39 | 243.90 | 265.79 | 213.41 | 477.25 | 473.83 | 835.38 | adenyl cyclase beta |
| PHT_0310300 | 158.37 | 43.19 | 106.90 | 84.73 | 78.70 | 148.11 | 209.54 | 396.93 | ADP-ribosylation factor, putative |
| PHT_0211700 | 48.35 | 79.24 | 67.83 | 83.93 | 107.64 | 33.55 | 45.22 | 83.66 | ADP/ATP carrier protein, putative |
| PHT_0212100 | 2737.72 | 3710.66 | 4450.78 | 3641.05 | 5810.61 | 2869.41 | 2829.42 | 2956.32 | ADP/ATP transporter on adenylate translocase |
| PHT_0303700 | 231.83 | 143.86 | 108.88 | 191.24 | 184.03 | 489.82 | 280.70 | 489.82 | alpha/beta holoenzyme membrane protein homologue |
| PHT_0110010 | 40.63 | 57.43 | 89.16 | 57.94 | 118.76 | 28.64 | 89.50 | 90.46 | alantoinase, putative |
| PHT_0105900 | 111.62 | 186.87 | 236.94 | 166.74 | 243.08 | 157.82 | 170.25 | 166.46 | alpha/beta hydrolase, putative |
| PHT_0303500 | 209.44 | 134.88 | 147.42 | 158.49 | 121.30 | 240.34 | 281.04 | 439.23 | alpha/beta hydrolase, putative |
| PHT_0219100 | 18.33 | 19.34 | 22.59 | 20.06 | 27.86 | 58.94 | 40.83 | 27.71 | alpha/beta hydrolase, putative |
| PHT_0201400 | 247.58 | 242.94 | 425.90 | 351.30 | 309.12 | 309.94 | 523.62 | 785.93 | alpha/beta hydrolase, putative |
| PHT_1200200 | 39.48 | 56.21 | 110.36 | 73.01 | 94.30 | 52.98 | 86.01 | 64.36 | aminodeoxychorismate lyase |
| PHT_0319800 | 26.54 | 7.84 | 11.59 | 16.06 | 10.34 | 43.71 | 25.01 | 61.12 | ankyrin-repeat protein, putative |
| PHT_0320300 | 74.46 | 50.16 | 40.65 | 65.24 | 41.85 | 97.95 | 113.59 | 167.70 | ankyrin, putative |
| PHT_0204500 | 77.80 | 91.03 | 134.98 | 120.13 | 598.45 | 79.55 | 38.78 | 410.66 | antigen 332, DBL-like protein |
| PHT_1240200 | 49.49 | 59.01 | 119.07 | 94.59 | 147.73 | 147.73 | 110.13 | 147.73 | AP-3 complex subunit beta, putative |
| PHT_0210800 | 87.39 | 168.36 | 149.35 | 147.25 | 199.85 | 139.54 | 106.72 | 94.02 | AP-3 complex subunit delta, putative |
| PHT_0318400 | 1788.34 | 362.28 | 1427.52 | 825.40 | 885.05 | 2306.04 | 2648.68 | 4329.16 | apical membrane antigen 1 |
| PHT_0303900 | 340.66 | 62.78 | 170.19 | 230.23 | 126.23 | 442.57 | 433.14 | 741.54 | apical sushi protein |
| PHT_0208500 | 184.70 | 274.64 | 289.99 | 308.88 | 375.09 | 187.69 | 212.56 | 267.00 | asparagine--RNA ligase |
| PHT_0311510 | 32.26 | 19.81 | 64.91 | 24.95 | 144.07 | 31.43 | 20.53 | 71.64 | asparaginase |
| PHT_0214800 | 480.86 | 883.14 | 857.60 | 804.60 | 1037.12 | 540.65 | 642.11 | 691.17 | aspartate carbonyltransferase |
| PHT_0206200 | 43.91 | 26.02 | 48.15 | 69.95 | 97.39 | 50.04 | 54.52 | 111.05 | ataxin-2-like protein, putative |
| PHT_0306500 | 39.90 | 43.44 | 42.45 | 31.93 | 35.16 | 24.45 | 19.36 | 80.57 | ATP dependent DEAD-box helicase, putative |
| PHT_0304800 | 37.52 | 13.06 | 21.52 | 26.05 | 32.76 | 67.63 | 38.26 | 81.72 | ATP-dependent helicase, putative |
| PHT_1150900 | 51.73 | 122.86 | 125.72 | 131.15 | 166.04 | 145.04 | 155.72 | 131.01 | ATP-dependent RNA helicase, putative |
| PHT_0303300 | 126.41 | 142.95 | 205.53 | 199.40 | 247.72 | 120.34 | 177.78 | 284.52 | ATP-dependent RNA helicase, putative |
| PHT_0317300 | 103.47 | 56.56 | 85.57 | 128.73 | 147.58 | 154.56 | 131.54 | 229.98 | ATP-dependent zinc metalloprotease FTSH 1 |
| PHT_0302400 | 811.55 | 350.26 | 742.80 | 641.37 | 523.11 | 1148.02 | 1592.10 | 2098.62 | autophagy-related protein 11, putative |
| PHT_0314000 | 387.41 | 68.63 | 276.67 | 229.06 | 171.71 | 473.39 | 683.22 | 1197.53 | autophagy-related protein 23, putative |
| PHT_0300100 | 39.09 | 45.77 | 45.99 | 38.74 | 45.23 | 64.26 | 64.26 | 45.99 | B-ITV1, C11-erythrocyte membrane protein 1, putative |
| PHT_0402700 | 34.64 | 67.27 | 111.39 | 92.57 | 105.27 | 69.33 | 140.56 | 84.52 | biotin carboxylase subunit of acetyl CoA carboxylase, putative |
| PHT_0104500 | 106.94 | 188.60 | 232.18 | 174.09 | 232.39 | 139.06 | 202.36 | 212.76 | BSD-domain protein, putative |
| PHT_0100900 | 25.71 | 12.01 | 53.36 | 37.13 | 66.04 | 23.15 | 33.25 | 34.37 | C-ITV5-erythrocyte membrane protein 1, PEMP1, putative |
| PHT_0206000 | 21.55 | 18.40 | 24.93 | 26.57 | 63.32 | 17.52 | 36.09 | 51.00 | calcium-dependent protein kinase, putative |
| PHT_0106400 | 383.18 | 762.39 | 770.74 | 755.04 | 893.51 | 475.34 | 679.11 | 489.82 | calmodulin binding protein, putative |
| PHT_0321500 | 96.43 | 154.77 | 145.31 | 128.86 | 154.65 | 101.53 | 149.35 | 211.68 | calponin homology domain-containing protein, putative |
| PHT_0208200 | 174.24 | 143.03 | 334.91 | 217.61 | 418.72 | 131.29 | 165.82 | 208.24 | calponin transcription factor P-ATF5 |
| PHT_0101010 | 43.44 | 33.61 | 113.10 | 68.27 | 152.08 | 42.24 | 108.34 | 97.95 | cdc2-related protein kinase 1 |
| PHT_0305700 | 87.82 | 25.57 | 62.93 | 70.92 | 38.07 | 117.02 | 134.90 | 200.20 | centrosomal protein CEP76, putative |
| PHT_0321100 | 115.72 | 18.93 | 83.90 | 67.43 | 162.04 | 144.17 | 149.71 | 32.14 | CEMP-dependent protein kinase |
| PHT_0314000 | 58.84 | 11.57 | 34.41 | 36.13 | 33.24 | 40.29 | 70.04 | 144.83 | CGMP-specific phosphodiesterase |
| PHT_0203200 | 77.36 | 100.84 | 108.16 | 126.63 | 226.36 | 55.13 | 92.33 | 175.58 | chaperone protein Ctp1B |
| PHT_0306800 | 3514.55 | 1308.73 | 3195.44 | 1690.27 | 1605.36 | 3384.56 | 5250.74 | 9030.87 | choline/ethanolaminephosphotransferase, putative |
| PHT_0209300 | 85.50 | 164.25 | 131.33 | 133.16 | 183.90 | 88.00 | 112.58 | 107.77 | citrate synthase-like protein, putative |
| PHT_0220400 | 27.83 | 126.73 | 49.77 | 42.78 | 50.60 | 37.74 | 64.30 | 48.26 | co-chaperone p23 |
| PHT_0900100 | 38.25 | 65.03 | 157.39 | 72.42 | 139.07 | 30.43 | 122.82 | 91.20 | conserved membrane protein, unknown function |
| PHT_0616500 | 357.78 | 826.98 | 958.26 | 700.55 | 944.76 | 730.82 | 891.05 | 824.72 | conserved Plasmodium membrane protein, unknown function |
| PHT_0207600 | 48.04 | 127.34 | 121.64 | 82.37 | 140.45 | 60.30 | 63.31 | 77.83 | conserved Plasmodium membrane protein, unknown function |
| PHT_1129900 | 81.40 | 148.15 | 179.00 | 157.03 | 253.63 | 82.78 | 109.99 | 221.77 | conserved Plasmodium membrane protein, unknown function |
| PHT_1129100 | 124.61 | 152.15 | 387.63 | 171.90 | 299.60 | 240.42 | 297.43 | 232.97 | conserved Plasmodium membrane protein, unknown function |
| PHT_0101400 | 803.82 | 1376.00 | 2478.58 | 1047.65 | 2807.62 | 292.24 | 795.74 | 1407.01 | conserved Plasmodium membrane protein, unknown function |
| PHT_0103400 | 67.15 | 121.05 | 185.10 | 102.05 | 195.01 | 83.30 | 108.18 | 77.39 | conserved Plasmodium membrane protein, unknown function |
| PHT_0103800 | 816.08 | 1466.88 | 1663.22 | 1342.86 | 1759.48 | 1115.50 | 1177.23 | 1314.22 | conserved Plasmodium membrane protein, unknown function |
| PHT_0103900 | 142.40 | 247.45 | 287.88 | 242.55 | 391.95 | 200.45 | 213.24 | 169.44 | conserved Plasmodium membrane protein, unknown function |
| PHT_0206100 | 501.79 | 903.73 | 995.99 | 823.46 | 1135.70 | 657.40 | 790.70 | 1063.40 | conserved Plasmodium membrane protein, unknown function |
| PHT_0213700 | 9.92 | 25.21 | 44.47 | 20.68 | 55.59 | 18.98 | 32.36 | 35.68 | conserved Plasmodium membrane protein, unknown function |
| PHT_0301000 | 38.23 | 27.80 | 11.99 | 36.19 | 21.18 | 62.14 | 34.60 | 81.12 | conserved Plasmodium membrane protein, unknown function |
| PHT_0308600 | 39.15 | 5.89 | 20.71 | 33.60 | 16.72 | 54.49 | 50.99 | 80.64 | conserved Plasmodium membrane protein, unknown function |
| PHT_0310100 | 26.20 | 2.77 | 11.36 | 17.47 | 10.38 | 43.87 | 25.75 | 64.31 | conserved Plasmodium membrane protein, unknown function |
| PHT_0310800 | 34.26 | 14.74 | 29.24 | 23.57 | 40.42 | 38.85 | 29.91 | 72.41 | conserved Plasmodium membrane protein, unknown function |
| PHT_0311200 | 100.87 | 84.42 | 129.59 | 138.04 | 149.59 | 101.96 | 122.66 | 219.19 | conserved Plasmodium membrane protein, unknown function |
| PHT_0311300 | 26.36 | 10.77 | 24.17 | 39.53 | 29.60 | 31.39 | 48.86 | 81.16 | conserved Plasmodium membrane protein, unknown function |
| PHT_0311900 | 998.52 | 1988.19 | 1102.08 | 1448.18 | 1801.52 | 692.08 | 1049.00 | 2849.04 | conserved Plasmodium membrane protein, unknown function |
| PHT_0312100 | 119.79 | 20.10 | 45.90 | 88.06 | 39.91 | 148.11 | 136.73 | 327.11 | conserved Plasmodium membrane protein, unknown function |
| PHT_0318000 | 104.58 | 14.65 | 53.72 | 36.33 | 28.07 | 96.18 | 90.98 | 215.87 | conserved Plasmodium membrane protein, unknown function |
| PHT_0322300 | 316.23 | 56.55 | 127.61 | 180.92 | 88.13 | 342.84 | 314.52 | 673.90 | conserved Plasmodium membrane protein, unknown function |
| PHT_0322400 | 89.77 | 91.00 | 153.17 | 126.50 | 160.31 | 110.06 | 146.70 | 184.83 | conserved Plasmodium membrane protein, unknown function |
| PHT_0312000 | 399.91 | 704.21 | 186.09 | 637.57 | 490.93 | 453.49 | 362.55 | 1034.11 | conserved Plasmodium protein (10b antigen), unknown function |
| PHT_bin10900 | 127.74 | 289.69 | 693.42 | 317.11 | 108 | | | | |

| | | | | | | | | | |
|--------------|---------|---------|---------|---------|---------|---------|---------|---------|--|
| FR1_011200 | 245.48 | 520.55 | 521.09 | 441.62 | 493.35 | 487.83 | 474.25 | 341.79 | conserved Plasmodium protein, unknown function |
| FR1_140020 | 83.43 | 152.24 | 274.40 | 198.83 | 256.94 | 156.96 | 212.60 | 196.35 | conserved Plasmodium protein, unknown function |
| FR1_bin09400 | 149.39 | 243.46 | 355.11 | 305.44 | 449.37 | 144.26 | 318.11 | 338.39 | conserved Plasmodium protein, unknown function |
| FR1_bin00200 | 27.92 | 46.96 | 74.34 | 64.51 | 103.27 | 64.14 | 53.53 | 73.56 | conserved Plasmodium protein, unknown function |
| FR1_bin09100 | 171.44 | 214.18 | 343.88 | 377.97 | 1140.83 | 272.85 | 317.18 | 632.86 | conserved Plasmodium protein, unknown function |
| FR1_bin10500 | 209.11 | 359.77 | 428.94 | 420.64 | 450.28 | 326.55 | 342.62 | 342.62 | conserved Plasmodium protein, unknown function |
| FR1_053760 | 26.24 | 49.30 | 52.73 | 59.29 | 79.67 | 25.61 | 50.28 | 94.27 | conserved Plasmodium protein, unknown function |
| FR1_bin08950 | 24.94 | 39.77 | 70.21 | 67.98 | 86.05 | 21.14 | 58.27 | 45.27 | conserved Plasmodium protein, unknown function |
| FR1_140010 | 154.96 | 287.83 | 366.79 | 312.52 | 337.23 | 290.15 | 288.07 | 281.35 | conserved Plasmodium protein, unknown function |
| FR1_011330 | 153.14 | 268.39 | 282.48 | 313.54 | 353.29 | 159.22 | 208.09 | 331.78 | conserved Plasmodium protein, unknown function |
| FR1_023400 | 88.83 | 145.14 | 70.29 | 79.21 | 101.12 | 43.91 | 68.86 | 87.21 | conserved Plasmodium protein, unknown function |
| FR1_bin04200 | 178.33 | 278.96 | 420.65 | 288.32 | 382.30 | 319.78 | 371.68 | 358.40 | conserved Plasmodium protein, unknown function |
| FR1_bin10300 | 23.71 | 11.51 | 97.33 | 40.14 | 74.04 | 47.34 | 99.43 | 79.92 | conserved Plasmodium protein, unknown function |
| FR1_140190 | 48.21 | 55.60 | 176.44 | 84.06 | 160.12 | 31.57 | 92.84 | 105.92 | conserved Plasmodium protein, unknown function |
| FR1_022130 | 13.65 | 33.93 | 54.75 | 33.22 | 62.39 | 15.55 | 25.73 | 51.62 | conserved Plasmodium protein, unknown function |
| FR1_023400 | 48.83 | 39.89 | 113.94 | 90.17 | 132.88 | 47.79 | 70.17 | 110.17 | conserved Plasmodium protein, unknown function |
| FR1_041190 | 19.07 | 37.95 | 50.98 | 36.59 | 52.88 | 23.28 | 26.92 | 55.50 | conserved Plasmodium protein, unknown function |
| FR1_053800 | 21.64 | 35.09 | 54.80 | 36.95 | 55.42 | 25.05 | 32.42 | 54.41 | conserved Plasmodium protein, unknown function |
| FR1_bin08600 | 17.48 | 20.89 | 58.89 | 28.61 | 97.87 | 11.50 | 37.51 | 53.98 | conserved Plasmodium protein, unknown function |
| FR1_010020 | 129.45 | 197.46 | 277.38 | 232.09 | 339.53 | 213.10 | 249.60 | 272.10 | conserved Plasmodium protein, unknown function |
| FR1_010040 | 167.85 | 228.03 | 510.99 | 215.24 | 421.91 | 100.71 | 138.28 | 385.52 | conserved Plasmodium protein, unknown function |
| FR1_110220 | 31.10 | 56.43 | 69.17 | 46.66 | 73.05 | 52.55 | 64.07 | 35.57 | conserved Plasmodium protein, unknown function |
| FR1_083560 | 22.04 | 21.08 | 67.51 | 41.32 | 67.33 | 30.94 | 54.99 | 25.78 | conserved Plasmodium protein, unknown function |
| FR1_bin11100 | 303.09 | 495.03 | 876.56 | 500.63 | 700.38 | 460.47 | 637.31 | 503.72 | conserved Plasmodium protein, unknown function |
| FR1_081190 | 30.14 | 21.48 | 84.22 | 35.27 | 62.02 | 32.02 | 62.13 | 52.99 | conserved Plasmodium protein, unknown function |
| FR1_010100 | 9.26 | 27.65 | 59.65 | 25.05 | 61.86 | 27.52 | 36.34 | 39.69 | conserved Plasmodium protein, unknown function |
| FR1_010130 | 216.06 | 218.85 | 481.29 | 266.38 | 460.99 | 233.04 | 254.14 | 295.87 | conserved Plasmodium protein, unknown function |
| FR1_010210 | 47.18 | 42.36 | 105.69 | 37.41 | 105.00 | 37.75 | 29.30 | 59.19 | conserved Plasmodium protein, unknown function |
| FR1_010500 | 60.60 | 107.54 | 145.63 | 108.38 | 127.83 | 74.80 | 115.60 | 107.11 | conserved Plasmodium protein, unknown function |
| FR1_010700 | 249.80 | 446.80 | 698.85 | 410.33 | 1273.09 | 254.09 | 387.11 | 328.19 | conserved Plasmodium protein, unknown function |
| FR1_010720 | 54.13 | 59.11 | 158.91 | 59.22 | 138.31 | 48.18 | 89.10 | 59.63 | conserved Plasmodium protein, unknown function |
| FR1_010740 | 113.35 | 103.71 | 387.22 | 129.10 | 343.88 | 158.63 | 194.24 | 150.94 | conserved Plasmodium protein, unknown function |
| FR1_010750 | 14.94 | 22.77 | 52.96 | 27.40 | 70.58 | 20.99 | 28.68 | 48.87 | conserved Plasmodium protein, unknown function |
| FR1_010840 | 22.11 | 39.66 | 74.74 | 42.85 | 77.16 | 18.47 | 38.03 | 36.99 | conserved Plasmodium protein, unknown function |
| FR1_010850 | 49.44 | 19.43 | 105.38 | 59.81 | 68.52 | 78.92 | 78.92 | 92.48 | conserved Plasmodium protein, unknown function |
| FR1_020150 | 31.64 | 44.31 | 58.03 | 57.17 | 70.68 | 42.66 | 63.68 | 84.64 | conserved Plasmodium protein, unknown function |
| FR1_020200 | 20.43 | 15.95 | 28.30 | 35.32 | 68.92 | 10.26 | 32.07 | 78.65 | conserved Plasmodium protein, unknown function |
| FR1_020230 | 268.24 | 439.85 | 424.82 | 475.06 | 590.24 | 363.67 | 466.00 | 826.08 | conserved Plasmodium protein, unknown function |
| FR1_020270 | 53.86 | 33.77 | 95.45 | 86.05 | 150.84 | 69.21 | 60.24 | 151.27 | conserved Plasmodium protein, unknown function |
| FR1_020390 | 253.89 | 307.82 | 307.82 | 345.53 | 494.24 | 235.67 | 235.67 | 477.09 | conserved Plasmodium protein, unknown function |
| FR1_020440 | 21.00 | 5.74 | 24.89 | 30.85 | 51.52 | 29.39 | 18.99 | 66.41 | conserved Plasmodium protein, unknown function |
| FR1_020490 | 72.25 | 32.74 | 104.52 | 85.77 | 235.46 | 79.92 | 66.76 | 211.23 | conserved Plasmodium protein, unknown function |
| FR1_020530 | 36.28 | 43.02 | 68.20 | 60.56 | 104.51 | 39.65 | 47.58 | 103.57 | conserved Plasmodium protein, unknown function |
| FR1_020550 | 27.91 | 35.21 | 50.80 | 45.15 | 60.97 | 43.83 | 46.76 | 55.46 | conserved Plasmodium protein, unknown function |
| FR1_020560 | 29.59 | 20.56 | 49.77 | 34.45 | 69.11 | 35.74 | 22.76 | 100.30 | conserved Plasmodium protein, unknown function |
| FR1_020580 | 34.12 | 53.66 | 42.84 | 42.71 | 79.62 | 29.26 | 38.64 | 79.93 | conserved Plasmodium protein, unknown function |
| FR1_020630 | 113.46 | 73.58 | 117.50 | 101.17 | 249.61 | 73.60 | 127.44 | 311.14 | conserved Plasmodium protein, unknown function |
| FR1_020190 | 38.76 | 59.42 | 70.83 | 64.45 | 78.75 | 38.46 | 80.25 | 72.96 | conserved Plasmodium protein, unknown function |
| FR1_020690 | 136.46 | 227.75 | 264.47 | 237.19 | 297.93 | 253.45 | 204.60 | 201.05 | conserved Plasmodium protein, unknown function |
| FR1_020780 | 8.28 | 16.53 | 26.41 | 21.24 | 45.08 | 4.08 | 21.60 | 47.07 | conserved Plasmodium protein, unknown function |
| FR1_020990 | 25.14 | 34.09 | 39.89 | 35.38 | 51.07 | 19.57 | 29.51 | 37.62 | conserved Plasmodium protein, unknown function |
| FR1_021150 | 61.58 | 113.98 | 94.51 | 93.19 | 123.48 | 59.73 | 77.61 | 75.60 | conserved Plasmodium protein, unknown function |
| FR1_021200 | 40.79 | 77.20 | 570.13 | 771.95 | 822.12 | 633.25 | 639.60 | 652.04 | conserved Plasmodium protein, unknown function |
| FR1_021240 | 48.78 | 95.01 | 85.79 | 96.69 | 110.46 | 66.13 | 86.21 | 65.18 | conserved Plasmodium protein, unknown function |
| FR1_021330 | 72.40 | 153.80 | 139.10 | 145.55 | 177.04 | 144.46 | 109.67 | 122.49 | conserved Plasmodium protein, unknown function |
| FR1_021390 | 37.29 | 69.21 | 58.71 | 57.75 | 75.73 | 36.56 | 39.11 | 69.33 | conserved Plasmodium protein, unknown function |
| FR1_021420 | 18.48 | 5.09 | 36.83 | 8.88 | 66.90 | 9.00 | 14.63 | 24.85 | conserved Plasmodium protein, unknown function |
| FR1_021490 | 46.44 | 57.74 | 90.64 | 92.62 | 103.67 | 65.17 | 92.54 | 85.96 | conserved Plasmodium protein, unknown function |
| FR1_021510 | 44.44 | 79.88 | 63.06 | 67.30 | 89.76 | 49.42 | 50.12 | 60.52 | conserved Plasmodium protein, unknown function |
| FR1_021590 | 31.96 | 25.44 | 50.04 | 48.27 | 71.72 | 46.13 | 28.13 | 52.25 | conserved Plasmodium protein, unknown function |
| FR1_010940 | 30.20 | 17.29 | 66.75 | 16.75 | 39.06 | 43.56 | 71.92 | 30.87 | conserved Plasmodium protein, unknown function |
| FR1_010970 | 30.41 | 40.24 | 76.31 | 44.65 | 46.74 | 49.50 | 69.09 | 58.48 | conserved Plasmodium protein, unknown function |
| FR1_010980 | 228.51 | 359.10 | 480.44 | 352.43 | 454.69 | 253.05 | 394.55 | 428.41 | conserved Plasmodium protein, unknown function |
| FR1_010990 | 47.09 | 28.46 | 107.90 | 38.05 | 70.87 | 31.75 | 53.42 | 50.84 | conserved Plasmodium protein, unknown function |
| FR1_011000 | 29.94 | 49.53 | 71.73 | 45.20 | 55.42 | 28.53 | 84.60 | 41.20 | conserved Plasmodium protein, unknown function |
| FR1_011020 | 262.95 | 260.98 | 589.40 | 317.14 | 511.21 | 304.88 | 426.29 | 357.71 | conserved Plasmodium protein, unknown function |
| FR1_011040 | 159.57 | 299.66 | 319.23 | 241.63 | 318.64 | 199.58 | 240.10 | 269.73 | conserved Plasmodium protein, unknown function |
| FR1_011050 | 36.34 | 23.17 | 100.48 | 28.07 | 68.54 | 16.06 | 51.90 | 20.82 | conserved Plasmodium protein, unknown function |
| FR1_011060 | 1269.91 | 1843.06 | 2553.11 | 1718.76 | 2358.45 | 2214.00 | 2153.25 | 2355.24 | conserved Plasmodium protein, unknown function |
| FR1_011080 | 72.40 | 114.04 | 30.04 | 101.70 | 145.95 | 101.41 | 67.70 | 85.54 | conserved Plasmodium protein, unknown function |
| FR1_011090 | 17.81 | 25.94 | 55.83 | 30.71 | 34.48 | 14.72 | 33.71 | 39.70 | conserved Plasmodium protein, unknown function |
| FR1_011110 | 47.93 | 76.46 | 112.61 | 62.16 | 89.15 | 74.13 | 46.70 | 65.32 | conserved Plasmodium protein, unknown function |
| FR1_011130 | 87.47 | 115.74 | 177.83 | 132.69 | 144.08 | 88.23 | 162.98 | 146.01 | conserved Plasmodium protein, unknown function |
| FR1_011170 | 25.49 | 27.85 | 52.96 | 27.71 | 47.17 | 14.44 | 36.53 | 33.62 | conserved Plasmodium protein, unknown function |
| FR1_011180 | 89.62 | 153.04 | 131.29 | 142.71 | 164.89 | 93.72 | 156.14 | 122.27 | conserved Plasmodium protein, unknown function |
| FR1_011200 | 107.19 | 77.40 | 221.04 | 95.10 | 183.85 | 48.56 | 110.87 | 139.79 | conserved Plasmodium protein, unknown function |
| FR1_011210 | 29.68 | 34.33 | 60.77 | 18.49 | 40.13 | 13.72 | 11.01 | 14.77 | conserved Plasmodium protein, unknown function |
| FR1_011230 | 43.94 | 49.09 | 93.47 | 60.94 | 67.20 | 62.12 | 74.09 | 52.21 | conserved Plasmodium protein, unknown function |
| FR1_022000 | 39.70 | 36.01 | 74.02 | 59.76 | 78.97 | 68.22 | 88.71 | 81.96 | conserved Plasmodium protein, unknown function |
| FR1_022020 | 1176.35 | 373.68 | 1491.73 | 817.93 | 1002.52 | 1746.08 | 2498.99 | 3003.53 | conserved Plasmodium protein, unknown function |
| FR1_021680 | 160.75 | 55.09 | 117.10 | 163.20 | 107.78 | 345.86 | 219.35 | 553.82 | conserved Plasmodium protein, unknown function |
| FR1_021720 | 3322.09 | 4776.97 | 4349.07 | 4049.77 | 3643.90 | 7178.64 | 5523.72 | 7497.33 | conserved Plasmodium protein, unknown function |
| FR1_030170 | 131.72 | 29.49 | 70.92 | 95.69 | 65.35 | 198.89 | 130.94 | 281.76 | conserved Plasmodium protein, unknown function |
| FR1_030190 | 441.11 | 81.80 | 298.33 | 210.74 | 212.27 | 441.97 | 644.24 | 898.24 | conserved Plasmodium protein, unknown function |
| FR1_030210 | 145.22 | 100.30 | 73.30 | 98.30 | 75.56 | 120.96 | 173.07 | 296.13 | conserved Plasmodium protein, unknown function |
| FR1_030260 | 54.09 | 77.57 | 80.85 | 80.79 | 106.85 | 57.64 | 83.69 | 126.21 | conserved Plasmodium protein, unknown function |
| FR1_030270 | 195.72 | 85.66 | 199.20 | 198.26 | 211.31 | 339.38 | 262.89 | 496.57 | conserved Plasmodium protein, unknown function |
| FR1_030280 | 65.86 | 6.58 | 29.96 | 36.29 | 18.20 | 69.55 | 66.95 | 146.54 | conserved Plasmodium protein, unknown function |
| FR1_030290 | 97.85 | 19.40 | 50.44 | 52.83 | 38.79 | 128.28 | 129.92 | 202.27 | conserved Plasmodium protein, unknown function |
| FR1_030310 | 164.13 | 28.85 | 62.97 | 74.41 | 51.33 | 147.63 | 174.66 | 362.35 | conserved Plasmodium protein, unknown function |
| FR1_030320 | 52.80 | 47.32 | 51.70 | 68.61 | 64.78 | 81.80 | 82.30 | 127.19 | conserved Plasmodium protein, unknown function |
| FR1_030400 | 190.65 | 65.58 | 139.73 | 118.75 | 108.00 | 201.78 | 227.74 | 471.16 | conserved Plasmodium protein, unknown function |
| FR1_030410 | 336.88 | 46.89 | 228.80 | 188.99 | 141.88 | 383.65 | 518.18 | 1040.22 | conserved Plasmodium protein, unknown function |
| FR1_030500 | 103.51 | 32.70 | 51.70 | 62.01 | 56.11 | 126.04 | 135.07 | 207.78 | conserved Plasmodium protein, unknown function |
| FR1_030510 | 70.51 | 11.44 | 64.32 | 33.63 | 29.62 | 98.51 | 94.45 | 213.59 | conserved Plasmodium protein, unknown function |
| FR1_030530 | 180.22 | 26.79 | 67.24 | 85.08 | 59.53 | 232.41 | 199.51 | 420.99 | conserved Plasmodium protein, unknown function |
| FR1_030540 | 173.00 | 198.92 | 244.44 | 218.13 | 200.20 | 200.88 | 318.67 | 349.13 | conserved Plasmodium protein, unknown function |
| FR1_030550 | 42.32 | 72.60 | 60.77 | 62.81 | 55.42 | 62.65 | 75.61 | 104.75 | conserved Plasmodium protein, unknown function |
| FR1_030600 | 35.57 | 2.26 | 22.59 | 24.45 | 17.86 | 64.39 | 50.19 | 78.49 | conserved Plasmodium protein, unknown function |
| FR1_030630 | 40.13 | 30.33 | 33.37 | 56.69 | 54.52 | 38.49 | 49.33 | 93.52 | conserved Plasmodium protein, unknown function |
| FR1_030640 | 173.71 | 35.27 | 86.96 | 94.61 | 58.67 | 147.29 | 194.34 | 375.03 | conserved Plasmodium protein, unknown function |
| FR1_030690 | 55.74 | 18.70 | 37.55 | 45.78 | 26.58 | 72.88 | 85.36 | 132.61 | conserved Plasmodium protein, unknown function |
| FR1_030720 | 28.57 | 23.55 | 30.50 | 30.47 | 24.05 | 36.10 | 52.66 | 66.15 | conserved Plasmodium protein, unknown function |
| FR1_030740 | 170.98 | 138.52 | 233.79 | 184.73 | 185.11 | 236.10 | 323.90 | 428.76 | conserved Plasmodium protein, unknown function |
| FR1_030760 | 46.14 | 36.76 | 45.50 | 42.31 | 41.11 | 62.63 | 70.23 | 97.19 | conserved Plasmodium protein, unknown function |
| FR1_030810 | 23.13 | 34.26 | 45.50 | 43.11 | 45.19 | 32.86 | 40.47 | | |

| | | | | | | | | | |
|---------------|----------|----------|----------|----------|----------|----------|----------|----------|--|
| PFIT_0312200 | 214.81 | 99.22 | 152.36 | 146.37 | 117.88 | 229.74 | 245.01 | 486.32 | conserved Plasmodium protein, unknown function |
| PFIT_0312300 | 3327.07 | 1044.40 | 2628.65 | 1795.82 | 1773.62 | 4473.17 | 5719.90 | 8404.33 | conserved Plasmodium protein, unknown function |
| PFIT_0312500 | 548.41 | 198.43 | 267.61 | 293.43 | 241.65 | 652.47 | 572.29 | 1131.38 | conserved Plasmodium protein, unknown function |
| PFIT_0312700 | 22.63 | 34.42 | 38.49 | 35.63 | 44.88 | 24.86 | 40.79 | 58.07 | conserved Plasmodium protein, unknown function |
| PFIT_0313600 | 95.23 | 35.37 | 57.27 | 60.75 | 42.94 | 111.79 | 88.45 | 199.28 | conserved Plasmodium protein, unknown function |
| PFIT_0313700 | 49.43 | 44.27 | 25.47 | 27.13 | 42.50 | 64.63 | 42.63 | 168.10 | conserved Plasmodium protein, unknown function |
| PFIT_0314500 | 100.68 | 14.86 | 31.49 | 46.21 | 32.94 | 111.15 | 88.37 | 211.93 | conserved Plasmodium protein, unknown function |
| PFIT_0314600 | 99.37 | 22.25 | 47.61 | 61.07 | 39.26 | 114.03 | 78.10 | 205.38 | conserved Plasmodium protein, unknown function |
| PFIT_0314900 | 53.35 | 47.10 | 33.37 | 49.64 | 30.01 | 52.25 | 59.18 | 125.35 | conserved Plasmodium protein, unknown function |
| PFIT_0315600 | 56.50 | 12.76 | 55.02 | 38.34 | 29.31 | 53.65 | 97.01 | 118.89 | conserved Plasmodium protein, unknown function |
| PFIT_0315100 | 37.84 | 16.02 | 59.29 | 80.68 | 42.50 | 196.30 | 110.72 | 310.74 | conserved Plasmodium protein, unknown function |
| PFIT_0315200 | 32.88 | 59.38 | 63.65 | 61.80 | 53.69 | 59.15 | 59.97 | 94.69 | conserved Plasmodium protein, unknown function |
| PFIT_0315300 | 13.68 | 27.12 | 15.32 | 26.22 | 14.74 | 7.48 | 16.53 | 92.47 | conserved Plasmodium protein, unknown function |
| PFIT_0315500 | 158.18 | 41.55 | 119.12 | 122.90 | 86.32 | 240.89 | 203.12 | 475.86 | conserved Plasmodium protein, unknown function |
| PFIT_0315600 | 80.19 | 17.99 | 59.83 | 90.04 | 46.98 | 135.37 | 119.06 | 213.35 | conserved Plasmodium protein, unknown function |
| PFIT_0315500 | 52.41 | 31.10 | 37.42 | 35.66 | 49.48 | 71.70 | 65.58 | 127.25 | conserved Plasmodium protein, unknown function |
| PFIT_0316900 | 24.70 | 7.63 | 21.96 | 11.34 | 10.84 | 25.56 | 38.25 | 60.50 | conserved Plasmodium protein, unknown function |
| PFIT_0318200 | 44.01 | 7.64 | 27.13 | 29.88 | 20.53 | 46.46 | 74.47 | 101.14 | conserved Plasmodium protein, unknown function |
| PFIT_0318300 | 128.82 | 50.32 | 62.75 | 104.56 | 57.43 | 156.04 | 181.78 | 394.68 | conserved Plasmodium protein, unknown function |
| PFIT_0318500 | 253.23 | 172.25 | 257.10 | 236.31 | 293.26 | 270.80 | 354.42 | 534.35 | conserved Plasmodium protein, unknown function |
| PFIT_0318700 | 47.82 | 23.07 | 23.54 | 31.49 | 21.68 | 34.19 | 42.45 | 108.85 | conserved Plasmodium protein, unknown function |
| PFIT_0318800 | 77.62 | 34.75 | 77.71 | 106.52 | 102.14 | 120.32 | 109.30 | 185.83 | conserved Plasmodium protein, unknown function |
| PFIT_0319000 | 114.39 | 133.03 | 128.33 | 116.19 | 95.63 | 121.79 | 180.93 | 258.25 | conserved Plasmodium protein, unknown function |
| PFIT_0319500 | 219.18 | 43.85 | 167.58 | 148.78 | 106.03 | 358.83 | 397.33 | 650.98 | conserved Plasmodium protein, unknown function |
| PFIT_0319600 | 260.99 | 545.54 | 1695.63 | 1549.84 | 1180.31 | 3300.86 | 3594.48 | 7271.46 | conserved Plasmodium protein, unknown function |
| PFIT_0319900 | 921.94 | 247.53 | 747.01 | 471.80 | 497.89 | 1239.52 | 1477.89 | 2374.48 | conserved Plasmodium protein, unknown function |
| PFIT_0320100 | 218.43 | 100.38 | 219.28 | 148.18 | 144.61 | 295.76 | 423.17 | 709.39 | conserved Plasmodium protein, unknown function |
| PFIT_0320400 | 21.26 | 24.15 | 37.78 | 45.00 | 40.66 | 45.55 | 37.51 | 80.80 | conserved Plasmodium protein, unknown function |
| PFIT_0320700 | 31.21 | 7.29 | 22.37 | 23.69 | 19.13 | 41.01 | 34.25 | 76.41 | conserved Plasmodium protein, unknown function |
| PFIT_0320900 | 110.96 | 37.99 | 71.24 | 89.74 | 61.83 | 106.57 | 116.64 | 294.11 | conserved Plasmodium protein, unknown function |
| PFIT_0321400 | 30.81 | 15.53 | 31.16 | 18.82 | 32.57 | 23.24 | 4.11 | 86.87 | conserved Plasmodium protein, unknown function |
| PFIT_0321600 | 301.74 | 495.38 | 542.29 | 533.60 | 540.62 | 547.72 | 598.05 | 615.00 | conserved Plasmodium protein, unknown function |
| PFIT_0321700 | 130.03 | 35.05 | 101.19 | 171.93 | 109.87 | 236.80 | 164.12 | 301.26 | conserved Plasmodium protein, unknown function |
| PFIT_0321800 | 64.49 | 14.01 | 27.89 | 40.04 | 19.77 | 68.23 | 58.69 | 131.18 | conserved Plasmodium protein, unknown function |
| PFIT_0322000 | 333.23 | 172.25 | 230.55 | 170.16 | 181.28 | 278.67 | 350.28 | 532.20 | conserved Plasmodium protein, unknown function |
| PFIT_0322100 | 75.08 | 81.91 | 47.34 | 84.52 | 71.61 | 59.24 | 87.72 | 155.94 | conserved Plasmodium protein, unknown function |
| PFIT_0322200 | 63.68 | 63.25 | 24.21 | 59.42 | 39.13 | 55.80 | 125.09 | 133.44 | conserved Plasmodium protein, unknown function |
| PFIT_0322500 | 16.17 | 12.82 | 19.76 | 31.96 | 15.49 | 28.13 | 37.75 | 84.06 | conserved Plasmodium protein, unknown function |
| PFIT_0220500 | 24.23 | 35.20 | 39.48 | 43.67 | 41.60 | 30.70 | 52.74 | 45.43 | conserved Plasmodium protein, unknown function |
| PFIT_0220900 | 38.59 | 33.99 | 22.05 | 36.58 | 22.05 | 30.78 | 26.88 | 31.18 | conserved Plasmodium protein, unknown function |
| PFIT_0221700 | 203.18 | 253.21 | 396.42 | 259.34 | 367.33 | 374.67 | 426.62 | 336.69 | conserved Plasmodium protein, unknown function |
| PFIT_0217800 | 23.63 | 23.75 | 33.73 | 19.38 | 31.52 | 51.34 | 14.41 | 28.07 | conserved Plasmodium protein, unknown function |
| PFIT_0218600 | 54.66 | 64.30 | 34.49 | 46.03 | 51.06 | 156.40 | 53.04 | 53.68 | conserved Plasmodium protein, unknown function |
| PFIT_0218900 | 78.64 | 136.18 | 133.94 | 122.33 | 154.78 | 165.26 | 98.12 | 117.07 | conserved Plasmodium protein, unknown function |
| PFIT_0218100 | 324.17 | 32.75 | 340.90 | 365.85 | 371.81 | 371.81 | 301.15 | 301.15 | conserved Plasmodium protein, unknown function |
| PFIT_0213900 | 29.42 | 43.31 | 47.79 | 61.15 | 70.56 | 33.43 | 37.61 | 28.91 | conserved protein, unknown function |
| PFIT_0900300 | 21.52 | 6.21 | 81.07 | 20.58 | 213.16 | 15.12 | 17.49 | 59.36 | conserved protein, unknown function |
| PFIT_bin09200 | 33.31 | 53.77 | 80.27 | 63.14 | 85.81 | 45.79 | 68.39 | 65.47 | conserved protein, unknown function |
| PFIT_0710600 | 19.21 | 32.41 | 74.47 | 43.26 | 100.40 | 16.23 | 51.28 | 48.43 | conserved protein, unknown function |
| PFIT_0110300 | 21.59 | 56.36 | 55.43 | 31.15 | 41.59 | 18.70 | 22.39 | 40.75 | conserved protein, unknown function |
| PFIT_0314300 | 45.75 | 59.34 | 69.58 | 61.92 | 80.09 | 79.41 | 58.82 | 102.97 | conserved protein, unknown function |
| PFIT_0317600 | 1987.76 | 374.20 | 1088.87 | 851.92 | 803.13 | 2056.46 | 2349.09 | 4182.75 | coronin |
| PFIT_0315700 | 19.92 | 14.17 | 29.64 | 11.42 | 20.96 | 18.06 | 7.60 | 57.22 | cysteine repeat modular protein 3 |
| PFIT_0302500 | 2155.17 | 506.74 | 1381.80 | 1470.15 | 817.44 | 3438.93 | 3464.03 | 8014.72 | cytochrome linked asexual protein 3.1 |
| PFIT_0200100 | 166.77 | 337.89 | 275.20 | 339.71 | 371.48 | 222.60 | 280.02 | 256.65 | cytochrome c heme lyase, putative |
| PFIT_0215600 | 147.85 | 241.27 | 258.89 | 217.82 | 329.02 | 180.10 | 164.00 | 182.61 | cytochrome c, putative |
| PFIT_0111500 | 19.44 | 21.26 | 50.94 | 27.27 | 31.42 | 18.73 | 21.43 | 22.68 | cytochrome c1 heme lyase, putative |
| PFIT_0210000 | 20.16 | 27.10 | 32.07 | 32.07 | 52.66 | 15.82 | 17.85 | 43.79 | cytoskeleton associated protein, putative |
| PFIT_0315900 | 270.11 | 78.07 | 245.02 | 160.89 | 194.72 | 352.98 | 499.78 | 872.50 | cytosolic iron-sulfur protein assembly protein 1, putative |
| PFIT_0205500 | 14.88 | 43.72 | 30.27 | 88.42 | 30.38 | 24.66 | 40.60 | 55.27 | DB1-containing protein, unknown function |
| PFIT_0101600 | 198.46 | 376.60 | 522.61 | 324.98 | 468.15 | 239.95 | 305.51 | 347.45 | DEAD box ATP-dependent RNA helicase, putative |
| PFIT_0205200 | 25.73 | 25.07 | 46.98 | 34.16 | 60.64 | 17.98 | 43.69 | 74.80 | DEAD box helicase, putative |
| PFIT_0207000 | 707.78 | 1194.02 | 1380.08 | 1140.18 | 1445.83 | 1128.04 | 1247.01 | 1265.80 | DEAD box helicase, putative |
| PFIT_bin02200 | 34.94 | 87.98 | 94.87 | 93.01 | 107.15 | 62.52 | 73.61 | 72.97 | DEAD/DEAH box helicase, putative |
| PFIT_0201300 | 64.99 | 132.37 | 115.08 | 131.56 | 141.39 | 120.21 | 162.82 | 137.72 | DBP1-like protein, putative |
| PFIT_0201700 | 43.80 | 56.89 | 86.51 | 66.86 | 87.85 | 44.24 | 96.35 | 83.14 | diacylglycerol O-acyltransferase |
| PFIT_bin02100 | 79.35 | 168.76 | 209.09 | 179.54 | 246.00 | 79.36 | 162.96 | 119.24 | dicarboxylate/tricarboxylate carrier |
| PFIT_0711400 | 191.86 | 337.42 | 639.54 | 299.30 | 915.37 | 142.36 | 241.77 | 551.26 | dihydropteroate synthetase |
| PFIT_0303600 | 347.11 | 49.16 | 105.42 | 155.46 | 97.79 | 330.38 | 242.96 | 697.22 | dipeptidyl aminopeptidase 3 |
| PFIT_0102700 | 149.58 | 337.57 | 350.80 | 317.45 | 344.89 | 334.99 | 331.77 | 207.42 | diphthine methyltransferase, putative |
| PFIT_0104400 | 210.94 | 352.21 | 448.85 | 345.21 | 477.08 | 237.49 | 340.14 | 317.84 | DNA helicase 40 |
| PFIT_0316100 | 47.43 | 68.14 | 68.77 | 70.52 | 76.65 | 65.10 | 82.10 | 114.20 | DNA helicase MCM8, putative |
| PFIT_0107800 | 105.16 | 136.85 | 247.36 | 163.56 | 217.31 | 147.64 | 148.16 | 179.58 | DNA helicase, putative |
| PFIT_0306600 | 24.21 | 14.27 | 40.83 | 32.45 | 43.72 | 15.54 | 25.06 | 51.89 | DNA polymerase 1, putative |
| PFIT_0304600 | 1326.48 | 299.04 | 943.03 | 601.52 | 590.78 | 1710.01 | 82.41 | 91.19 | DNA polymerase alpha |
| PFIT_0105700 | 287.13 | 542.75 | 588.41 | 528.77 | 841.32 | 291.94 | 428.70 | 501.31 | DNA-directed RNA polymerase |
| PFIT_0710800 | 21.41 | 27.85 | 59.69 | 39.32 | 51.30 | 30.92 | 61.20 | 31.37 | DnaJ protein, putative |
| PFIT_0108700 | 386.46 | 377.56 | 935.38 | 533.52 | 978.52 | 505.75 | 693.96 | 473.94 | DnaJ protein, putative |
| PFIT_0210900 | 78.36 | 110.23 | 129.23 | 99.90 | 198.73 | 75.45 | 110.25 | 137.08 | DnaJ protein, putative |
| PFIT_0217400 | 4.93 | 0.00 | 15.05 | 6.64 | 1.07 | 54.31 | 27.26 | 8.13 | DnaJ protein, putative |
| PFIT_0313100 | 464.87 | 104.38 | 233.25 | 295.77 | 183.27 | 721.97 | 517.74 | 1212.07 | duffy binding-like merozoite surface protein |
| PFIT_bin09000 | 64.72 | 147.87 | 154.29 | 167.75 | 137.54 | 126.37 | 231.26 | 109.44 | dynein heavy chain, putative |
| PFIT_0320500 | 31.11 | 32.61 | 23.13 | 37.63 | 28.94 | 27.89 | 33.12 | 108.51 | dynein-associated protein, putative |
| PFIT_0204200 | 148.10 | 188.81 | 260.69 | 213.36 | 541.79 | 183.09 | 192.62 | 342.35 | early transcribed membrane protein 10.2 |
| PFIT_0209100 | 10067.47 | 13777.11 | 19450.37 | 14847.83 | 23442.78 | 16877.37 | 13959.47 | 13417.94 | early transcribed membrane protein 5 |
| PFIT_0102500 | 53.69 | 65.01 | 150.87 | 81.47 | 162.18 | 62.47 | 98.81 | 103.29 | elongation factor G, putative |
| PFIT_0103500 | 790.55 | 1438.71 | 1644.53 | 1227.01 | 3204.49 | 752.59 | 1258.15 | 1496.92 | EMPI1-trafficking protein |
| PFIT_0103000 | 40.76 | 25.42 | 89.61 | 44.97 | 124.23 | 32.60 | 70.27 | 81.00 | endonuclease III homologue, putative |
| PFIT_0214600 | 59.76 | 79.60 | 98.10 | 85.54 | 123.41 | 43.13 | 65.73 | 109.37 | endopeptidase, putative |
| PFIT_0317800 | 1326.48 | 299.04 | 943.03 | 601.52 | 590.78 | 1710.01 | 82.41 | 91.19 | erythrocyte binding antigen-140 |
| PFIT_0219700 | 86.43 | 33.90 | 126.08 | 66.33 | 105.43 | 171.11 | 240.21 | 407.38 | erythrocyte binding antigen-145, pseudogene |
| PFIT_0308200 | 5542.69 | 1538.69 | 4382.58 | 2955.00 | 2694.41 | 8901.27 | 9441.50 | 21327.92 | erythrocyte binding antigen-175 |
| PFIT_0219200 | 582.69 | 169.72 | 559.61 | 304.06 | 373.06 | 959.98 | 1209.00 | 2339.97 | erythrocyte binding antigen-181 |
| PFIT_0216600 | 515.83 | 119.92 | 364.17 | 461.48 | 529.48 | 1301.13 | 1288.22 | 3457.84 | erythrocyte binding like protein 1, pseudogene |
| PFIT_bin08900 | 49.70 | 65.06 | 815.39 | 569.84 | 1251.38 | 309.26 | 168.75 | 231.59 | erythrocyte membrane protein 1, PIEMP1 |
| PFIT_0200700 | 58.97 | 21.34 | 15.09 | 132.31 | 84.69 | 44.40 | 87.24 | 111.29 | erythrocyte membrane protein 1, PIEMP1 |
| PFIT_0300600 | 29.42 | 18.60 | 38.81 | 39.35 | 37.25 | 58.79 | 53.67 | 99.83 | erythrocyte membrane protein 1, PIEMP1 |
| PFIT_0300400 | 16.66 | 10.24 | 41.50 | 15.49 | 44.74 | 24.73 | 28.06 | 54.75 | erythrocyte membrane protein 1, PIEMP1, putative |
| PFIT_0300700 | 65.92 | 28.30 | 86.28 | 69.95 | 81.97 | 95.55 | 114.58 | 150.63 | erythrocyte membrane protein 1, PIEMP1, putative |
| PFIT_0204000 | 265.72 | 67.21 | 277.32 | 336.00 | 799.56 | 195.61 | 180.34 | 811.13 | erythrocyte membrane protein 2 |
| PFIT_0217600 | 1.68 | 0.00 | 17.38 | 4.28 | 4.24 | 103.63 | 17.19 | 30.68 | erythrocyte membrane protein 3 |
| PFIT_0304200 | 1339.02 | 1348.87 | 2037.48 | 1718.15 | 1825.33 | 2267.39 | 2190.93 | 3127.42 | erythrocyte vesicle protein 1 |
| PFIT_0536300 | 101.18 | 230.54 | 235.64 | 197.40 | 264.50 | 165.10 | 168.19 | 241.42 | exonuclease I, putative |
| PFIT_0204300 | 77.84 | 102.51 | 78.33 | 139.56 | 191.39 | 87.37 | 88.09 | 212.80 | exonuclease, putative |

| | | | | | | | | | |
|--------------|----------|----------|----------|----------|----------|----------|----------|----------|--|
| PF1_0308500 | 313.24 | 113.36 | 351.60 | 171.77 | 182.80 | 414.22 | 467.86 | 642.75 | gamele release protein, putative |
| PF1_0112200 | 47.91 | 114.90 | 114.90 | 77.54 | 69.53 | 85.40 | 85.40 | 85.40 | gamma-bublin complex component, putative |
| PF1_0318400 | 255.06 | 49.81 | 142.47 | 150.88 | 98.44 | 312.59 | 239.36 | 562.10 | glideosome associated protein with multiple membrane spans 1 |
| PF1_0316400 | 503.29 | 76.27 | 207.02 | 194.90 | 143.86 | 442.21 | 436.83 | 1065.30 | glideosome-associated protein 45 |
| PF1_0108200 | 1115.61 | 1730.95 | 2384.71 | 1567.21 | 3366.57 | 813.95 | 1550.36 | 1912.90 | glucose-6-phosphate isomerase |
| PF1_0600100 | 847.12 | 1152.57 | 2281.43 | 1329.34 | 4404.66 | 521.39 | 775.31 | 2042.43 | glutamate dehydrogenase, putative |
| PF1_0314000 | 54.25 | 57.45 | 39.35 | 46.11 | 50.68 | 39.20 | 36.19 | 121.21 | glutamate--RNA ligase, putative |
| PF1_0312800 | 774.15 | 155.59 | 622.13 | 514.63 | 406.39 | 946.88 | 1133.09 | 2602.84 | glutamate-rich protein |
| PF1_bin09800 | 5764.70 | 8424.51 | 14130.52 | 10198.15 | 16376.10 | 5758.22 | 5340.50 | 12983.80 | glutamic acid-rich protein |
| PF1_0221000 | 683.99 | 881.67 | 1202.33 | 859.04 | 862.78 | 1097.37 | 1463.48 | 966.66 | glutamine--fructose-6-phosphate aminotransferase [isomerizing], putative |
| PF1_0213100 | 68.50 | 151.07 | 105.69 | 127.37 | 160.07 | 90.30 | 108.61 | 108.66 | glutathione peroxidase-like thioredoxin peroxidase |
| PF1_0101900 | 30.91 | 48.93 | 108.75 | 65.39 | 111.47 | 46.64 | 79.20 | 60.03 | glutathione synthetase |
| PF1_0215500 | 46.18 | 45.58 | 79.15 | 54.17 | 94.85 | 29.45 | 66.22 | 75.32 | glycine cleavage system T protein, putative |
| PF1_0107100 | 215.36 | 248.27 | 648.86 | 287.66 | 502.75 | 255.42 | 405.58 | 302.78 | glycophorin binding protein |
| PF1_0212500 | 127.39 | 186.26 | 159.50 | 197.16 | 257.78 | 96.18 | 104.99 | 212.30 | Grp protein homolog, mitochondrial, putative |
| PF1_0204600 | 28.20 | 29.57 | 55.74 | 39.76 | 100.16 | 21.22 | 36.34 | 77.95 | GTP cyclohydrolase I |
| PF1_0310000 | 22.19 | 11.99 | 22.41 | 35.99 | 38.76 | 37.47 | 28.68 | 61.06 | GTP-binding protein, putative |
| PF1_0208300 | 45.48 | 48.03 | 73.08 | 71.27 | 94.46 | 59.63 | 57.41 | 83.98 | GTPase-activating protein, putative |
| PF1_0101500 | 579.61 | 1108.10 | 1185.04 | 1009.63 | 1191.62 | 1012.00 | 1039.61 | 1025.33 | heat shock protein 40 |
| PF1_0211900 | 130.73 | 162.28 | 176.34 | 191.36 | 433.27 | 108.00 | 132.59 | 260.55 | heat shock protein 60 |
| PF1_0212700 | 1538.20 | 3921.77 | 3557.32 | 3404.12 | 4753.54 | 2770.80 | 3015.37 | 3109.81 | heat shock protein 70 |
| PF1_0305700 | 342.76 | 79.68 | 136.01 | 197.46 | 81.52 | 303.68 | 254.44 | 751.33 | HECT-domain (ubiquitin-transferase), putative |
| PF1_0111400 | 260.11 | 303.98 | 548.21 | 310.95 | 496.19 | 239.30 | 416.69 | 281.51 | heterochromatin protein 1 |
| PF1_1240500 | 27.30 | 28.79 | 94.14 | 41.65 | 62.07 | 47.32 | 62.42 | 38.72 | high mobility group protein B4, putative |
| PF1_0309600 | 3576.24 | 419.39 | 1583.88 | 1879.55 | 934.96 | 4420.76 | 3707.30 | 9356.22 | high molecular weight rhoty protein 3 |
| PF1_0411000 | 26.74 | 40.00 | 76.81 | 50.32 | 73.69 | 28.88 | 57.42 | 47.80 | histidine--RNA ligase, putative |
| PF1_0104500 | 3214.54 | 42505.84 | 7605.87 | 4239.51 | 6432.93 | 5191.36 | 46724.55 | 3411.36 | histidine-rich protein II |
| PF1_0103700 | 42114.48 | 78821.05 | 87035.44 | 64790.25 | 99014.72 | 47745.62 | 54558.82 | 54387.43 | histidine-rich protein III |
| PF1_0221100 | 21.39 | 9.78 | 41.95 | 17.83 | 34.28 | 28.08 | 60.79 | 39.48 | HSP20-like chaperone |
| PF1_0317200 | 18.88 | 8.14 | 16.89 | 19.91 | 32.82 | 26.30 | 20.36 | 52.35 | hydroxyethylthiazole kinase |
| PF1_0314100 | 101.44 | 151.09 | 58.03 | 139.51 | 87.14 | 95.43 | 143.23 | 270.26 | hypothetical protein |
| PF1_0314000 | 26.14 | 11.99 | 16.08 | 19.46 | 16.39 | 16.72 | 64.33 | 535.17 | IMP-specific 5'-nucleotidase, putative |
| PF1_0219300 | 95.97 | 17.66 | 86.60 | 66.11 | 49.21 | 111.28 | 210.55 | 229.03 | inner membrane complex protein 1e, putative |
| PF1_0319100 | 1143.66 | 296.68 | 1012.30 | 608.72 | 624.04 | 1330.45 | 1958.64 | 2980.59 | inner membrane complex protein 1f, putative |
| PF1_0111000 | 29.00 | 32.65 | 67.87 | 27.68 | 48.03 | 12.42 | 28.18 | 53.97 | inner membrane complex protein 1l, putative |
| PF1_0218800 | 106.78 | 132.82 | 131.47 | 147.09 | 132.63 | 226.45 | 204.30 | 176.26 | inositol polyphosphate kinase, putative |
| PF1_0319200 | 136.62 | 166.62 | 165.43 | 186.64 | 185.68 | 290.97 | 185.84 | 290.97 | inositol polyphosphate 5-phosphatase, putative |
| PF1_0218300 | 19487.55 | 31229.87 | 28993.64 | 25960.43 | 24256.55 | 50161.98 | 27740.00 | 31821.76 | interspersed repeat antigen |
| PF1_0213400 | 9.59 | 33.74 | 36.25 | 37.77 | 81.81 | 9.33 | 33.57 | 46.06 | isoleucine--RNA ligase, putative |
| PF1_0314200 | 824.96 | 182.92 | 553.38 | 433.54 | 410.21 | 915.14 | 1257.68 | 1991.36 | kelch protein, putative |
| PF1_0314300 | 900.01 | 414.56 | 748.84 | 540.44 | 552.83 | 933.55 | 1559.62 | 2182.83 | kelch protein, putative |
| PF1_0209900 | 31.71 | 36.63 | 46.36 | 64.00 | 47.10 | 43.48 | 37.33 | 57.33 | kinase, putative |
| PF1_0220100 | 29.27 | 25.13 | 53.09 | 39.86 | 46.26 | 45.74 | 68.32 | 68.75 | kinasin-2, putative |
| PF1_0301200 | 50.01 | 16.67 | 26.59 | 53.75 | 28.92 | 70.50 | 58.94 | 115.56 | kinasin-8, putative |
| PF1_0217500 | 1.69 | 0.00 | 29.87 | 2.38 | 1.67 | 400.29 | 31.03 | 8.84 | knob associated heat shock protein 40 |
| PF1_0108900 | 19.63 | 0.65 | 30.56 | 23.52 | 20.41 | 3096.87 | 341.39 | 230.64 | knob-associated histidine-rich protein |
| PF1_0311500 | 242.99 | 383.01 | 346.59 | 307.41 | 287.84 | 377.52 | 554.25 | 71.77 | L-serine-RNA(Sec) kinase, putative |
| PF1_0321300 | 46.11 | 41.76 | 28.57 | 55.24 | 39.70 | 33.04 | 54.85 | 94.97 | leucine carboxyl methyltransferase, putative |
| PF1_bin10500 | 111.92 | 178.21 | 259.40 | 239.07 | 348.14 | 107.59 | 197.03 | 289.74 | leucine--RNA ligase, putative |
| PF1_0214000 | 46.21 | 135.50 | 119.97 | 99.34 | 140.67 | 88.29 | 129.41 | 67.46 | lipotein-protein ligase 1 |
| PF1_0303800 | 131.90 | 176.72 | 46.89 | 145.90 | 99.72 | 81.71 | 132.28 | 268.87 | liver specific protein 2, putative |
| PF1_0305800 | 1176.40 | 992.62 | 1347.58 | 671.59 | 748.86 | 1796.08 | 1857.69 | 2891.33 | long chain polyunsaturated fatty acid elongation enzyme, putative |
| PF1_0305200 | 28.59 | 35.43 | 13.65 | 43.54 | 29.27 | 29.97 | 36.88 | 57.46 | longevity-assurance (LAG1) protein, putative |
| PF1_0207700 | 46.54 | 13.51 | 34.45 | 23.44 | 119.44 | 22.85 | 24.25 | 52.50 | lysine decarboxylase, putative |
| PF1_0411300 | 25.18 | 50.54 | 82.96 | 61.16 | 125.75 | 19.13 | 62.69 | 82.72 | lysine--RNA ligase, putative |
| PF1_bin07600 | 372.54 | 900.86 | 1718.52 | 958.18 | 2658.65 | 427.91 | 829.62 | 1191.60 | lysine-rich membrane-associated PHISb protein |
| PF1_0223000 | 243.99 | 383.01 | 346.59 | 307.41 | 287.84 | 377.52 | 554.25 | 71.77 | lysophospholipase, putative |
| PF1_0104700 | 314.82 | 575.20 | 650.85 | 574.35 | 794.33 | 336.70 | 444.06 | 555.59 | M18 aspartyl aminopeptidase |
| PF1_0209600 | 52.84 | 87.69 | 91.90 | 89.73 | 136.33 | 55.01 | 61.69 | 92.60 | maleate:quinone oxidoreductase, putative |
| PF1_0107900 | 11122.21 | 20564.00 | 24773.28 | 21696.68 | 26997.31 | 18655.82 | 17675.87 | 12650.89 | membrane associated histidine-rich protein |
| PF1_0313300 | 259.99 | 42.48 | 185.37 | 123.52 | 119.98 | 339.07 | 354.06 | 548.22 | merozoitin surface protein |
| PF1_0318500 | 38.61 | 7.44 | 16.71 | 33.86 | 21.03 | 39.82 | 34.34 | 72.03 | merozoitin surface protein |
| PF1_0310700 | 6925.09 | 951.19 | 4437.32 | 3468.97 | 2674.56 | 10115.42 | 8632.89 | 18402.89 | merozoitin surface protein 1 |
| PF1_0219800 | 32.86 | 8.25 | 22.01 | 26.61 | 22.91 | 60.61 | 66.64 | 146.32 | merozoitin surface protein 10 |
| PF1_0301800 | 4668.68 | 1218.10 | 2416.10 | 2423.25 | 1750.06 | 6814.41 | 4262.80 | 9675.34 | merozoitin surface protein 2 |
| PF1_0312900 | 1317.35 | 272.44 | 1198.64 | 764.09 | 661.23 | 2147.42 | 2241.32 | 4757.13 | merozoitin surface protein 3 |
| PF1_0313000 | 910.49 | 217.71 | 846.28 | 475.74 | 467.93 | 1193.75 | 1651.59 | 2755.61 | merozoitin surface protein 4 |
| PF1_0312400 | 654.32 | 104.06 | 409.10 | 234.76 | 252.89 | 713.36 | 840.35 | 1497.76 | merozoitin TRAP-like protein |
| PF1_1219200 | 51.97 | 89.63 | 174.18 | 100.03 | 248.24 | 36.71 | 100.44 | 135.77 | melabolite/drug transporter, putative |
| PF1_0419300 | 49.54 | 75.49 | 118.94 | 86.25 | 101.00 | 61.57 | 140.67 | 66.85 | melocapsin-1 |
| PF1_0321200 | 133.50 | 107.12 | 218.43 | 149.81 | 257.81 | 159.61 | 202.43 | 358.09 | melocapsin-like protein |
| PF1_0104900 | 25.51 | 18.79 | 57.18 | 26.28 | 58.34 | 30.86 | 39.14 | 38.43 | metallopeptidase, putative |
| PF1_0107300 | 101.99 | 84.84 | 228.17 | 108.37 | 260.34 | 78.50 | 119.66 | 108.21 | methyltransferase-like protein, putative |
| PF1_0216000 | 85.87 | 138.37 | 135.96 | 160.13 | 330.00 | 70.72 | 97.52 | 170.64 | mitochondrial acidic protein MAM3, putative |
| PF1_0213000 | 19.78 | 12.38 | 16.04 | 27.98 | 52.45 | 12.69 | 17.43 | 35.02 | mitochondrial ACP precursor |
| PF1_0102800 | 65.53 | 52.04 | 169.07 | 84.59 | 153.81 | 56.71 | 113.21 | 115.50 | mitochondrial cardiolipin synthase, putative |
| PF1_0215300 | 85.89 | 165.81 | 115.89 | 165.97 | 172.41 | 130.27 | 96.17 | 110.27 | mitochondrial import inner membrane translocase subunit TIM23, putative |
| PF1_0210300 | 38.96 | 82.50 | 56.33 | 77.21 | 95.67 | 45.21 | 44.84 | 58.58 | mitochondrial import inner membrane translocase subunit TIM50, putative |
| PF1_0208900 | 312.89 | 750.85 | 728.37 | 682.59 | 860.83 | 530.30 | 609.24 | 689.30 | mitochondrial processing peptidase alpha subunit, putative |
| PF1_0101100 | 49.99 | 70.97 | 142.34 | 70.59 | 110.14 | 65.48 | 75.63 | 67.50 | mitochondrial ribosomal protein L12 precursor, putative |
| PF1_0106300 | 62.97 | 118.63 | 140.33 | 106.09 | 129.95 | 80.42 | 92.98 | 94.35 | mitochondrial ribosomal protein S18 precursor, putative |
| PF1_0307500 | 44.89 | 29.62 | 46.67 | 45.70 | 67.31 | 49.93 | 64.98 | 95.22 | mitochondrial ribosomal protein S8 precursor, putative |
| PF1_0208600 | 36.85 | 56.29 | 36.16 | 81.50 | 72.71 | 65.74 | 45.46 | 64.20 | monocarboxylate transporter, putative |
| PF1_0312400 | 66.95 | 30.45 | 48.78 | 59.39 | 44.06 | 86.37 | 71.91 | 207.45 | MORN repeat-containing protein 1 |
| PF1_0109100 | 26.25 | 58.84 | 66.48 | 55.80 | 57.27 | 43.91 | 75.58 | 38.99 | mRNA-binding protein PUF1 |
| PF1_0205400 | 20.79 | 17.35 | 34.36 | 21.95 | 65.24 | 13.45 | 28.49 | 71.56 | MSP7-like protein |
| PF1_0302000 | 44.78 | 29.95 | 33.10 | 46.40 | 47.95 | 46.44 | 52.45 | 94.28 | multidrug efflux pump, putative |
| PF1_bin00100 | 129.20 | 229.17 | 298.69 | 291.72 | 514.02 | 144.57 | 231.48 | 256.94 | multidrug resistance protein 2 |
| PF1_0202100 | 19.43 | 15.56 | 43.93 | 36.65 | 69.97 | 21.47 | 42.88 | 66.85 | multidrug resistance-associated protein 1 |
| PF1_0318900 | 3868.38 | 900.52 | 2745.18 | 1870.82 | 1844.64 | 4569.41 | 5629.75 | 9595.05 | myosin A |
| PF1_0312900 | 1308.96 | 366.09 | 1014.65 | 663.33 | 859.70 | 1560.00 | 1902.81 | 3405.22 | myosin A tail domain interacting protein |
| PF1_0214400 | 393.89 | 290.81 | 428.24 | 403.15 | 809.88 | 331.79 | 370.79 | 765.35 | myosin C |
| PF1_0318800 | 272.60 | 52.53 | 193.72 | 168.51 | 141.96 | 410.42 | 393.49 | 891.40 | myosin D |
| PF1_0306200 | 876.43 | 197.23 | 736 | | | | | | |

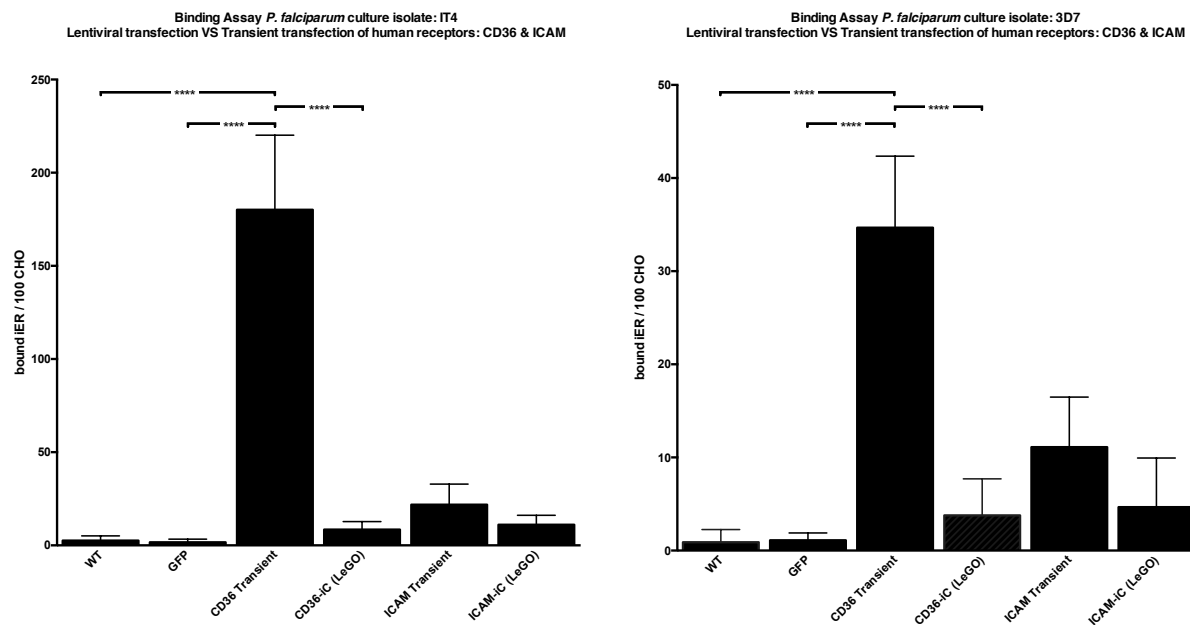
| | | | | | | | | | |
|---------------|----------|----------|----------|---------|----------|---------|---------|---------|---|
| PFIT_0217300 | 1.27 | 0.60 | 5.03 | 3.46 | 0.87 | 81.42 | 6.09 | 2.07 | PHISTb domain-containing RESA-like protein 1 |
| PFIT_0107700 | 231.79 | 269.17 | 543.67 | 312.92 | 821.99 | 280.14 | 369.88 | 426.39 | phosphoenolpyruvate carboxykinase |
| PFIT_0307000 | 107.64 | 130.49 | 179.09 | 153.75 | 189.62 | 125.95 | 189.78 | 279.76 | phosphoinositide-binding protein, putative |
| PFIT_0230600 | 62.99 | 60.25 | 92.26 | 69.44 | 164.99 | 164.99 | 164.99 | 35.55 | phosphoinositide-binding protein, putative |
| PFIT_1003300 | 81.88 | 84.66 | 189.95 | 107.25 | 583.50 | 36.24 | 53.10 | 224.40 | Plasmodium exported protein (hyp11), unknown function |
| PFIT_bin11000 | 679.66 | 1754.10 | 3985.84 | 1705.57 | 4933.59 | 505.87 | 1774.87 | 2312.97 | Plasmodium exported protein (hyp12), unknown function |
| PFIT_0204000 | 25.35 | 9.70 | 44.11 | 15.99 | 83.23 | 1.80 | 8.87 | 102.36 | Plasmodium exported protein (hyp12), unknown function |
| PFIT_bin06900 | 54.00 | 153.42 | 827.58 | 187.46 | 1310.70 | 62.91 | 191.46 | 478.11 | Plasmodium exported protein (hyp17), unknown function |
| PFIT_0201000 | 73.10 | 103.66 | 725.06 | 230.05 | 1074.54 | 66.95 | 186.07 | 508.82 | Plasmodium exported protein (hyp17), unknown function |
| PFIT_0211300 | 22.68 | 59.74 | 34.36 | 35.23 | 121.44 | 16.03 | 21.40 | 43.33 | Plasmodium exported protein (PHISTa-like), unknown function |
| PFIT_0205100 | 20.02 | 33.03 | 46.76 | 22.58 | 57.60 | 5.85 | 12.52 | 90.08 | Plasmodium exported protein (PHISTa-like), unknown function, pseudogene |
| PFIT_0210500 | 16.80 | 86.66 | 64.99 | 81.12 | 87.80 | 17.11 | 68.01 | 61.48 | Plasmodium exported protein (PHISTa), unknown function |
| PFIT_0202200 | 105.27 | 42.82 | 120.16 | 154.45 | 443.32 | 54.45 | 46.92 | 341.77 | Plasmodium exported protein (PHISTa), unknown function |
| PFIT_0218000 | 299.43 | 145.95 | 438.62 | 253.43 | 268.86 | 914.07 | 401.60 | 317.15 | Plasmodium exported protein (PHISTb), unknown function |
| PFIT_0219000 | 84.54 | 54.98 | 99.31 | 57.04 | 81.44 | 230.38 | 85.62 | 79.59 | Plasmodium exported protein (PHISTa), unknown function |
| PFIT_0102400 | 30.00 | 32.18 | 64.05 | 41.45 | 80.41 | 30.08 | 50.77 | 42.34 | Plasmodium exported protein (PHISTa), unknown function, pseudogene |
| PFIT_0108800 | 142.48 | 393.32 | 598.20 | 351.02 | 919.90 | 252.39 | 218.12 | 365.94 | Plasmodium exported protein (PHISTb), unknown function |
| PFIT_0109800 | 89.13 | 97.43 | 328.21 | 101.72 | 792.88 | 31.94 | 53.10 | 291.02 | Plasmodium exported protein (PHISTb), unknown function |
| PFIT_0102300 | 6058.94 | 9924.00 | 15919.32 | 8984.27 | 20464.63 | 5375.95 | 8084.13 | 8851.04 | Plasmodium exported protein (PHISTb), unknown function |
| PFIT_0103400 | 97.29 | 165.47 | 204.82 | 146.19 | 438.82 | 58.99 | 120.87 | 184.74 | Plasmodium exported protein (PHISTb), unknown function |
| PFIT_0207400 | 557.07 | 521.88 | 1088.94 | 750.30 | 4197.25 | 463.22 | 312.95 | 1040.68 | Plasmodium exported protein (PHISTb), unknown function |
| PFIT_0211200 | 11.15 | 17.73 | 32.79 | 10.86 | 65.34 | 4.27 | 18.85 | 32.02 | Plasmodium exported protein (PHISTb), unknown function |
| PFIT_0212900 | 331.21 | 132.23 | 245.12 | 319.00 | 1048.13 | 129.55 | 113.04 | 610.32 | Plasmodium exported protein (PHISTb), unknown function |
| PFIT_0217900 | 381.76 | 98.10 | 260.88 | 178.39 | 149.11 | 804.52 | 280.33 | 197.97 | Plasmodium exported protein (PHISTb), unknown function |
| PFIT_0218400 | 891.70 | 296.31 | 1004.46 | 477.83 | 581.34 | 1920.52 | 848.55 | 1704.13 | Plasmodium exported protein (PHISTb), unknown function |
| PFIT_0203600 | 23.49 | 20.86 | 34.90 | 31.94 | 76.25 | 14.46 | 35.25 | 54.01 | Plasmodium exported protein (PHISTb), unknown function, pseudogene |
| PFIT_0104000 | 1181.29 | 2627.32 | 4244.68 | 2418.88 | 4930.37 | 964.38 | 2510.67 | 2469.93 | Plasmodium exported protein (PHISTc), unknown function |
| PFIT_0208000 | 60.01 | 65.61 | 43.88 | 72.30 | 240.78 | 47.14 | 68.71 | 100.77 | Plasmodium exported protein (PHISTc), unknown function |
| PFIT_0112200 | 116.63 | 56.12 | 135.26 | 88.63 | 282.43 | 61.09 | 99.06 | 132.46 | Plasmodium exported protein, unknown function |
| PFIT_0302200 | 70.92 | 69.09 | 172.57 | 90.48 | 505.77 | 41.37 | 65.84 | 170.58 | Plasmodium exported protein, unknown function |
| PFIT_0103200 | 342.68 | 587.36 | 917.82 | 579.36 | 1505.15 | 383.59 | 434.25 | 455.06 | Plasmodium exported protein, unknown function |
| PFIT_0203400 | 85.81 | 34.49 | 39.13 | 115.83 | 226.80 | 28.61 | 17.74 | 210.01 | Plasmodium exported protein, unknown function |
| PFIT_0211100 | 77.81 | 68.19 | 101.16 | 76.71 | 288.00 | 35.99 | 63.35 | 154.56 | Plasmodium exported protein, unknown function |
| PFIT_0213500 | 302.76 | 58.27 | 446.57 | 54.58 | 207.47 | 456.58 | 57.28 | 60.89 | Plasmodium exported protein, unknown function |
| PFIT_0108000 | 51.30 | 70.61 | 110.94 | 67.02 | 119.23 | 44.89 | 70.72 | 63.01 | prefoldin subunit 2, putative |
| PFIT_0208400 | 145.21 | 299.84 | 296.63 | 238.24 | 369.92 | 109.25 | 199.05 | 213.26 | prefoldin subunit, putative |
| PFIT_0105100 | 369.45 | 686.48 | 1743.08 | 662.39 | 2818.10 | 154.75 | 458.94 | 638.57 | probable protein, unknown function |
| PFIT_0315200 | 934.25 | 140.96 | 631.52 | 353.81 | 305.90 | 1154.49 | 1150.54 | 2902.17 | probable protein, unknown function |
| PFIT_0313400 | 353.3400 | 78.70 | 182.89 | 174.68 | 156.63 | 430.87 | 871.29 | 620.98 | probable protein, unknown function |
| PFIT_0211800 | 61.28 | 158.69 | 126.26 | 146.15 | 233.56 | 42.25 | 103.08 | 132.42 | prohibitin, putative |
| PFIT_0208800 | 476.72 | 743.37 | 808.01 | 769.95 | 968.87 | 555.43 | 653.70 | 635.90 | proteasome subunit beta type-1, putative |
| PFIT_0214700 | 24.76 | 35.06 | 26.28 | 33.77 | 70.80 | 20.35 | 27.12 | 34.04 | protein kinase 6 |
| PFIT_0201000 | 67.79 | 123.80 | 119.61 | 140.85 | 130.53 | 115.73 | 122.62 | 95.41 | protein kinase, putative |
| PFIT_0301400 | 116.63 | 62.03 | 154.60 | 81.76 | 112.93 | 148.69 | 182.48 | 263.88 | protein kinase, putative |
| PFIT_0303000 | 25.56 | 6.40 | 12.80 | 20.99 | 13.42 | 23.46 | 35.25 | 60.49 | protein kinase, putative |
| PFIT_0304700 | 23.25 | 11.78 | 41.37 | 19.50 | 49.02 | 23.09 | 33.21 | 51.75 | protein kinase, putative |
| PFIT_0310400 | 53.12 | 57.05 | 51.92 | 66.08 | 57.11 | 53.61 | 99.80 | 171.20 | protein kinase, putative |
| PFIT_0311000 | 215.44 | 74.18 | 176.75 | 172.70 | 131.48 | 344.69 | 332.38 | 469.51 | protein MAM3, putative |
| PFIT_0308800 | 602.76 | 86.66 | 320.57 | 263.57 | 207.47 | 472.88 | 222.79 | 132.61 | protein phosphatase PPM5, putative |
| PFIT_bin10700 | 41.97 | 113.45 | 130.89 | 117.38 | 168.64 | 76.98 | 123.17 | 107.98 | protein prenyltransferase alpha subunit, putative |
| PFIT_0203700 | 62.94 | 113.32 | 120.15 | 118.61 | 128.52 | 106.11 | 109.19 | 131.43 | pseudouridylyl synthase, putative |
| PFIT_0203000 | 26.73 | 43.05 | 39.62 | 37.05 | 34.28 | 19.37 | 55.32 | 54.86 | pyridine nucleotide transhydrogenase, putative |
| PFIT_0203800 | 46.63 | 62.88 | 82.16 | 67.78 | 402.75 | 40.66 | 78.02 | 103.40 | pyridoxal 5'-phosphate dependent enzyme class III, putative |
| PFIT_0209700 | 1093.54 | 1639.73 | 1845.06 | 1524.10 | 2504.87 | 1507.51 | 1409.61 | 871.29 | pyridoxal biosynthesis protein PDX1 |
| PFIT_0411400 | 138.87 | 264.00 | 468.42 | 291.33 | 624.81 | 118.96 | 285.66 | 270.13 | pyrolysine-S-carboxylate reductase |
| PFIT_bin07650 | 44.30 | 115.96 | 120.20 | 116.36 | 219.71 | 45.56 | 100.46 | 144.93 | pyruvate kinase 2 |
| PFIT_0104800 | 206.07 | 347.04 | 457.13 | 324.22 | 466.85 | 273.92 | 347.31 | 389.74 | queuine tRNA-ribosyltransferase, putative |
| PFIT_0314400 | 64.80 | 79.06 | 43.77 | 71.86 | 63.78 | 55.58 | 75.09 | 132.33 | rad kinase inhibitor |
| PFIT_0113000 | 33.28 | 103.00 | 115.84 | 115.84 | 159.21 | 34.69 | 53.69 | 120.98 | RAP protein, putative |
| PFIT_0214300 | 149.99 | 353.16 | 294.02 | 272.95 | 372.44 | 192.99 | 238.16 | 232.84 | RAP protein, putative |
| PFIT_0202500 | 30.76 | 44.98 | 29.24 | 53.03 | 74.55 | 28.74 | 43.06 | 105.63 | RAP protein, putative |
| PFIT_0204700 | 21.64 | 42.07 | 45.50 | 43.37 | 69.11 | 36.02 | 38.90 | 56.15 | RAP protein, putative |
| PFIT_0216100 | 48.97 | 71.52 | 81.86 | 72.40 | 123.52 | 51.96 | 77.90 | 74.83 | RAP protein, putative |
| PFIT_0214000 | 264.67 | 295.12 | 485.42 | 325.23 | 439.27 | 345.92 | 361.64 | 262.07 | RAP protein, putative |
| PFIT_0221200 | 360.92 | 505.83 | 685.78 | 535.58 | 621.76 | 538.03 | 830.17 | 637.43 | ras-related protein Rab-2 |
| PFIT_0211400 | 237.40 | 256.83 | 309.92 | 343.47 | 538.89 | 189.47 | 271.60 | 405.46 | ras-related protein RAB7 |
| PFIT_0215200 | 82.91 | 100.53 | 129.81 | 122.70 | 189.82 | 82.75 | 86.79 | 108.04 | reactive oxygen species modulator 1, putative |
| PFIT_0101000 | 495.34 | 1023.15 | 939.75 | 872.22 | 1096.83 | 586.00 | 830.85 | 776.72 | regulator of chromosome condensation, putative |
| PFIT_0110100 | 70.10 | 81.16 | 169.21 | 88.32 | 115.63 | 76.47 | 97.74 | 105.32 | regulator of chromosome condensation, putative |
| PFIT_0304500 | 202.76 | 63.03 | 178.59 | 132.10 | 132.99 | 261.57 | 390.45 | 651.19 | regulator of chromosome condensation, putative |
| PFIT_0710900 | 405.85 | 706.87 | 887.92 | 851.37 | 1018.74 | 648.37 | 832.25 | 944.26 | regulator of nonsense transcripts, putative |
| PFIT_0301500 | 99.70 | 31.28 | 98.05 | 72.10 | 67.28 | 186.17 | 187.20 | 201.27 | repetitive organelle protein, putative |
| PFIT_0109200 | 80.83 | 132.86 | 166.96 | 115.54 | 118.47 | 131.44 | 194.68 | 107.35 | replication termination factor, putative |
| PFIT_0107400 | 43.05 | 26.45 | 90.78 | 64.83 | 413.31 | 15.29 | 30.91 | 66.11 | RESA-like protein with PHST and DnaI domains |
| PFIT_0219500 | 1719.79 | 439.36 | 2624.56 | 836.38 | 1112.59 | 3165.50 | 4200.28 | 7893.80 | reticulocyte binding protein homologue 1 |
| PFIT_0317700 | 369.02 | 119.09 | 354.09 | 180.61 | 214.13 | 404.65 | 653.74 | 1191.50 | reticulocyte binding protein homologue 3, pseudogene |
| PFIT_0219600 | 108.77 | 31.45 | 108.83 | 72.46 | 73.08 | 175.00 | 242.71 | 323.31 | reticulocyte binding protein homologue 4 |
| PFIT_0311400 | 103.07 | 15.24 | 40.78 | 69.83 | 35.76 | 138.16 | 109.50 | 206.51 | rhoGAP GTPase, putative |
| PFIT_0321900 | 506.96 | 29.86 | 294.30 | 290.94 | 154.61 | 416.12 | 437.16 | 1064.69 | rhophy neck protein 2 |
| PFIT_0313800 | 386.10 | 67.18 | 198.26 | 304.27 | 143.86 | 655.88 | 473.66 | 1313.08 | rhophy neck protein 4 |
| PFIT_0309100 | 363.03 | 55.09 | 144.54 | 225.35 | 112.23 | 486.81 | 398.27 | 1115.40 | rhophy neck protein 5 |
| PFIT_0302300 | 521.99 | 108.33 | 338.22 | 373.50 | 184.62 | 724.42 | 836.46 | 1316.02 | rhophy neck protein 6 |
| PFIT_0306100 | 176.91 | 27.39 | 91.45 | 102.88 | 69.38 | 231.67 | 193.76 | 403.62 | rhophy protein ROP14 |
| PFIT_0307700 | 324.43 | 109.24 | 318.23 | 352.51 | 215.46 | 775.92 | 743.54 | 1563.03 | rhophy-associated leucine zipper-like protein 1 |
| PFIT_0307300 | 1633.05 | 172.55 | 625.10 | 721.49 | 347.88 | 1642.82 | 1703.32 | 3596.45 | rhophy-associated membrane antigen |
| PFIT_0319700 | 1735.32 | 162.18 | 683.00 | 736.11 | 388.69 | 1753.36 | 1724.47 | 3535.55 | rhophy-associated protein 1 |
| PFIT_0304300 | 99.02 | 42.62 | 102.72 | 78.47 | 98.55 | 138.44 | 141.39 | 267.67 | ribosome biogenesis GTPase A, putative |
| PFIT_0112800 | 44.41 | 98.26 | 71.06 | 109.04 | 110.69 | 59.06 | 79.77 | 105.41 | ribon |
| PFIT_0113700 | 27.81 | 29.86 | 294.30 | 204.84 | 67.16 | 35.51 | 27.21 | 44.17 | ribon |
| PFIT_0203500 | 122.29 | 21.10 | 135.56 | 127.19 | 791.20 | 28.59 | 38.65 | 258.84 | ribon |
| PFIT_0220400 | 49.95 | 4.68 | 24.48 | 25.60 | 33.69 | 83.94 | 110.27 | 100.11 | ribon |
| PFIT_0218100 | 1.66 | 0.00 | 12.04 | 1.07 | 0.75 | 233.86 | 18.00 | 126.70 | RING zinc finger protein, putative |
| PFIT_0311500 | 59.41 | 7.46 | 29.69 | 29.21 | 18.16 | 63.78 | 62.60 | 166.70 | RING zinc finger protein, putative |
| PFIT_0309800 | 51328.40 | 34753.27 | 50344.34 | | | | | | |

| | | | | | | | | | |
|---------------|----------|----------|----------|----------|----------|----------|----------|----------|--|
| PFIT_0419500 | 67.11 | 114.99 | 233.29 | 132.58 | 372.89 | 66.49 | 144.66 | 144.87 | serine/threonine protein phosphatase CPED1, putative |
| PFIT_0216200 | 1350.79 | 2060.47 | 2517.46 | 2033.93 | 2838.60 | 1559.84 | 1854.30 | 1957.65 | signal peptide peptidase |
| PFIT_0213500 | 77.49 | 50.24 | 118.81 | 74.68 | 168.36 | 47.86 | 104.16 | 105.30 | signal recognition particle receptor, beta subunit |
| PFIT_0202900 | 47.84 | 110.77 | 84.99 | 100.80 | 134.08 | 39.83 | 82.61 | 116.22 | smn3 associated polypeptide p18-like protein |
| PFIT_0218200 | 21872.82 | 33377.12 | 40658.10 | 35407.14 | 37417.83 | 44357.21 | 36489.29 | 28661.04 | skeleton-binding protein 1 |
| PFIT_0103100 | 392.47 | 488.88 | 937.27 | 539.37 | 1326.08 | 348.82 | 486.97 | 366.31 | small exported membrane protein 1 |
| PFIT_1241100 | 14.59 | 28.75 | 70.07 | 40.01 | 73.20 | 18.23 | 54.38 | 32.79 | SNARE protein, putative |
| PFIT_0202600 | 54.63 | 102.40 | 88.58 | 83.02 | 109.68 | 56.95 | 93.23 | 122.35 | sorting assembly machinery 50 kDa subunit, putative |
| PFIT_0305900 | 41.85 | 8.86 | 23.31 | 39.04 | 13.16 | 70.49 | 51.05 | 88.83 | spindle assembly abnormal protein 6, putative |
| PFIT_0101200 | 26.67 | 42.60 | 60.55 | 37.41 | 63.42 | 34.61 | 36.00 | 40.73 | SRRI-like protein |
| PFIT_0301100 | 445.63 | 155.59 | 290.20 | 210.57 | 206.61 | 455.26 | 571.36 | 1085.48 | STAR-related lipid transfer protein |
| PFIT_0101700 | 45.21 | 26.43 | 122.94 | 46.56 | 113.68 | 42.48 | 59.51 | 67.41 | steroid dehydrogenase, putative |
| PFIT_0212600 | 66.03 | 105.30 | 105.94 | 110.66 | 155.21 | 61.09 | 100.26 | 129.30 | steryl ester hydrolase, putative |
| PFIT_0210600 | 17.72 | 53.97 | 27.71 | 33.23 | 115.65 | 13.28 | 18.74 | 42.61 | stevor, pseudogene |
| PFIT_0207300 | 43.32 | 57.10 | 43.34 | 62.51 | 109.38 | 34.58 | 46.65 | 85.35 | stomatol-like protein |
| PFIT_0309800 | 48.23 | 11.87 | 29.91 | 42.44 | 27.92 | 73.72 | 52.69 | 116.48 | subpellicular microtubule protein 1, putative |
| PFIT_0301300 | 4.00 | 4.69 | 3.37 | 3.99 | 5.07 | 3.37 | 1.58 | 63.44 | surface-associated interspersed protein 1.1 (SURFIN 1.1) |
| PFIT_0214500 | 50.46 | 101.28 | 88.89 | 74.65 | 66.59 | 112.77 | 115.92 | 108.52 | surface-associated interspersed protein 1.2 (SURFIN 1.2) |
| PFIT_0317900 | 10.60 | 14.28 | 25.20 | 17.11 | 17.45 | 28.74 | 16.12 | 149.57 | surface-associated interspersed protein 13.1 (SURFIN 13.1) |
| PFIT_0303400 | 243.52 | 76.93 | 135.33 | 158.38 | 189.65 | 421.10 | 372.33 | 602.38 | surface-associated interspersed protein 4.1 (SURFIN 4.1) |
| PFIT_0203300 | 12.89 | 19.90 | 48.15 | 20.48 | 60.26 | 5.06 | 46.70 | 90.52 | surface-associated interspersed protein 8.1 (SURFIN 8.1) |
| PFIT_0317100 | 28.04 | 16.04 | 118.58 | 32.94 | 99.21 | 36.31 | 78.78 | 110.33 | surface-associated interspersed protein 8.2 (SURFIN 8.2) |
| PFIT_0209400 | 75.78 | 75.91 | 108.65 | 110.44 | 163.62 | 69.92 | 98.46 | 133.40 | synactin binding protein, putative |
| PFIT_0218700 | 35.87 | 56.91 | 61.13 | 53.82 | 43.60 | 72.39 | 65.72 | 65.54 | telomerase reverse transcriptase |
| PFIT_0108600 | 210.76 | 310.84 | 455.53 | 325.74 | 556.37 | 205.96 | 278.46 | 310.69 | thioredoxin 1 |
| PFIT_0210200 | 62.49 | 95.18 | 122.76 | 99.28 | 144.02 | 83.23 | 69.52 | 96.25 | thioredoxin-like protein |
| PFIT_0310200 | 70.95 | 12.49 | 72.23 | 31.82 | 51.67 | 98.74 | 125.67 | 23.42 | thioredoxin-like protein 1, putative |
| PFIT_0202200 | 53.39 | 130.28 | 107.22 | 137.16 | 137.35 | 104.76 | 94.98 | 91.88 | thioredoxin, putative |
| PFIT_0401500 | 300.12 | 477.37 | 714.45 | 450.55 | 633.68 | 482.44 | 575.07 | 604.62 | trafficking protein particle complex subunit 8, putative |
| PFIT_0212800 | 1272.37 | 2650.67 | 2380.86 | 2110.61 | 3283.23 | 700.31 | 1079.50 | 1370.55 | transcription factor with AP2 domain(s) |
| PFIT_0204100 | 258.10 | 142.78 | 348.24 | 371.44 | 855.70 | 369.45 | 298.23 | 646.61 | transcription factor with AP2 domain(s) |
| PFIT_0212300 | 1245.69 | 1642.03 | 1773.49 | 1427.82 | 3390.56 | 776.67 | 1019.01 | 1939.70 | transcription factor with AP2 domain(s) |
| PFIT_0214100 | 35.88 | 27.90 | 65.35 | 32.83 | 173.97 | 8.01 | 22.43 | 57.76 | transcription factor with AP2 domain(s) |
| PFIT_0215800 | 16.46 | 30.29 | 38.94 | 27.19 | 51.94 | 27.16 | 33.07 | 38.94 | transcription factor with AP2 domain(s), putative |
| PFIT_0220700 | 1501.39 | 2472.56 | 2743.53 | 2320.80 | 2111.64 | 1773.94 | 3661.33 | 2032.45 | transcription factor with AP2 domain(s), putative |
| PFIT_0104000 | 77.09 | 100.64 | 234.20 | 122.21 | 203.99 | 120.93 | 113.21 | 106.17 | translation initiation factor IF-2, putative |
| PFIT_0104400 | 282.92 | 586.55 | 599.63 | 516.95 | 672.92 | 334.01 | 507.22 | 433.97 | transporter, putative |
| PFIT_0105800 | 269.60 | 343.06 | 542.06 | 295.64 | 577.33 | 184.01 | 203.50 | 341.14 | transporter, putative |
| PFIT_0100500 | 12.99 | 15.55 | 55.74 | 25.71 | 73.56 | 26.14 | 48.40 | 71.01 | TRAP-like protein |
| PFIT_0206400 | 157.35 | 169.79 | 247.00 | 173.02 | 328.28 | 131.16 | 135.31 | 198.20 | triose phosphate transporter |
| PFIT_0109300 | 381.03 | 549.85 | 794.28 | 576.62 | 660.82 | 550.81 | 787.07 | 538.17 | (RNA delta(2))-isopentenylpyrophosphate transferase, putative |
| PFIT_0109000 | 370.90 | 589.02 | 770.60 | 735.73 | 727.28 | 741.25 | 970.44 | 758.30 | RNA m(5C)-methyltransferase, putative |
| PFIT_0102000 | 557.43 | 731.11 | 1324.77 | 579.26 | 1349.04 | 478.60 | 701.72 | 691.36 | RNA pseudouridine synthase, putative |
| PFIT_0201200 | 171.14 | 302.72 | 318.82 | 340.14 | 347.88 | 347.85 | 340.48 | 316.60 | trophozoite exported protein 1 |
| PFIT_0106900 | 66.41 | 106.14 | 132.82 | 83.60 | 160.34 | 53.95 | 58.84 | 117.94 | tryptophan--tRNA ligase, putative |
| PFIT_0308400 | 65.51 | 82.53 | 80.00 | 64.90 | 77.64 | 66.64 | 62.76 | 142.17 | tubulin gamma chain |
| PFIT_0311600 | 132.39 | 40.26 | 62.17 | 75.35 | 48.23 | 147.84 | 128.26 | 273.78 | tubulin--lysine ligase, putative |
| PFIT_0206400 | 33.81 | 40.21 | 54.98 | 43.42 | 84.48 | 25.19 | 30.46 | 38.99 | tubulin-specific chaperone a, putative |
| PFIT_0313900 | 46.00 | 20.54 | 28.93 | 44.30 | 54.81 | 30.48 | 55.13 | 116.71 | tyrosine--tRNA ligase |
| PFIT_0104200 | 87.60 | 168.06 | 193.45 | 156.72 | 195.35 | 100.93 | 172.18 | 123.55 | U6 snRNA-associated Sm-like protein LSM8, putative |
| PFIT_0318600 | 162.98 | 187.67 | 269.86 | 190.52 | 285.30 | 216.77 | 270.22 | 375.37 | ubiquitin-activating enzyme |
| PFIT_0317400 | 487.47 | 133.00 | 385.83 | 312.04 | 314.06 | 698.25 | 843.20 | 1375.53 | ubiquitin-conjugating enzyme E2, putative |
| PFIT_0319300 | 96.75 | 19.80 | 48.60 | 78.86 | 47.14 | 163.18 | 126.06 | 260.51 | ubiquitin-conjugating enzyme, putative |
| PFIT_0207100 | 229.86 | 340.57 | 427.52 | 341.79 | 542.20 | 337.65 | 316.63 | 391.44 | ubiquitin-protein ligase, putative |
| PFIT_0113100 | 1473.68 | 2931.70 | 2607.60 | 3448.71 | 4218.01 | 2793.31 | 1996.47 | 3296.90 | unspecified product |
| PFIT_0201100 | 734.68 | 1066.64 | 414.95 | 1546.92 | 625.19 | 756.45 | 406.00 | 1026.28 | unspecified product |
| PFIT_0217000 | 40.62 | 67.40 | 64.14 | 80.44 | 59.56 | 104.80 | 67.53 | 202.40 | unspecified product |
| PFIT_0317100 | 87.36 | 16.77 | 41.05 | 64.81 | 32.16 | 125.36 | 108.70 | 236.87 | V-type K+-independent H+-translocating inorganic pyrophosphatase |
| PFIT_0213800 | 51.69 | 23.93 | 65.26 | 54.44 | 104.57 | 40.14 | 49.12 | 86.04 | vacuolar protein sorting-associated protein 26, putative |
| PFIT_0105500 | 98.24 | 156.28 | 200.28 | 146.82 | 244.89 | 159.00 | 148.25 | 196.45 | vacuolar protein sorting-associated protein 35, putative |
| PFIT_bin01000 | 82.91 | 180.27 | 225.98 | 192.45 | 253.45 | 153.82 | 205.70 | 198.09 | vacuolar protein sorting-associated protein 53, putative |
| PFIT_0309000 | 255.37 | 84.78 | 208.54 | 167.61 | 250.38 | 313.45 | 301.59 | 582.08 | vacuolar protein sorting-associated protein 9, putative |
| PFIT_bin07000 | 291.04 | 596.48 | 666.49 | 597.63 | 662.62 | 302.53 | 628.19 | 515.85 | vesicle-associated membrane protein, putative |
| PFIT_0203000 | 21.62 | 84.54 | 70.52 | 76.02 | 103.33 | 37.93 | 79.23 | 86.52 | von Willebrand factor A domain-related protein |
| PFIT_bin06100 | 26.45 | 52.43 | 91.36 | 53.25 | 79.39 | 51.84 | 57.66 | 58.70 | zinc finger protein, putative |
| PFIT_0209000 | 42.20 | 20.36 | 53.23 | 30.36 | 180.55 | 12.38 | 18.57 | 32.17 | zinc finger protein, putative |
| PFIT_0309200 | 306.12 | 76.85 | 242.51 | 140.10 | 159.32 | 305.70 | 395.51 | 653.06 | zinc finger protein, putative |
| PFIT_0310500 | 57.56 | 7.67 | 38.67 | 29.72 | 21.74 | 89.08 | 56.14 | 125.57 | zinc finger protein, putative |
| PFIT_0318000 | 165.87 | 38.23 | 114.40 | 113.90 | 121.25 | 202.78 | 190.15 | 371.73 | zinc finger transcription factor, putative |
| PFIT_0300900 | 326.63 | 177.08 | 394.50 | 273.14 | 315.35 | 391.56 | 595.80 | 716.72 | zinc-carboxypeptidase, putative |

Annex II

Static binding assay of stable and transient transfected CHO cell.

Initial binding capability of culture isolate IT4 and 3D7 towards human CD36 and ICAM-1.



LANGUAGE CERTIFICATE

By Eva Pansegrau

I am a native speaker, have read the present PhD thesis and hereby confirm that it complies with the rules of the English language. Date, Signature

19. MARCH 2019,

A handwritten signature in blue ink, appearing to read 'E. Pansegrau', written in a cursive style.

Date, Signature

ACKNOWLEDGEMENTS

An dieser Stelle möchte ich mich bei den Menschen bedanken, die diese Doktorarbeit möglich gemacht und mich auf dem Weg dorthin begleitet haben.

Mein besonderer Dank gilt meiner Doktormutter Prof. Dr. Iris Bruchhaus, die mich über die Jahre hinweg betreut, beraten, aufgebaut und unterstützt hat. Vielen Dank für die Möglichkeit in deiner Laborgruppe zu lernen und zu wachsen.

Ebenfalls möchte ich mich bei Prof. Dr. Tim Gilberger für die Begutachtung der Dissertation, sowie den Mitgliedern der Prüfungskommission Prof. Dr. Dr. Jonas Schmidt-Chanasit und PD Dr. Hartwig Lüthen bedanken.

Insbesondere gilt mein Dank der Joachim Herz Stiftung und der PIER Helmholtz Graduate School, für das erhaltene Stipendium und die fachübergreifende Betreuung. Ganz besonders möchte ich mich bei Dr. Eva Ackermann, Stefanie Tepass und Mirko Siemssen bedanken. Ihr wart wunderbare Ansprechpartner und habt mir die schweren Phasen besonders erleichtert!

Auch möchte ich mich bei Olaf Kern und dem Team von Printarena bedanken, die mir den wunderbaren Druck meiner Dissertation ermöglicht haben.

Ein ganz lieber Dank geht auch an die ehemalige und die aktuelle Arbeitsgruppe Protozoologie und die Arbeitsgruppe Molekulare Infektionsimmunologie, oder auch Labor 4,5 und 6. Ganz besonders an Nahla, Heidrun, Corinna, Siew Ling und Jill. Ohne euch wäre die Zeit nie so bunt und die Kaffeepausen nie so lebhaft geworden!

Von ganzem Herzen möchte ich mich auch bei meinen geliebten Eltern Norbert und Bärbel und bei meinem Bruderherz Florian bedanken. Für alles was war, was ist und was jemals kommen wird. Ihr seid einfach wunderbar!

Tausend Dank auch an die Hamburger Clique, vor allem an Melanie, Liliana, Anne, Marleen, Anika, Malina, Jan, Yannik, Babsi und Gabriel für all die Zerstreung, den Rückhalt und die Freundschaft. Ihr habt mit mir die Welt entdeckt, den Kiez und das Meer – und der Rest kommt auch noch. Destination: Anywhere. Wunderbare Freunde, die ich nie missen möchte! Auch Constantin, Salek und ganz besonders Clemens möchte ich danken. Ihr seid in so kurzer Zeit ein so großer Teil meines Lebens geworden und werdet es hoffentlich immer sein!

Regrets, I've had a few,
But then again, too few to mention.

(Frank Sinatra)

It was amazing!

DECLARATION

by **Lisa Katharina Roth**

Hiermit bestätige ich, dass die vorliegende Arbeit mit dem Titel: 'The effects on the malaria parasite *Plasmodium falciparum* (WELCH, 1897) in response to an interaction of parasitized erythrocytes with various human endothelial receptors' von mir selbständig verfasst wurde und ich keine anderen als die angegebenen Quellen und Hilfsmittel verwendet habe. Die Dissertation wurde von mir vorher nicht bei einem anderen Prüfungsverfahren zur Erreichung eines akademischen Titels eingereicht.

Die eingereichte schriftliche Fassung entspricht der auf dem elektronischen Speichermedium.

Ich bin damit einverstanden, dass die Doktorarbeit veröffentlicht wird.

Hereby, I declare that I have developed and written the enclosed dissertation entitled: 'The effects on the malaria parasite *Plasmodium falciparum* (WELCH, 1897) in response to an interaction of parasitized erythrocytes with various human endothelial receptors' by myself and have not used sources or means without declaration in the text.

The dissertation was not used in the same or in a similar version to achieve an academic grading. The written dissertation matches the digital one.

I hereby agree that the dissertation will be published.

Date, Signature